

1-1-2008

Performance of full scale self consolidating concrete structural elements in shear, bond and under corrosion attack

Assem adel abdel Aal Hassan
Ryerson University

Follow this and additional works at: <http://digitalcommons.ryerson.ca/dissertations>

 Part of the [Civil Engineering Commons](#)

Recommended Citation

Hassan, Assem adel abdel Aal, "Performance of full scale self consolidating concrete structural elements in shear, bond and under corrosion attack" (2008). *Theses and dissertations*. Paper 861.

This Dissertation is brought to you for free and open access by Digital Commons @ Ryerson. It has been accepted for inclusion in Theses and dissertations by an authorized administrator of Digital Commons @ Ryerson. For more information, please contact bcameron@ryerson.ca.

TA
440
.1437
2008

**PERFORMANCE OF FULL SCALE SELF CONSOLIDATING
CONCRETE STRUCTURAL ELEMENTS IN SHEAR, BOND
AND UNDER CORROSION ATTACK**

By
Assem Adel Abdel Aal Hassan
Master of Applied Science in Structural Engineering
Ryerson University, Toronto, Canada 2003
Master of Science in Structural Engineering,
Ain Shams University, Cairo, Egypt 1999

A Dissertation
presented to Ryerson University
in partial fulfillment of the
requirements for the degree of
Doctor of Philosophy
in
Civil Engineering
Toronto, Ontario, Canada, 2008
© (Assem Hassan) 2008

Author's Declaration

I hereby declare that I am the sole author of this dissertation.

I authorize Ryerson University to lend this dissertation to other institutions or individuals for the purpose of scholarly research.

SIGNATURE

I further authorize Ryerson University to reproduce this dissertation by photocopying or by other means, in total or in part, at the request of other institutions or individuals for the purpose of scholarly research.

SIGNATURE

PERFORMANCE OF FULL SCALE SELF CONSOLIDATING CONCRETE STRUCTURAL ELEMENTS IN SHEAR, BOND AND UNDER CORROSION ATTACK

By
@ Assem Adel Abdel Aal Hassan 2008
Doctor of Philosophy
in
Civil Engineering
Ryerson University
Toronto, Ontario, Canada

ABSTRACT

This research program focuses on investigating the shear resistance, bond characteristics, and corrosion performance of self-consolidating concrete (SCC) compared to those of normal concrete (NC). The shear strength, cracking behavior, and deflection characteristics were tested in full-scale beams. A total of twenty reinforced concrete beams, with no shear reinforcements, were tested under mid-span concentrated load until shear failure occurred.

The experimental test parameters included concrete type/coarse aggregate content, beam depth and the longitudinal reinforcing steel ratio (ρ_s). The beam depth ranged from 150 to 750 mm while the shear span-to-depth ratio (a/d) was kept constant in all beams. The two longitudinal reinforcing steel ratios used were 1% and 2%.

The performance of SCC/NC beams was evaluated based on the results of crack pattern, crack widths, loads at the first flexure/diagonal cracking, ultimate shear resistance, post-cracking shear resistance/ductility, load-deflection response, and failure modes. Code-based equations or procedures are used to predict the crack width, first flexural cracking moment/load, and ultimate shear resistance as well as to simulate load-deflection response.

The bond strength of reinforcing bars embedded in full-scale heavy reinforcing beams (4000 mm length \times 1200 mm depth \times 300 mm width) made with SCC was investigated and compared with that of NC. The flowability of SCC mixture through the dense reinforcement was visually monitored from a transparent formwork.

The bond stress was tested for bars located at three different heights (150 mm, 510 mm, and 870 mm from the bottom of the beam) and at different concrete ages (1, 3, 7, 14, and 28 days). The bond stress-free end slip relationship, the top bar effect, and the effect of age on bond

stress were investigated in both SCC and NC beams. Bond stresses predicted based on some major Codes were compared with those obtained from experiments.

The corrosion of steel reinforcement embedded in full-scale SCC beams was investigated and compared to that embedded in NC beams. The corrosion performance of 400 mm width \times 363 mm depth \times 2340 mm length beams containing epoxy and non-epoxy coated stirrups was monitored by partial immersion in a sodium chloride solution and an impressed current. Half-cell potential tests were implemented at 25 different locations on each beam to evaluate the probability of steel corrosion along the beam length/perimeter.

At the same locations where the half-cell potential tests were implemented, the chloride ion content near the bar surface was measured to study the variation of the chloride-ion penetrability along the beam length/perimeter. The mass loss and bar diameter degradation along the length of each bar were investigated at the end of the test. Predicted rebar mass loss due to corrosion based on Faraday's law was compared with experimental mass loss for each beam.

Small-scale cylinder specimens made of NC and SCC with centrally located embedded reinforcing bar was also tested to investigate the effect of segregation and bleeding on corrosion performance. The corrosion performance of various SCC with different types of high range water reducers (HRWRs) were also investigated with small-scale cylinder specimens.

The structural performance and cracking behavior of full-scale corroded reinforced concrete beams made with SCC was investigated and compared with those of NC. Six reinforced concrete beams (2340 mm length \times 363 mm depth \times 400 mm width) without web reinforcement designed to fail in shear were tested under mid-span concentrated load after three degrees of corrosion obtained (0, 8%, and 25% degree of corrosion). The performance of corroded SCC/NC beams was evaluated based on the results of crack patterns, crack widths, loads at the first flexure and first diagonal cracks, mid span deflection, ultimate load, and failure modes. In addition, the results of the crack widths and the mid-span deflections were compared with some major Code-based equations.

Based on the results of the shear strength investigation, the ultimate shear strength of SCC beams was found to be slightly lower than that of NC beams. The difference was more pronounced with the reduction of longitudinal steel reinforcement and with the increase of beam depth. However, the results of testing the bond strength in heavily reinforced beams indicated that casting SCC beam was faster, easier, required less labor, and did not result in blockage of

concrete among the heavy reinforcements when compared with NC. The results of the bond strength also indicated that the bond stress was slightly higher in SCC beam compared with NC beams and the difference was more pronounced in the top bars and at 28 days of testing.

The results of the corrosion investigation showed that SCC beams had superior performance compared to their NC counterparts in terms of corrosion cracking, corrosion rate, half-cell potential, time of corrosion initiation, rebar mass loss and rebar diameter reduction. The SCC beams showed severe localized corrosion of stirrups and longitudinal rebars at the far end of the beam (away from the casting point). The SCC beams also had spalling of concrete cover at the corners due to inadequate local compaction and distribution of concrete. A strong correlation between the predicted rebar mass loss (using Faraday's law) and actual rebar mass loss, due to corrosion, validates the use of theoretical estimates to examine the effect of corrosion over time. The difference between SCC and NC mixtures in terms of corrosion was only pronounced in large-scale beams and types of HRWR have no influence on corrosion performance.

Acknowledgments

I am deeply indebted to my advisor, Dr. Mohamed Lachemi, for his constant support and continued advice. His extensive knowledge together with his gentle way encouraged me to love and finish this research work. He has been everything that one could want in an advisor.

I also would like to express my deepest sense of gratitude to Dr. Anwar Hossain for his valuable advice, suggestions and incredible knowledge which made this work successful. Without his help, this work would not be possible.

I'm gratefully acknowledging the financial assistance of the Natural Sciences and Engineering Research Council (NSERC) of Canada for this research project. Special thank to Mr. John Pontarollo and Mr. Dennis Baker of St. Lawrence Cement, Canada, for their great support.

Special thanks to my examining committee members, Dr. Kamal Khayat, Dr. Hesham Marzouk, Dr. Medhat Shehata, and Dr. Farnaz Sadeghpour for their helpful advice and suggestions.

I am deeply and forever indebted to my parents for their love, support and encouragement throughout my entire life. I am also very grateful to my sister and my brothers for their support and constant encouragement.

Above all, my deepest appreciation and love to my wife Sherine Khattab for her infinite love and tender. She was every time beside me supporting and encouraging me to complete this work. Without her in my life the completion of this research would not have been possible to me.

Table of Contents

Abstract	iii
Acknowledgments	vi
Table of Contents	vii
List of Figures	xii
List of Tables	xxi
List of Symbols	xxii
1 Introduction	1
1.1 Background.....	1
1.2 Scope and objectives.....	5
1.3 Outline of thesis.....	7
2 Background of Self-Consolidating Concrete	8
2.1 Introduction.....	8
2.2 History of SCC.....	8
2.3 Applications of SCC.....	9
2.4 Production of SCC.....	11
2.4.1 High range water reducer.....	11
2.4.2 Viscosity modifying admixture.....	12
2.4.3 Mineral admixtures.....	12
2.5 Properties of SCC.....	13
2.5.1 Slump flow.....	13
2.5.2 Passing ability.....	13
2.5.3 Segregation resistance.....	13
2.5.4 Hardened properties and structure performance of SCC.....	14
3 Literature Review	15
3.1 Shear strength.....	15
3.1.1 Stresses in uncracked elastic beams without transverse reinforcement.....	15
3.1.2 Stresses between cracks in beams without transverse reinforcement.....	18
3.1.3 Principle mechanism of shear.....	19
3.1.4 Mechanism of shear transfer for beams without transverse reinforcement.....	20

3.1.5	Factor influencing shear strength	22
3.1.5.1	Influence of shear span/effective depth ratio on failure mode	22
3.1.5.2	Longitudinal reinforcement ratio	25
3.1.5.3	Beam size	27
3.1.5.4	Axial force.....	27
3.1.5.5	Aggregate type and size	28
3.1.5.6	Concrete tensile strength	29
3.1.6	Shear strength in concrete beams with transverse reinforcement	29
3.1.6.1	General	29
3.1.6.2	Truss analogy.....	30
3.1.7	Equations for shear in beams.....	32
3.1.8	Review of shear tests in reinforced concrete beams	34
3.2	Bond strength	40
3.2.1	Introduction	40
3.2.2	Bar-concrete interaction.....	41
3.2.2.1	Stage I (Uncracked stage)	42
3.2.2.2	Stage II (Microcracks).....	42
3.2.2.3	Stage III (splitting cracks)	42
3.2.2.4	Stage IVa (Bond failure of plain bars)	43
3.2.2.5	Stage IVb (Bond failure of deformed bars surrounded by light confinement) .	44
3.2.2.6	Stage IVc (Bond failure of deformed bars surrounded by heavy confinement)	44
3.2.3	Effect of bar profile on bond strength.....	45
3.2.4	Effect of geometry and shape of the bar	46
3.2.5	Effect of rib angle, rib spacing, and rib height.....	47
3.2.6	Effect of casting position and concrete confinement on the bond strength	48
3.2.7	Effect of member depth on the bond strength	51
3.2.8	Bond Strength in SCC.....	53
3.2.8.1	General	53
3.2.8.2	Review of research work.....	54
3.3	Durability and corrosion resistance of self consolidating concrete.....	56
3.3.1	Introduction	56

3.3.2	Reinforcing steel corrosion	56
3.3.3	Concrete as an electrolyte	59
3.3.3.1	Solid phases	59
3.3.3.2	Non-solid phases	60
3.3.3.2.1	Pores	60
3.3.3.2.2	Water	61
3.3.3.3	Aggregate paste interface	61
3.3.3.4	Concrete Porosity	62
3.3.4	Review of previous work	63
4	Experimental Program	65
4.1	Introduction	65
4.2	Materials used	65
4.2.1	Concrete mix parameters	65
4.2.2	Reinforcing steel	66
4.2.3	Testing concrete properties	66
4.3	Shear investigations	67
4.3.1	Shear behavior of large-scale SCC beams	67
4.3.2	Studying the cracking and deflection characteristics of large-scale SCC beams ..	67
4.3.3	Specimens details	68
4.3.4	Formwork preparation and casting of beam specimens	68
4.3.5	Test setup, instrumentation and loading procedure	69
4.4	Bond investigation	70
4.4.1	Specimens details	70
4.4.2	Formwork preparation and casting of beam specimens	71
4.4.3	Test setup, instrumentation, and loading procedure	72
4.5	Corrosion investigations	72
4.5.1	Testing the performance of SCC/NC in terms of corrosion resistance	72
4.5.2	Strength and cracking of full-scale corroded SCC/NC beams	73
4.5.3	Specimens details	74
4.5.4	Accelerated corrosion setup and current measurements	75
4.5.5	Half-cell potential measurements	76

4.5.6	Chloride ions measurements	77
4.5.7	Measurement of mass loss and reduction of bar diameter	77
5	Shear Resistance - Results and Discussion	97
5.1	Shear behavior of large-scale SCC beams	97
5.1.1	Cracking and failure characteristics.....	97
5.1.2	Cracking load and crack width characteristics of SCC/NC beams	97
5.1.3	Shear resistance characteristics of SCC/NC beams.....	98
5.1.4	Influence of concrete type, beam depth and longitudinal steel ratio on normalized shear load (V_{nz})	99
5.1.5	Performance of Code-based shear prediction of SCC beams	101
5.2	Cracking and deflection characteristics of large-scale SCC beams	102
5.2.1	Experimental and theoretical analyses of crack width.....	102
5.2.2	Experimental load-deflection response and strength characteristics	104
5.2.2.1	Experimental load-deflection response.....	104
5.2.2.2	Post-cracking shear resistance and ductility.....	105
5.2.3	Theoretical formulations of load-deflection response	106
5.2.4	Comparison of experimental and theoretical shear load /moment	110
5.2.5	Comparison of experimental and theoretical load-deflection response.....	110
6	Bond Resistance - Results and Discussion.....	145
6.1	General observation.....	145
6.2	Effect of concrete age on bond and compressive strength	145
6.3	Effect of mixture type bond stress.....	146
6.4	Comparison between experimental and predicted bond stresses	148
6.5	Bond stress-slip relationship	149
6.6	Effect of bar location on bond stress	150
7	Corrosion Resistance - Results and Discussion	161
7.1	Performance of SCC/NC specimens under corrosion attack	161
7.1.1	General cracking observation.....	161
7.1.2	Time-dependent corrosion test results	162
7.1.2.1	Current results.....	162
7.1.2.2	Half-cell potential measurements	163

7.1.3	After corrosion test results	164
7.1.3.1	Results of chloride content, mass loss and rebar's diameter reduction	164
7.1.4	Comparison of theoretical and actual corrosion mass loss	165
7.1.5	Results of the small concrete cylinders samples	166
7.2	Results of testing the strength and cracking of full-scale corroded SCC/NC beams ..	167
7.2.1	Ultimate failure load and mode of failure	167
7.2.2	Load cracking observations.....	169
7.2.2.1	Non-corroded and first degree corroded beams	169
7.2.2.2	Second degree corroded beams	169
7.2.3	Crack width calculation	170
7.2.4	Experimental load deflection response	172
7.2.5	Post-cracking shear resistance and ductility.....	173
7.2.6	Comparison between actual and theoretical deflection	174
8	Conclusions and Recommendations	208
8.1	Summary	208
8.2	Conclusions	208
8.3	Recommendations	213
	References	215
	Appendices	229
	Appendix A	229

List of Figures

Figure 4-1: Schematic diagram of experimental beam specimens (Dimensions are in mm)	82
Figure 4-2: Cross sections and reinforcement layout of beams with 1% and 2% ρ_w (mm)	83
Figure 4-3: 750 mm depth beam formwork (contained 1% and 2% ρ_w)	83
Figure 4-4: Formwork reinforcing bar placement	84
Figure 4-5: Test setup, instrumentation and testing of a beam specimen (shear test)	84
Figure 4-6: Schematic diagram of the shear test beam specimens	85
Figure 4-7: Beam specimens; (a) Front view, (b) Back view (bond test)	86
Figure 4-8: Schematic diagram of the beam specimens; (a) Front view, (b) Back view (bond test)	87
Figure 4-9: Schematic diagram of the pull out test setup	88
Figure 4-10: Plastic sleeve covering 150 mm of the pull out bar to insure only 150 mm of the bar is in contact with the concrete	88
Figure 4-11: Transparent plastic front side of the bond test formwork	89
Figure 4-12: Formwork details of the bond test specimen	90
Figure 4-13: Formwork details for corrosion test beams a) non-epoxy coated stirrups for moderate corrosion stage b) epoxy-coated stirrups for severe corrosion stage	91
Figure 4-14: Cylinder sample for corrosion tests	91
Figure 4-15: Steel bars preparation	92
Figure 4-16: Adjustment of the bar verticality	92
Figure 4-17: Accelerated corrosion tank for corrosion test	93
Figure 4-18: Schematic diagram of the accelerated corrosion test	93
Figure 4-19: Corrosion current monitoring by data-acquisition system	94
Figure 4-20: Typical layout of the tested points along the beam length/perimeter	94
Figure 4-21: Half-cell potential measurements	95
Figure 4-22: Chloride ion electrometer for measuring the chloride ion content	95
Figure 4-23: Cleaning the embedded bars with HCL before measuring the mass loss	96
Figure 4-24: Embedded longitudinal bar segments for measuring the mass loss	96
Figure 5-1: Typical failure modes of SCC/NC beams of various sizes	117

Figure 5-2: Crack development and crack widths (in mm) for 1% and 2% ρ_w 750 mm SCC beams at different load levels (50%, 75%, and 100% of failure load).....	118
Figure 5-3: Crack development and crack widths (in mm) for 1% and 2% ρ_w 750 mm NC beams at different load levels (50%, 75%, and 100% of failure load)	119
Figure 5-4: Crack development and crack widths (in mm) for 1% and 2% ρ_w 500 mm SCC beams at different load levels (50%, 75%, and 100% of failure load).....	120
Figure 5-5: Crack development and crack widths (in mm) for 1% and 2% ρ_w 500 mm NC beams at different load levels (50%, 75%, and 100% of failure load)	121
Figure 5-6: Crack development and crack widths (in mm) for 1% and 2% ρ_w 363 mm SCC beams at different load levels (50%, 75%, and 100% of failure load).....	122
Figure 5-7: Crack development and crack widths (in mm) for 1% and 2% ρ_w 363 mm NC beams at different load levels (50%, 75%, and 100% of failure load)	123
Figure 5-8: Crack development and crack widths (in mm) for 1% and 2% ρ_w 250 mm SSC beams at different load levels (50%, 75%, and 100% of failure load)	124
Figure 5-9: Crack development and crack widths (in mm) for 1% and 2% ρ_w 250 mm NC beams at different load levels (50%, 75%, and 100% of failure load)	125
Figure 5-10: Crack development and crack widths (in mm) for 1% and 2% ρ_w 150 mm depth SCC beams at different load levels (50%, 75%, and 100% of failure load)	126
Figure 5-11: Crack development and crack widths (in mm) for 1% and 2% ρ_w 150 mm depth SCC beams at different load levels (50%, 75%, and 100% of failure load)	127
Figure 5-12: Normalized ultimate shear load (V_{nz}) for both SCC and NC beams	128
Figure 5-13: Effect of beam depth on normalized shear stress (v_{nz}) for both SCC and NC beams	128
Figure 5-14: Percentage ratio (r_L) of normalized ultimate shear loads ($r_L = 100 * U_{NZ-NC} / U_{NZ-SCC}$)	129
Figure 5-15: Ultimate shear strength (V_u)- experiments and Code predictions (SCC beams with 1% ρ_w).....	129
Figure 5-16: Ultimate shear strength (V_u)- experiments and Code predictions (NC beams with 1% ρ_w).....	130
Figure 5-17: Ultimate shear strength (V_u) - experiments and Code predictions (SCC beams with 2% ρ_w).....	130

Figure 5-18: Ultimate shear strength (V_u) - experiments and Code predictions (NC beams with 2% ρ_w).....	131
Figure 5-19: Calculated / experimental crack widths for NC in both 1% and 2% ρ_w	131
Figure 5-20: Calculated / experimental crack widths for SCC in both 1% and 2% ρ_w	132
Figure 5-21: β as a function of beam depth and ρ_w	132
Figure 5-22: Comparison of experimental and Code-based load-mid span deflection responses (1NC150).....	133
Figure 5-23: Comparison of experimental and Code-based load-mid span deflection responses (2NC150).....	133
Figure 5-24: Comparison of experimental and Code-based load-mid span deflection responses (1SCC150).....	134
Figure 5-25: Comparison of experimental and Code-based load-mid span deflection responses (2SCC150).....	134
Figure 5-26: Comparison of experimental and Code-based load-mid span deflection responses (1NC250).....	135
Figure 5-27: Comparison of experimental and Code-based load-mid span deflection responses (2NC250).....	135
Figure 5-28: Comparison of experimental and Code-based load-mid span deflection responses (1SCC250).....	136
Figure 5-29: Comparison of experimental and Code-based load-mid span deflection responses (2SCC250).....	136
Figure 5-30: Comparison of experimental and Code-based load-mid span deflection responses (1NC363).....	137
Figure 5-31: Comparison of experimental and Code-based load-mid span deflection responses (2NC363).....	137
Figure 5-32: Comparison of experimental and Code-based load-mid span deflection responses (1SCC363).....	138
Figure 5-33: Comparison of experimental and Code-based load-mid span deflection responses (2SCC363).....	138
Figure 5-34: Comparison of experimental and Code-based load-mid span deflection responses (1NC500).....	139

Figure 5-35: Comparison of experimental and Code-based load-mid span deflection responses (2NC500).....	139
Figure 5-36: Comparison of experimental and Code-based load-mid span deflection responses (1SCC500).....	140
Figure 5-37: Comparison of experimental and Code-based load-mid span deflection responses (2SCC500).....	140
Figure 5-38: Comparison of experimental and Code-based load-mid span deflection responses (1NC750).....	141
Figure 5-39: Comparison of experimental and Code-based load-mid span deflection responses (2NC750).....	141
Figure 5-40: Comparison of experimental and Code-based load-mid span deflection responses (1SCC750).....	142
Figure 5-41: Comparison of experimental and Code-based load-mid span deflection responses (2SCC750).....	142
Figure 5-42: Post cracking shear resistance of SCC/NC beams.....	143
Figure 5-43: Post cracking shear ductility of SCC/NC beams.....	143
Figure 5-44: Ratio of Code to experimental first cracking load for NC in both 1% and 2% ρ_w .	144
Figure 5-45: Ratio of Code to experimental first cracking load for NC in both 1% and 2% ρ_w .	144
Figure 6-1: SCC beam during casting.....	153
Figure 6-2: Typical pull out failure.....	153
Figure 6-3: Development of bond stress with age for the SCC beam	154
Figure 6-4: Development of bond stress with age for the NC beam	154
Figure 6-5: Development of compressive strength with age for both SCC and NC beams	155
Figure 6-6: Normalized bond stress with age for both SCC and NC beams.....	155
Figure 6-7: Typical bond stress-free end displacement relationship	156
Figure 6-8: Bond stress-free end slip relationship at 28 days for SCC and NC beams at different bar elevations	156
Figure 6-9: Bond stress-free end slip relationship at 14 days for SCC and NC beams at different bar elevations	157
Figure 6-10: Bond stress-free end slip relationship at 7 days for SCC and NC beams at different bar elevations	157

Figure 6-11: Normalized bond stress in SCC and NC beams (top bars)	158
Figure 6-12: Normalized bond stress in SCC and NC beams (middle bars)	158
Figure 6-13: Normalized bond stress in SCC and NC beams (bottom bars)	159
Figure 6-14: Top bar factor at various free end slip for SCC and NC (28 days tested age)	159
Figure 6-15: Top bar factor at various free end slip for SCC and NC (14 days tested age)	160
Figure 6-16: Top bar factor at various free end slip for SCC and NC (7 days tested age)	160
Figure 7-1: Corrosion performance, crack pattern and widths in non-epoxy coated stirrups SCC-1 beam	186
Figure 7-2: Corrosion performance, crack pattern and widths in non-epoxy coated stirrups NC-1 beam	187
Figure 7-3: Corrosion performance, crack pattern and widths in epoxy coated stirrups SCC-2 beam	188
Figure 7-4: Corrosion performance, crack pattern and widths in epoxy coated stirrups NC-2 beam	189
Figure 7-5: Current-time measurements for non-epoxy coated stirrup beams in moderate corrosion stage	190
Figure 7-6: Current-time measurements for non-epoxy coated stirrup beams in severe corrosion stage.....	190
Figure 7-7: Average cross section half-cell reading at each point along SCC-N beam length ...	191
Figure 7-8: Average cross section half-cell reading at each point along NC-N beam length	191
Figure 7-9: Average cross section half-cell reading at each point along SCC-E beam length....	192
Figure 7-10: Average cross section half-cell reading at each point along NC-E beam length....	192
Figure 7-11: Chloride content, rebar mass loss, maximum crack width and the reduction of bar diameter along the front external bars of NC-E.....	193
Figure 7-12: Chloride content, rebar mass loss, maximum crack width and the reduction of bar diameter along the front external bars of SCC-E.....	193
Figure 7-13: Chloride content, rebar mass loss, maximum crack width and the reduction of bar diameter along the internal bar of NC-E	194
Figure 7-14: Chloride content, rebar mass loss, maximum crack width and the reduction of bar diameter along the internal bars of SCC-E.....	194

Figure 7-15: Chloride content, rebar mass loss, maximum crack width and the reduction of bar diameter along the back external bars of NC-E	195
Figure 7-16: Chloride content, rebar mass loss, maximum crack width and the reduction of bar diameter along the back external bar of SCC-E	195
Figure 7-17: Comparison of theoretical and actual mass loss in all tested beams	196
Figure 7-18: Corrosion performance in the small concrete cylinders	196
Figure 7-19: Failure of NC-0 beam	197
Figure 7-20: Failure of SCC-0 beam	197
Figure 7-21: Failure of NC-1 beam	198
Figure 7-22: Failure of SCC-1 beam	198
Figure 7-23: Failure of NC-2 beam	199
Figure 7-24: Failure of SCC-2 beam	199
Figure 7-25: SCC-2 Rebar slippage.....	200
Figure 7-26: Reduction of mass loss and bar diameter in NC-2	200
Figure 7-27: Reduction of mass loss and bar diameter in SCC-2	201
Figure 7-28: NC-0 crack development and crack widths at different load levels (50, 75, and 100% of failure load).....	201
Figure 7-29: SCC crack development and crack widths at different load levels (50, 75, and 100% of failure load)	202
Figure 7-30: NC-1 crack development and crack widths at different load levels (50, 75, and 100% of failure load) of uncorroded beam.....	202
Figure 7-31: SCC-1 crack development and crack widths at different load levels (50, 75, and 100% of failure load) of uncorroded beam.....	203
Figure 7-32: NC-2 crack development and crack widths at different load levels (50, 75, and 100% of failure load) of uncorroded beam.....	203
Figure 7-33: SCC-2 crack development and crack widths at different load levels (50, 75, and 100% of failure load) of uncorroded beam.....	204
Figure 7-34: Comparison of experimental and Code-based load-mid span deflection response for NC-0	204
Figure 7-35: Comparison of experimental and Code-based load-mid span deflection response for SCC-0	205

Figure 7-36: Comparison of experimental and Code-based load-mid span deflection response for NC-1	205
Figure 7-37: Comparison of experimental and Code-based load-mid span deflection response for SCC-1	206
Figure 7-38: Comparison of experimental and Code-based load-mid span deflection response for NC-2	206
Figure 7-39: Comparison of experimental and Code-based load-mid span deflection response for SCC-2	207

Appendix A Figures

A 1: Experimental load-free end displacement (top bar embedded in the NC beam at 28 days tested age) [Bond stress (MPa) = 0.106 Load (kN)]	230
A 2: Experimental load-free end displacement (middle bar embedded in the NC beam at 28 days tested age) [Bond stress (MPa) = 0.106 Load (kN)]	230
A 3: Experimental load-free end displacement (bottom bar embedded in the NC beam at 28 days tested age) [Bond stress (MPa) = 0.106 Load (kN)]	231
A 4: Experimental load-free end displacement (top bar embedded in the SCC beam at 28 days tested age) [Bond stress (MPa) = 0.106 Load (kN)]	231
A 5: Experimental load-free end displacement (middle bar embedded in the SCC beam at 28 days tested age) [Bond stress (MPa) = 0.106 Load (kN)]	232
A 6: Experimental load-free end displacement (bottom bar embedded in the SCC beam at 28 days tested age) [Bond stress (MPa) = 0.106 Load (kN)]	232
A 7: Experimental load-free end displacement (top bar embedded in the NC beam at 14 days tested age) [Bond stress (MPa) = 0.106 Load (kN)]	233
A 8: Experimental load-free end displacement (middle bar embedded in the NC beam at 14 days tested age) [Bond stress (MPa) = 0.106 Load (kN)]	233
A 9: Experimental load-free end displacement (bottom bar embedded in the NC beam at 14 days tested age) [Bond stress (MPa) = 0.106 Load (kN)]	234

A 10: Experimental load-free end displacement (top bar embedded in the SCC beam at 14 days tested age) [Bond stress (MPa) = 0.106 Load (kN)].....	234
A 11: Experimental load-free end displacement (middle bar embedded in the SCC beam at 14 days tested age) [Bond stress (MPa) = 0.106 Load (kN)].....	235
A 12: Experimental load-free end displacement (bottom bar embedded in the SCC beam at 14 days tested age) [Bond stress (MPa) = 0.106 Load (kN)].....	235
A 13: Experimental load-free end displacement (top bar embedded in the NC beam at 7 days tested age) [Bond stress (MPa) = 0.106 Load (kN)].....	236
A 14: Experimental load-free end displacement (middle bar embedded in the NC beam at 7 days tested age) [Bond stress (MPa) = 0.106 Load (kN)].....	236
A 15: Experimental load-free end displacement (bottom bar embedded in the NC beam at 7 days tested age) [Bond stress (MPa) = 0.106 Load (kN)].....	237
A 16: Experimental load-free end displacement (top bar embedded in the SCC beam at 7 days tested age) [Bond stress (MPa) = 0.106 Load (kN)].....	237
A 17: Experimental load-free end displacement (middle bar embedded in the SCC beam at 7 days tested age) [Bond stress (MPa) = 0.106 Load (kN)].....	238
A 18: Experimental load-free end displacement (bottom bar embedded in the SCC beam at 7 days tested age) [Bond stress (MPa) = 0.106 Load (kN)].....	238
A 19: Experimental load-free end displacement (top bar embedded in the NC beam at 3 days tested age) [Bond stress (MPa) = 0.106 Load (kN)].....	239
A 20: Experimental load-free end displacement (middle bar embedded in the NC beam at 3 days tested age) [Bond stress (MPa) = 0.106 Load (kN)].....	239
A 21: Experimental load-free end displacement (bottom bar embedded in the NC beam at 3 days tested age) [Bond stress (MPa) = 0.106 Load (kN)].....	240
A 22: Experimental load-free end displacement (top bar embedded in the SCC beam at 3 days tested age) [Bond stress (MPa) = 0.106 Load (kN)].....	240
A 23: Experimental load-free end displacement (middle bar embedded in the SCC beam at 3 days tested age) [Bond stress (MPa) = 0.106 Load (kN)].....	241
A 24: Experimental load-free end displacement (bottom bar embedded in the SCC beam at 3 days tested age) [Bond stress (MPa) = 0.106 Load (kN)].....	241

A 25: Experimental load-free end displacement (top bar embedded in the NC beam at 1 day tested age) [Bond stress (MPa) = 0.106 Load (kN)].....	242
A 26: Experimental load-free end displacement (middle bar embedded in the NC beam at 1 day tested age) [Bond stress (MPa) = 0.106 Load (kN)].....	242
A 27: Experimental load-free end displacement (bottom bar embedded in the NC beam at 1 day tested age) [Bond stress (MPa) = 0.106 Load (kN)].....	243
A 28: Experimental load-free end displacement (top bar embedded in the SCC beam at 1 day tested age) [Bond stress (MPa) = 0.106 Load (kN)].....	243
A 29: Experimental load-free end displacement (middle bar embedded in the SCC beam at 1 day tested age) [Bond stress (MPa) = 0.106 Load (kN)].....	244
A 30: Experimental load-free end displacement (bottom bar embedded in the SCC beam at 1 day tested age) [Bond stress (MPa) = 0.106 Load (kN)].....	244

List of Tables

Table 4-1: Mixture proportions for SCC and NC mixtures	78
Table 4-2: Physical and chemical analysis of cement	78
Table 4-3: Physical and chemical analysis of slag	79
Table 4-4: Sieve analysis of coarse and fine aggregate	79
Table 5-1: Cracking loads and crack characteristics of experimental SCC/NC beams	112
Table 5-2: Shear resistance of SCC/NC beams from experiments and Code-based predictions	113
Table 5-3: Calculated and experimental crack widths for SCC and NC beams	114
Table 5-4: Strength-deflection results of SCC and NC beams with 1% and 2% ρ_w	115
Table 5-5: Central deflection and longitudinal steel strain development in SCC/NC beams	116
Table 6-1: Measured and predicted bond stress for SCC and NC beams at different heights and ages	152
Table 7-1: Half-cell potential readings at 25 points along SCC-E beam length/ perimeter	176
Table 7-2: Half-cell potential readings at 25 points along NC-E beam length/ perimeter	177
Table 7-3: Half-cell potential readings at 25 points along SCC-N beam length/ perimeter	178
Table 7-4: Half-cell potential readings at 25 points along NC-N beam length/ perimeter	179
Table 7-5: Chloride content, rebar mass loss, maximum crack width and the reduction of bar diameter at each point along NC-E beam length/perimeter	180
Table 7-6: Chloride content, rebar mass loss, maximum crack width and the reduction of bar diameter at each point along SCC-E beam length/perimeter	181
Table 7-7: Chloride content, rebar mass loss, maximum crack width and the reduction of bar diameter at each point along NC-N beam length/perimeter	182
Table 7-8: Chloride content, rebar mass loss, maximum crack width and the reduction of bar diameter at each point along SCC-N beam length/perimeter	183
Table 7-9: Ultimate failure load and mode of failure for each level of corrosion	184
Table 7-10: Comparison between calculated and experimental crack widths for uncorroded SCC and NC beams	185
Table 7-11: Strength-deflection results of SCC and NC beams in different corrosion stages	185

List of Symbols

τ_1^{Ds}	The maximum bond stress that the deformed bar can resist without occurring a transverse microcracks
τ_1^{ps}	The maximum bond stress that the plain bar can resist without slipping
$(C_b+K_{tr})/d_b$	The contribution of confining reinforcement across potential splitting plan
f_y	The flexure stress
Δ	The total deflection due to flexure and shear
ΔM	The change of the beam's bending moment over ΔX
ΔT	The change of the tension force over ΔX
ΔX	The width of a specific part of the beam
$1/r$	The flexural curvature of the beam
a/d	The shear span-to-depth ratio
a/h	The span-to-total depth ratio
A_b	The area of the tested pullout bar
a_g	The maximum size of aggregate in concrete.
A_g	The gross area of the section
A_s	The steel reinforcing area
A_{sv}	The cross-section area of shear reinforcement
A_v	The cross-sectional area of the stirrups
b_w	The thickness of the beam web
CSE	The copper-copper sulfate electrode
d	The beam's effective depth
d_b	The nominal diameter of the rebar
d_c	The distance from the extreme tension fiber to the centre of the reinforcing bar located closest to it
d_v	The effective shear depth which can be taken as the greater of $0.9d$ or $0.72h$
E_c	The modulus of elasticity of concrete
E_e	The effective elastic modulus (Euro Code)
E_s	The modulus of elasticity of non-prestressed reinforcement

F	Faraday's constant which is the amount of electrical charge in one mole of electron ($F= 96487$).
FBECR	Fusion-bonded epoxy-coating reinforcement
f_c	The concrete compressive strength
f_{cf}	The characteristic flexural tensile strength of the concrete (Australian Standard)
f_{ck}	The characteristic compressive cylinder strength of the concrete at 28 days
f_{ct}	The concrete tensile strength
f_{ctm}	The mean value of axial tensile strength of concrete
f_s	The stress in the longitudinal reinforcement
f_{yv}	The yield strength of shear reinforcement
G	The shear modulus
h	The height of the section
HPC	High-performance concrete
HRWR	High range water reducers
HWC	High workability concrete
i	The current passed (Amperes)
I	The moment of inertia
I_c	The moment of inertia of the cracked section (Euro Code)
I_{cr}	The moment of inertia of cracked section transformed to concrete (ACI)
I_e	The effective moment of inertia of the beam
I_g	The moment of inertia of gross concrete section about centroidal axis (ACI)
I_u	The moment of inertia of the un-cracked section (Euro Code)
jd	The beam's lever arm and is approximately equal $0.875 d$
L	The effective beam span
l	The embedded length of the pullout rebar
l_d	The developmental length of the deformed bar
LVDT	Linear Variable Displacement Transducers
M	The applied bending moment at specific cross section
M	The atomic weight (for iron $M = 55.847$ g/mol)
M_a	The maximum moment in member at load stage at which deflection is computed
M_{cr}	The cracking moment

M_f	The factor bending moment at a specific section
NA	The neutral axis of the beam
NaCl	Sodium chloride
NC	Normal concrete
N_u	The axial compression applied on the member
\emptyset	The strength reduction factor
P	The applied load
p^*	The bearing stresses in the concrete produced by the bar ribs
P_d	The first diagonal cracking load
PFA	Pulverized fly ash
P_{nz}	The normalized ultimate failure load
P_u	The ultimate failure load
Q	The first moment of area about specific neutral axis
RC	Reinforced concrete
r_L	The percentage ratio of normalized ultimate shear load of NC beam to that of SCC beam
SCC	Self consolidating concrete
SCM	Supplementary cementing materials
S_v	The stirrups spacing
S_z	The crack spacing parameter dependent on crack control characteristics of longitudinal reinforcement
t	The time passed (sec)
T	The tension force acting on a specific section
τ	The bond stress
u	The steel-concrete bond stress
U_{bot}/U_{top}	The average bond stress ratio of bottom-to-top bars
U_{bottom}	The bond stress of the bottom bars
u_{nn}	The normalized bond stress of NC
u_{ns}	The normalized bond stress of SCC
u_{nz}	The normalized bond stress.
U_{top}	The bond stress of the top bars

V	The applied shear force at specific cross section
v	The shear stress
V_a	The portion of the shear force carried by the vertical component of the aggregate interlock
V_c	The total shear force carried by the concrete
V_{cz}	The portion of the shear force carried by the uncracked concrete in the compression zone
V_d	The portion of the shear force carried by the longitudinal flexural reinforcement
V_f	The factor shear force at a specific section
VMA	Viscosity modifying admixtures
V_n	The nominal shear resistance = $V_c + V_s$
V_{nz}	The normalized shear load
v_{nz}	The normalized shear stress
V_{nz-NC}	The normalized ultimate shear load of NC beam
V_{nz-SCC}	The normalized ultimate shear load of SCC beam
V_s	The portion of the shear force carried by stirrups
V_u	The ultimate shear force
w	The crack width in mm
w/c	The water/cement ratio
w/cm	The water/cementitious material ratios
x_u	The distance from centroidal axis of the section to the extreme tension fiber
y_t	The distance from centroidal axis of the gross section to the extreme tension fiber
Z	The section modulus of the uncracked section - The ion charge (2 moles of electrons)
δ_d	The first diagonal crack deflection
δ_f	The deflection at failure load
δ_u	The deflection at peak (failure) load
ϵ_x	The longitudinal strain at mid-depth of the member due to factored loads
θ	The angle of the inclined crack
λ	The density of the concrete
ρ_w	Longitudinal reinforcing steel ratio = $A_s / (b_w d)$

ϕ	The creep coefficient at relevant loading time and duration
ϕ	The strength reduction factor, taken equal to 0.85 for shear
ψ_e	The bar coating factor (for calculating the bond stress)
ψ_s	The bar diameter factor (for calculating the bond stress)
ψ_t	The location factor (for calculating the bond stress)

1 Introduction

1.1 Background

The problem of casting concrete in heavily reinforced sections has been a major topic of interest over the years. Providing proper consolidation and placement of concrete in such heavy reinforced sections requires adequate compaction by either internal or external mechanical vibrators operated by skilled workers. However, excessive vibration can lead to segregation, bleeding, and blockage of concrete particles when passing through narrow spaces. Therefore, self-consolidating concrete (SCC) is used to reduce the intensive labor demand for vibration whilst eliminating the problems which arise from bleeding and segregation.

Self consolidating concrete is one of the latest innovations in concrete technology, it is a highly flowable, high-performance concrete that spreads readily under its own weight without the use of vibrators. It also achieves good consolidation without segregation, even in a very congested structural member with a large amount of steel reinforcement (Avery 2004; Bouzoubaâ and Lachemi 2001; Lachemi et al. 2003, 2004; Patel et al. 2004; Khayat 1999; Khayat 1998; Khayat et al. 2001; Khayat et al. 2004). In addition, SCC facilitates pouring concrete from higher free falls. This was seen during the construction of the Akashi-Kaikyo suspension bridge in Japan in 1998 when the concrete free fall was more than 3 meters in depth, accomplished without segregation (Avery 2004).

The production of SCC is normally achieved by increasing the quantity of fines in the mixture by incorporating mineral admixtures (such as fly ash, ground granulated blast furnace slag, volcanic ash, cement kiln dust etc.) and/or viscosity modifying admixtures (VMA) (Bouzoubaâ and Lachemi 2001; Lachemi et al. 2003, 2004; Patel et al. 2004; Hossain and Lachemi 2004; Khayat 1999; Khayat et al. 2004). In addition, the coarse aggregate content in a SCC mixture is usually less than in normal concrete (NC).

Somewhat problematic, however, is the lack of information regarding the in-situ properties and the structural performance of SCC members which has prohibited the widespread use of this material by designers/engineers in practical applications [Khayat 2001 and Domone 2007]. In particular, there are concerns among designers/engineers that SCC may not be strong enough at resisting shear because of the presence of a significantly smaller amount of coarse aggregates,

compared to NC. This, of course, can lead to the formation of smooth fractured surfaces and subsequent development of weak aggregate interlock mechanism (Lachemi et al. 2005).

Taylor (1974) investigated reinforced normal concrete beams without shear reinforcement, and reported that the shear strength is derived from the contributions of a compression shear zone ranging between 20% and 40 %, an aggregate interlock mechanism ranging between 35% and 50 %, and a dowel action of longitudinal reinforcement ranging between 15% and 25 %. Hence, a major component of the shear transfer in the fractured interface arises from the friction forces that develop across the diagonal shear cracks due to “aggregate interlock” which provides resistance against slip.

The aggregate interlock is greatly influenced by the beam size. As the depth of the beam increases, the crack widths at points above the main longitudinal reinforcement tend to increase. This leads to a reduction in aggregate interlock across the crack, resulting in the reduction of shear stress (Collins 1996; Bazant and Kim 1984 and 1991; Walraven and Lehwalter 1994). Also, the aggregate interlock is influenced by the longitudinal reinforcement ratio and this component of shear strength is more significant if the cracks are narrow. Thus, a higher percentage of longitudinal reinforcing steel (which reduces the shear crack width) would allow the concrete to resist more shears (Bentz 2005 and Tompos and Frosch 2002].

The substantial difference in the rheology of the cement paste matrix in SCC compared to NC relates to the average aggregate diameter and aggregate spacing (Bui et al. 2002; Lachemi et al. 2007), which also affects SCC’s shear resistance. Lack of research studies in this area warrants experimental investigations of full-scale SCC beams that are subjected to shear failure. This should include a performance study of Code-based procedures in predicting strength, and deformability and cracking characteristics taking into consideration various SCC mix parameters such as aggregate size, aggregate volume, etc. and beam parameters such as size, longitudinal reinforcement ratio, etc. (Lachemi et al. 2005; Yurugi et al. 1993; Sonebi et al. 2003, Grunewald and Walraven 2001).

Segregation of aggregate is one of the major concrete casting problems. Segregation causes settlement of the unhydrated cement grains in the fresh concrete stage. As the downward movement of the concrete occurs during settlement, the contact between the lower portion of the steel bar and the concrete loosens, which reduces the bond strength.

Surface cracking above the top reinforcing bar is another factor that results from surface settlement. Surface cracking reduces the interface area between the bar rib and the concrete which contributes to reduced the bond strength (Dakhil et al. 1975).

In addition, settlement of relatively big concrete particles in the fresh concrete state forces some of the free water to move upward causing bleeding. This bleeding water either reaches the surface of the concrete or is trapped in upper concrete layers, which affects the mechanical properties of the concrete. Moreover, bleeding water may accumulate below the horizontal reinforcement and cause porous concrete area which results in reduced bond strength (Hoshino 1988).

A greater amount of bleeding, segregation, and surface settlement can be expected as the specimens height increases because of the increase in the quantity of fresh concrete contributing to such bleeding, segregation, and settlement (Hoshino 1989). Therefore, one can conclude that the top bars in a beam will have poorer bond characteristics than the bottom bars, since the water and air gain will be greater under top bars. The ACI and CSA codes recognizes this phenomenon by requiring 30% excess development length for top-cast deformed bars.

SCC is sufficiently cohesive to prevent segregation or blockage of aggregates during flowing. The enhanced cohesiveness can ensure better suspension of solid particles in the fresh concrete and, therefore, good deformability and filling capability during the spread of fresh concrete through various obstacles. In addition, bleeding, segregation and surface settlement that results from a high w/c ratio or excessive vibration is not a factor in the application of SCC. Therefore, the application of SCC is expected to increase the concrete mechanical properties and bond strength even in greater depth sections.

Corrosion of steel reinforcement in concrete is considered as one of the major threats to concrete durability. When concrete is subjected to severe environment, the chloride ions can penetrate and diffuse through the body of the concrete and ultimately reach the steel bars and cause corrosion. Concrete that has low permeability and dense microstructure is believed to have high resistivity to some degree, which helps in reducing the rate of corrosion of the embedded reinforcing steel.

Corrosion of steel reinforcement also reduces the beams shear capacity as well as flexural and/or longitudinal bars anchorage capacity. Corrosion of steel reinforcement may occurs along the whole length of the beams or accumulate in a specific area. The concentration of the

corrosion at the beams mid-span subsequently reduces the longitudinal bars diameter at this particular area and decrease the overall beams flexural capacity. Meanwhile the reduction of the longitudinal bar's cross section as a consequence of corrosion reduces the dual action of the longitudinal bars and causes a dropping in the beams shear capacity (more pronounced in beams without web reinforcement). In addition to these factors, the concentration of the corrosion at the beams ends/supports reduces the anchorage capacity of the flexural reinforcing bars and causes anchorage splitting failure before shear or flexural failure (Uomoto et al. 1984; Tachibana et al. 1990; Tachibana 1999). This said, SCC is expected to have dense and less permeable microstructure because of its superior resistance to bleeding and segregation especially in absence of excessive vibration. In addition, the production of SCC involves using a high range water reducer (HRWR), and/or supplementary cementing materials (SCM). A HRWR helps to disperse cement particles in the mixture and reduce overall concrete permeability (Haque and Kayyali 1995; McCurrich 1986), while SCM has been proven to increase the concrete corrosion resistance (Hussain and Rasheeduzzafar 1994; Al-Amoudi et al. 1993; Rasheeduzzafar 1992)

Although the durability of SCC mixtures has been investigated by number of researchers (Khayat 2000; Zhu and Bartos 2003; Persson 2003; Nehdi et al. 2004) and proved to be excellent, the tested samples were always relatively small and the durability properties of those samples may not reflect the in-situ durability and uniformity performance of large SCC beams. The durability of large SCC beams may differ from the small laboratory samples because of the segregation and bleeding effects that are manifested in large concrete elements only. In addition, the quality of concrete below the lower horizontal bars in large concrete beams is weak and porous due to the insufficient compaction and the restraint from the horizontal bars in this area (Park and Paulay 1975). This is likely to occur in full-scale beams rather than small laboratory samples and would definitely affect the concrete durability and the rebar corrosion at this area. Therefore, testing the durability of full-scale SCC/NC beams is essential. Particularly because SCC mixtures are likely to present distinct advantage over NC mixtures in such situations.

A number of researchers (Khayat et al. 1997; Khayat et al. 1999; Sonebi 2003; Zhu 2001) have investigated the uniformity of SCC mixtures in both small and full-scale samples and have confirmed its uniformity. However, their results were mainly based on testing the mechanical properties, and not necessary considering the variation of the durability properties along the length of the element. Therefore, the durability and uniformity of full-scale SCC beams, in terms

of corrosion performance and cracking, is important and requires further investigation. This will alleviate omissions from previous studies and shed light on the affect that the particular location of the corrosion on the beam has on the overall beam strength and mode of failure (as described before).

1.2 Scope and objectives

As mentioned, there are some concerns among designers/engineers that SCC may not be strong enough in resisting shear (due to the weak aggregate interlock resulting from decreasing the volume of coarse aggregate) although it does have more capacity than the normal vibrated concrete in bond strength (because of its superior resist to segregation, bleeding and surface settlement which can affect the quality of the concrete around the reinforcement bar).

Also, because SCC mixtures usually contain an increased amount of finesse and the excess use of SCM, it is expected that SCC mixtures will have denser and less permeable microstructures than would NC. This warrants more corrosion protection to the steel reinforcements.

Meanwhile, the enhanced corrosion protection of SCC mixtures may benefit the beams shear resistance. This is due to the reduction of the longitudinal bar cross sectional area, which results from corrosion, affecting the dowel action and reducing the beam's shear capacity. Therefore an investigation of the shear, bond and rebar corrosion protection of same SCC mixture was done in order to evaluate the performance of that mixture according to the overall bond, shear and corrosion test results. The scope of this investigation was detailed as follows:

- **Investigate the shear strength, cracking behavior and deflection of full-scale beams made with self-consolidating concrete as well as normal concrete.**
 - The performance of SCC/NC beams was evaluated based on the results of crack pattern, crack widths, loads at the first flexure/diagonal cracking, ultimate shear resistance, post-cracking shear resistance/ductility, load-deflection response and failure modes.
- **Investigate and evaluate the performance of Code-based equations in predicting the shear resistance of SCC/NC beams.**

- **Investigate and evaluate the performance of Code-based equations in predicting crack width, first flexural cracking moment/load, as well as to simulate load-deflection response of SCC/NC beams.**
- **Investigate the bond strength of reinforcing bars embedded in full-scale heavy reinforcing beams made with SCC and compare the results with that of NC.**
 - The investigation included evaluating the bond stress-free end slip relationship, the top bar effect and the effect of age on bond stress.
- **Investigate and evaluate the performance of Code-based equations in the prediction of the bond stress of the reinforcing bars embedded in full-scale heavy reinforcing SCC/NC beams.**
- **Investigate the flowability of SCC mixture through a dense reinforcing concrete beam.**
- **Study and test the corrosion performance of steel reinforcement embedded in full-scale SCC beams and compare the results with that in NC beams.**
 - The evaluation of SCC/NC beams corrosion performance included testing the corrosion cracking, corrosion rate, probability of corrosion by half-cell potential tests monitoring, measuring the chloride ion content near the bar surface and measuring the actual mass loss and bar diameter degradation along the length of the embedded reinforcing bars.
- **Validate the use of theoretical estimates by Faraday's law to calculate the mass loss with time during corrosion.**
- **Investigate the corrosion performance in small concrete cylinders made with the same NC/SCC mixtures and other SCC mixtures made with different SCC admixture types.**
 - This was to test the effect of admixture type and the effect of non-vibrated large SCC beams in corrosion inhibition.
- **Study the structural performance and cracking of full-scale corroded reinforced concrete beams (designed to fail in shear) made with SCC as well as NC.**
 - The performance of the corroded SCC/NC beams was evaluated based on the results of crack patterns, crack widths, loads at the first flexure and first diagonal cracks, mid span deflection, ultimate load, and failure modes

- **Investigate and evaluate the performance of Code-based equations in predicting the crack widths and the mid span deflections of corroded SCC/NC beams.**

1.3 Outline of thesis

This thesis is divided into 8 chapters.

Chapter 1 addresses the goals of this specific research program, within an overall strategic research program.

Chapter 2 presents a background on self consolidating concrete including the historical development of SCC, lights on some applications using SCC, design and production of SCC outlining definitions of some major SCC ingredients, and the outstanding fresh and hardened properties of SCC.

Chapter 3 presents some of the latest literature review of the concrete shear strength and the factors influencing the resistance of concrete beams against shear, the mechanism of the concrete-reinforcement bond strength in NC/SCC structural elements and how this bond is affected by some factors, and overview of the durability and corrosion resistance of SCC.

Chapter 4 describes the research experimental work, which is divided into three parts; 1) shear tests 2) corrosion tests 3) bond tests. The description of the experimental work in this chapter includes the concrete mix parameters, the physical, chemical, and mechanical properties of the materials used, the properties of the concrete mixture including the test results of the fresh and hardened concrete, casting of concrete specimens, and description of specimen's preparation and the tests setup.

Chapter 5 summarizes the test results of the shear strength investigation in full-scale SCC/NC reinforced concrete beams made without shear reinforcement.

Chapter 6 presents the results of the bond strength investigation of reinforcing bars embedded in full-scale heavy reinforced SCC/NC concrete elements.

Chapter 7 summarized the test results of the corrosion investigation of SCC/NC in full-scale concrete beams and in small concrete cylinders.

Finally, conclusions are drawn from the investigation, and suitable recommendations for further research are made in **chapter 8**.

2 Background of Self-Consolidating Concrete

2.1 Introduction

The ease of placing, consolidating, and finishing freshly mixed concrete and the degree to which it resists segregation is called workability. Concrete should be workable but the ingredients should not separate during transport and handling.

With an increase in the use of congested reinforced concrete, there is a growing need for highly flowable concrete to ensure proper filling of the formwork. Congested elements restrict the access of vibrators required to adequately consolidate normal concrete. Moreover, excessive vibration can cause undesirable segregation and bleeding in non-flowable concrete. The use of high water content in concrete mixtures increases the flowability of the mixture but also proves to increase segregation and bleeding. In addition, high water content in the concrete mixture contributes to the formation of capillary pores, which will predominate capillary porosity in the matrix leading to less dense structure, less bond between the aggregate and the matrix and weakness of overall concrete strength (Neville 1981). Therefore, the need to find a flowable concrete to improve the in-situ application and to maintain the required concrete quality have become essential in the field of the concrete technology.

Self-compacting or self-consolidating concrete (SCC) is defined as the concrete that is able to flow under its own weight and completely fill the formwork, even in the presence of dense reinforcement, without the need of any vibration, whilst maintaining homogeneity (EFNARC 2002). SCC is the latest innovation in concrete technology; the advent of self-compacting concrete has reduced construction noise which can affect humans physically, psychologically and socially. Noise has numerous undesirable consequences such as interfering with communication, causing fatigue, reducing efficiency, and even damaging hearing.

2.2 History of SCC

Self-consolidating concrete was developed in Japan in the late 1980s to reduce the labor required to properly place concrete. After its development, the technology was quickly accepted and embraced by the Japanese civil community. Several large structures were made using SCC, including the two support anchorages for the Akashi-Kaikyo suspension bridge. The use of SCC on these pours reduced the placement time from 2.5 to 2 years. Also, concrete free fall of more

than 3 meters in depth was accomplished without segregation and without the use of vibration (Avery 2004).

The technology was taken from Japan to Europe in the early '90s by a few of the major international construction material companies. During the next several years, they refined these products in their labs (during which time new material understandings and newer admixtures were evolving). By late 1998, the first of these products was being offered commercially in Europe. The following year, France-based Lafarge, introduced its branded "Agilia" SCC in North America. For a "new" material, it was accepted quickly and used for the supporting columns of a 50-story building in Vancouver.

This building, which is located in a seismic zone, required massive, 16-foot-high columns measuring 8 square feet. The reinforcing steel configuration made vibrating virtually impossible, so the engineers and owners were open to using SCC. They realized an unexpected benefit upon stripping these non-vibrated columns: the surface finish was excellent. Since that project was accomplished in late 1999, the use of ready-mixed SCC has grown quickly in the markets where it is currently being offered (Hall 2004).

The use of SCC concrete has been increasing in the United States in the last 5 years. Currently the technology is being applied to the precast industry. Other segments being targeted are flatwork, columns and wall construction. The applications of SCC are numerous and limited only by the industry's knowledge of it, the ability to produce it and overall acceptance.

2.3 Applications of SCC

Since the development of the prototype of SCC in 1988, the use of SCC in actual structures has gradually increased. Currently, the percentage of self-compacting concrete in annual production of ready mixed concrete in Japan is around 0.1%.

A typical application example of SCC is the two anchorages of the Akashi-Kaikyo Bridge which opened in April 1998. This is a suspension bridge with the longest span in the world (1,991 meters). The volume of the cast concrete in the two anchorages amounted to 290,000 m³. In the final analysis, the use of SCC shortened the anchorage construction period by 20%, from 2.5 to 2 years.

Researchers at the University of Tokyo, Japan, began developing SCC in the late 1980's. By the early 1990's, Japan had developed and used SCC which did not require

vibration to achieve full compaction. More and more applications of SCC in construction have been reported in Japan as shown in Figure 2.1. As of the year 2000, the amount of SCC used for prefabricated products (precast members) and ready-mixed concrete (cast-in-place) in Japan was about 400,000 m³ (Ouchi et al., 2003).

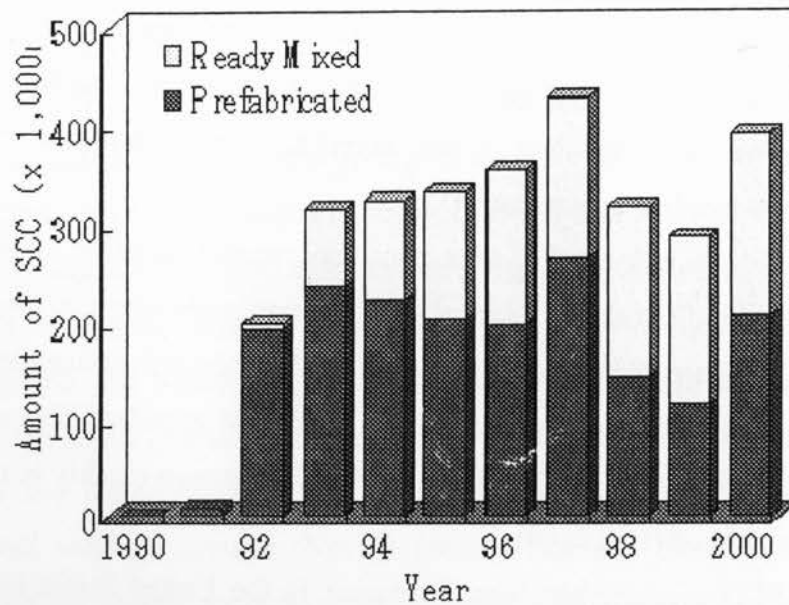


Figure 2.1: Amount of SCC Placement in Japan (Ouchi et al., 2003)

SCC can be used in any concrete application, precast or cast-in-place. Precast concrete products can be categorized as architectural, structural, or utility. In precast applications, SCC has been used and is suitable for use in any structural elements such as double-Tees, inverted-Tees, I-beams, columns, box beams, girders, etc.

Ready-mixed concrete applications can also benefit from the use of SCC mixtures. Areas containing congested reinforcement such as columns, walls and specialty applications like insulated concrete forms are particularly challenging. Highly fluid, stable concrete mixtures permit faster placeability with minimal effort.

Like any other concrete mixture, a SCC mixture must be suitable for the application. For example, a 3.7 m high wall would require different mixture proportions than a 100 mm slab because of an increased risk of segregation and bleeding. The use of SCC instead of a conventional concrete mixture in deep concrete sections would be the appropriate choice because it provides the required stability and minimize the high potential for segregation and bleeding.

2.4 Production of SCC

Self-consolidating concretes are developed by altering the mix design and possibly by the use of mineral admixtures (SCM). First, a high-range water-reducing admixture (super plasticizer) is used to provide the high flowability of the mixture, much like a high slump concrete. Second, the aggregate content is proportioned. The size and shape of the coarse aggregate are very important to the successful manufacturing of SCC. Third, the fluid properties are altered to provide a cohesive mixture that will keep the aggregate and paste together.

Aggregate size, shape, content and gradation play a critical role in the successful development of an SCC. As with any concrete mixture, aggregate size must be limited to that which will pass through rebar openings. In SCC, the top size is often 10 to 20 mm. Rounded aggregate is desirable over angular aggregate because angular aggregate will have a tendency to lock together. The coarse aggregate content will usually drop in an SCC mixture, resulting in a sand to aggregate ratio of 0.50 or greater. The combined aggregate grading is the most important aspect of achieving a good SCC mixture. A poorly graded aggregate source may make it impossible to develop an SCC mixture.

The viscous properties of an SCC mixture are achieved through one of three ways:

- Higher fine content - the fines can be: cement, fly ash, limestone screenings, finely ground glass and granulated ground blast furnace slag
- The addition of viscosity modifying admixtures (VMA) and/or high range water reducer admixtures (HRWRA)
- The addition of a combination of both fine content and VMA or HRWRA

The type of VMA used is generally irrelevant. The major requirement of the VMA is that it produces an economic SCC mixture that meets the hardened and long-term requirements of the concrete. Other admixtures may be used in an SCC mixture once the general mix design has been developed, such as air entraining agents, retarders or hydration control agents, and corrosion inhibiting admixtures (Avery 2004).

2.4.1 High range water reducer

It is important to use HRWRA in the production of SCC since it increase the flowability of the mixture while maintaining reasonable water-to-cement ratio (w/c) (Okamura and Ouchi 1999, Okamura and Ozawa 1995, Ghezal et al. 2002). High range water reducer admixtures (also

known as superplasticizers) are water-soluble organic polymers which have long molecules of high molecular mass. HRWRA can disperse cement grains and reduce particles' friction. The ability of HRWRA to isolate cement particles provides an even distribution of cement particles throughout the cement paste and allows for a greater water exposure to each particle, which increases the early and long term strength. The structure of the hydrated cement paste however remains the same (Neville 1996 and Berke 2002). The proper use of HRWRAs allows SCC to be developed with a reasonably low w/c leading to a higher strength, and more durable concrete (Khayat 1999 and Mindess et al. 2003).

2.4.2 Viscosity modifying admixture

Viscosity modifying admixtures are used to modify the cohesion of SCC without significantly altering its fluidity. Using VMA results in a more stable and cohesive concrete mixture. VMA enhances the viscosity of the mixture which reduces aggregate segregating, bleeding and settlements (Mindess 2003). The incorporation of VMA imbibes some of the free water in the system causing an increase in the viscosity of the cement paste; as a result, less free water is available for bleeding. The enhanced viscosity of the cement paste can improve the capacity of the paste to suspend solid particles, which decreases the rate of segregation (Khayat 1998).

2.4.3 Mineral admixtures

Additional mineral admixtures such as silica fume, ground granulated blast furnace slag, fly ash, and silica fume proved to improve the concrete microstructure and enhances the overall concrete performance (Mehta 1981). The use of these minerals also proved to be effective in the field of SCC technology. The addition of mineral admixtures to a concrete mixture tends to reduce segregation and bleeding tendencies. When very fine particles are added to the concrete (such as mineral admixture particles), the size of the water channels in the concrete paste are greatly reduced. This is because these particles are able to find their way into the empty spaces between two cement grains, and consume part of the mixing water to get their surface wet. This leaves very little free water left in the mixture for bleeding. Also, due to an increase in the number of solid to solid contact points, the cohesiveness of the concrete mixture is greatly improved when mineral admixture is added (Mehta 1981).

2.5 Properties of SCC

2.5.1 Slump flow

Slump flow is one of the most important properties of SCC. According to the ACI Manual of Concrete Practice (2005), slump is defined as “a measure of consistency of freshly mixed concrete, mortar, or stucco equal to the subsidence measured to the nearest 0.25 in (6mm) of the molded specimen immediately after removal of the slump cone”. The flowability of SCC is tested using a slump flow test, which tests the radial spread of a freshly mixed concrete filled in the slump cone after lifting the cone up and allowing the concrete to flow on a horizontal metal surface. The amount of the spread indicates the slump flow properties of SCC. For a typical SCC mixture, the slump flow value is over 24 in (600mm), and the maximum time taken after lifting the cone until the spread stops should be less than 8 seconds (Bonen and Shah 2005).

2.5.2 Passing ability

Passing ability is the ability of the fresh concrete to flow and pass through small openings or tight and congested reinforcement. SCC has superior passing ability and easily passes through confined areas. The maximum size of coarse aggregate used in SCC mixtures is usually small (10-20mm) which helps to increase the SCC passing ability. Also, the mixture of SCC has sufficient viscosity (Khayat 1999) enabling the mixture in motion to easily pass through encountered obstacles (rebar). However, since there is collision and friction between coarse aggregate and obstacles, the coarse aggregate may not be able to pass through the obstacles which can result in a blockage. Therefore it is always important to avoid the blockage by proper selection of the minimum rebar distance, flowability of SCC, paste content, and the maximum size, distribution, and shape of the coarse aggregate.

2.5.3 Segregation resistance

Concrete segregation is considered as one of the major problems in the field of concrete technology. Segregation is the resistance of the mixture to retain its homogeneity. There should be no separation of aggregate from the paste or water from solids, and no tendency for the coarse aggregate to sink downwards under its own weight through the fresh concrete mass.

The result of segregation is basically an increase in the paste's volume at the top surface and settling of the coarse aggregate toward the bottom. Besides the reduction of the concrete

strength at the top part (due to the lack of coarse aggregate content), the redistribution of the coarse aggregate also causes an increase in the differential thermal expansion stresses. This results in top cracks due to greater shrinkage (Bonen and Shah, 2005). Therefore, careful attention must be paid to the selection of the constituent materials as well as the proportioning of SCC mixtures since segregation resistance is one of the keys necessary for SCC success.

2.5.4 Hardened properties and structure performance of SCC

As mentioned, SCC is a new concrete technology that saves labor time and energy required for vibration. Like any other concrete, SCC should satisfy the desired mechanical properties to meet the required concrete performance. The same hardened concrete tests and procedures, used for conventional concrete, are used for SCC. Most of the research studies have been carried out to compare conventional concrete with SCC in terms of mechanical properties (Abrishami 1993 and Persson 2001) and the in-situ properties of full-scale structural elements (Khayat 1996 and Zhu 2001). The results of these studies show that the mechanical properties of SCC do not vary significantly from those of normal, well compacted concrete. Also, most full-scale SCC structure elements do not have obvious variation in strength between any two parts of the element.

While a sufficient number of studies have been carried out to evaluate the hardened properties of SCC, much less is known about the performance of structure elements cast using SCC. The studies performed thus far have mainly focused on compressive strength, elastic modulus of elasticity, and to a lesser extent on creep and shrinkage (Persson 2001). While these properties were found to be similar to those corresponding with traditional vibrated samples, SCC has been found to exhibit a higher early age creep coefficient (Persson 2001), higher bond strength (Chan et al. 2003) and lower concrete shear capacity (especially when the design of SCC mixture involves the reduction of coarse aggregate content) (Lachemi et al. 2005 and Kim et al. 2007).

3 Literature Review

3.1 Shear strength

3.1.1 Stresses in uncracked elastic beams without transverse reinforcement

In the case of a simply supported beam with a uniformly distributed load (as shown in Figure 3.1), the values of both the shear strength (V) and the bending moment (M), at any cross section of the beam, can be obtained directly from the shear force and the bending moment diagram, respectively. Assuming an elastic uncracked beam, the flexure stress (f), at any point of the cross section of the beam, (Fig. 3.1-f) can be calculated as:

$$f = \frac{My}{I} \tag{3.1}$$

Also the shear stress (v), at the same point, can be calculated as:

$$v = \frac{VQ}{Ib} \tag{3.2}$$

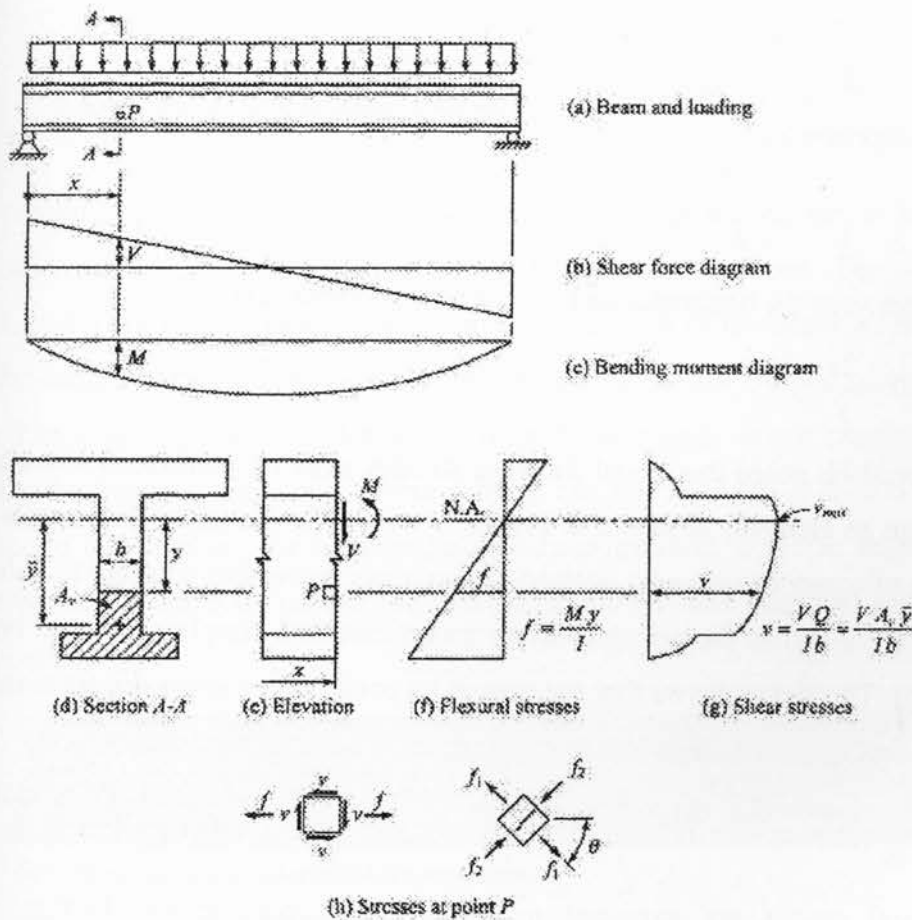


Figure 3.1: Elastic analysis of uncracked beam (Robberts and Marshall 2005)

Where:

V = shear force

Q = first moment of the cross-hatched area A_v about the neutral axis (Fig. 3.1-d)
= $A_v \bar{y}$

I = second moment of area of the total section about the neutral axis

b = width of the section at the depth where the shear stress is calculated

The element P in Figure 3.1-h is subjected to combined normal stresses due to flexure (f) and shearing stresses (v). The largest and smallest normal stresses acting on that element are referred to as *principal stresses*. The principal stresses, and the planes they act on, are found using a Mohr's circle for stress and are as follows:

Maximum (tension):

$$f_1 = \frac{f}{2} + \sqrt{v^2 + \left(\frac{f}{2}\right)^2} \quad (3.3)$$

Minimum (compression):

$$f_2 = \frac{f}{2} - \sqrt{v^2 + \left(\frac{f}{2}\right)^2} \quad (3.4)$$

The angle θ between the horizontal and f_1 can be determined from

$$\tan 2\theta = \frac{2v}{f} \quad (3.5)$$

It should be noted that equal shearing stresses exist on both the horizontal and vertical planes through an element, as shown in Figure 3.1-h. The horizontal shear stresses are important in the design of construction joints, web-to-flange joints, or regions adjacent to holes in beams.

Figure 3.2 shows the principle stress trajectories in a simply supported beam (Park and Paulay, 1975). The figure shows that the maximum compressive stress occurs at mid-span, in the top of the beam, with the stress trajectories forming an arch toward the supports. The maximum tensile stress occurs at mid-span, bottom center of the beam and changes direction closer to the support.

Vertical cracks are expected to form at mid-span, in the bottom of the beam, perpendicular to f_1 . Away from mid-span, a crack initiating at the bottom of the beam will

progress upwards and change direction as v increases and the direction of f_1 changes. At the neutral axis $f = 0$ and the shear stresses will cause cracks to form at 45° to the horizontal as shown in Figure 3.2-b.

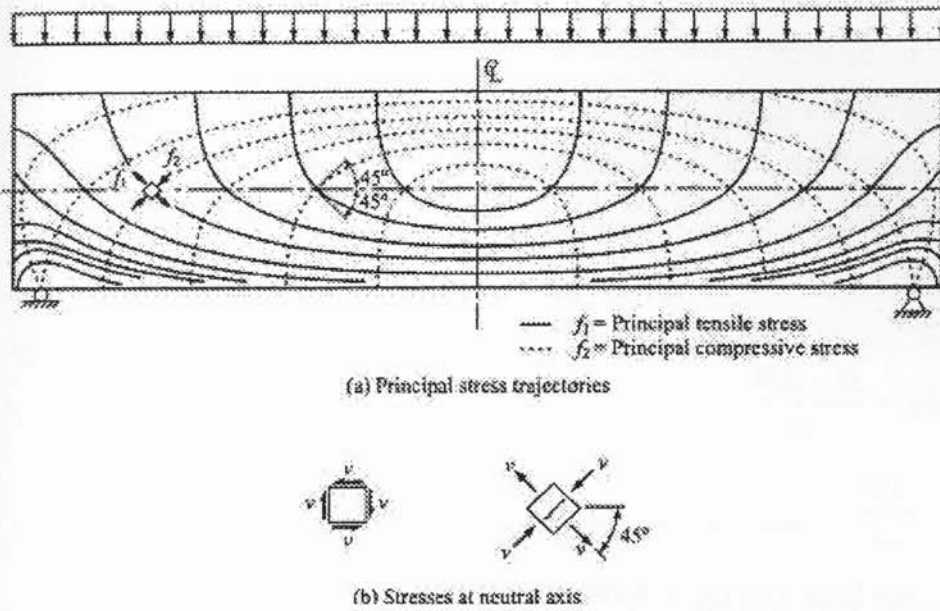


Figure 3.2: Principle stress trajectories (Park and Paulay, 1975)

The cracking pattern in a simply supported tested beam is shown in Figure 3.3 (MacGregor and Bartlett 2000) where two types of cracks can be seen. The vertical cracks occurred first, due to flexural stresses. These start at the bottom of the beam where the flexural stresses are the largest. The inclined cracks at the ends of the beam are due to combined shear and flexure. These are commonly referred to as *inclined cracks*, *shear cracks*, or *diagonal tension cracks*. Such cracks must exist before a beam can fail in shear. It should be noted that once the concrete has cracked, the assumption of a homogeneous isotropic material does not apply. However, it will correctly predict the first crack and remains useful to explain cracking observed in beams.

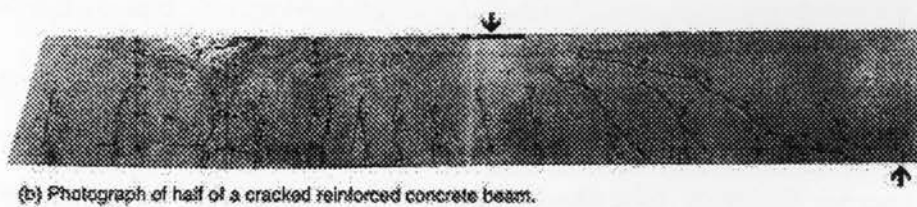


Figure 3.3: Cracking pattern in a simply supported test beam (MacGregor and Bartlett 2000)

3.1.2 Stresses between cracks in beams without transverse reinforcement

As shown in Figure 3.4, the moment has been replaced by the horizontal forces acting on the section. These forces are the resultants of the stresses in the concrete and reinforcement. Two assumptions are made regarding the cracked concrete below the neutral axis:

1. There are no longitudinal tensile stresses.
2. Vertical shear stresses can be transmitted across cracks.

The equilibrium of the section of the beam between such cracks can be obtained from the following equations:

$$T = \frac{M}{jd}$$

And
$$T + \Delta T = \frac{M + \Delta M}{jd}$$

$$\Delta T = \frac{\Delta M}{jd}$$

Where jd is the lever arm and is approximately equal $0.875d$ (Fig. 3.4-b)

Also

$$\Delta M = V\Delta X$$

$$\Delta T = \frac{V\Delta X}{jd}$$

If the shaded portion of Figure 3.4-b is isolated as shown in Figure 3.4-c, the force ΔT must be transferred by horizontal shear stress on the top of the element. The average value of these horizontal shear stresses must be equal to the vertical shear stress and can be calculated as:

$$v = \frac{\Delta T}{b_w \Delta X}$$

or
$$v = \frac{V}{b_w jd} \quad (3.6)$$

Where b_w is the thickness of the beam web

Figure 3.4-d shows the distribution of the vertical shear stress (equal to the horizontal shear stress) across the crack. The shear stresses below the neutral axis remains constant with depth for a constant width b . Note that shear stresses in the uncracked concrete above the neutral

axis are influenced by the flexural stresses, as in the elastic analysis, and can be determined from equation (3.2).

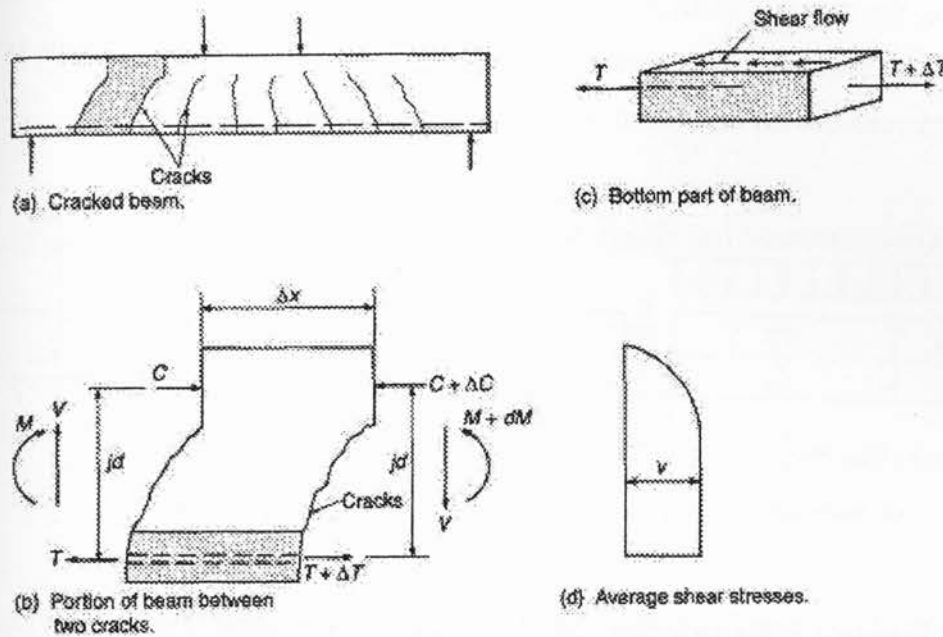


Figure 3.4: Calculation of average shear stress between cracks (MacGregor and Bartlett 2000)

3.1.3 Principle mechanism of shear

As mentioned, $\Delta M = V\Delta X$ (Fig. 3.4). The internal shear resistance of a beam can be found by rewriting this equation as follows (Park and Paulay 1975):

$$V = \frac{d}{dx}(Tjd)$$

or
$$V = \frac{d(T)}{dx}jd + \frac{d(jd)}{dx}T$$

Two extreme cases can be identified. If the lever arm (jd) remains constant as assumed in normal elastic beam theory.

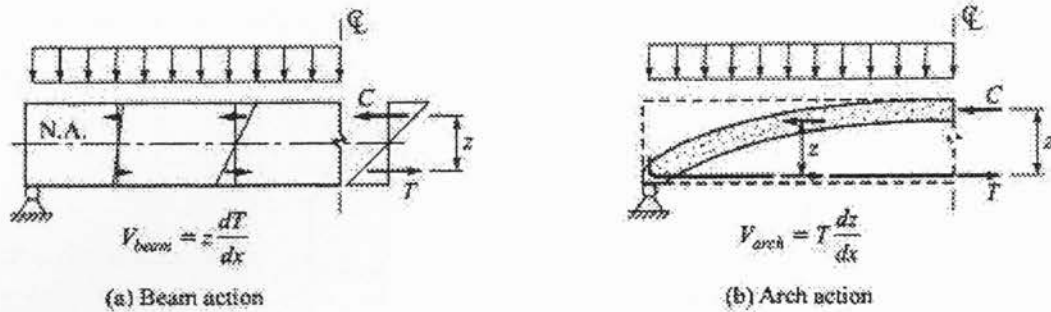
$$\frac{d(jd)}{dx} = 0 \quad \text{and} \quad V = \frac{d(T)}{dx}jd$$

where $d(T)/dx$ is the shear flow across any horizontal plane between the reinforcement and the compression zone as shown in Figure 3.4-c. For beam action to exist, this shear flow must exist.

The other extreme occurs if the shear flow ($d(T)/dx$) equals zero, giving:

$$V = \frac{d(jd)}{dx}T$$

This occurs if the shear flow cannot be transmitted due to the steel being unbonded, or if the transfer of shear flow is prevented by an inclined crack extending from the load to the reactions. In such a case, the shear is transferred by *arch action* rather than beam action, as illustrated in Figure 3.5. In this member, the compression force (C) in the inclined strut and the tension force (T) in the reinforcement are constant over the length of the shear span.



* $z = jd$

Figure 3.5: Beam action and arch action (Robberts and Marshall 2005)

The relative importance of the arch action is directly related to the shear span-to-depth ratio (a/d) (i.e. the distance from the support to the load over the effective depth). Beams without stirrups, with an a/d ratio of less than 2.5 develop inclined cracks and, after a redistribution of internal forces, are able to carry an additional load due in part to arch action (Kong and Evans, 1987; MacGregor and Bartlett 2000)

3.1.4 Mechanism of shear transfer for beams without transverse reinforcement

Consider the free-body diagram of the cracked concrete beams shown in Figure 3.6. The summation of the vertical component of the forces along the diagonal crack is equal to the shear resistance:

$$V_c = V_{cz} + V_d + V_a$$

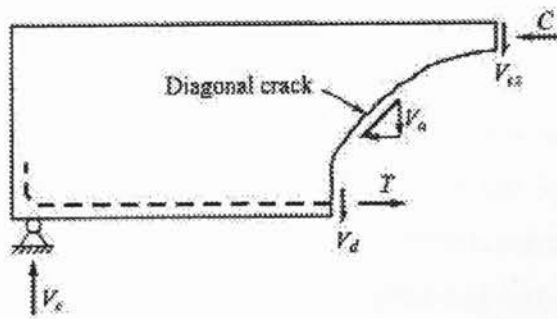


Figure 3.6: Mechanism of shear transfer (Robberts and Marshall 2005)

Where the contributing components are:

V_{cz} = the uncracked concrete in the compression zone

V_d = the dowel force produced by the longitudinal flexural reinforcement

V_a = the vertical component of the aggregate interlock

Taylor (1970), reported tests of beams without web reinforcement in which he found that about a quarter of the shear was transferred by the compression zone, a quarter by dowelling action of the flexural reinforcement, and about half by aggregate interlock along the cracks.

The contribution of each component to the total shear resistance was also determined experimentally by Taylor (1974). He found that for normal test beams, the components of shear resistance were: compression zone shear (20-40%), crack friction (35-50%) and dowel action (15-25%). He also concluded that the dowel force reaches its capacity first, transferring the shear to the aggregate interlock. It is believed that the aggregate interlock is next to fail, transmitting all shears to the concrete in the compression zone which then fails explosively.

The shear stresses in uncracked concrete (the compression zone) are not very important mechanisms for slender members without axial compressions, because the depth of the compression zone is relatively small. On the other hand, at locations of maximum moment for less slender beams, much of the shear is resisted in the compression zones, particularly after significant yielding of the longitudinal reinforcement.

The shear transfer in the interface of the crack is due primarily to “the aggregate interlock”, and hence, caused by those aggregates that protruded from the crack surface and provided resistance against slip. However, as cracks go through the aggregate in lightweight and high-strength concrete they still have the ability to transfer shear by mean of friction. The four

basic parameters involved are the crack interface shear stress, normal stress, crack width, and crack slip. Walraven (1981) made numerous tests and developed a model that considered the probability that aggregate particles, idealized as spheres, would project from the crack interface (Fig. 3.7). As slips develop, the matrix phase deforms plastically, coming into contact with projecting aggregates. The stresses in the contact zones are comprised of a constant pressure (σ) and a constant shear ($\mu\sigma$). The geometry of the crack surface is described statistically in terms of the aggregate content of the mixture and the probability of particles projecting out at different degrees.

Dowel action is not very significant in members without transverse reinforcement, as the maximum shear in a dowel is limited by the tensile strength of the concrete cover supporting the dowel. Nevertheless, it may be significant in members with large amounts of longitudinal reinforcement, particularly when the longitudinal reinforcement is distributed in more than one layer.

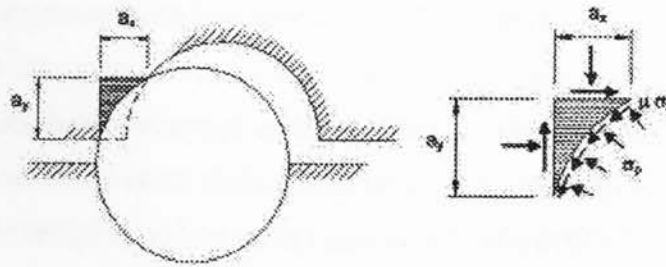


Figure 3.7: Walraven's model of crack friction (Walraven 1981)

3.1.5 Factor influencing shear strength

3.1.5.1 Influence of shear span/effective depth ratio on failure mode

Based on experimental results, Kong and Evans (1987) identified the following failure modes as illustrated in Figure 3.8:

1. Case of $a_v/d > 6$

For $a_v/d > 6$, beams fail in bending rather than shear (Fig. 3.8-b). Beams are designed so that the flexural reinforcement yields before the concrete crushes, ensuring a ductile failure.

2. $6 > a_v/d > 2.5$

Beams with $a_v/d < 6$ tend to fail in shear before their bending capacity is reached. Two failure modes are identified for the range $6 > a_v/d > 2.5$:

High a_v/d ratio: As the load on the beam increases, the flexural crack $a-h$ closest to the support changes direction and propagates toward the loading point (Fig. 3.8-c). This type of crack $a-b-c$ is referred to as a *flexure-shear crack*, or simply a *diagonal crack*. With an increase in load, the crack rapidly extends to e causing the beam to break in two (Fig. 3.8-d). This type of failure is referred to as a *diagonal-tension* failure. The important characteristic of this type of failure is that the failure load is approximately the same as the load at which the diagonal crack forms.

Low a_v/d ratio: The diagonal crack ceases its upward progression (at j) and further cracks develop around the tension reinforcement (Fig. 3.8-e). As the load increases, the diagonal crack opens further while a crack develops along the tension reinforcement ($g-h$). The reinforcement to the left of the crack is forced down, further reducing the bond between the concrete and reinforcement. If hooks are not provided at the ends of the reinforcement, collapse follows almost immediately. With hooks provided, the beam behaves like a tied arch and fails when the concrete around the hook fails. This mode of collapse is called a *shear-tension* failure. The failure load is only slightly greater than the diagonal cracking load.

3. Case of $2.5 > a_v/d > 1$

The diagonal crack often forms independently from a flexural crack. Once developed, the crack will be stable under a sustained load. As the load increases, the crack progresses into the compression zone, eventually causing the compression zone to fail explosively. This type of failure is referred to as a *shear-compression* failure. The failure load can be twice the load at diagonal cracking.

4. Case of $a_v/d < 1$

Beams with $a_v/d < 1$ are generally referred to as deep beams. The diagonal crack initiates approximately $d/3$ from the bottom of the beam and simultaneously propagates towards the support and the loading point. Failure occurs by crushing of the concrete, either at the loading point or at the support. This mode of collapse is called a *deep beam* failure. The failure load is usually several times the diagonal cracking load.

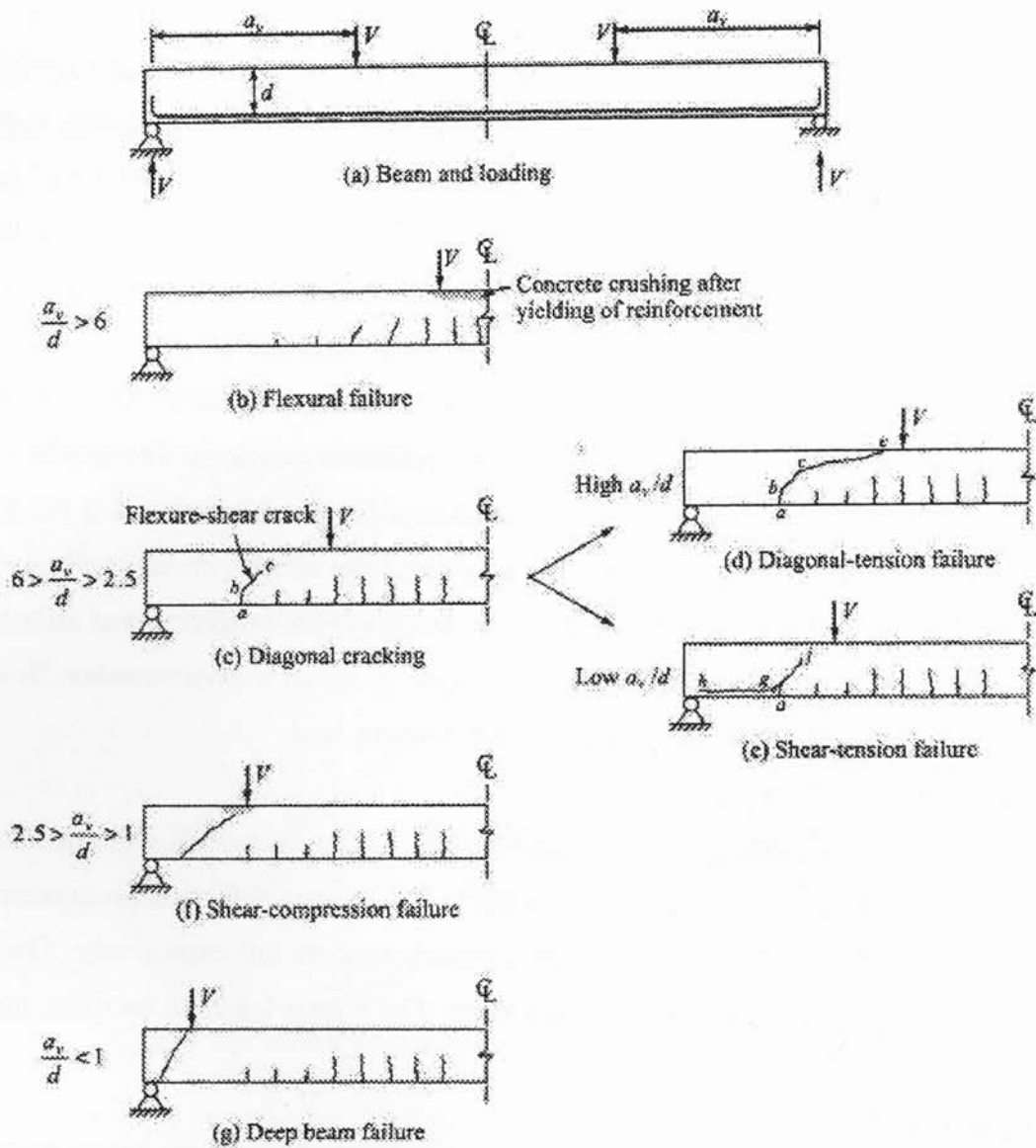


Figure 3.8: Shear failure mode (Kong and Evans, 1987)

Beams without stirrups, with a/d ratio less than 2.5 develop inclined cracks and, after a redistribution of internal forces, are able to carry an additional load due in part to the arch action. Figure 3.9 shows the comparison of experimental shear capacity of beams with different shear-span-to-depth ratios

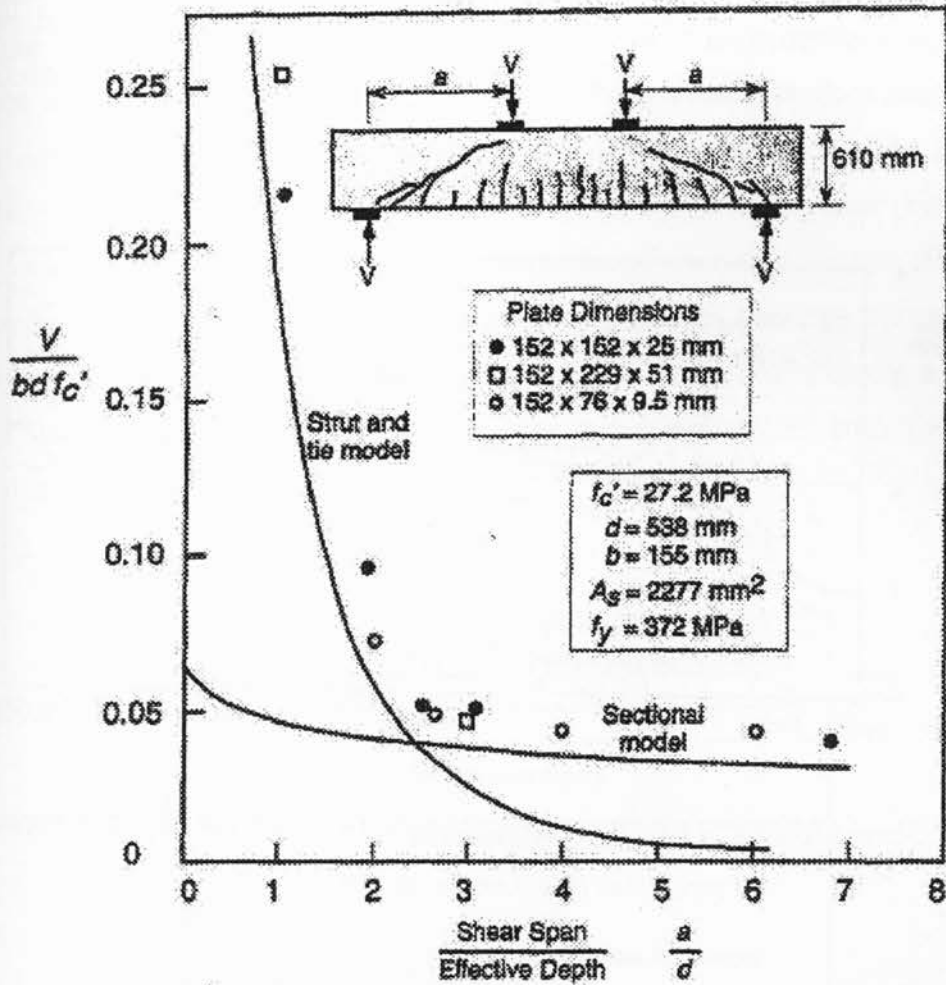


Figure 3.9: Comparison of experimental shear capacity of beams with different shear-span-to-depth ratios with predictions by strut and tie models and sectional models (Collins and Mitchell 1991)

3.1.5.2 Longitudinal reinforcement ratio

Figure 3.10 (MacGregor and Gergely 1977) shows the shear capacity of simply supported beams without stirrups as a function of the steel ratio $\rho_w = A_s/(b_w d)$. When the steel ratio (ρ_w) is small, flexural cracks extend higher into the beam and open wider than would be the case for large values of ρ_w . As a result, inclined cracking occurs earlier leading to a reduction of the shear stress. The practical range of ρ_w for beams developing shear failures is about 0.0075 to 0.025. In this range, the shear strength is approximately:

$$V_{cu} = 0.167 \sqrt{f'_c} b_w d$$

Figure 3.11 presents the shear capacities of simply supported beams without stirrups as a function of the steel ratio, $\rho_w = A_s/b_w d$. As indicated by the horizontal dashed line in, this equation tends to overestimate V_{cu} for beams with small steel percentages (MacGregor and Bartlett 2000)

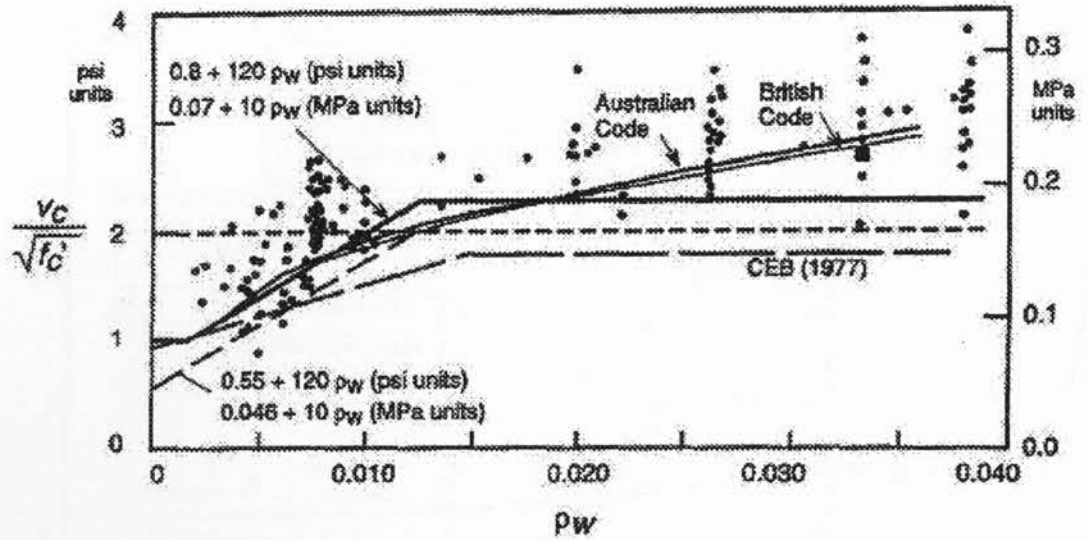


Figure 3.10: Shear capacity of simply-supported beams ($a/d > 2.5$) without stirrups as a function of steel ratio (MacGregor and Gergely 1977)

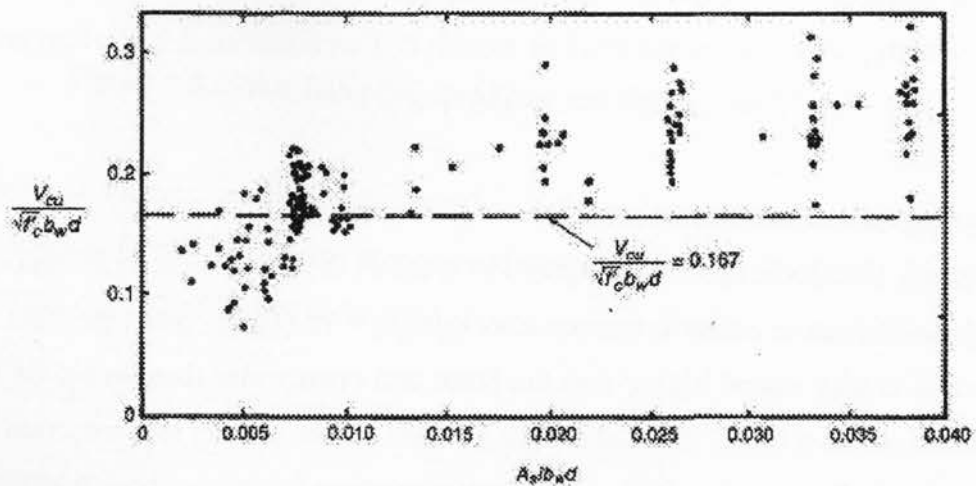


Figure 3.11: Effect of reinforcement ratio on the shear capacity of beams without stirrups (MacGregor and Bartlett 2000)

3.1.5.3 Beam size

As the depth of the beam increases, the crack widths at points above the main reinforcement tend to increase. This leads to a reduction in aggregate interlock across the crack, resulting in earlier inclined cracking and reduction of the shear stress. Collins and Mitchell (1991), Collins et al. (1996) show the well-known size effect in beam shear (Fig. 3.12). The Modified Compression Field Theory does a reasonable job of predicting the size effect, whereas the ACI provisions can be unconservative for large beams. Figure 3.12 shows a strong size effect in beams without web reinforcement, while in beams with web reinforcement a reduction in shear due to size is not believed to occur because the web reinforcement holds the crack faces together so that the aggregate interlock is not lost.

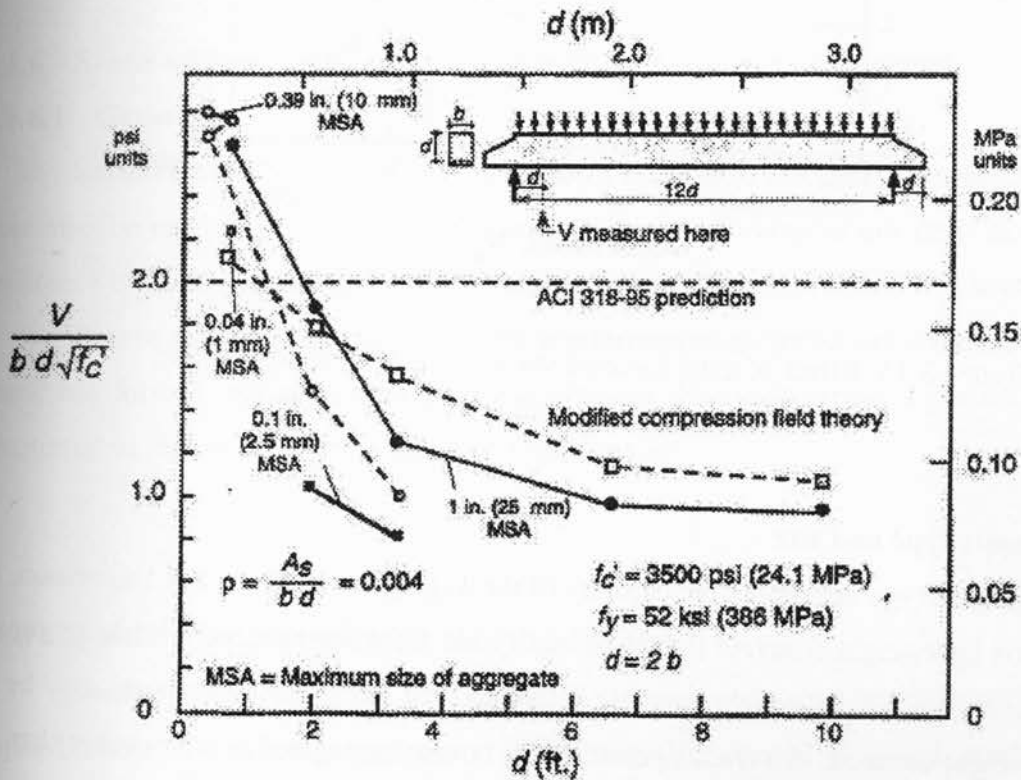


Figure 3.12: Effect of beam size on shear stress at failure at distance d from support (Collins and Mitchell 1991 and Collins et al. 1996)

3.1.5.4 Axial force

Axial tensile forces tend to decrease the inclined cracking load, while axial compressive forces tend to increase the inclined cracking load. This is shown in Figure 3.13 (MacGregor

1992). As the axial compressive force is increased, the onset of flexural cracking is delayed and the flexural cracks do not penetrate as far into the beam. As a result, a larger shear is required to cause principal tensile stresses equal to the tensile strength of the concrete.

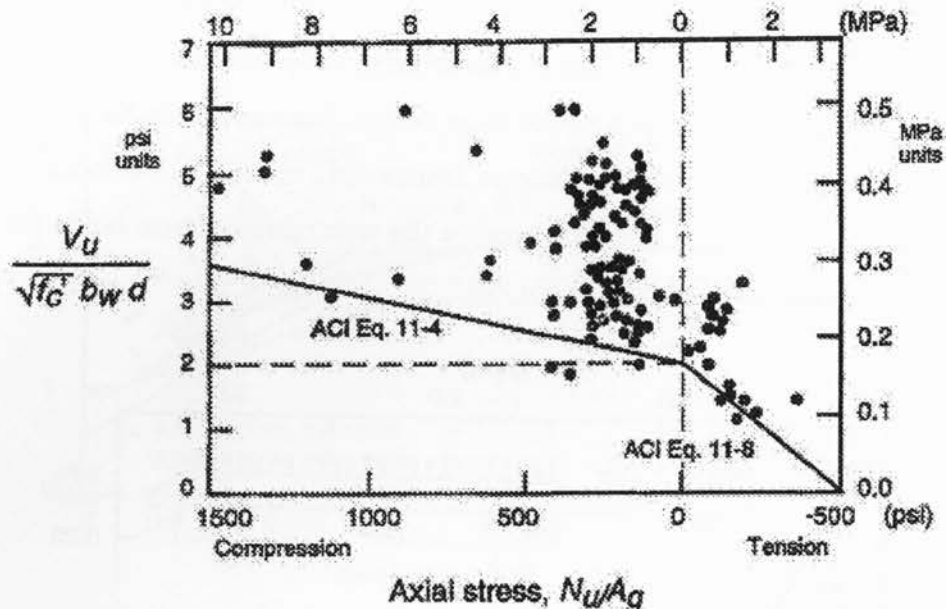


Figure 3.13: Effect of axial force on shear force at inclined cracking
(MacGregor 1992)

3.1.5.5 Aggregate type and size

The aggregate type influences the capacity of the aggregate interlock. For this reason, the shear strength of lightweight concrete (which normally has light and relatively weak aggregate) will be less than that of normal weight concrete, although their compressive strengths may be the same. In lightweight concrete, the cracks penetrate the coarse aggregate (as it is weaker than the mortar) forming smoother surface along the diagonal failure crack. The shear in that case transfer along the diagonal crack by mean of friction which is less than the case of aggregate interlock shear transfer. The shear transfer in high strength concrete is somehow similar to that in lightweight concrete. In high strength concrete the cracks also penetrate the coarse aggregate as it is weaker than the relatively stronger mortar.

The use of large size aggregate is also believed to affect the aggregate interlock (Lachemi 2005), the presence of large size aggregate extends the path of the shear crack around the aggregate and subsequently improves the post cracking shear resistance.

3.1.5.6 Concrete tensile strength

The inclined cracking load is a function of the tensile strength of the concrete. The stress state in the web of the beam involves biaxial principal tension and compression stresses. The flexural cracking which precedes the inclined cracking disrupts the elastic stress field to such an extent that inclined cracking occurs at a principal tensile stress, based on the uncracked section, of roughly a third of f_{ct} (MacGregor and Bartlett 2000).

3.1.6 Shear strength in concrete beams with transverse reinforcement

3.1.6.1 General

Shear reinforcement normally consists of links, also referred to as stirrups. Bent-up bars may also be used in combination with links. Shear reinforcement not only increases the shear resistance of the beam, but also the ductility as it reduces the probability of a brittle failure.

Before diagonal cracking, the shear reinforcement is almost stress free. Once the diagonal crack has formed, the shear reinforcement crossing the crack carries a portion of the shear as illustrated in Figure 3.14. The total shear resistance is:

$$\begin{aligned} V &= V_c + V_s \\ &= V_{cz} + V_d + V_a + V_s \end{aligned}$$

where V_s is the shear resisted by the shear reinforcement.

Shear reinforcement not intercepted by a crack remains practically stress free. As the applied shear force increases beyond the force that caused diagonal cracking, the shear reinforcement will yield at some point, reaching a constant value. Any increase in shear force has to be carried by V_{cz} , V_a and V_d . An increase in crack width reduces V_a , rapidly increasing V_{cz} and V_d . Failure is caused by splitting of the concrete along the longitudinal reinforcement or crushing of the concrete in the compression zone.

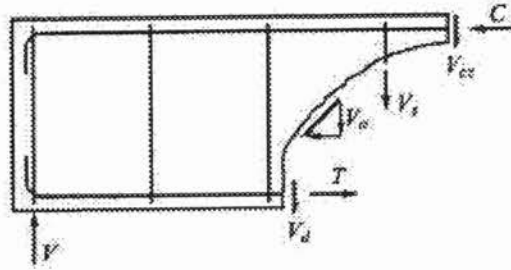


Figure 3.14: Shear components including shear reinforcement

3.1.6.2 Truss analogy

In 1899 and 1902, respectively, the Swiss engineer Ritter and the German engineer Morsch, independently published papers proposing the truss analogy for the design of reinforced concrete beams for shear. These procedures provide an excellent conceptual model to show the forces that exist in a cracked concrete beam.

To determine the stresses in the shear reinforcement by using a truss analogy. Consider the general case shown in Figure 3.15a where the shear reinforcement is spaced at a distance s_v and placed at an angle α to the horizontal. The shear reinforcement can be bent-up bars or inclined links, as shown in figure 3.15. It is assumed that compressive struts develop in the concrete at an angle β to the horizontal. The truss is completed by a top chord, consisting of concrete in compression and a bottom chord made up of the tensile reinforcement.

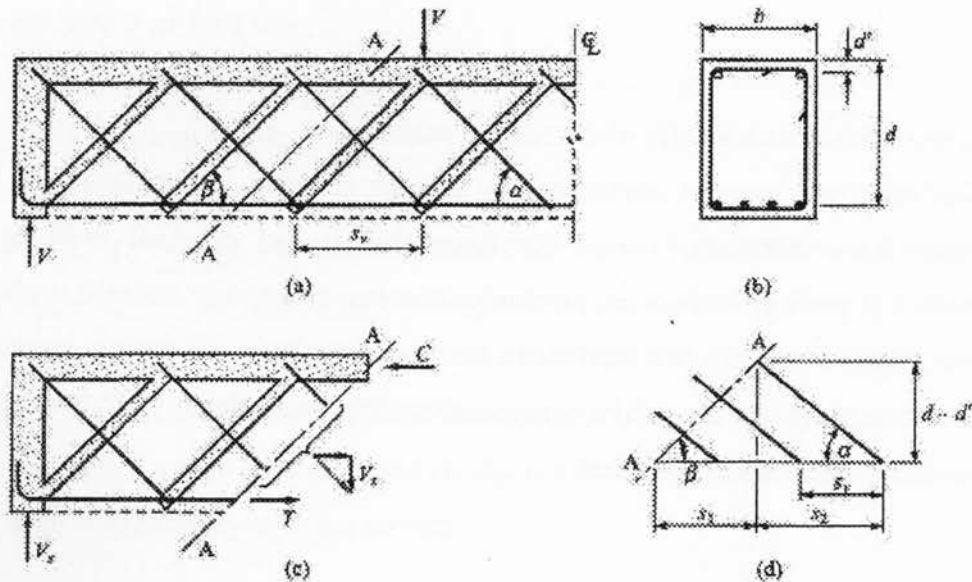


Figure 3.15: Shear components including shear reinforcement

The vertical component of the force in the shear reinforcement is determined by:

$$V_s = n_s A_{sv} f_{yv} \sin \alpha \quad (3.7)$$

Where A_{sv} = cross-section area of shear reinforcement
 f_{yv} = yield strength of shear reinforcement
 n_s = number of bars intersected by A-A

The number of bars intersected by A-A is determined from Figure 3.15-d

$$\begin{aligned} n_s &= \frac{s_1 + s_2}{s_v} = \frac{(d - d') \cot \beta + (d - d') \cot \alpha}{s_v} \\ &= [\cot \alpha + \cot \beta] \frac{(d - d')}{s_v} \end{aligned}$$

Substituting the above into Eq. (3.7)

$$\begin{aligned} V_s &= A_{sv} f_{yv} \sin \alpha [\cot \alpha + \cot \beta] \left(\frac{d - d'}{s_v} \right) \\ &= A_{sv} f_{yv} [\cos \alpha + \sin \alpha \cot \beta] \left(\frac{d - d'}{s_v} \right) \end{aligned} \quad (3.8)$$

The above equation applies to bent-up bars or inclined links.

Vertical links

For vertical links, the angle between the horizontal and the links $\alpha = 90^\circ$ so that:

$$V_s = A_{sv} f_{yv} \cot \beta \left(\frac{d - d'}{s_v} \right) \approx A_{sv} f_{yv} \left(\frac{d}{s_v} \right) \cot \beta$$

Experimental results indicate $\beta = 45^\circ$ so that:

$$V_s = A_{sv} f_{yv} \left(\frac{d}{s_v} \right)$$

The total shear resistance can be determined from:

$$V = V_c + V_s = V_c + A_{sv} f_{yv} \left(\frac{d}{s_v} \right)$$

$$\frac{V}{bd} = \frac{V_c}{bd} + \frac{A_{sv}}{s_v} f_{yv} \frac{1}{b}$$

$$\frac{A_{sv}}{s_v} = \frac{b}{f_{yv}} \left(\frac{V - V_c}{bd} \right) = \frac{(v - v_c)b}{f_{yv}}$$

Where v = nominal shear stress in the concrete = $\frac{V}{bd}$

v_c = shear strength of the reinforced concrete without shear reinforcement = $\frac{V_c}{bd}$

3.1.7 Equations for shear in beams

In the ACI Code (ACI 318M-05), the basic design equation for the shear capacity of a concrete beam is:

$$V_u \leq \phi V_n$$

Where V_u is the shear force due to the factored loads, ϕ is the strength reduction factor, taken equal to 0.75 for shear, and V_n is the nominal shear resistance.

$$V_n = V_c + V_s$$

V_c is the shear carried by the concrete and V_s , the shear carried by the stirrups, which is based on the 45° truss. The number of vertical stirrups spaced s apart crossed by a crack is therefore d/s , where d is the beam effective depth. Assuming that all stirrups yield at failure, the shear resisted by the stirrups where shear reinforcement perpendicular to the axis of member is as follows (ACI 318M-05):

$$V_s = \frac{A_v f_{yt} d}{s} \leq 0.66 \sqrt{f'_c} b_w d$$

where A_v is the stirrups cross-sectional area, f_{yt} is the specified yield strength of transverse reinforcement, b_w is the beam width, d is the beam depth, and f'_c is the concrete compressive strength.

The ACI Code (ACI 318M-05) assumes that V_c is equal to the shear strength of a beam without stirrups, which in turn, is taken equal to the load at which inclined cracking occurs:

$$V_c = \left(0.16 \sqrt{f'_c} + 17 \frac{\rho_w V_u d}{M_u} \right) b_w d \leq 0.29 \sqrt{f'_c} b_w d \quad \text{mm-Newton system} \quad (3.9)$$

Where ρ_w is the longitudinal reinforcement ratio, M_u is the factored moment at section, and $M_u / (V_u d)$ expresses the shear span to depth ratio a/d .

This equation was developed by ACI-ASCE Committee 326 in 1962 and is still in current use (ACI 318M-05). Taking V_c equal to the shear at inclined cracking is based on empirical observations and is approximately true if the truss angle θ is assumed to be 45° .

The mechanism of shear failure of beams with shear reinforcement is totally different from beams without shear reinforcement. Yet, ACI and many other design codes use the same V_c for both types of members. Thus, the shear resistance due to the concrete and stirrups are considered additive, when in fact they form part of a complex interaction (Chana 1987). For the normal range of variables, the second term in equation (3.9) will be equal to about $0.008\sqrt{f'_c}$. Therefore equation 3.9 could be written as follows (ACI 318M-05):

$$V_c = 0.17\sqrt{f'_c}b_w d \quad (3.10)$$

In Canadian Code (CSA-A23.3 2004), a concrete resistance factor (ϕ_c), factor account for the concrete density (λ), and a factor account for shear resistance (β) are used. Also, the concrete depth is taken as the effective shear depth (d_v) as follows:

$$V_c = \beta\lambda\phi_c\sqrt{f'_c}b_w d_v \quad (3.11)$$

where

λ = factor defined in ACL. 8.6.5 (CSA-A23.3 2004) to account for the lower tensile strength of structure low-density concrete. Where $\lambda = 1.0$ for normal weight concrete, $\lambda = 0.85$ for sand-light weight concrete, and $\lambda = 0.75$ for all-lightweight concrete.

ϕ_c = factor concrete strength, where $\phi_c = 0.65$

d_v = effective shear depth, taken as the greater of 0.9 or 0.72 the member height

The value of β shall be taken as 0.21 for beams with an overall thickness not greater than 250 mm otherwise, the value of β can be determined using the simplified method (CSA-A23.3 2004) as follows:

- If the section contains at least the minimum transverse reinforcement as specified by CSA-A23.3 (2004), β shall be taken as 0.18.

- If the section contains no transverse reinforcement and the specified nominal maximum size of coarse aggregate is not less than 20 mm, β shall be taken as

$$\beta = 230 / (1000 + d_v) \quad (3.12)$$

- Alternatively, the value of β for sections containing no transverse reinforcement may be determined for all aggregate sizes by replacing the parameter d_v in Equation (3-12) by the equivalent crack spacing parameter s_{ze}

$$s_{ze} = \frac{35s_z}{15 + a_g} \leq 0.85s_z \quad (3.13)$$

Where a_g is the specified nominal maximum coarse aggregate size and the crack spacing parameter, s_z , shall be taken as d_v or as the maximum distance between layers of distributed longitudinal reinforcement, whichever is less. Each layer of such reinforcement shall have an area at least equal to $0.003b_w s_z$ (CSA-A23.3 2004).

3.1.8 Review of shear tests in reinforced concrete beams

Wilkins Air Force Depot warehouse in Shelby, Ohio, collapsed in 1955 due to shear failure. The failed beams were 914 mm deep beams and did not contain any stirrups at the location of failure (Collins and Kuchma, 1997 and Collins and Mitchell, 1997). These beams had a longitudinal steel ratio of 0.45%. They failed at a shear stress of only about 0.5 MPa whereas the ACI Building Code of the time (ACI 318 1951) permitted an allowable working stress of 0.62 MPa for the 20 MPa concrete used in the beams. Experiments on twelve 305 mm deep model beams indicated that the beams could resist about 1.0 MPa. However, the application of an axial tension stress of about 1.4 MPa reduced the shear capacity by about 50%. It was thus concluded that tensile stresses caused by thermal and shrinkage movements were the reason for the shear reduction and the beam failures.

In the late 1960's Fenwick and Paulay (1968) investigated the shear transfer across cracks by interlocking particles. They examined the principal mechanisms of shear resistance in reinforced concrete beams. The concrete strength and the crack width were among the studied parameters. The concrete strength ranged from about 20 to 60 MPa. The results showed that there was a substantial reduction in shear transmitted by aggregate interlock action when the crack width was increased. Also, as the concrete strength was increased to 60 MPa, the shear transmitted across the cracks increased.

Kani (1966 and 1967) investigated the effect of member size on concrete shear strength. Kani's work consisted of beams without web reinforcement with varying member depths (d), longitudinal steel percentages (ρ_w), and shear span-to-depth ratios (a/d). He found that the member depth and steel percentage had a great effect on shear strength and that there is a transition point at a/d around 2.5 at which beams are shear critical. He also found that below an a/d value of about 2.5 the test beams developed arch action and had a considerable reserve of strength, beyond the first cracking point. In addition, he found that for a/d values greater than 2.5, the failure was sudden, brittle and in diagonal tension, soon after the first diagonal cracks appeared. Kani also looked at the effect of beam width and found that there is no significant effect on shear strength with different beam widths.

Fenwick and Paulay (1968) investigated the effect of longitudinal steel percentage (ρ_w) on concrete shear strength. They concluded that the transverse displacement at the level of the main longitudinal reinforcement (i.e., the shear slip across the crack), is greatly affected by the longitudinal steel percentage (ρ_w) in beams without stirrups. As the longitudinal steel percentage increased, the resistance to the shear slip across the crack increased, which result in an increase of the whole concrete shear strength.

Carrasquillo et al. (1981) tested the behavior and microcracking of high-strength concrete and compared it with normal strength concrete. They found that high-strength concrete had much less microcracking at all stress levels than did normal strength concrete. However, high-strength concrete fails more suddenly with fewer planes of failure than normal strength concrete.

They also found that under uniaxial compression, normal strength concrete developed highly irregular failure surfaces including numerous instances of bond failure between the coarse aggregates and mortar. Medium strength concrete developed a mechanism similar to the normal strength concretes but at a higher strain. The failure mode of high-strength concretes was typical of that of a nearly homogeneous material. Failure occurred suddenly in a vertical, nearly flat plane passing through the aggregate and the mortar.

Bazant and Kim (1984) derived a shear strength equation accounting for the size effect phenomenon as well as the longitudinal steel ratio and incorporating the effect of aggregate size. This equation was compared with the ACI Code equations at that time. The results showed that when different beam sizes are considered, the ACI Code does not yield a uniform safety margin

for design. It was also found that for very large specimen depths the factor of safety in the ACI Code almost disappears.

Elzanaty et al. (1986) found that the shear failure in high-strength concrete specimens had a smoother failure plane compared to normal strength concrete specimens. Eighteen specimens were studied in their investigation (3 of which contained stirrups). The concrete strengths used were ranging from 21 to 83 MPa. The test variables included ρ_w and the shear span-to-depth ratio, a/d . The results showed that for beams without stirrups, the shear strength increased with increasing compressive strength but less than that predicted using the ACI Code equations at that time. The results also concluded that for beams without stirrups an increase in the steel ratio led to an increase in the shear capacity of the specimens, regardless of concrete strength.

Ahmad et al. (1986) studied the effects of a/d and longitudinal steel percentage on the shear capacity of beams without web reinforcement. The concrete strength was maintained as constant as possible with f'_c in the range of 63 to 70 MPa. Their results were similar to that drawn by Elzanaty et al. (1986) with a transition in the failure mode at a/d of approximately 2.5. The envelope involving limits on a/d and ρ_w , which separates shear failures from flexural failures, was found to be similar to the envelope for the normal-strength concrete.

Walraven et al. (1987) investigated high strength concrete beams with maximum compressive strength of 115 MPa. The crack width and normal stress were also varied in the test program. Walraven et al. found that the shear friction capacity of cracks, in high-strength concrete, is significantly reduced due to fracture of the aggregate. They also found that the surface of a diagonal tension fracture in a high-strength concrete beam was relatively smooth. They attribute their results to the following; the aggregate particles, which protrude from the crack faces, play an important role in transmitting the shear forces, by virtue of the roughness. In concrete with normal and low strengths, the cracks intersect the cement matrix, but propagate around the relatively strong aggregate particles. With high strength concrete, however, the cracks intersect, and pass through the aggregate particles, such that the roughnesses of the crack faces are considerably different. Therefore, the number of contact areas can be significantly reduced, thus reducing the capability of transmitting shear forces.

Shioya (1989) investigated the influence of member depth and aggregate size on shear strength of large-scale beams. Lightly reinforced concrete beams without transverse reinforcement were tested under a uniformly distributed load. The beam depths were relatively

high and ranged from 100 to 3000 mm. Shioya found that the shear stress at failure decreased as the member size increased and as the aggregate size decreased.

In 1991, Bazant and Kazemi investigated beams with a size range of 1 to 16 and having a constant a/d ratio of 3.0 and a constant longitudinal steel ratio (ρ_w). The tested beams had a variation in depth from 25 to 406 mm. The main failure mode of the specimens tested was diagonal shear but the smallest specimen failed in flexure which confirmed the size effect phenomenon. However, because the tested beams were relatively small, the authors concluded that for beams larger than 406 mm, additional reductions in shear strength, due to size effect, were likely.

Kim and Park (1994) investigated beams with a higher strength than normal concrete (53.7 MPa). The test variables were longitudinal steel ratio (ρ_w), shear span-to-depth ratio (a/d), and effective depth (d). The beam heights varied from 170 to 1000 mm while the longitudinal steel ratio varied from 0.01 to 0.049 and a/d varied from 1.5 to 6.0. Their findings were similar to Kani's (1966 and 1967) concluding that the behavior of the higher strength concrete is similar to that of normal strength concrete. However, since only one concrete strength was investigated no general conclusions could be made with respect to concrete strength and shear capacity.

Walraven and Lehwalter (1994) conducted experimental work to investigate whether the size effect of the concrete beams without shear reinforcement can occur in short members, and how this can be described. They performed two series of studies. In the first series, the specimen size, reinforcement, and load application were kept constant, whereas the maximum particle diameter was varied between 8 and 32 mm. The grading curve and aggregate shape were also systematically varied (rounded or crushed). In the second series, the mix design was kept constant and the specimen sizes were varied. The depth of the member was varied between 200 and 1000 mm, whereas all other variables remained constant. Their results showed that there is no significant influence from the maximum particle diameter and the grading curve on the shear strength for deep beams ($a/d < 1$). In addition, the load at which inclined cracking occurs is hardly size dependant, however, the final bearing capacity ($\frac{V}{bdf_c}$) shows strong size dependency.

Kong and Rangan (1998), at the Curtin University of Technology in Western Australia, conducted an experimental work to examine the shear capacity for high-performance concrete beams with different longitudinal steel ratios. The tested parameters included the percentage of

longitudinal reinforcement, the beam depth, the shear span-to-depth ratio and the concrete strength. Test results showed that the increase in shear capacity found with increasing the percentage of longitudinal reinforcement from 1.66% to 2.79% was not as significant as that obtained by increasing it to 3.69%. The test results also showed that the concrete strength, ranging from 63.6 to 89.4 MPa, had essentially no influence on the concrete beams shear capacity.

Stanik (1998) conducted a large test program, which included 22 lightly reinforced concrete beams tested under 3-point loading, at the University of Toronto. The dimensions of these large, lightly reinforced specimens were; 1000 mm in height and 300 mm in width. The longitudinal reinforcement in that study varied between 0.5% and 1.19%. The other parameters studied were the concrete strength and the addition of transverse reinforcement. It was found that there was little gain in shear capacity for the specimens made with high-strength concrete. Stanik also concluded that, in general, as the concrete strength or member depth increased, or the percentage of longitudinal reinforcement decreased, for beams without stirrups, the ACI (ACI 318-95) predictions were very unconservative. In addition, his study concluded that an increase in the percentage of longitudinal reinforcement decreased the crack width and significantly increased the shear capacity of beams that did not contain transverse reinforcement.

Eric and Tompos (2003) studied the shear behavior of high workability concrete beams (HWC) containing shear reinforcement. Their investigation included 9 normal concrete and 11 HWC beams. The slump for normal concrete was less than 200 mm, while HWC slump was around 230mm. The slump flow in normal concrete was around 270 mm, while in HWC it was around 450 mm. The coarse aggregate content was around 900 kg/m in normal concrete and 1040 kg/m in HWC. The specimens dimension was 240 mm in width, 360 mm in depth and 3500 mm in length. The parameters used for their investigation were the concrete strength, shear span-depth ratio, spacing of shear reinforcement, and the strength of shear reinforcement.

The results of their investigation showed that HWC beams have slightly higher diagonal cracking strengths and ultimate strengths than normal concrete beams. In addition, HWC beams had more and finer cracks than normal concrete. The results also indicated that an increase of the concrete strength and decrease of the shear-span-depth ratio will increase the diagonal cracking strength

Cladera and Mari (2005) investigated the influence of the concrete compressive strength on the shear strength in beams with and without shear reinforcement. Eighteen reinforced concrete beams were tested as a part of an extensive research on shear design of reinforced high-strength concrete beams. The concrete compressive strength of the beams, at the age of the tests, ranged from 50 to 87 MPa. The only parameter which varied for all beams that did not contain shear reinforcement was the concrete mixture. The longitudinal reinforcement ρ_w was constant and equal to 2.24%. The results showed that the beams without web reinforcement presented a very brittle behavior. The higher their concrete compressive strength, the brisker their failure. The results also indicated that for beams without web reinforcement, the failure shear strength generally increased as the concrete compressive strength increased.

Lachemi et al. (2005) investigated the shear resistance of 18 flexurally reinforced self-consolidating concrete beams without shear reinforcements and compared the results to that in normal concrete beams. They investigated the shear strength in SCC based on the assumption that SCC mixtures have comparatively smaller amount of coarse aggregates content which may reduce the shear resistance of concrete by reducing the aggregate interlock between the fracture surfaces. The tested beams were varied in depth (150 to 300 mm) and have effective span of 800 mm. The test parameters in their investigation included concrete type, maximum size of coarse aggregate, coarse aggregate content, and beam shear span-to-depth ratio. Shear strength, shear ductility, crack patterns, and failure modes of all experimental beams were compared to analyze the shear resistance mechanisms of SCC and NC beams in both pre- and post-cracking stages.

The results of their investigation showed that SCC with the same maximum size of coarse aggregate but having a lower coarse aggregate content (as is the case for a typical SCC) showed similar concrete shear resistance characteristics in pre-cracking stage as compared with an NC. The results also revealed the development of lower post-cracking shear resistance in SCC due to lesser aggregate interlock and dowel action as a consequence of the presence of lower quantity of coarse aggregate compared with NC.

Kim et al. (2007) investigated the shear characteristics of self-consolidating concrete for precast prestressed concrete members and compared the results with those obtained from similar conventional concrete samples. Their study involved investigating the influence of SCC aggregate and paste volumes on shear capacity as the SCC mixtures commonly has higher paste and lower coarse aggregate volumes than the conventional concrete. The test variables in their

investigation included concrete strength (35 and 48 MPa), coarse aggregate type (river gravel and limestone), and three coarse aggregate volumes. The aggregate interlock was evaluated based on the crack slip, crack width, normal stress, and shear stress. The results indicated that SCC samples exhibit less aggregate interlock than the conventional concrete samples. As the crack width increases, the decreasing value of the normalized shear stress in SCC samples indicates the decrease in aggregate interlock.

3.2 Bond strength

3.2.1 Introduction

Bond between reinforcement and concrete is necessary to ensure composite action of the two materials. The normal assumptions of plain section behavior, used in section analysis and design, rely on composite interaction being achieved. Bond stress is the shear stress over the surface of the bar, which is a considerably simplified representation of the "actual" conditions.

Bond stress is defined as the change in the force within the reinforcing bar divided by the area of that bar surface, over which the change in the force takes place. In other words, bond stress is the shear stress transferred from the concrete to the reinforcing bar to change the bar stress from point to point, which depends on the development length and the change in the bending moment along the member.

Bond stress initially comes from the weak chemical bonds between the steel and the hardened hydrated cement paste of that concrete. However, with a little increase of the applied load on the steel bar, this resistance is lost. Once slip occurs, friction contributes to the bond, but with increasing slip between the bar and the concrete, bond resistance is derived principally from the bearing, or mechanical interlock, of the ribs on the surface of the bar with the concrete. At this stage, the reinforcing bar generates bursting forces resulting from the horizontal component of the force, acting between the concrete and the rib face angle. This force tends to split the surrounding concrete. Consequently, the resistance provided by the concrete cover and the confining reinforcement to these bursting forces may limit the failure load.

3.2.2 Bar-concrete interaction

Based on a previous study by Leroy et al. (1967), the force in the steel bar, which is transmitted to the surrounding concrete by bond, can be classified into three components: (a) chemical adhesion, (b) friction, (c) mechanical interaction between the concrete and the steel.

Bond of plain bars depends primarily on the first two elements in addition to the effect of the end anchorage. Although there is some mechanical interlocking due to the roughness of the bar surface. Deformed bars, however, depend primarily on mechanical interlocking for superior bond properties. This does not mean that friction and chemical adhesion are negligible in the case of deformed bars, but that they are secondary. However, researchers, who have contributed to the knowledge of the many aspects of bond (CEB-FIP 2000), agree that the interaction between the concrete and the bar subjected to a tensile force is characterized by four different stages (Fig.3.16). These stages are:

- Stage I (Uncracked stage)
- Stage II (Microcracks)
- Stage III (Splitting cracking)
- Stage IVa (Bond failure of plain bars)
- Stage IVb (Bond failure of deformed bars surrounded by light confinement)
- Stage IVc (Bond failure of deformed bars surrounded by heavy confinement)

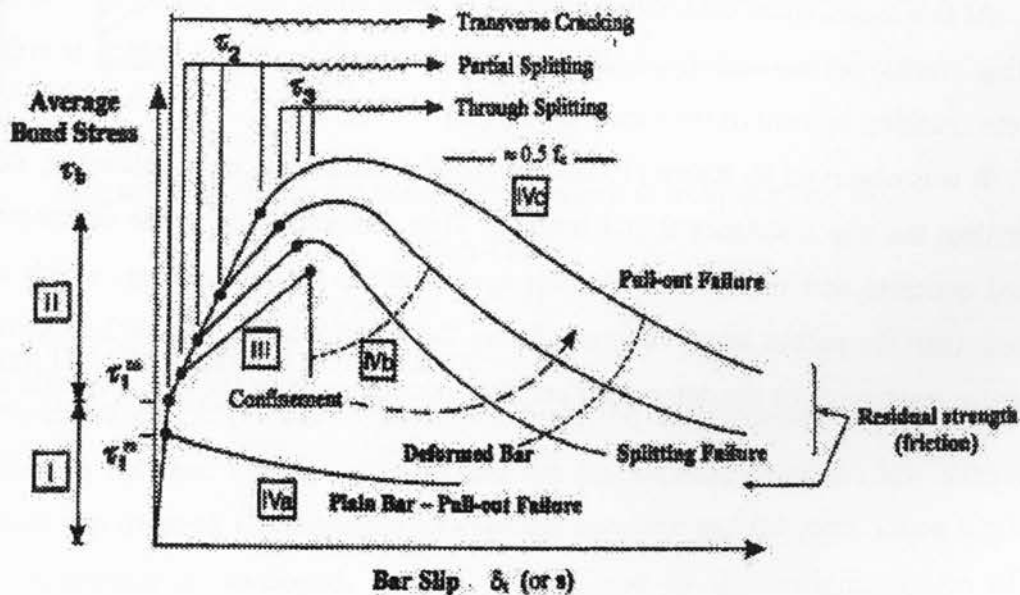


Figure 3.16: Local bond stress-slip law (CEB-FIP 2000)

3.2.2.1 Stage I (Uncracked stage)

The maximum bond stress that the plain bar can resist without slipping is defined as τ_1^{Ps} (Fig. 3.16). At this stage, the bond stress (τ) is less than the maximum bond stress (τ_1^{Ps}), and chemical adhesion is responsible for the bond efficiency. No bar slip occurs, however localized stress occurs close to the lug tips. Choi and Lee (2002) found that an adhesion range from 1.0 to 2.0 MPa is appropriate for the analysis of the bond of deformed bars and concrete.

3.2.2.2 Stage II (Microcracks)

The maximum bond stress that the deformed bar can resist, without causing transverse microcracks, is defined as τ_1^{Ds} (Fig. 3.16). At this stage, the bond stress (τ) is higher than τ_1^{Ps} , the chemical adhesion breaks down, and the lugs induce large bearing stresses in the concrete p^* (defined as the reaction of the bar lugs bearing against the concrete) (Fig. 3.17.a). Also, transverse microcracks originate at the tips of the lugs at this stage along with compressing of the porous concrete in front of the lug (in some cases due to lack of compaction) allowing the bar to slip. However, the wedging action of the lugs remains limited, and there is no concrete splitting. (Fig. 3.17. b)

3.2.2.3 Stage III (splitting cracks)

At this stage, when continuous increase of bond stress takes place, the longitudinal cracks (splitting cracks) spread radially, contributing to the wedging action, which is enhanced by the concrete crushing in front of the lugs (Fig. 3.17.c).

It was observed by Rehm (1968) that the slip resistance, upon reloading, is considerably higher than the slip resistance found initially. This was attributed to the compacted nonporous crushed concrete that the ribs are bearing against at the second loading, which was distinctly different than the porous intact concrete during the initial loading. Figure 3.18 shows a decrease of the slip resistance for the deformed bars after reloading, when the rib face angle is greater than 40° .

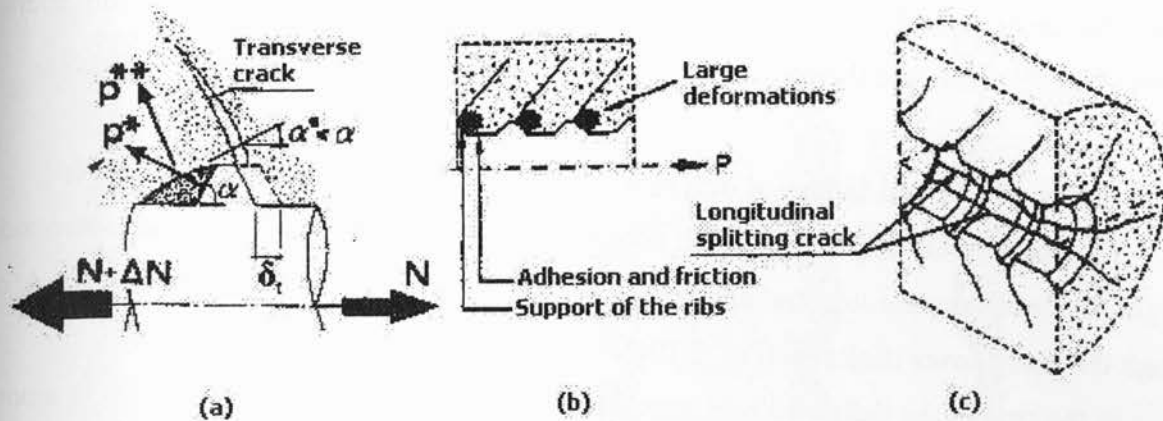


Figure 3.17: (a) Bar-concrete: slipping and wedging action of the bar; (b) friction and bearing action; (c) transverse cracking and splitting (CEB-FIP 2000)

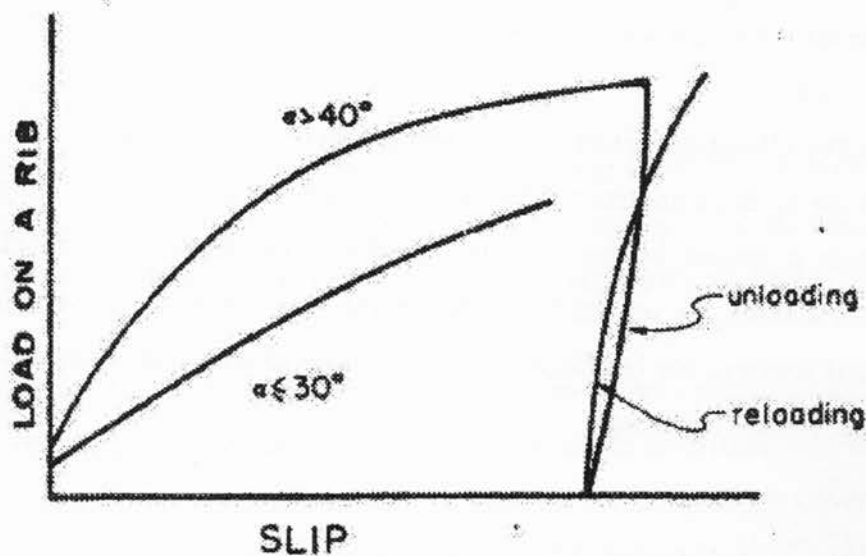


Figure 3.18: Load slip curve for the action in front of every rib (Rehm 1968)

3.2.2.4 Stage IVa (Bond failure of plain bars)

As explained earlier, in the case of plain bars, the bond resistance is assumed to be chemical adhesion between the mortar paste and the bar surface, however, low stresses will cause sufficient slip to break the adhesion between the concrete and the steel. Once slip occurs, further bond resistance is developed, only by friction and by the wedging action of small dislodged sand particles between the bar and the surrounding concrete. This stage immediately

follows the depletion of adhesive bond, and failure occurs when the adhesion and friction resistance is overcome, and the bars usually pull out from the encasing concrete.

3.2.2.5 Stage IVb (Bond failure of deformed bars surrounded by light confinement)

The bond in this stage tends to fail abruptly. In the case of the deformed bars surrounded by light confinement; the longitudinal cracks, accompanied by slip on the rib face, break out through the entire cover thickness (Fig. 3.19c).

In the case of the deformed bars surrounded by medium confinement, a sufficient amount of transverse reinforcement is provided, and longitudinal cracks accompanied by crushing or shearing-off, in the concrete below the ribs, will occur through the entire cover thickness (Fig. 3.19 b). The bond stress values as high as $1/3$ to $1/2 f_c$ can be developed during this stage, with the unavoidable and often unacceptable side-effect represented by very high slip values.

3.2.2.6 Stage IVc (Bond failure of deformed bars surrounded by heavy confinement)

In the case of deformed bars surrounded by heavy confinement, splitting does not occur and bond failure is caused by bar pullout. The force transfer mechanism changes from rib bearing to friction along the vertical line between the tops of the ribs as seen in Figure 3.19 a. Under continued loading, the interface is smoothed due to wear and compaction, leading to a further decrease of bond resistance.

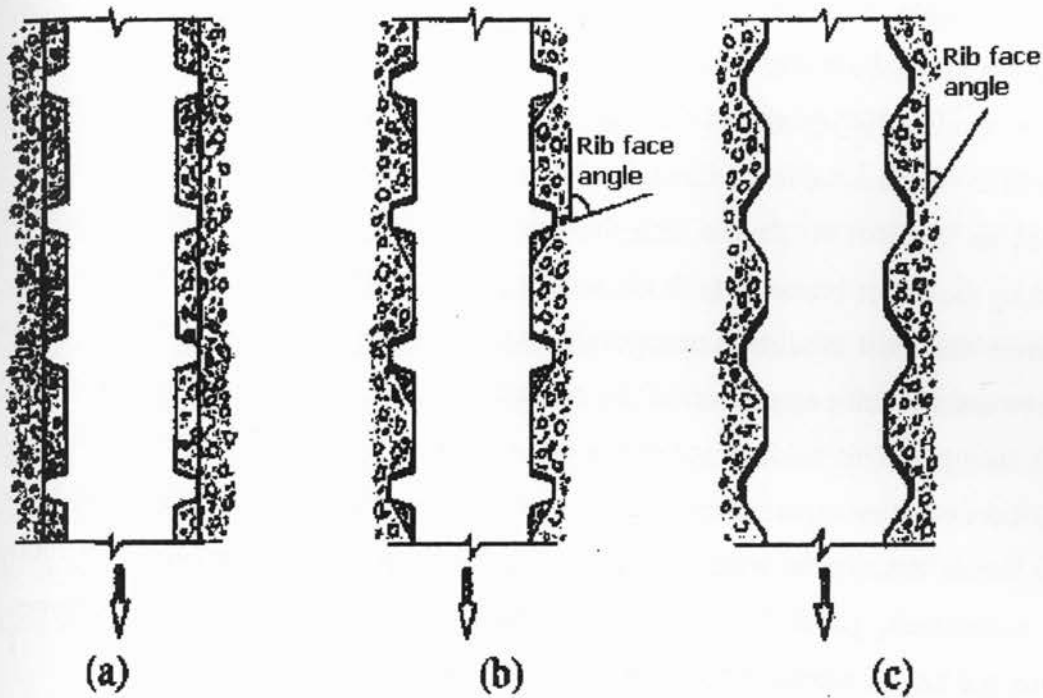


Figure 3.19: Modes of bond failure: (a) heavy confinement pull out; (b) medium confinement, splitting induced pull out accompanied by crushing and/or shearing-off in the concrete below the ribs; and (c) light confinement splitting accompanied by slip on the rib face (CEB-FIP 2000)

As far as Stage III is concerned, due to the build-up of the wedging action exerted by the bars and to the propagation of the splitting cracks, all possible contribution to the confinement are mobilized. In fact, the confinement efficiency depends on the concrete cover thickness, bar spacing (Ferguson 1966; Edwards and Jannopoulos, 1978; Ferguson et al., 1954; Morita and Kaku, 1979), reinforcement, and transverse pressure.

3.2.3 Effect of bar profile on bond strength

As is well known, the theory of reinforced concrete is based on stress transfer between the reinforcing steel bars and the surrounding concrete. This transfer of load or stress is made possible by the resistance to relative motion, or slippage between the concrete and the surface of the embedded steel bar. The resistance to slippage occurs due to the bond at the steel-concrete interface.

Choi and Lee (2002) found that the effective rib face angle (as a result from the crushing of the concrete in front of the rib) ranges between 25 and 35 degrees, which is lower than the

actual rib face angle. Also, the relative rib area has little effect on the bond strength of deformed bars when the bars are not confined by transverse reinforcement.

Lutz et al. (1966) predicted that bars with a large rib face angle would be less affected by grease or other friction-reducing agents than bars with a flatter rib face angle. If the face of the rib formed an angle of 90 degree with the axis of the bar, all of the bond strength would be produced by the direct bearing of the rib against the concrete key. In this case, friction between the concrete and steel would be unnecessary. On the other hand, bars with 90 degree angles could have insufficient compaction of the concrete in front of the rib, which oppositely affects the bond strength. This said, for plain bars (a rib face angle of 0 degree), friction caused by adhesion between the concrete and steel would be the only bond component and loss of this adhesion would destroy the bond. As the rib face angle becomes larger, the contribution of the friction component, parallel to the face of the rib, to the bond strength becomes smaller. Therefore, the loss of adhesion becomes less significant.

3.2.4 Effect of geometry and shape of the bar

David (1941) investigated the effect of different bar geometry on bond stress. He found that the stress transmission from the loaded end to the free end was higher in the case of plain bars than in the case of ribbed bars. Also, it was observed that the stress in the ribbed steel bar was higher near the loaded end than in case of plain bars. This may attributed to the increase of bond resistance due to the ribs action, which is not available.

Another study by Maslehuddin et al. (1990) evaluated the effect of the steel surface condition on the bond with the concrete. One of their objectives was to evaluate the effect of several rust degrees on the steel surface and the corresponding bond with the concrete. The study was conducted for several bar diameters subjected to different degrees of atmosphere exposure. The results of this experimental work indicated that there was no change in the bond between concrete and 16 mm diameter bars due to atmospheric corrosion. In the case of 32 mm diameter bars, there was a slight increase in the bond resistance as the periods of atmospheric exposure were increased. The slight increase in the bond resistance in larger size bars was attributed to the increased roughness developed due to atmospheric exposure.

3.2.5 Effect of rib angle, rib spacing, and rib height

Several researches have evaluated the effect of the rib geometry on the bond performance of the steel bar. Cairns and Abdullah (1994) studied the effect of the reduction of bond stress in fusion-bonded epoxy-coating reinforcement (FBECR). They also evaluated the variation in bond stress with different rib face angles for machined bars. Figure 3.20 shows the variation in rib face angle from 30 to 75°, with the bond stress and the corresponding slips.

At slips 0.01 and 0.1 mm, the bond stress slightly increases with the increase in the rib face angle. At the failure load (slip 1 mm), the bond stress increases with the increase of rib angle from 30 to about 55 or 60. This may be attributed to the increase of bearing force, due to the increase of bearing area. It should be mentioned that the large increase in the rib face angle can result in an insufficient concrete compaction below the rib and this factor should be taken into consideration when designing the rib face angle.

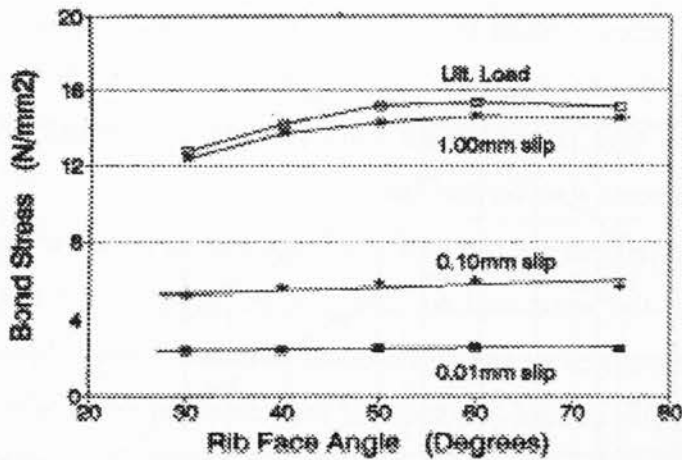


Figure 3.20: Variation in bond stress with rib face angle (Cairns an Abdullah 1994)

Previous bond research (Rehm1961, Soretz and Holzenbein 1979, Kimura and Jirsa 1992, Darwin and Ebeneze 1993) involving pullout and beam-end tests of regular and specially machined bars indicate that the geometry and shape of bar deformations affect the bond strength of anchored bars. It was concluded from their studies that bond performance of deformed bars would improve with: an increase in the rib height or decrease in rib spacing, an increase in rib bearing area-to-rib shearing area ratio (approximately rib height-to-rib spacing ratio), or an increase in the rib face angle above 45 degrees. Today, the ratio of rib bearing area-to-rib

shearing area is alternately known as the relative rib area R_r . That is the ratio of the projected rib area (normal to bar axis) to the product of the nominal bar perimeter, by the center-to-center rib spacing.

3.2.6 Effect of casting position and concrete confinement on the bond strength

According to Park and Paulay (1975), the load-bond slip relationship for deformed bars is primarily affected by the quality of the concrete in front of the bar ribs. The quality of the concrete in this region depends on its relative position of casting. Figure 3.21 shows the effect of different casting positions on the bond slip relationship. A soft and spongy layer of concrete can form under the ribs when casting is perpendicular to the bar length (number 3 in Fig. 3.21). This results in a higher slip (compared to the other casting positions) due to the crushing of the weak concrete under the ribs.

The effect of casting position on bond is even more severe for plain bars. Figure 3.22 shows the effect of different casting positions for 16 mm plain bars. The upper curves of each pair in the figure were obtained for heavily rusted and pitted bars. The lower curves of each pair are for smooth surface bars. The ultimate bond strength is drastically reduced in the case of horizontal bars as compared with vertical bars.

It is to be expected that the top bars in a beam will have poorer bond characteristics than the bottom bars, since the water and air gain will be greater under top bars. In addition, the relative downward movement of the surrounding concrete, caused by settlement of the fresh mixture, can be large. The amount of settlement that can occur depends on the extent of bleeding of the fresh concrete and the rate of the water that is permitted to escape from the formwork (Park and Paulay 1975).

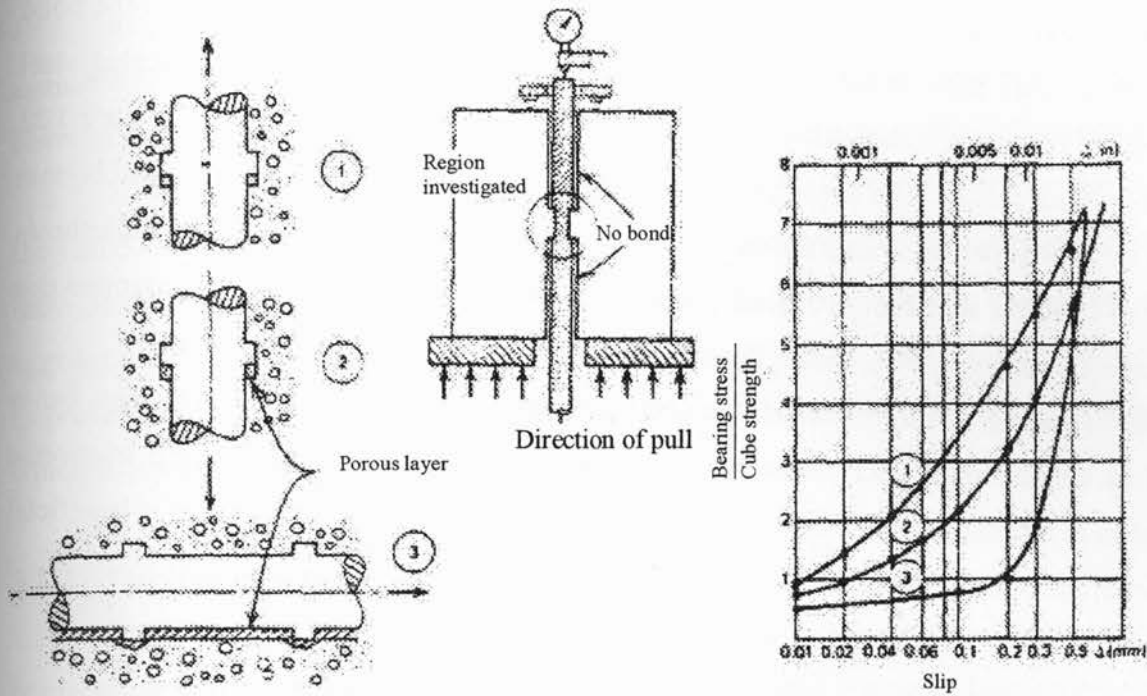


Figure 3.21: The influence of casting position on bond performance (Park and Paulay 1975)

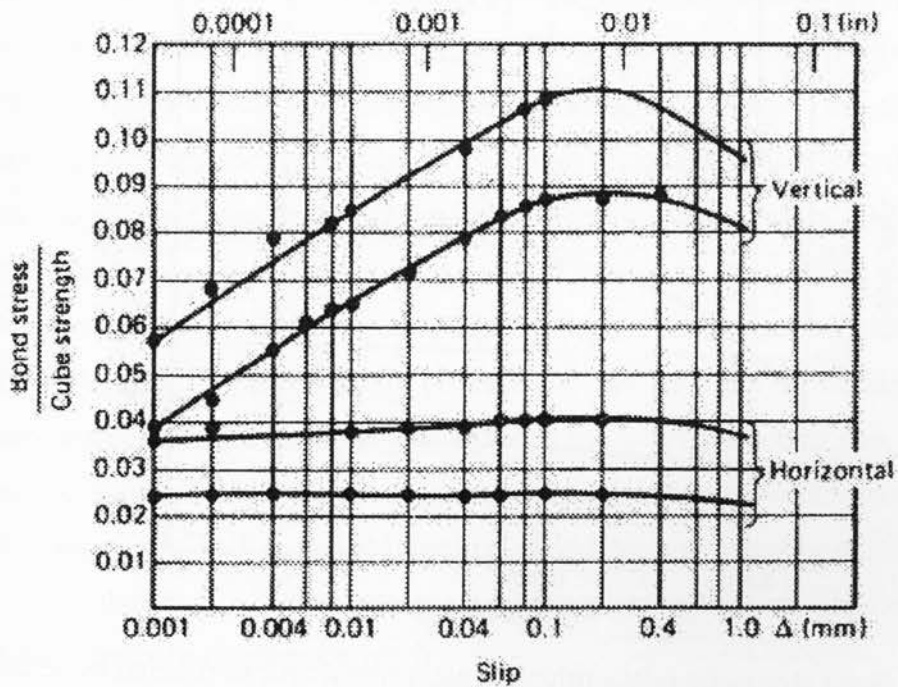


Figure 3.22: The load-slip relationship for No. 5 (16 mm) plain rounded bar in different casting positions (Park and Paulay 1975)

Welch and Patten (1967) studied the effect of casting positions and compared the bond performance of bars surrounded by concrete in leaky timber molds and in well-sealed steel moulds. In the latter, they also delayed the placing of the concrete by 40 minutes. Figure 3.23 demonstrates their results. The upper two curves indicate the delayed placing for top and bottom bars, and the lower part indicates the leaky timber mold placing for the same bars. This shows the effect of concrete settlement on bond, particularly for top bars. The ACI code recognizes this phenomenon by requiring 30% excess development length for top-cast deformed bars.

The widening of splitting cracks can be restricted, if the concrete that surrounds a bar is confined in certain areas such as at the simply supported ends of beams where transverse compression is normally available from the reaction force. Transverse compression is beneficial to the anchorage of reinforcement.

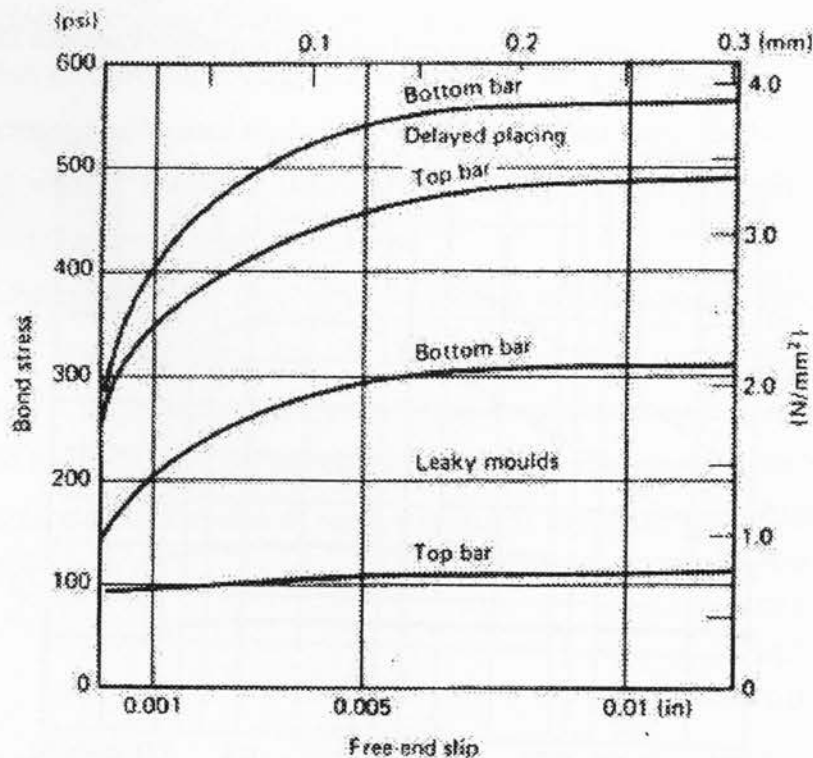


Figure 3.23: Bond stress-slip relationship for plain round bars as affected by settlement of fresh concrete. (Park and Paulay 1975)

Increasing the concrete cover was found to produce some increase in the resistance against splitting. However, the improved bond performance is not proportional to the additional cover thickness. Extra cover does not provide protection against excessive surface crack width.

Stirrups, particularly when closely spaced, prevent the opening of cracks that form along the embedded bars and enable greater bond forces to be transmitted. In many situations, this is only possible if the shearing stresses are transmitted across splitting cracks by means of aggregate interlock. The aim of confinement by means of stirrups or transverse reinforcement is to prevent a failure along a potential splitting crack and to enforce, if necessary, a shear failure, which is associated with the maximum attainable bond strength.

3.2.7 Effect of member depth on the bond strength

Segregation of the aggregate in concrete can lead to settlement of unhydrated cement grains along with some early hydration products in the plastic concrete. The settlement of fresh concrete around rigidly held reinforcement can reduce the effective projection of the lugs and lead to a minute separation between the lower portions of the reinforcement and the concrete that contributes to reducing the bond. Surface settlement can also lead to the formation of surface cracks above top-cast bars because of the restraining action of the bar to the settling of plastic concrete. Such surface settlement cracking, that reduces the quality of the interface between the reinforcement and concrete, increases with the increase in free water content (Dakhil et al. 1975).

With the increase in specimen height, a greater amount of bleeding, segregation, and surface settlement can be expected because of the increase in the quantity of fresh concrete (Hoshino 1989). As a result, bond strength between top-cast bars and surrounding concrete can be significantly lower than that with bars embedded at the lower portion of cast specimens. The effect of bleeding, segregation, and settlement on weakening bond between concrete and rigidly held reinforcements is related to several factors, including: the stability of the concrete, the position of the embedded bar, the extent of vibration consolidation, the leakage and the roughness of the formwork (Brettmann 1986).

Khayat (1998) investigated the effectiveness of incorporating a viscosity modifying admixture (VMA) to enhance stability of fluid and highly flowable concrete and reduce the top-bar effect. 18 concrete mixtures were prepared with 220 mm slump and contained various concentrations of VMA corresponding to 0, 0.035, and 0.07 percent by mass of cementitious

materials. The mixtures were used to cast specimens measuring 500, 700, and 1100 mm in height. These specimens were used to evaluate the effect of concrete type and height on stability and bond to horizontally embedded anchored bars. The mixtures containing 0.035 percent of VMA were prepared with blended silica fume cement, whereas those made without VMA and those with 0.07 percent of VMA did not contain any silica fume. Nine of the 18 specimens were hand-consolidated, and the remaining specimens were subjected to excessive external vibration. This was carried out to evaluate the effectiveness of incorporating a VMA to enhance stability and reduce top-bar factor in fluid concrete when subjected to excessive consolidation.

The results showed that the increase in specimen height resulted in some increase in the average bond stress ratio of bottom-to-top bars (U_{bot}/U_{top}) value, as well as an increasing in bleeding, settlement, and segregation of the rodded concrete. As expected, increasing the compaction effort, which reduces the stability of the investigated mixtures, also resulted in an increase in the U_{bot}/U_{top} value. For example, in the case of rodded concrete, the U_{bot}/U_{top} values of mixtures cast with concrete containing 0.035 percent VMA in specimens measuring 500 and 700 mm in height were approximately 1.20 and 1.35, respectively. Meanwhile, U_{bot}/U_{top} values of mixtures consolidated by external vibration were 1.50 and 1.75, for 500 and 700 mm specimens' heights respectively (Figs. 3.24 and 3.25).

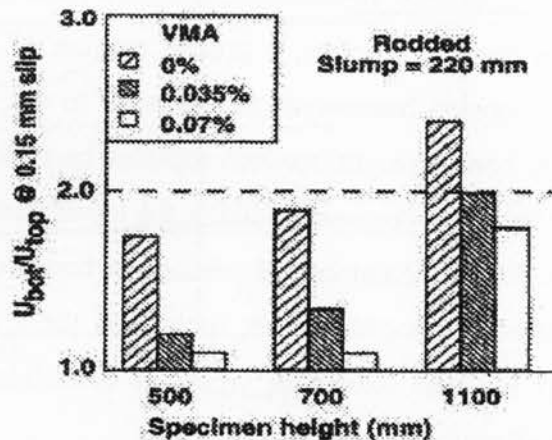


Figure 3.24: Effect of VMA dosage and specimen height on top-bar effect of rodded concrete (Khayat 1998)

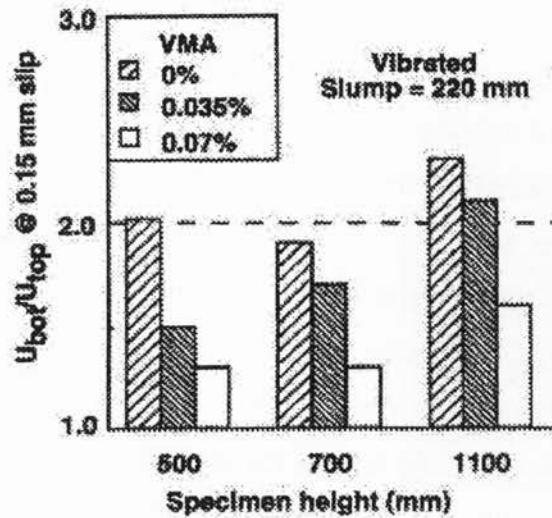


Figure 3.25: Effect of VMA dosage and specimen height on top-bar effect of vibrated concrete (Khayat 1998)

3.2.8 Bond Strength in SCC

3.2.8.1 General

Self-consolidating concrete (SCC) is a specially proportioned concrete that can flow under its own gravity and fill in the formworks without the need of any internal or external vibration. SCC is sufficiently cohesive to prevent segregation or blockage of aggregates during flowing. The enhanced cohesiveness can ensure better suspension of solid particles in the fresh concrete and, therefore, good deformability and filling capability during the spread of fresh concrete through various obstacles (Bouzoubaâ and Lachemi 2001; Lachemi et al. 2003, 2004; Patel et al. 2004; Khayat 1999; Khayat 1998; Khayat et al. 2001; Khayat et al. 2004)

The application of SCC is expected to increase the flexure behavior and load capacity of moment-resisting member due to the superior filling capability of SCC that may directly enhance the bond between reinforcements and concrete. The effects of bleeding, segregation, and surface settlement that are more pronounced in big size members (as mentioned earlier) are not significant in SCC mixtures. Moreover, the influence of intrinsic deficiencies and material defects, due to bleeding or segregation induced by improper vibration practice, can be avoided in SCC. As a result, the homogeneity of SCC can be ensured to substantially enhance the mechanical properties of members.

3.2.8.2 Review of research work

Khayat (1998) investigated the effect of incorporating viscosity modifying admixture to enhance the bond strength and stability of various self-consolidation concretes (slump flow from 600 to 690) and normal concretes (190 mm slump). The specimens used were 200 x 200 mm and 200 x 300 mm cross sections and 500, 700, and 1100 mm in heights to evaluate the effect of concrete type and height on stability and bond to horizontally embedded bars. Each specimen had two horizontally anchored reinforcing bars measuring 25 mm in diameter positioned at 75 mm from the upper and lower ends of the specimen. The results showed that regardless of the height of the specimens (500 to 1100 mm) and the mode of consolidation, the incorporation of VMA was shown to substantially enhance stability and reduce the top-bar factor (the average bond stress ratios of bottom-to-top bars U_{bot}/U_{top}). The results also indicated that the optimized SCC mixtures, which contained proper VMA contents, exhibited low settlement and low value of bond strength.

Sonebi et al. (2001) evaluated the bond strength in SCC and compared the results with those of the conventional vibrated concrete. Two optimized SCC mixtures were used (35 and 60 MPa). Deformed reinforcing steel bars with 12 mm and 20 mm effective diameters were used to evaluate the bond strength. The test specimen was a prism with a cross section of 100 × 100 mm and a length of 150 mm. The anchorage length was 120 mm for all bars. Average bond stresses were evaluated by pull out test and the deformation of the bar was measured. The results showed that the maximum bond strength decreased when the diameter of the steel bar increased from 12 to 20 mm. The normalized bond strengths of the SCC mixtures were found to be about 10-40% higher than those of the reference mixtures for both bar diameters (12 and 20 mm).

Chan et al. (2003) investigated the bond between SCC and reinforcements. The bonding strengths of reinforcing bars were measured using full-scale reinforced concrete (RC) members of SCC and of ordinary Portland concrete (OPC). Blast furnace slag and class F fly ash were used as cementitious materials to produce SCC. Full-scale RC walls were used as the pullout specimen, in which pullout reinforcing bars and transverse reinforcement were installed. The reinforcing bars for pullout were installed horizontally. The results showed that SCC members generated significantly higher bond to reinforcing bars than did ordinary concrete members. It was also found in their investigation that the reduction in bond, due to bleeding and

inhomogeneous nature in the case of ordinary concrete, was prevented in the case of SCC. Figures 3.26 and 3.27 show the trends of bond strength development of SCC and OPC.

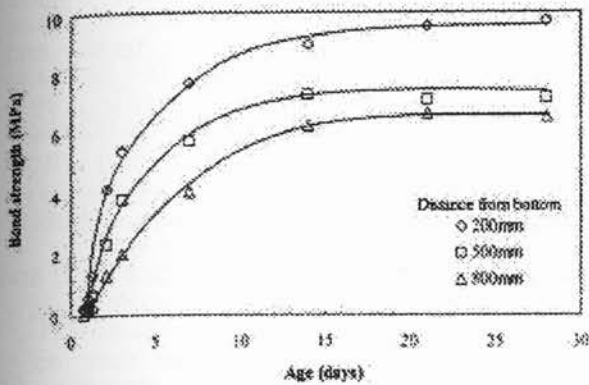


Figure 3.26: Bond strength in SCC
(Chan et al. 2003)

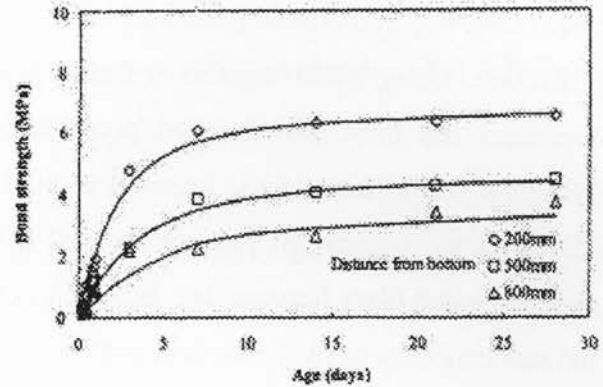


Figure 3.27: Bond strength in OPC
(Chan et al. 2003)

Chan et al. (2004) also investigated the effect of consolidation on concrete-steel bond strength. Three different types of concrete were adopted: normal concrete with low slump (75 mm), high-performance concrete with high slump (220 mm), and SCC that contained a high content of pozzolanic materials which consisted of 200 kg/m³ of slag and fly ash in total. Different consolidation conditions were adopted to simulate various situations that might occur during practical concrete placement, including: standard vibration (10s duration), overvibration (12-30s duration), no vibration, and improper vibration (the vibrator contacting the steel bars).

The experimental results indicated that consolidation is absolutely important to the bond strength development of reinforcing bars in normal concrete. The bond strength of normal concrete is significantly reduced when no vibration is applied. In addition, the application of vibration in high-performance concrete (HPC) is so crucial that overvibration or improper vibration would result in a substantial reduction in bond strength. The results also indicated that without any consolidation, SCC is capable of developing remarkably higher bond strength than the control case. Furthermore, the application of vibration in SCC may affect the bond strength and should be prevented.

3.3 Durability and corrosion resistance of self consolidating concrete

3.3.1 Introduction

The properties of high performance concrete (HPC) which contain supplementary cementing materials (SCM) are well known in terms of durability and reinforcement corrosion protection. Using SCM together with low w/c ratio to produce HPC increases the density and decreases the total porosity and permeability of the concrete (Aïtcin and Neville 1993, Midgley and Illston 1983, Lessard et al. 1992, Mehta 1980 and 1986, Sarkar and Aïtcin 1987). In most cases, the production of SCC involves the use of SCM such as fly ash, limestone and/or ground blast furnace slag, but such concrete mixture is different in design than HPC and the susceptibility of reinforcement corrosion in SCC could be different than in the case of HPC.

Corrosion of steel reinforcement could also affect the concrete shear strength. As mentioned, the shear strength in concrete beams without web reinforcement is transferred by the compression shear zone (20-40 %), aggregate interlock (35-50 %), and the dowel action (15-25 %). The dowel action of the longitudinal steel bars is greatly affected by the rebar corrosion, as the cross sectional area of the steel bar is decreased after corrosion takes place. Also, the cracks associated with corrosion are expected to strongly influence the shear strength. The flexure and shear cracks associated with the applied load are expected to be wider (because of the decreased rebar cross sectional area), which contributes to a reduction in the aggregate interlock and the overall shear strength.

3.3.2 Reinforcing steel corrosion

The steel reinforcement embedded in concrete is normally immune from corrosion because of the high alkalinity of the concrete. By alkaline we mean a high pH (versus acidic), which is a measure of hydroxyl ion (OH⁻) concentration. Higher pH values are due to the hydroxyl ions from sodium and potassium hydroxides (NaOH and KOH). On a scale of 0 to 14, the pH of concrete can be about 12.5 or higher. Generally, steel is chemically passive in concrete because of concrete's alkalinity, but if conditions change, and the alkalinity of the concrete dropped, corrosion rate could increase to problematic proportions. The two major causes of the breakdown of passivity on the embedded steel in concrete and the consequent initiation of active corrosion are:

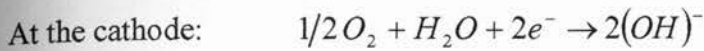
1. The presence of chloride ions in the concrete

2. The decrease in the pH value of the aqueous solution in the concrete pores because of the reaction of the cement paste with the atmospheric CO₂.

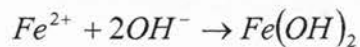
The mechanism of corrosion can be described by chemical half-cell reactions occurring at anodic and cathodic areas (Mehta, 1993). At active sites on the steel bar, called anodes, iron atoms lose electrons and move into the surrounding concrete as ferrous ions. This process is called a half-cell oxidation reaction, or the anodic reaction, and is represented as:



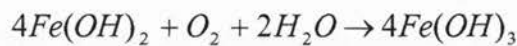
The electrons remain in the bar and flow to sites called cathodes, where they combine with water and oxygen in the concrete. The reaction at the cathode is called a reduction reaction. A common reduction reaction is:



The hydroxyl ions, OH arriving at the anodic area electrically neutralize the Fe²⁺ ions dissolved in pore water and form a solution of ferrous hydroxide at the anode:



This compound Fe (OH)₂ react further with additional hydroxide and available oxygen, to form the water insoluble red rust



The transfer of electrons between the anode and the cathode is characteristic of the corrosion process. For corrosion to take place the electrons released by the oxidation reaction must equal the electrons used up in the reduction reaction. If the reduction reaction cannot consume all the electrons released at the anode, the entire corrosion process, inducing the oxidation at the anode will be slowed down. Generally, a lack of oxygen and water at the reduction site are the primary cause for a slow cathodic reaction.

The physical distribution of the anode and the cathode on the metal, and their position relative to each another influence the presence of corrosion cells. Minor differences in the metal composition are mostly responsible for the locations for the anode and the cathode. Localized stress differences and local environmental conditions also influence the location of each site on the reinforcing metal. Sites can be permanently anodic, or permanently cathodic, or in other cases, they will alternate between each state as a result of changing physical conditions, {i.e.,

temperature, moisture, oxygen availability, etc.). Both the anodic and cathodic sites are dormant in dry conditions, however, when wetted, they regain their properties and activity is resumed.

The rate determining mechanisms in corrosion are (Bentur et al 1997):

- The availability of oxygen at the cathode which depends on the diffusion of gaseous or dissolved oxygen through the concrete. The reduction is the rate controlling reaction, so that any shortage of oxygen will abort the corrosion reaction.
- The presence of water solution in the concrete pores to promote ionic transport. The lack of moisture in the concrete cover inhibits the flow of ions through the concrete cover, or any other material separating the two sites.
- The flow rate of the ionic charges, the resistance between the anodic and cathodic site all influence the rate of corrosion. However, their effect is secondary to the availability of oxygen or moisture.

Red rust is not the only product of corrosion of steel in concrete. Compounds such as black rust, Fe_3O_4 , green rust, $FeCl_2$, and other ferric and ferrous oxides, hydroxides, chlorides, and hydrates are also formed. Their composition depends on the availability of the pore water, its pH and composition, and oxygen supply. Figure 2.28 shows the relative increase in the volumes of the various oxides and hydroxides of iron, which increases considerably when water molecules combine with them. These large volume increases lead to large pressures (similar to bursting pressures in pipes) and cause cracking of the concrete and its delamination.

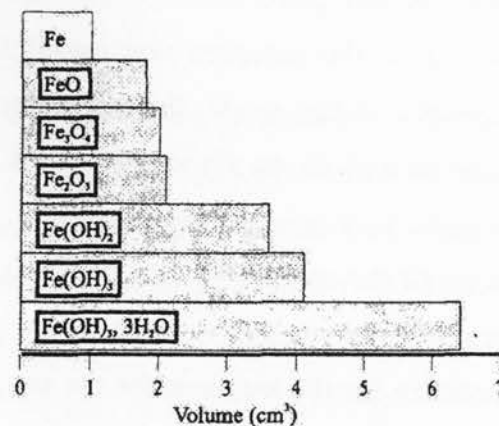


Figure 3.28: The relative volumes of iron and its corrosion reaction products, Nielsen (1985)

3.3.3 Concrete as an electrolyte

In order to discuss the factors influencing corrosion, it is essential to overview the concrete structure. The concrete consist of cement paste and coarse and fine aggregates, and the aggregates usually do not play a significant role in the corrosion process. Basically, the hydrated cement paste phase of the concrete acts as electrolyte for the transportation of ions and the ionic current. To a very large extent, the chemistry and particularly the physical structure of the cement paste determines the durability of the concrete and the nature of any deterioration (Lea, 1971). In general, the aggregates of concrete do not play a significant role in the protection or corrosion of reinforcing steel as there are no leachable ions. Also, the aggregates are usually less permeable than hydrated cement paste, however, its inclusion in the concrete creates low-density transition zones and makes concrete more permeable.

As an introduction to the microstructure of the hydrated cement paste, a brief discussion of the structure at different phases in the hydrated cement paste is given. The phases in hydrated cement can be divided into two main categories: Solid phase and Non-Solid phase

3.3.3.1 Solid phases

These solid phases are anhydrous clinker, calcium hydroxide (CH), calcium silicate hydrate (C-S-H), ettringite (Aft) and monosulphoaluminate (Afm).

After long periods of hydration some anhydrous clinker grains still exist in the microstructure of hydrated cement (Mehta 1986) the amount of which mainly depends on the particle size distribution of the anhydrous cement grains, the water /cement ratio and the degree of hydration.

Calcium hydroxide (CH) is released during the hydration process of the C_3S (tricalcium silicate) and C_2S (dicalcium silicate) the mineral compounds of the cement grains (Neville 1981). The CH crystals tend to have a well-defined crystal structure, and they are large, weak and relatively pure hexagonal prism crystals (Mehta 1986). The presence of CH crystals especially at the aggregate cement interface contributes to weaken the concrete strength and increases the overall porosity. The available space for hydration, hydration temperature and the percentage of impurities all affect the morphology of CH which usually varies from non-descript to large stacked plates (Mehta 1986).

The calcium silicate hydrate (C-S-H) phase is the main product of hydration of C_2S and C_3S mineral compounds of cement. The properties of the hardened paste are mainly determined by the C-S-H (Mehta 1986). The composition of the C-S-H is uncertain and possibly variable (Scrivener 1989).

Ettringite (Aft) is produced during the early hydration reaction of C_3A (tricalcium aluminate) in the presence of gypsum. The produced Aft phase has needle shaped prismatic crystals. Barnes et al. (1980) reported that the ettringite needles could either be solid or hollow with some variation in the composition. Different size of the ettringite needles have been reported (Jennings 1983). The available space, the sulphate ion concentration and the solution pH value are considered the main factors that control the Aft morphology (Scrivener 1984, and Jennings 1983).

The monosulphoaluminate phase (Afm) is produced at the late stage of C_3A hydration, when the Aft further reacts with more C_3A (Neville 1981, Taylor 1990). Afm has hexagonal plate crystals (Taylor 1990, Mehta 1986, Scrivener 1989). The presence of Afm crystals makes concrete vulnerable to sulphate attack (Mehta 1986)

3.3.3.2 Non-solid phases

3.3.3.2.1 Pores

The pore system of concrete consists of a very wide range of pore size. Generally, the pore space can be divided into two distinct classes gel pores and capillary pores.

Gel pores are the interconnected interstitial space between the interlayer spaces of the C-S-H gel. The average width of these pores as calculated based on the thickness of adsorbed water layer from adsorption isotherms for cement pastes of different w/c ratios is $0.0018 \mu\text{m}$. It was found that gel pores have a characteristic porosity, which is independent on w/c ratio and age, but limited to normally cured paste. The volume of the gel pores is about 28% of the total volume of the gel (Soroka 1979).

Capillary pores exist when the hydration products do not fill the original pore volume, which held the mixing water. These pores are in a continuous dynamic change in terms of geometry and connectivity as hydration proceeds with time and until the ultimate or terminal degree of hydration is reached. The w/c ratio and the degree of hydration influence the size of the capillary pores. Depending on the w/c ratio, and for well-hydrated cement, capillary pores

ranging from 0.01 μm up to 5 μm is being reported (Mehta 1986). For fluid flow, only capillary pores dominate and not the total pore space (Oberholster 1986, Hughes 1985).

3.3.3.2.2 Water

Water is one of the important phases in concrete, as its properties and behavior vary depending on the amount of water held in the pore system. The water can be classified into two main classes; evaporable water and non-evaporable water. Non-evaporable water is the chemically combined water, which is seen as an integral part of the various hydration products. This water can only be liberated on the decomposition of the hydrate structure.

According to the degree of firmness evaporable water can be classified into three types: interlayer water, adsorbed water and capillary water. The interlayer water (water in gel pores), is bonded to the surface of the gel with hydrogen bonds, which gives it the highest level of firmness. Consequently, it is unlikely to have normal hydraulic freedom (Peer 1990) this water can be only removed by drying (below 11% R.H), and while it affects shrinkage and creep, it takes no part in influencing permeability. The adsorbed water is the water close to the surface of the C-S-H and which is physically adsorbed to the solid surface (Mehta 1986). The capillary water, sometimes called free water is the water filling the large capillary pores with minimum or no binding force to the solid surface (Mehta 1986).

3.3.3.3 Aggregate paste interface

The interface between the aggregates and the cement paste is of significant importance to many of the concrete properties, such as compressive strength, tensile strength, bond strength, mode of failure, and permeability. The interface is always regarded as a weakest link in concrete. The volume of the interface zone was found to represent approximately 30% to 50% of the total volume of the cement matrix in concrete (Larbi 1993), which makes it a significant component of the concrete structure. Therefore any improvement of this zone is expected to show in the overall performance of concrete.

Mehta (1986) observed that calcium hydroxide crystals would grow preferentially in the contact zone between the cement past and the aggregate. Monteiro et al. (1985) studied the interface by using mortar against rock forming a composite specimen and they found that the surface effects produced by the aggregate face create zones of matrix with a higher w/c ratio at

the interface. This extra water permits the ions to diffuse more easily and at the same time eliminates some of the geometrical constraints that exist in the bulk matrix, causing higher porosity and the formation of large crystals of CH in the transition zone.

3.3.3.4 Concrete Porosity

The open microstructure of the transition zone and the occurrence of relatively large and better crystallized hydrates of CH, the growth of which enhanced in an open system (Larbi 1993), indicate that the interfacial region has higher porosity than the bulk cement paste. Ping et al. (1991) studied the structural feature of the transition zone by means of electric conductivity and showed that it is always less dense than the bulk paste; this indicates higher porosity.

The higher porosity in this region is attributed to two reasons. The first reason, is the lack of packing of cement grains (10-30 μm average diameter) close to the aggregate particles, known as "wall effect" (Scrivener 1989, Larbi 1993, Scrivener and Gartner 1987, Scrivener and Pratt 1987). The second reason is the micro bleeding entrapping water pockets or film around the aggregate particles (Larbi 1993, Mehta 1986, Maso 1980). Hoshino (1988) studied the pore volume at the lower and upper boundaries of coarse aggregate particles, and found that the total pore volume is higher at the lower surface than the upper surface at any w/c ratio. Also he observed large numbers of CH crystals at the lower boundary, many of which were of large size on the contrary, at the upper boundary, the number and size of CH crystals was smaller.

In comparison with other engineering materials, such as steel and polymer, concrete can be considered unique in its composition. On macroscopic level, it is a two-phase system composed of aggregate particles dispersed throughout the cement paste matrix. On microscopic level, it is a multi-phase material, which is composed of at least three components; aggregate particles, cement paste, and the interface between them (Scrivener 1989). The inclusion of aggregate into cement paste adds to the complexity of characterizing the main features of the microstructure. The aggregate and the aggregate paste interfacial regions are added as extra phase to the already multiphase cement paste. Also, aggregate affects each of the following: -

The amount of entrapped air and segregation during mixing and casting, the composition the form and size of the formed hydrates, the pore structure and pore size distribution and rate of hydration (Scrivener 1989, Kreijger 1987). All these features depend on the kind, particle size and particle size distribution of the aggregate. For these reasons, many researches have

concluded that concrete is different than mortar and cement paste, and there are some differences in the composition and structure between concrete, mortar and paste.

The production of SCC usually involves using SCM and/or VMA. In addition, the coarse aggregate content in SCC is commonly less than what is usually used in NC mixtures. SCM helps to densify the concrete microstructure and increase the corrosion resistance while VMA helps to disperse cement particles in the mixture and reduce the overall concrete permeability which contributes to increase the concrete corrosion resistance as well. Moreover, using less amount of coarse aggregate in SCC mixtures reduces the total volume of the transition zone (as mentioned before) and therefore reduces the total porosity of the concrete.

3.3.4 Review of previous work

A study was carried out by Khayat (2000) which involved testing air entrained SCC in a rapid chloride permeability test and water permeation test. His study was undertaken to optimize and evaluate the air entrained SCC made with different dosages of fly ash, ground blast furnace slag and silica fume. The mixtures were proportioned with 370, 450, and 550 kg/m³ of cementitious materials and water-cementitious material ratios (w/cm) of 0.45 to 0.50. Ternary binders containing 20% Class C fly ash or 40% ground blast-furnace slag, with 3% silica fume were used. The results of this study indicated that the rapid chloride-ion permeability and water permeability coefficient values were substantially lower in mixtures made with 0.45 w/c compared to those made with 0.5 w/c ratio. Khayat also found that all optimized SCC mixtures had favorable air-void systems and excellent durability to freezing and thawing.

Zhu and Bartos (2003) investigated the permeability properties of SCC made with two strength levels (40 and 60 MPa) and three design mixtures. The first mixture was designed using limestone powder, the second mixture was designed using pulverized fly ash (PFA) and the third mixture was designed using no additional powders but with a viscosity modifying agent. The permeability tests in their investigation consisted of the oxygen permeability, capillary water absorption and chloride diffusivity tests. The results of their investigation indicated that SCC mixtures showed significantly lower values of coefficient of permeability and sorptivity of water compared to the traditional vibrated reference concretes of the same strength grade. They also found that the chloride diffusivity was very much dependent on the type of additional powder used in concrete. In addition, both the SCC and the reference mixtures using PFA showed much

lower values of chloride migration coefficient than the other mixtures. The results also indicated that among the three different SCC mixtures, it appeared that the SCC mixture using no additional powder but a viscosity modifying agent to maintain stability of the fresh mixture, had the highest permeability, sorptivity and chloride diffusivity.

Persson (2003) investigated the sulfate resistance of SCC made with Portland cement and lime stone powder. Forty concrete cylinders were used; those concrete cylinders were subjected to a solution with sodium sulfate, sea or distilled water for a period up to 900 days. The results showed that when cured in a solution with sodium sulfate, larger loss of mass occurred with SCC than with normally vibrated concrete. Persson attributed this result to the effect of limestone filler content in SCC. He also concluded that if the content of sulfates in the groundwater is not known, it is not suitable to use SCC with large amounts of limestone powder.

Nehdi et al. (2004) performed some durability tests on SCC such as: the rapid chloride ion permeability test, sulfate expansion and deicing salt surface scaling resistance. Their investigation included normal vibrating concrete and different SCC types that contain fly ash, slag, silica fume and rice husk with different dosages. The results indicated that SCC that can be made with high-volume replacement of cement can achieve very low chloride ion permeability compared to the conventional concrete. They also found that 50% ordinary Portland cement, 24% fly ash and 6% slag was the best percentage of replacement which delivered the minimum chloride ion permeability diffusion compared to other selected percentages of cement replacement. The results also showed that SCC made with a high-volume replacement of cement can achieve good workability, high long-term strength, good deicing salt surface scaling resistance, and low sulfate expansion.

4 Experimental Program

4.1 Introduction

This investigation was divided into three stages; 1) testing the shear resistance of SCC members, 2) testing the rebar-concrete bond strength of SCC, and 3) testing the performance of SCC in protecting the reinforcing bars from corrosion. All tests in the three stages were performed at Ryerson University structural laboratory. Each SCC and NC consisted of the same mixture design for all performed tests used in the three stages (shear, bond, and corrosion investigation). Both SCC and NC were delivered to Ryerson University Structures laboratory in ready mixed concrete trucks by Dufferin Concrete Group, Toronto – Canada. The delivered SCC mixture was similar to that successfully used in Pearson International airport project in Toronto, Canada, in the year of 2000 (Lessard et al. 2002). Immediately after concrete delivery, tests on fresh properties of the concrete mixtures as well as casting of beams in prepared wooden forms were carried out. NC was cast using an electrical vibrator while SCC samples were cast without consolidation. In addition, SCC samples were poured in the formworks from one side until the mixture flowed and reached the other side under its own weight.

4.2 Materials used

4.2.1 Concrete mix parameters

Two distinct mixtures were used in each of the three experimental stages (shear, bond, and corrosion investigation); One SCC mixture with 900 kg/m^3 of coarse aggregate content, and one NC mixture with 1130 kg/m^3 of coarse aggregate (approximately 25% more coarse aggregate content than SCC). SCC/NC mixtures were designed to study the effect of lower coarse aggregate content in SCC compared with that in NC. Such a significant difference in coarse aggregate content was intended to study the effect of aggregate interlock on the shear strength reduction (during the shear stage investigation). The water-to-cementitious materials ratio was kept constant at 0.4 for both SCC and NC mixtures. SCC and NC mixtures were designed to achieve similar compressive strength and were typical in terms of material types, but different in mixture proportions.

In the corrosion test stage, two extra SCC mixtures were used to study the effect of adding different commercial high range water reducers (HRWR) on corrosion performance. The two extra SCC mixtures are similar in proportions to the mixture used in all other stages, the only

difference was replacing the original HRWR with two other commercial types (with different dosages to obtain the same slump flow). Details of SCC/NC concrete mixture proportions are presented in Table 4.1.

Type GU Canadian cement, similar to ASTM Type I and slag cement (ground granulated blast furnace slag) were used as cementitious materials for both SCC and NC. The chemical and physical properties of cement and slag are given in Tables 4.2 and 4.3. Natural sand and 10 mm maximum size stone were used as fine and coarse aggregates, respectively. Sieve analysis of the used coarse and fine aggregates is shown in Table 4.4.

High range water reducer admixture, similar to Type F of ASTM C 494 (15), and water reducer (WR), similar to Type A of ASTM C 494 (15), were used to adjust the flowability of SCC and NC mixtures.

4.2.2 Reinforcing steel

The diameters of the deformed bars used in all stages (shear, bond and corrosion test stages) were No. 10, 15, 20, 25 and 35M bars. All deformed bars are made out of regular carbon steel; they are manufactured locally and conformed to the ASTM Standard A615-72. The average yield and tensile strength of the used steel were 480 MPa and 725 MPa, respectively.

4.2.3 Testing concrete properties

The traditional slump test according to ASTM C 143/C 143M (2001) was conducted for the NC mixture. The slump flow test (ASTM C1611 / C1611M – 05) was conducted to evaluate the flowability of the SCC mixture while the V-funnel (Ozawa et al. 1994) and L-box (Sonebi et al. 2000) tests were conducted to evaluate the stability and the passing ability, respectively. 100×200 mm control cylinders were used to determine the compressive strength (f'_c) and the indirect tensile strength (f'_{ct}) as per ASTM standards C 39/C 39M (2001) and C 496-96 (2001) respectively. The fresh and hardened properties of the used SCC/NC concrete are presented in Tables 4.5 and 4.6

4.3 Shear investigations

4.3.1 Shear behavior of large-scale SCC beams

This part of the investigation is dealing with the overall shear behavior of full-scale reinforced concrete beams with no shear reinforcement made with SCC and NC. It is important to study the shear failure mechanism of large-scale reinforced concrete beams, without web reinforcement, to better understand the failure mechanisms in beams with stirrups (Zararis and Papadakis 2001). A total of 20 flexurally reinforced concrete beams, with no shear reinforcements, were tested under mid-span concentrated load until shear failure occurred. The test parameters included: concrete type (SCC or NC), coarse aggregate content, beam depth, and longitudinal reinforcing steel ratio. Shear strength, crack patterns, and crack width of the experimental beams with SCC and NC are compared. The performance of Code-based design equations in predicting the shear resistance of SCC/NC beams is also presented.

4.3.2 Studying the cracking and deflection characteristics of large-scale SCC beams

The objective of this part is to analytically investigate the shear strength, cracking behavior and deflection characteristics of large-scale SCC beams made without web (shear) reinforcement and compare these traits to those of the NC beams. The aggregate interlock mechanism (affecting the shear load, cracking and deflection behavior) is greatly influenced by the beam size (Collins and Mitchell 1991; Collins et al. 1996; Walraven and Lehwalter 1994; Bazant and Kim 1984; Bazant and Kazemi 1991). Hence, to study the effect of beam size (size effect) the tested SCC/NC beams were chosen to have variable beam depth (h) but having constant shear span-to-total depth ratio (a/h). The longitudinal tensile steel ratio (ρ_w) is also a factor influencing the shear capacity and deformability of reinforced concrete (RC) beams (Tempos and Frosch 2002). To study the effect of longitudinal steel ratio, half of the SCC/NC beams had low ρ_w ($= 1\%$) and the other half had comparatively high ρ_w ($= 2\%$).

The experimental crack widths (from SCC/NC beams) were compared with those obtained from Gergely and Lutz equation (ACI 224R 1992) (as both the current Canadian Code and the early ACI Code are handling the crack width based on this equation). Experimental first flexural cracking moments were compared with those calculated from Canadian (CSA-A23.3 2004), ACI (ACI 318 2005), Australian (AS 3600 1988) and Euro (EC2 1992) Code-based equations while ultimate shear resistances were compared to those obtained from Canadian

Standards (CSA-A23.3 2004). Moreover, the experimental load-mid span deflection curves were compared with those obtained from ACI (ACI 318 2005) and Euro (EC2 1992) Code-based equations.

4.3.3 Specimens details

Twenty reinforced concrete beams (10 made with SCC and 10 with NC), designed only for adequate flexural reinforcements and having no shear reinforcements, were tested. Table 4.7, Figures 4.1 and 4.2 show the geometric dimensions of SCC/NC beams. All beams were 400 mm wide (b) with total depth (h) ranging from 150 to 750 mm. The shear span-to-total depth ratio (a/h) was kept constant at a value of 2.5 to ensure shear rather than bending failure of all beams (Kani 1966, 1967, 1979) (Table 4.7, Figs. 4.1 and 4.2). Two flexural reinforcement configurations were used for the beams with longitudinal reinforcement ratios (ρ_w) of 1% and 2%. Cross-sectional dimensions and reinforcement layouts of beams are shown in Fig. 4.2. The beams were designated by concrete type, total beam depth (h), and longitudinal reinforcement ratio (ρ_w). The beam designation included a combination of letters and numerics: SCC or NC to indicate the concrete type; 1 or 2 to indicate the longitudinal reinforcement ratio; and 150, 250, 363, 500 or 750 to designate the total height. For example, a SCC beam having 1% ρ_w with a total height of 750 mm is designated as 1SCC750.

4.3.4 Formwork preparation and casting of beam specimens

Two beams were cast simultaneously in each formwork; one beam contained 1% ρ_w while the other contained 2%. The beams formworks were constructed from 20 mm plywood sheets and 50x100 mm wooden bars. The two beams in each formwork shared a middle plywood sandwich sheet (two plywood sheet stiffened by two-by-fours in the middle). The two sides of each formwork and the middle plywood wall were laterally supported from the bottom by the formwork base and from the top by several two-by-four bars (Fig. 4.3).

The reinforcement cage was installed inside the formwork after the strain gauges were glued to the assigned individual rebar. Plastic chairs positioned on the formwork floor were used to support the bottom longitudinal bars, while round plastic spacers were used to support the two sides of the steel cage and maintain the required cover (Fig. 4.4). In order to support the top longitudinal bars, three 10M stirrups were added on each side of the beam, away from the beam

support, and one stirrup was located at the middle of the beam (below the loading point). The location of these stirrups was chosen so that beam shear resistance is not affected by these stirrups during loading.

After the inside formworks were oiled, the beams were cast using a large concrete bucket maneuvered by a 20-ton crane. The concrete mixture was delivered to Ryerson University Structures laboratory in ready mixed concrete trucks by Dufferin Concrete Group, Toronto – Canada. Immediately after concrete delivery, tests on fresh properties of the concrete mixtures were carried out. The NC was consolidated using an electrical vibrator, while SCC samples were cast without any mechanical consolidation. In SCC beams, the concrete was poured in the formwork from one side until it flowed and reached the other side.

Formworks were removed after 24 hours of casting, then the beams were moist cured for four days and subsequently air-cured until the date of testing (same as control cylinder samples).

4.3.5 Test setup, instrumentation and loading procedure

The beam specimens were tested as simply supported beams under three-point loading conditions. Figures 4.5 and 4.6 show a picture and schematic diagram of the test setup. The test setup included the use of a hydraulic jack that apply load gradually on the mid-span of beam specimens until failure. Four Linear Variable Displacement Transducers (LVDT's) were attached at 45° on the front surface of each beam to measure the shear strain and to detect the initiation of diagonal cracks (Figs. 4.5 and 4.6). Another LVDT was placed directly under the mid-span of each beam to measure central deflection. In order to monitor the development of strain in the longitudinal steel reinforcement with progressive loading, two electrical strain gauges were installed to the lower layer of the reinforcement, directly under the loading point at mid-span. A computer-aided data-acquisition system automatically monitored load, displacements and strains at pre-selected time intervals throughout the loading history. The tests also provided information on the overall behavior of beams including development of cracks, crack patterns, crack width, load transfer mechanisms and failure modes. The load was applied in a load control fashion in three stages. The first and second stages correspond to 50% and 75% of the expected failure load, respectively, while the third stage corresponds to the failure load.

4.4 Bond investigation

The main objective of this phase was to investigate the bond strength in heavy reinforced full-scale SCC sections and compare the results with those of NC sections. Both SCC and NC mixtures were commercially used concretes and were delivered in ready-mix concrete trucks to the laboratory. In this phase, the flowability of SCC in the heavy reinforced section was also investigated and monitored through a transparent formwork. The study included investigating the bond strength at various rebar heights (150 mm, 510 mm, and 870 mm from the bottom of the beam), different testing ages (1, 3, 7, 14, and 28 days) and comparing the experimental results of the bond stress against the results calculated using ACI and CSA Code provisions. The free end displacement was detected during the applied pull out load and stress-free end displacement was investigated in each tested bar.

4.4.1 Specimens details

Two heavy reinforced full-scale reinforced beams (one made with SCC and one made with NC) were tested in this phase. The beams were 4000 mm in length x 1200 mm in height x 300 mm in width. Each of the two beams had thirty 20M bars; each bar was embedded 150 mm into the concrete and protruded 500 mm and 20 mm from the front and back sides, respectively (Figs. 4.7 and 4.8). The 500 mm protruded portion of the bars was selected in order to have enough length to mount the hydraulic pullout jack, load cell and the end wedge; while the 20 mm protruded portion was selected to measure the free end displacement of the tested bar (Fig. 4.9). In order to ensure only 150 mm of the embedded 300 mm portion of the bar was in contact with the concrete, a plastic sleeve was erected to envelop 150 mm of the embedded bar isolating the concrete from contacting the bar in that area (Figs. 4.8-4.10).

The bars were installed at elevations 150, 510, and 870 mm from the bottom of the beam (Fig. 4.8). Such elevations were selected to investigate the effect of specimen depth on the bond strength. The thirty 20M bars in each beam were divided into five groups, each group had six bars (two bars at each elevation) tested in separate ages (1, 3, 7, 14 and 28 days) to study the development of the bond strength under different ages. It was suspected that any pullout steel bars located below the pouring side of the beam would have better bond strength due to the weight of the falling concrete. For this reason, no pullout steel bars were erected up to a distance of 800mm from the edge of the beam (Fig. 4.8)

Nine 35M and three 25M longitudinal steel bars were placed on the top and bottom of the beam, respectively, to simulate the case of negative moment sections. The number and size of the longitudinal steel bars were selected in accordance with CSA-23.3 (2004) standard of reinforcement placement. The concrete cover was selected in all beams to be 30 mm to simulate the case of a non-exposed structure.

According to previous researches (Ferguson 1966; Edwards and Jannopoulos 1978; Ferguson et al. 1954; Morita and Kaku 1979), the confinement efficiency which depends on the concrete cover thickness, bar spacing and transverse pressure, greatly affects the bond strength between the concrete and the steel bar. Therefore, eight 15M longitudinal steel bars were added along both beam sides to satisfy the requirement of CSA-23.3 (2004) standard for crack control and to ensure equal steel confinement around each embedded steel bar (Fig. 4.8).

4.4.2 Formwork preparation and casting of beam specimens

The two NC and SCC beams were identical in terms of the reinforcement details and the formwork size. The beams formwork was constructed from 20 mm plywood sheets and 50x100 mm wooden bars. The front side of the formwork was made out of a plastic transparent sheet to monitor and study the flowability of SCC through the heavy reinforcement (Fig. 4.11). The two sides of the formwork were laterally supported by triangles made with two-by-fours from the two sides while supported by several two-by-four bars from the top (Fig. 4.12).

The reinforcement cage was assembled separately outside and then placed inside the formwork using a 20-ton crane. Plastic chairs, positioned on the formwork floor, were used to support the bottom longitudinal bars while round plastic spacers were used to support the two sides of the steel cage and maintain the required cover. After the inside formworks were oiled, the beams were cast using a large concrete bucket maneuvered by 20-ton crane. The concrete mixture was delivered to Ryerson University Structures laboratory in ready mixed concrete trucks by Dufferin Concrete Group, Toronto – Canada. Immediately thereafter, tests on fresh properties of the concrete mixtures were carried out. NC was consolidated using an electrical vibrator while SCC samples were cast without any mechanical consolidation. The concrete in the SCC beam was poured in the formwork from one side until it flowed and reached the other side. After the completion of casting, the beams were moist cured for 4 days then left uncured in the laboratory area until the time of test (same as the control cylinder samples).

4.4.3 Test setup, instrumentation, and loading procedure

Figure 4.9 shows a typical pullout test setup for each embedded bar. The protruded part of the steel bar was erected inside a hollow hydraulic jack and a hollow load cell. The hydraulic jacking system was adopted to apply concentric pullout force to the steel bar. When the bond slip occurred, the free end displacement of the protruded bar was measured automatically by one LVDT attached to the free end of the pullout bar. A computer-aided data-acquisition system was automatically monitoring the load and the displacements at pre-selected time intervals throughout the loading history (10 reading per second).

4.5 Corrosion investigations

4.5.1 Testing the performance of SCC/NC in terms of corrosion resistance

This part of corrosion investigation was divided into two stages. The first stage was designed to study the corrosion performance and cracking of full-scale SCC beams and compare the results with those of NC beams. The corrosion performance was examined along the beam's length/perimeter to reflect the durability characteristics and to study the uniformity of the full-scale SCC beams.

This phase was designed to investigate the corrosion performance and cracking due to stirrup and longitudinal bar corrosion. The tested beams were divided into two sets; the first set (1 SCC and 1 NC beam measured 400 mm width, 2340 mm length, and 363 mm depth) contained non-epoxy coated stirrups and were investigated under a moderate corrosion stage, while the second set (1 SCC and 1 NC beam measured 400 mm width, 2340 mm length, and 363 mm depth) contained epoxy coated stirrups and were investigated under a severe corrosion stage. The test was terminated in the moderate corrosion stage after any of the two beams reached 10% theoretical mass loss and in severe corrosion stage after any of the two beams reached 30% theoretical mass loss. The beam designation included a combination of letters: SCC or NC to indicate the concrete type; E or N to indicate the epoxy and non-epoxy coated stirrups. For example, a SCC containing epoxy coated stirrups is designated as SCC-E.

The corrosion investigation was conducted under an accelerated corrosion test and the corrosion rate was monitored throughout the test by measuring the current passing with time. The corrosion performance along the beam's length/perimeter was studied in different locations on each beam by taking periodical half-cell potential measurements, chloride ion content near the

bar surface, crack patterns and widths, mass loss, and reduction of the longitudinal bar diameter along each embedded bar. At the end of the corrosion testing, the actual measurement of the mass loss was compared to that obtained theoretically by Faraday's equation in order to validate the use of theoretical estimations of the mass loss by Faraday's law.

The second stage was designed to study the corrosion performance in small concrete cylinders made with the same NC/SCC mixtures used in the first stage. In addition to the regular SCC and NC mixtures used in the first stage, the small concrete cylinders also contained two more types of SCC mixtures. The additional two SCC mixtures were similar to the SCC mixture used in the first stage, but had different types of HRWRs. The corrosion investigation was conducted under the accelerated corrosion test which investigated the corrosion initiation, corrosion rate, crack patterns and widths. The objective of this stage was to verify that the bleeding, segregation and casting techniques (which are manifested in full-scale beams rather than small laboratory cylinders) could be the only reasons behind enhancing SCC durability and corrosion protection. The second objective of this stage was to investigate the effect of different HRWR types in SCC corrosion protection (if any).

4.5.2 Strength and cracking of full-scale corroded SCC/NC beams

The objective of this investigation was to study the evolution of strength, mid-span deflection, failure load, mode of failure, and cracking of the full-scale SCC/NC beams in three corrosion levels (0, 1 or 2). The data of the beams in 0 corrosion level were taken from the beams tested in shear. The performance of Code-based design equations, in predicting the crack width and mid-span deflection of SCC/NC beams, is also considered. The tested beams were 400 mm wide \times 363 mm deep \times 2340 mm in length, having no web reinforcement.

The beams were first subjected to an accelerated corrosion test to reach the required degrees of corrosion. Then the beams were tested under mid-span concentrated load until failure. All beams were designed to fail in shear and had the exact anchorage length for flexural reinforcement bars according to A23.3-04 CL.11.3.9.1 (to check the sufficiency of the designed anchorage length after the occurrence of several degrees of corrosion). The beam designation included a combination of letters and numbers: SCC or NC to indicate the concrete type; 0, 1 or 2 to indicate the degree of corrosion. For example, a SCC in the second degree of corrosion is

designated as SCC-2. Test setup, instrumentation and loading procedure for the tested beams were carried out as mentioned in section 4.3.5.

4.5.3 Specimens details

A total of four concrete beams were used in testing the corrosion performance in full-scale beams; 2 made with SCC and 2 with NC. The four beams were divided into two sets. The first set contained one SCC beam and its counterpart NC beam, both of these beams had non-epoxy coated stirrups in certain locations (Fig. 4.13-a) and were designed for a moderate corrosion stage. The second set contained another typical SCC beam and its counterpart NC beam but had epoxy coated stirrups; these beams were designed for severe corrosion stage (Fig. 4.13-b). The four beams were cast with those designated for the shear investigation and were kept until the time of the tests (refer to 4.3.4 for casting of beam specimens). All beams were 400 mm wide, 363 mm deep and 2340 mm in length. The four beams contained three 25M longitudinal bars at the bottom and two 15M at the top. The longitudinal bars cover was 40 mm while the stirrups cover was 30 mm.

A total of 8 concrete cylinders (100 mm in diameter and 200 mm in height, reinforced axially with a single 25M bar and protruding at one end only) were used to investigate the corrosion performance in small concrete cylinders (Fig. 4.14). To protect the interface between the protruding steel bar and the surface of the concrete specimen from corrosion, 50 mm of the extension part of the bars, along with another length of 25 mm within the specimen top, was taped with an electrical tape (Fig. 4.15). To maintain the bar verticality during casting, a square wooden piece which had a centered hole of 21 mm in diameter, was mounted on the cylinder mold quickly after casting the concrete and the bar was then hammered until reaching the required depth (Fig. 4.16).

The 8 concrete cylinders were divided into 4 groups of 4 concrete types, each group contained 2 concrete cylinders from each concrete type. The four concrete types were NC and SCC (from the same mix design used in the full-scale beams test) and two more SCC mixtures containing two different HRWRs. All concrete cylinders were cast at Ryerson University Concrete Laboratory using 1/8 cubic meter electrical concrete mixer. The concrete materials and admixtures used in the small cylinders were the same as those used in the full-scale beams and were delivered from the same company. After casting the concrete, the same fresh and hardened

concrete tests performed for the ready mixed concrete (used in full-scale concrete beams) were carried out to verify that the laboratory cast concrete had the same properties as that of the full-scale beams.

4.5.4 Accelerated corrosion setup and current measurements

The corrosion of steel in a concrete environment is an electrochemical process; it requires an anode, a cathode, an electrolyte, and a contact between the anode and cathode. Several electrochemical techniques have been developed to obtain qualitative information on concrete corrosion processes in a relatively short period of a few weeks. Accelerated corrosion tests have been used successfully to determine the susceptibility of the reinforcing bars and other forms of structural steel for corrosion. In this technique, direct current is impressed into the steel reinforcement so that it becomes the anode, while an auxiliary element serves as a cathode. When a constant voltage is maintained between the anode and cathode, the current level is proportional to the speed of the corrosion process.

After the completion of casting and curing, the concrete beams and cylinders were placed in accelerated corrosion tanks (Figs. 4.17 and 4.18). The accelerated corrosion setup consisted of plastic tanks, electrolytic solution [5% sodium chloride (NaCl) by the weight of water] and a steel mesh placed in the bottom of each tank. Two tanks 2800 mm in length, 1500 mm in width and 500 mm in depth were used to test the four concrete beams, while the small concrete cylinders were placed in a 700 mm long, 700 mm wide and 500 mm deep tank. The concrete beams were partially immersed in the electrolytic solution up to one third of their height (to avoid the corrosion of the top longitudinal bars), while the small cylinders were immersed up to two thirds of their total height. To eliminate any change in the concentration of the NaCl and pH of the solution, the electrolyte solution was changed on a weekly basis.

The bottom steel mesh in each tank and the specimen's steel bars were connected to a 12 VDC power supply. The direction of the current was arranged so that the steel mesh served as cathode while the specimen bars served as anodes (Fig. 4.18). The accelerated corrosion test was continued until two degrees of corrosion occurred. After the power supply was turned on, the current flowing through the system was recorded at 1 hour interval using a computer-controlled data-acquisition system (Fig. 4.19). Based on Faraday's law (4.1), the amount of corrosion is

based on the electrical energy consumed and is a function of current and elapsed time. Therefore, the amount of corrosion can be estimated using equation 4.1, as follows:

$$\text{Mass loss} = \frac{t \times i \times M}{z \times F} \quad (4.1)$$

where

t = the time passed (s)

i = the current passed (Ampere)

M = atomic weight (for iron $M = 55.847$ g/mol)

z = ion charge (2 moles of electrons)

F = Faraday's constant, which is the amount of electrical charge in one mole of electron ($F = 96487$).

4.5.5 Half-cell potential measurements

Half-cell potential measurements were taken periodically at 25 points along the beam's length/perimeter. Figure 4.20 shows the typical layout for the tested points on each beam. This method was first developed in the late 1950's (Stratfull 1957) and has been used extensively since that time. It was adopted in 1977 as an ASTM method C876 (24). It is based on measuring the electrochemical potential of reinforcement against a reference CSE (copper-copper sulfate electrode) placed on a concrete surface (Fig. 4.21). The test instrument outputs a range of values, the more negative the values, the higher the probability of corrosion.

Half-cell potential measurements are usually affected by a number of factors (Klinghoffer 1995). Among these factors is the moisture condition of the concrete cover and its contamination by carbonation and/or chlorides. Also, the oxygen access strongly determines the half-cell reading. For example, low oxygen content resulting from wet surfaces shows low potentials and gives higher negative values. Therefore, it was intended to take biweekly readings for all beams at the same time, and in the same condition, in order to ensure a fair comparison between all beams.

4.5.6 Chloride ions measurements

Chloride ion determination was conducted using a high impedance electrometer with calibrated chloride electrode to measure the chloride content of concrete powders in the extraction solution as a percentage of concrete mass (Fig. 4.22). Five standard samples containing chloride ranging from 0.005% to 0.5% Cl^- -ions were used to calibrate the instrument before use. The concrete powder samples were taken near the bars' surfaces from the same locations tested in half-cell (Fig. 4.20) using an electrical drill. The concrete powders were then weighted, poured in small plastic vials containing extraction liquid and left over the night before testing.

4.5.7 Measurement of mass loss and reduction of bar diameter

After the completion of the designated corrosion stages, the beams were jack hammered and the corroded stirrups and longitudinal bars were removed. The corroded bars were cleaned and scrubbed with wired brush (to ensure that the bars were free from any adhering concrete or corrosion products) then soaked in chemical solution (Fig. 4.23) (1:1 of HCL and water) according to ASTM Standards G1-03 method (2003). The cleaned bars were then weighted and the percentage of mass loss for each bar was calculated based on the equation (4.2) below.

$$\% \text{ of mass loss} = \frac{(\text{initial weight} - \text{final weight})}{\text{initial weight}} \times 100 \quad (4.2)$$

In order to investigate the reduction of bar diameter and mass loss along the length of the beam, each bottom longitudinal bar was cut into 5 segments (Fig. 4.24) then the mass loss and bar diameters along each segment were measured.

Table 4-1: Mixture proportions for SCC and NC mixtures

Concrete type	Type GU Cement (kg/m ³)	Slag (kg/m ³)	10 mm coarse aggregate (kg/m ³)	Fine aggregate (kg/m ³)	Water (kg/m ³)	HRWR mL/100kg of binder	WR mL/100kg of binder
SCC	315	135	900	930	180	Variable to obtain same slump flow	0
NC	300	100	1130	725	160	0	300

* The specific gravity, volatile weight, and pH of the HRWRA were 1.2, 62% and 9.5 respectively

Table 4-2: Physical and chemical analysis of cement

Chemical Analysis (%)		Physical Analysis	
LOI	2.05	Residue 45um (%)	8.42
SiO ₂	19.64	Blaine (m ² /kg)	410
Al ₂ O ₃	5.48	Air Content (%)	7.78
Fe ₂ O ₃	2.38	Initial Set (mins.)	103
CaO	62.44	Auto. Exp. (%)	0.14
MgO	2.48	Sulf. Exp. (%)	0.013
SO ₃	4.32		
Total Alkali	0.97	Compressive Strength (MPa)	
Free Lime	1.03	1 day	19
Insol.	0.6	3 days	29
		7 days	34
		28 days	41
C3S	52.34		
C2S	16.83		
C3A	10.5		
C4AF	7.24		

Table 4-3: Physical and chemical analysis of slag

Chemical Analysis (%)		Physical Analysis	
LOI	0.65	Residue 45um (%)	3.14
SiO ₂	40.3	Blaine (m ² /kg)	422
Al ₂ O ₃	8.4		
		Compressive Strength	
Fe ₂ O ₃	0.5	(MPa)	
CaO	38.71	(50:50 cement:slag)	
MgO	11.06	7 days	24
SO ₃	2.31	28 days	42
K ₂ O	0.57		
Na ₂ O	0.37		
		Slag Activity Index	
		(% of 28 day control)	99.9

Table 4-4: Sieve analysis of coarse and fine aggregate

Sieve #	3/8"	0.265"	No. 4	No. 8	No. 16	No. 30	No. 50	No. 100	No. 200
Opening (mm)	9.5	6.7	4.75	2.36	1.18	0.6	0.3	0.15	0.075
% of passing	100	99.8	96.5	82.8	69.8	51.8	22.1	6	1.5
Standard specifications	Min.	100	95	80	50	25	10		
	Max.	100	100	100	85	60	30	10	3

Table 4-5: Fresh properties of SCC and NC mixtures

Concrete type	Slump (mm)	Slump flow		V-funnel flow time (s)	L-box		
		Flow (mm)	T500 (s)		Index (%)	T200 (s)	T400 (s)
SCC	-	700	3	5.5	90	1.5	2
NC	80	-	-	-	-	-	-

T500: flow time to achieve 500 mm slump flow, T200 and T400: times taken by concrete to travel a horizontal distance of 200 and 400 mm, respectively

Table 4-6: Hardened properties of SCC and NC mixtures

Concrete type	1-day f'_c (MPa)	3-day f'_c (MPa)	7-day f'_c (MPa)	14-day f'_c (MPa)	28-day f'_c (MPa)	28-day f'_{ct} (MPa)	300-d (corroded beams) f'_c (MPa)	300-d (corroded beams) f'_{ct} (MPa)
SCC	15	18	31	38	45	3.8	53	4.3
NC	14	19	32	42	47	4	56	4.4

Table 4-7: Details of experimental beams

Beam designation	Total length (L) mm	Effective span (S) mm	Total depth (h) mm	Effective depth (d) mm	Longitudinal steel ratio ($p_w = 100A_s/bd$) %
1SCC150 1NC150	1050	750	150	102.5	1%
2SCC150 2NC150				100.0	2%
1SCC250 1NC250	1750	1250	250	202.5	1%
2SCC250 2NC250				197.5	2%
1SCC363 1NC363	2340	1815	363	310.5	1%
2SCC363 2NC363				305.5	2%
1SCC500 1NC500	2500	3200	500	447.5	1%
2SCC500 2NC500				442.5	2%
1SCC750 1NC750	4500	3750	750	667.5	1%
2SCC750 2NC750				650.5	2%

A_s = area of longitudinal steel, b = width of the beam = 400 mm, a = shear span = $S/2$

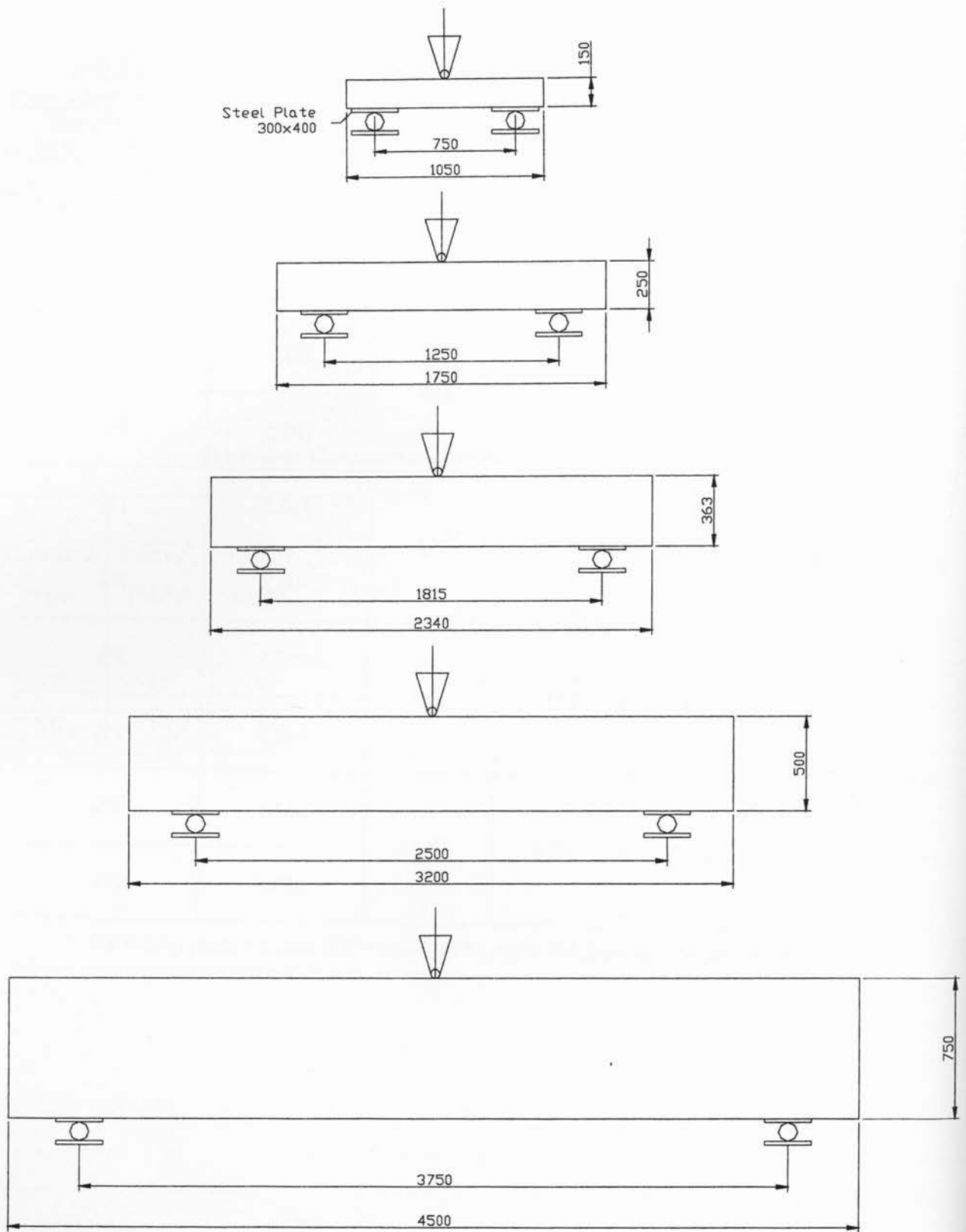


Figure 4-1: Schematic diagram of experimental beam specimens (Dimensions are in mm)

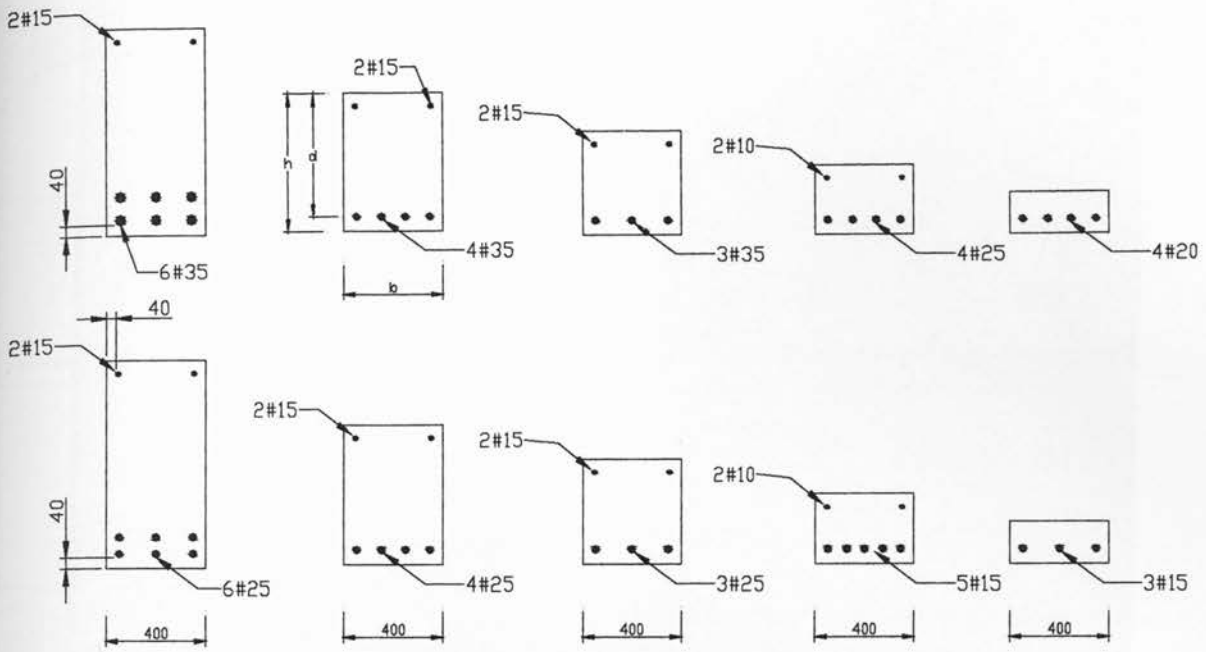


Figure 4-2: Cross sections and reinforcement layout of beams with 1% and 2% ρ_w (mm)

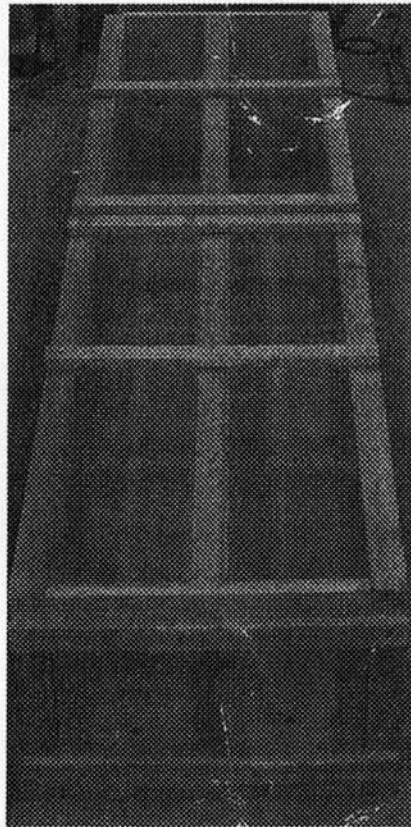


Figure 4-3: 750 mm depth beam formwork (contained 1% and 2% ρ_w)

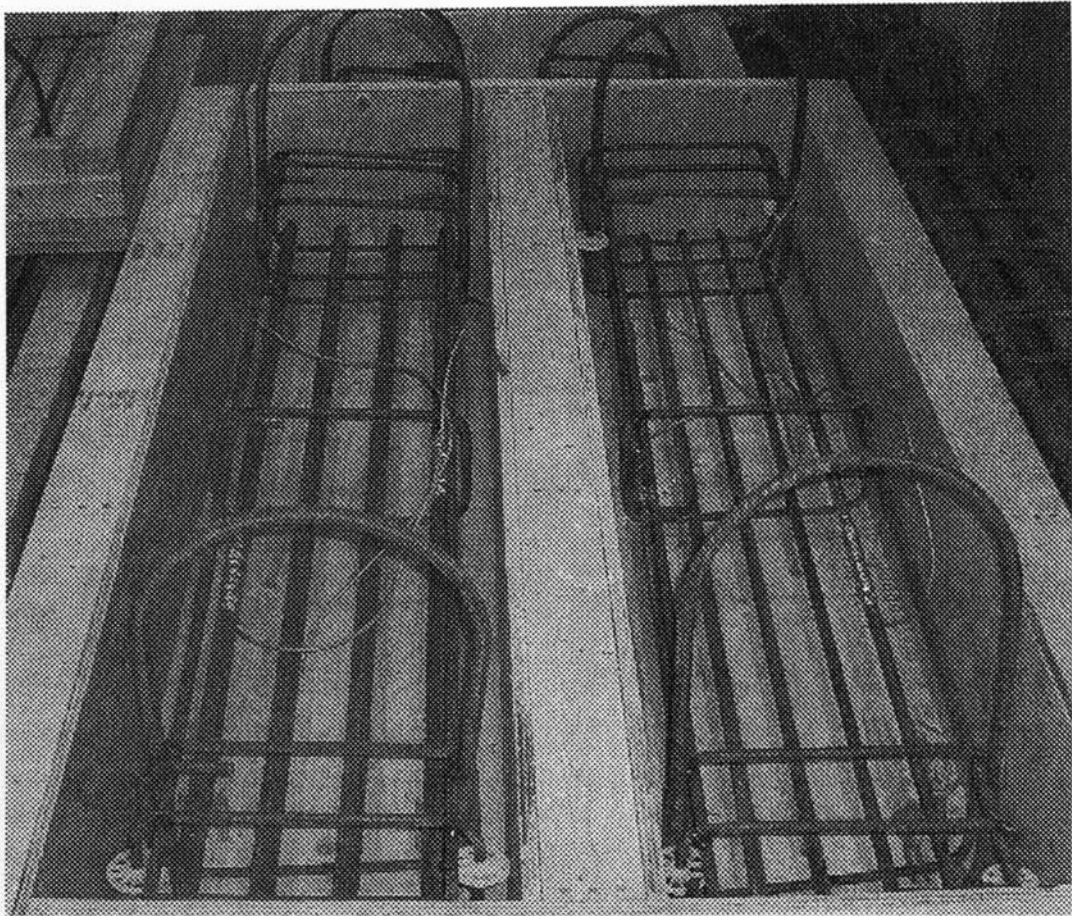


Figure 4-4: Formwork reinforcing bar placement

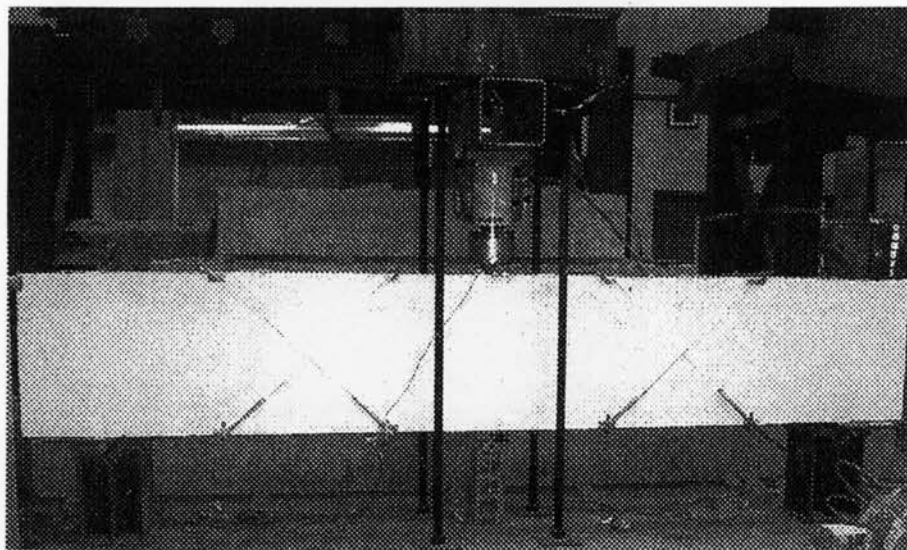


Figure 4-5: Test setup, instrumentation and testing of a beam specimen (shear test)

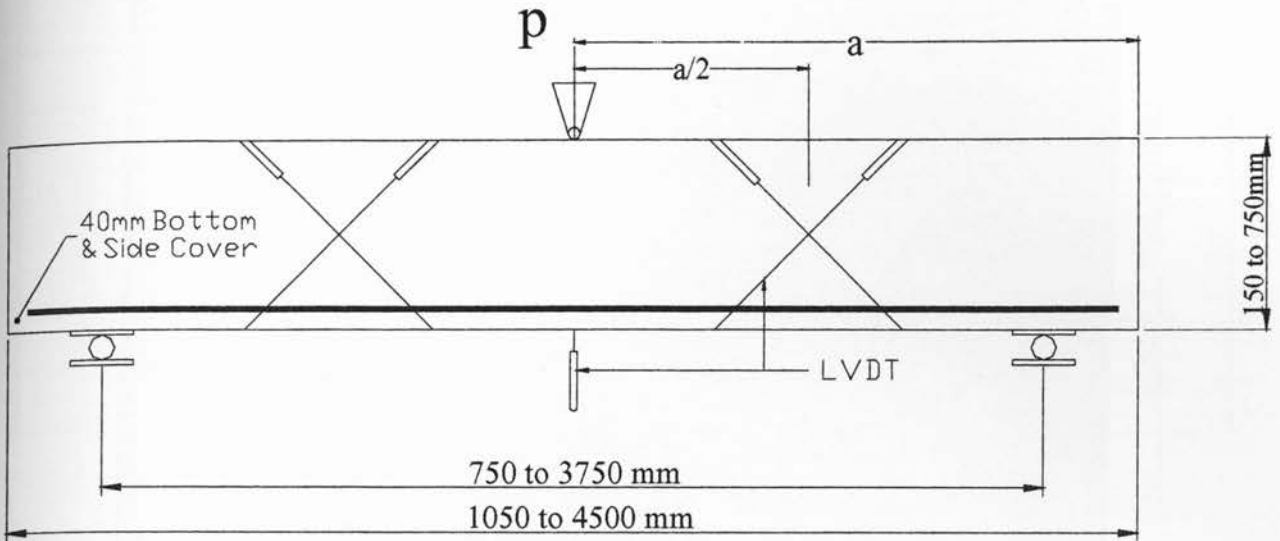
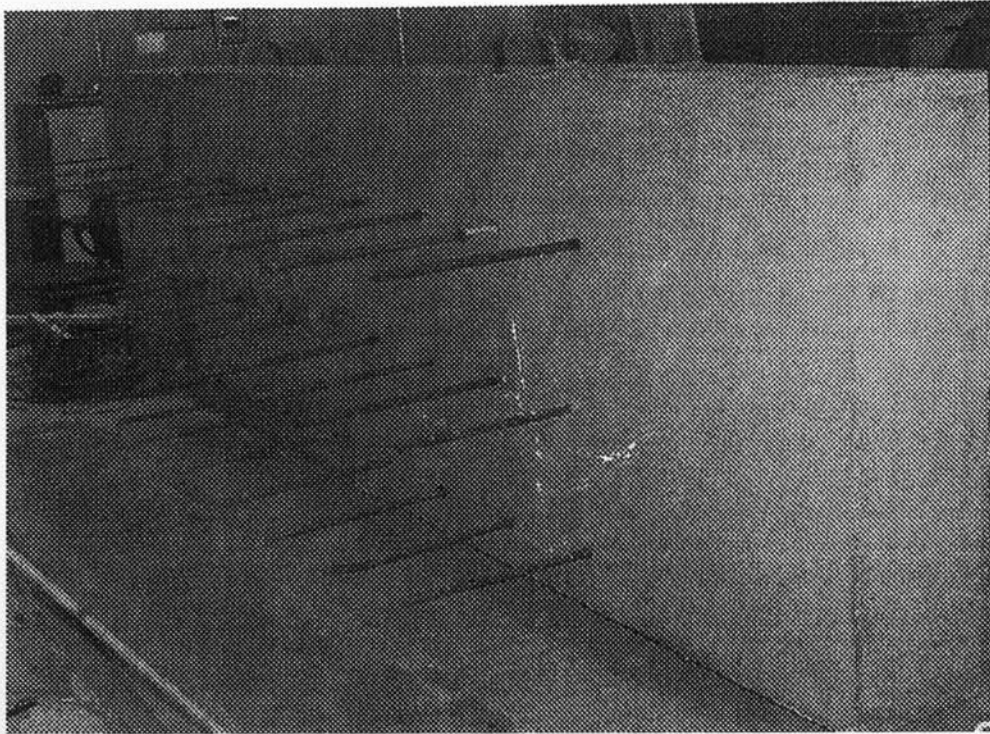
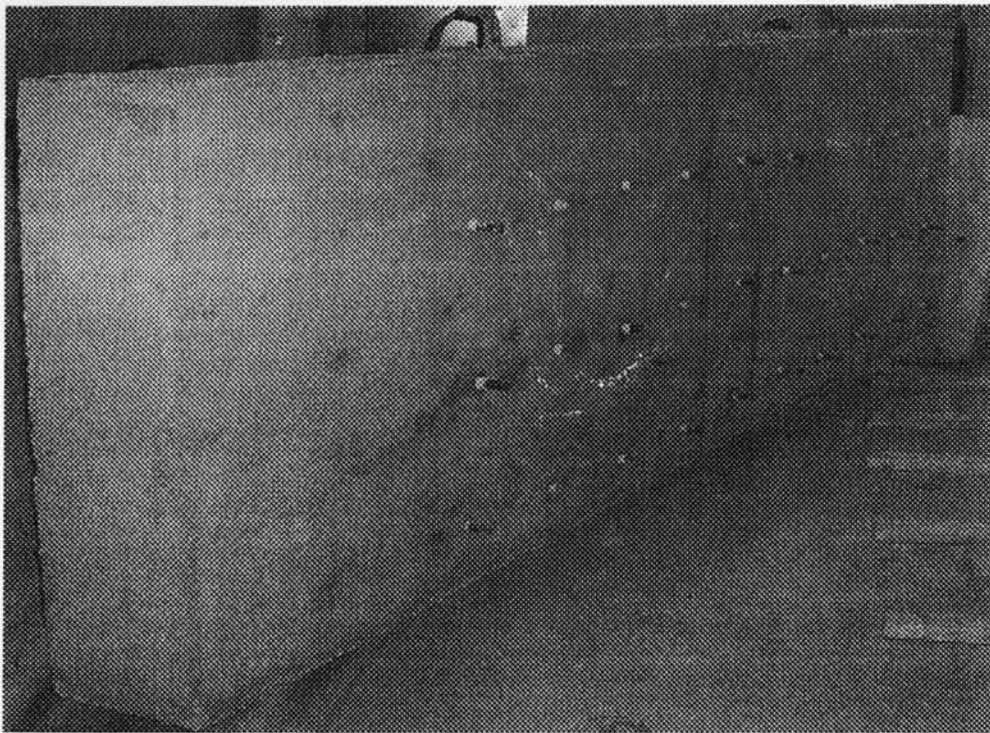


Figure 4-6: Schematic diagram of the shear test beam specimens



(a)



(b)

Figure 4-7: Beam specimens; (a) Front view, (b) Back view (bond test)

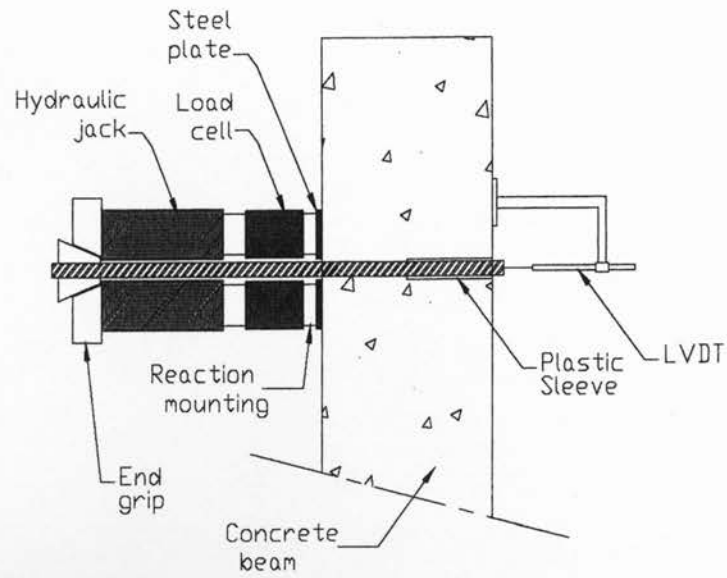


Figure 4-9: Schematic diagram of the pull out test setup

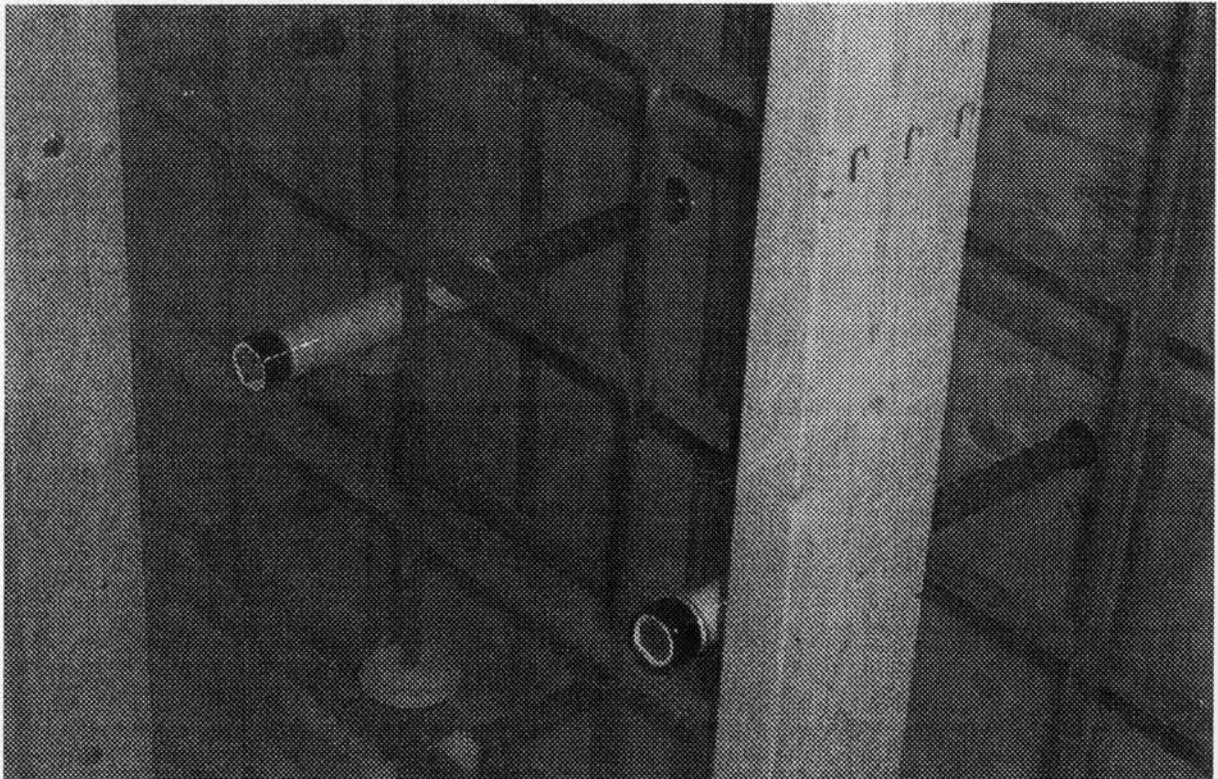


Figure 4-10: Plastic sleeve covering 150 mm of the pull out bar to insure only 150 mm of the bar is in contact with the concrete



Figure 4-11: Transparent plastic front side of the bond test formwork

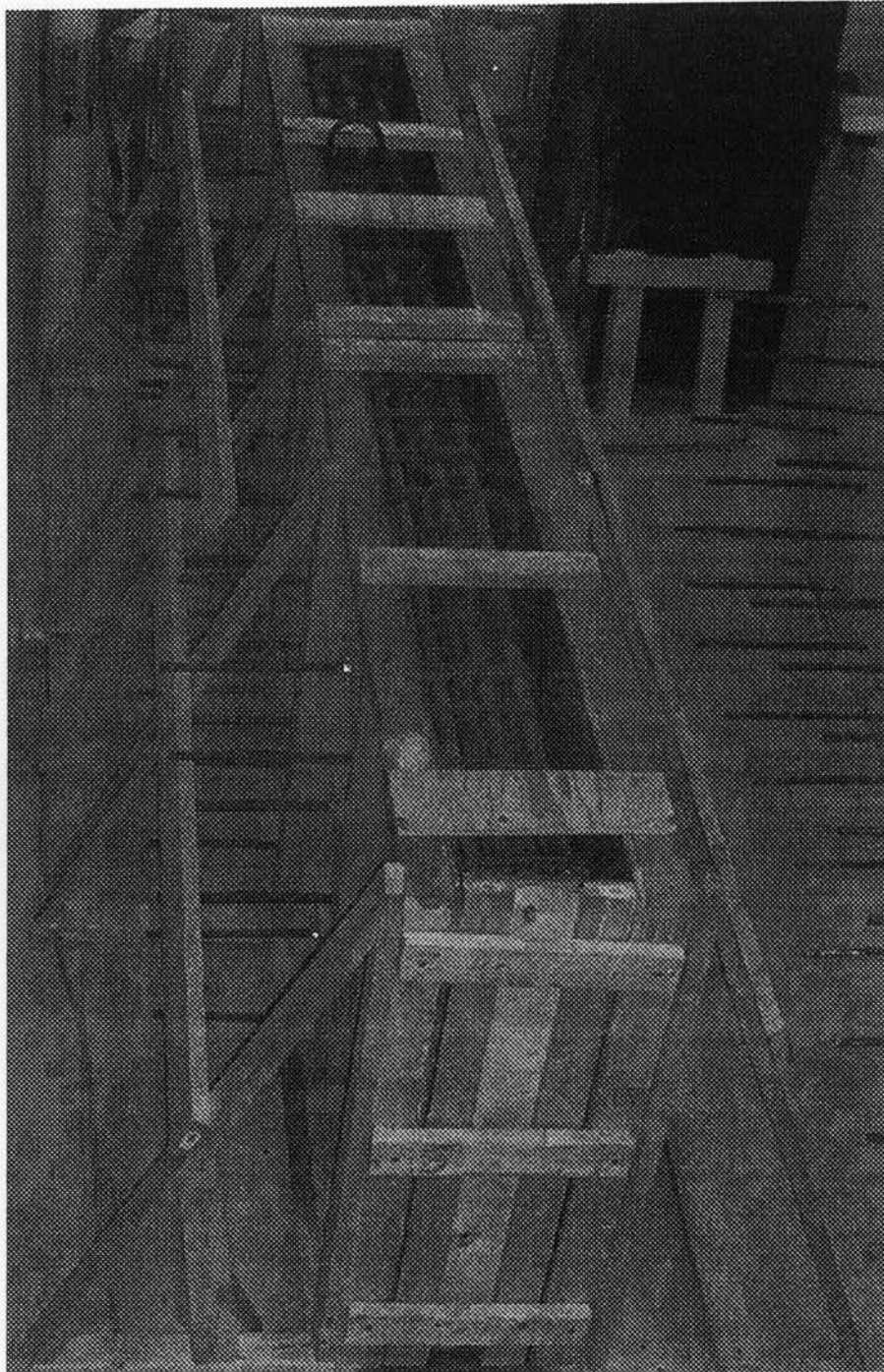
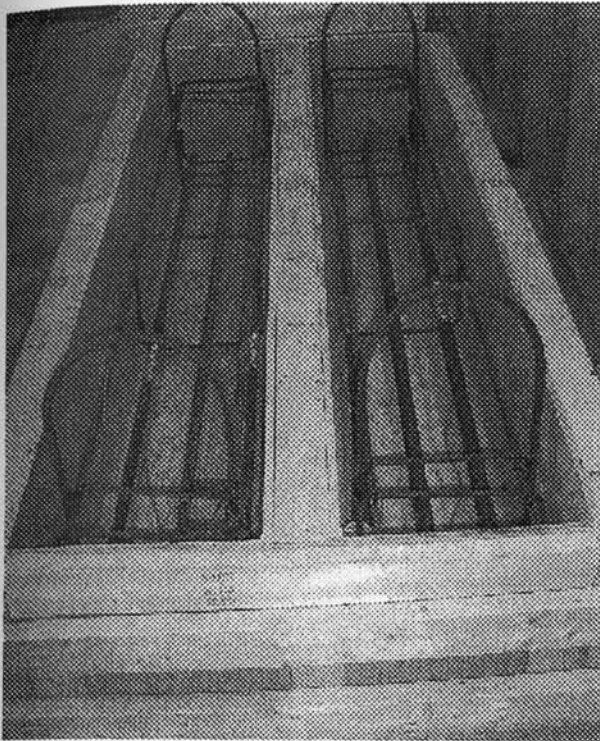
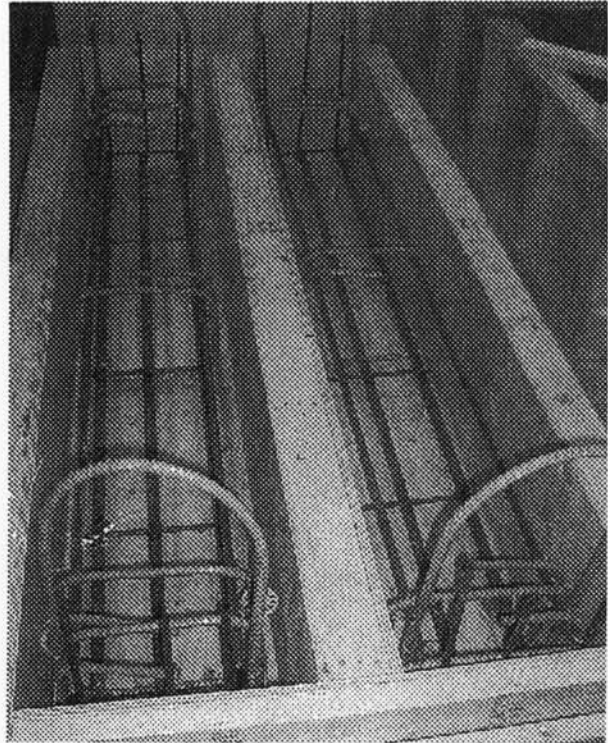


Figure 4-12: Formwork details of the bond test specimen



a)



b)

Figure 4-13: Formwork details for corrosion test beams a) non-epoxy coated stirrups for moderate corrosion stage b) epoxy-coated stirrups for severe corrosion stage

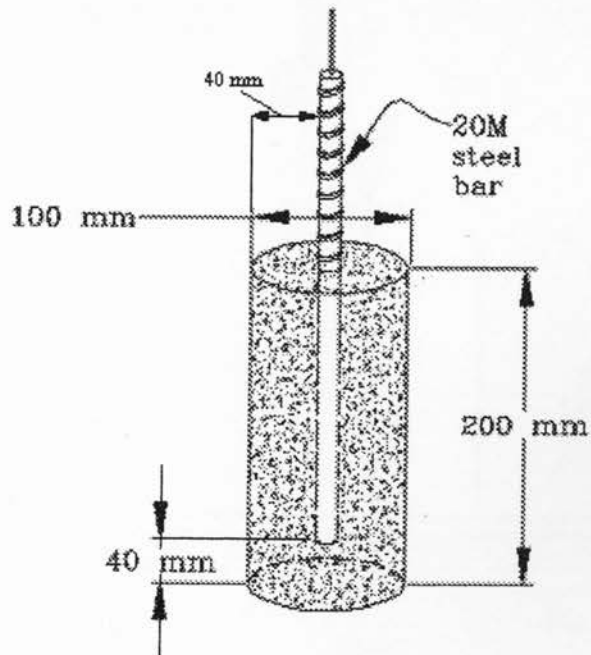


Figure 4-14: Cylinder sample for corrosion tests

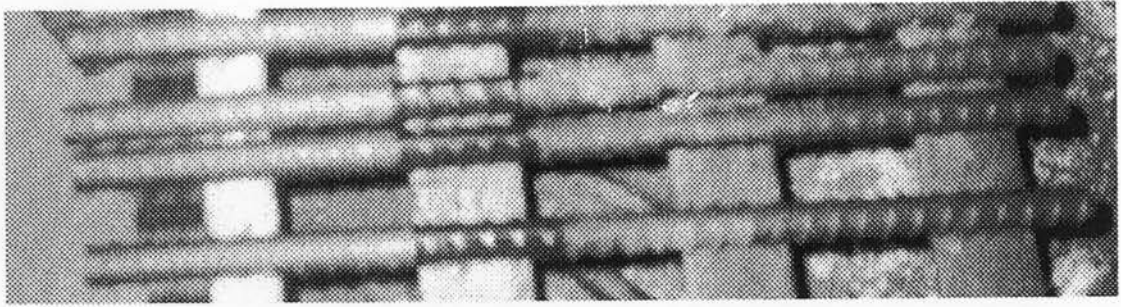


Figure 4-15: Steel bars preparation

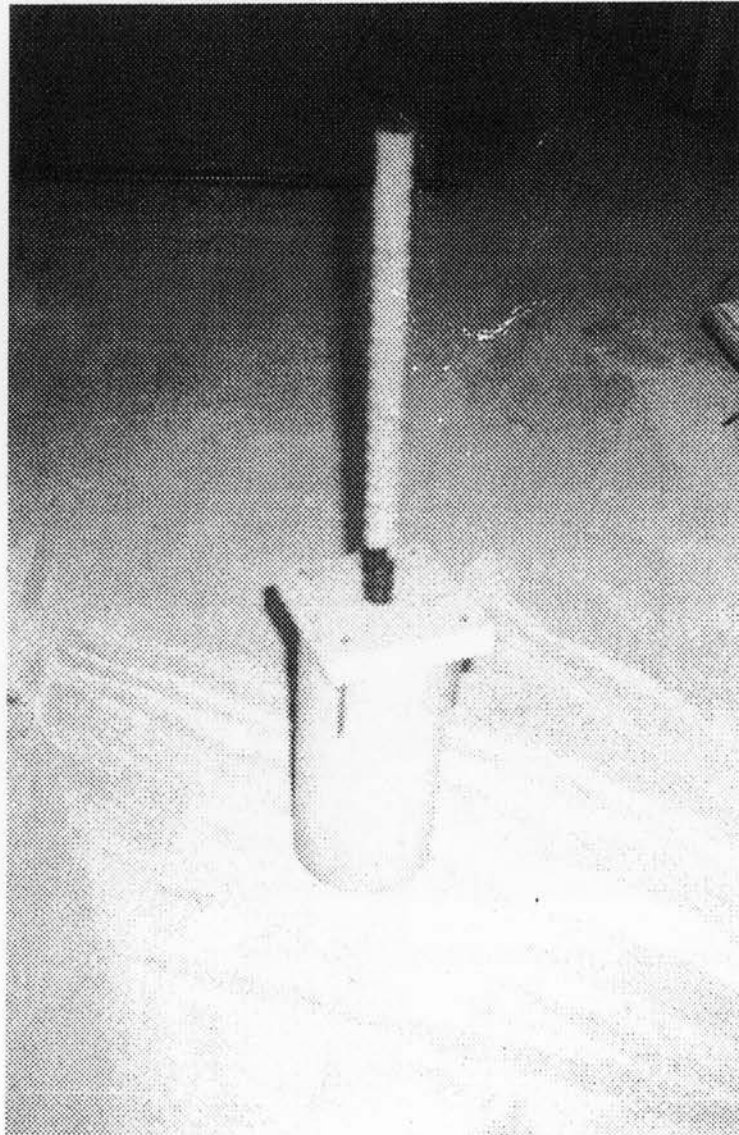


Figure 4-16: Adjustment of the bar verticality

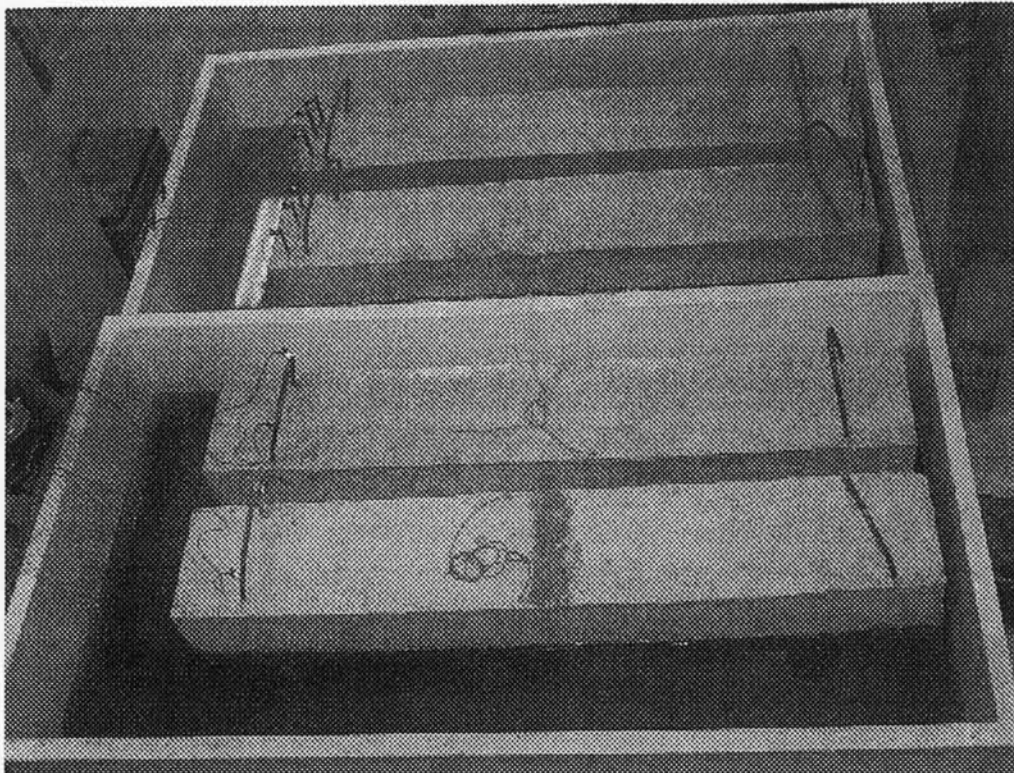


Figure 4-17: Accelerated corrosion tank for corrosion test

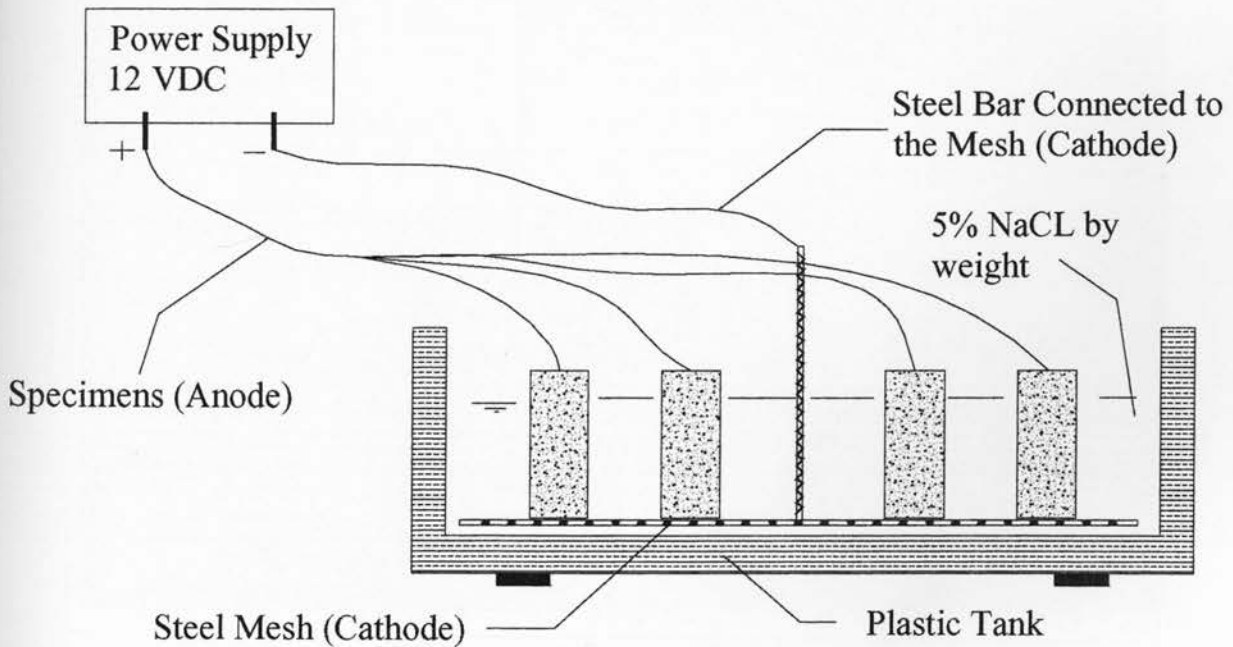


Figure 4-18: Schematic diagram of the accelerated corrosion test

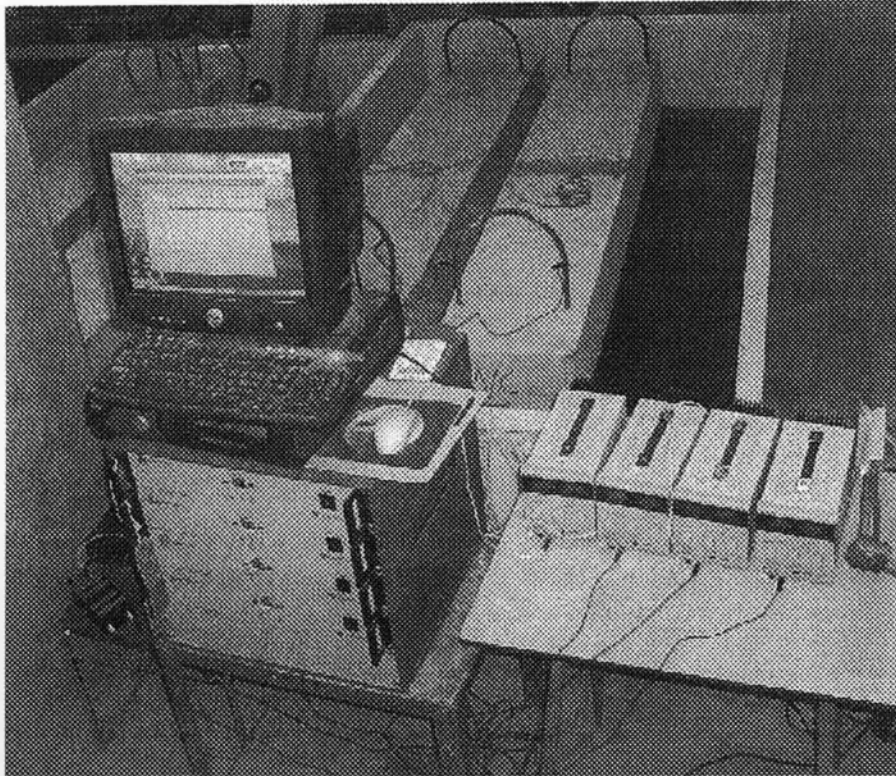
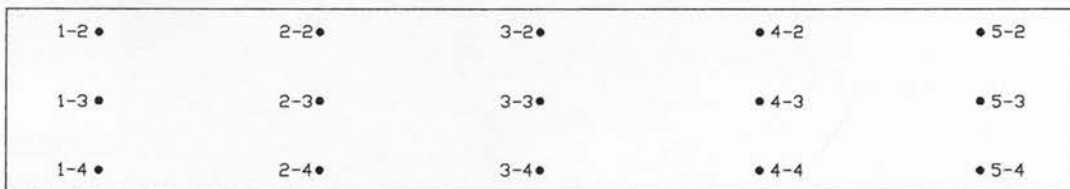
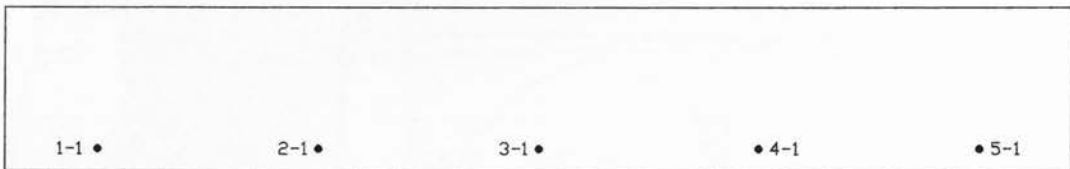


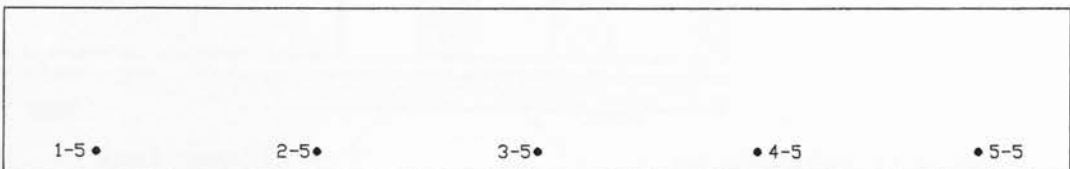
Figure 4-19: Corrosion current monitoring by data-acquisition system



Bottom view of the beam



Front view of the beam



Back view of the beam

Figure 4-20: Typical layout of the tested points along the beam length/perimeter

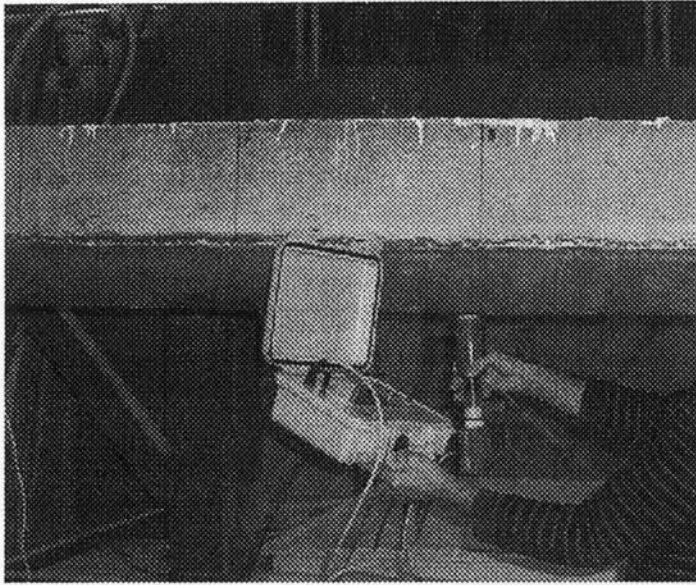


Figure 4-21: Half-cell potential measurements



Figure 4-22: Chloride ion electrometer for measuring the chloride ion content

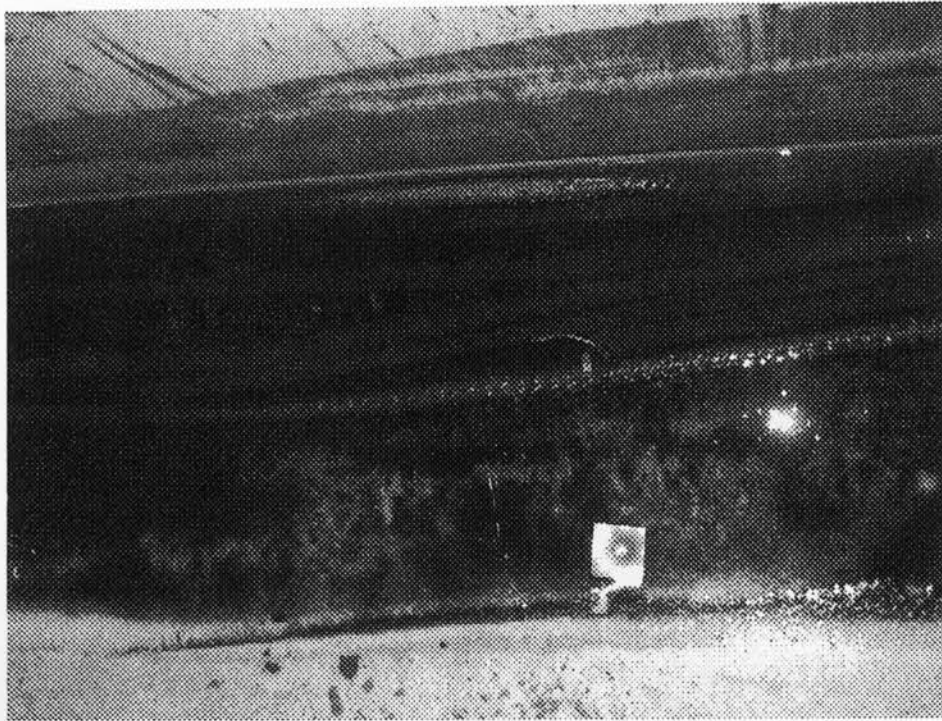


Figure 4-23: Cleaning the embedded bars with HCL before measuring the mass loss

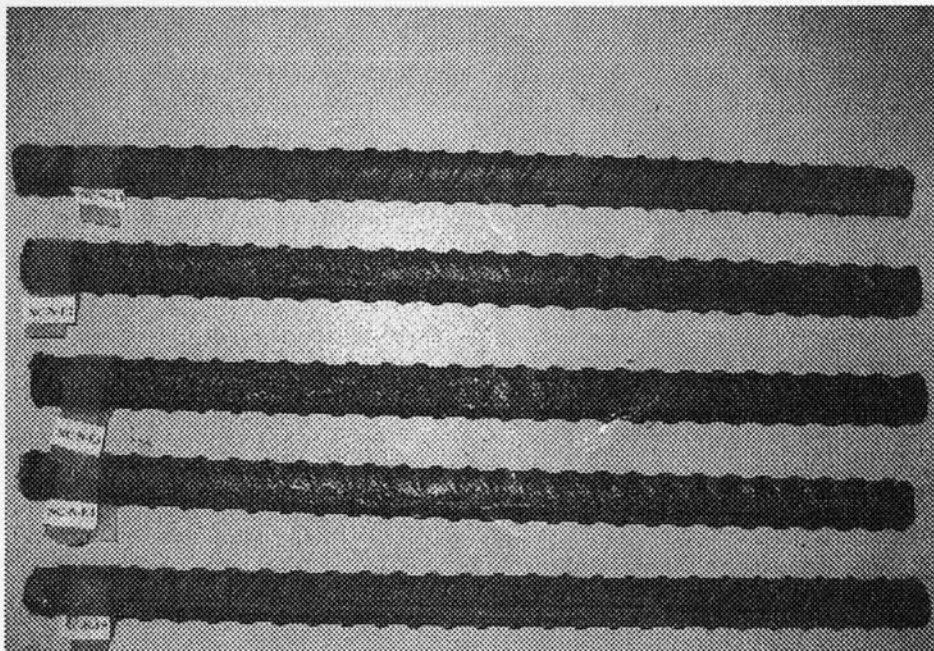


Figure 4-24: Embedded longitudinal bar segments for measuring the mass loss

5 Shear Resistance - Results and Discussion

5.1 Shear behavior of large-scale SCC beams

5.1.1 Cracking and failure characteristics

Figure 5.1 shows pictorial view of the shear failure of experimental SCC/NC beams having varying depths. Cracks are outlined with a black felt tip marker. The crack width was also determined and labeled at each loading stage. Figures 5.2-5.11 show schematic diagrams of all SCC/NC beams showing crack patterns and crack widths at 50% and 75% of the total failure load, as well as at failure.

As expected, during the early stages of loading, fine vertical flexural cracks appeared around the mid-span of all of the beams. With an increase in load, new flexural cracks formed away from the mid-span area. With a further increase in load, the flexural cracks started to propagate diagonally towards the loading point and other new diagonal cracks began to form separately in locations farther away from the mid-span along the beam (Figs. 5.2-5.11). In most cases, shear failure of the beams occurred shortly after a dominant diagonal shear crack (within one shear span or zone) extended to the top fiber. At the point of shear failure, the volume of the sound of crushing was positively related to the size of the beams. The larger beams were louder than the smaller beams.

In both SCC and NC beams, cracks extended up to 50% of the beam depth at 50% of the failure loading while up to 70% of the beam depth at 75% of the failure loading. The angle for the early diagonal dominant shear cracks was around 55° (to the beam longitudinal axis). The angle of the failure diagonal cracks was around 35° .

5.1.2 Cracking load and crack width characteristics of SCC/NC beams

The first flexural cracking load was visually observed and then compared with values associated with a change in the slope of the load-deflection and load-longitudinal steel strain curves, obtained from the test. The formation of the first diagonal crack was also observed visually during the loading, and was also verified most of the time by sudden jumps in the elongation for any of the four diagonal LVDT's mounted on the surface of the beam (Figs. 4.5, 4.6). Table 5.1 presents the loads at failure and first flexure/shear crack, number of cracks, crack height and the failure crack width of all SCC/NC beams.

As expected, no significant difference was observed between the behavior of SCC and NC beams, with respect to the first flexural crack load (Table 5.1). The ratio of the first flexural crack load to the failure load increased with the increase of beam depth in SCC/NC beams having 1% or 2% steel reinforcement (Table 5.1). First flexural crack load for SCC beams varied from 21% to 38% of the failure load (from shallow to deeper beams) compared with 20% to 33% of NC beams.

The first diagonal dominant shear cracks were developed around 32% of the failure load for shallow beams, compared to 60% of deep beams (Table 4). The failure crack widths varied from 1 to 3 mm in shallow beams while crack width of up to 27 mm was observed in deeper beams. In general, SCC beams exhibited slightly fewer cracks than NC beams. The number of diagonal shear cracks was also lower in SCC beams, compared to NC beams. Otherwise, no significant difference was noted between SCC and NC beams in terms of crack widths, crack heights, crack angles or overall failure mode.

From Table 5.1, it can be seen that the percentage ratio of the first diagonal crack load to the failure load in SCC beams increased from 34% to 65% with the increase of beam depth from 150 mm (shallow beam) to 750 mm (deep beam), compared with 32% to 54% increase of the corresponding NC beams. This indicates that SCC beams had lower post-diagonal cracking shear resistance capacity (derived from aggregate interlock plus dowel action) compared to NC beams. Generally SCC/NC beams with lower steel ratio (1%) developed wider crack widths during loading stages and at failure, compared to those with higher steel ratio (2%). This was expected, as the presence of higher longitudinal steel ratio increases the resistance for the cracks to open wider, and to extend vertically. The average height of cracks before failure was more in beams with 1% reinforcement steel ratio (71% of the beam height) compared to beams with 2% reinforcement steel ratio (63% of the beam height). In general, cracks extended vertically up to the theoretically calculated neutral axis for each cracked SCC/NC beams (with both 1% and 2% steel reinforcement) with a maximum difference of 10%.

5.1.3 Shear resistance characteristics of SCC/NC beams

To analyze and compare the shear strength of beams, the ultimate shear load (V_u) is normalized to count for the difference in compressive strength between SCC and NC. Since the

shear strength is proportional to the square root of the compressive strength of concrete (f'_c), the normalized shear load (V_{nz}) was calculated as follows:

$$V_{nz} = \frac{V_u}{\sqrt{f'_c}} \quad (5.1)$$

The normalized shear stress (v_{nz}) is then calculated as:

$$v_{nz} = \frac{V_{nz}}{bd} \quad (5.2)$$

Normalized shear load and stress for all experimental SCC/NC beams are tabulated in Table 5.2.

5.1.4 Influence of concrete type, beam depth and longitudinal steel ratio on normalized shear load (V_{nz})

While the shear span to total depth ratio (a/h) of all beams was kept constant, the shear resistance of beams was found to depend on the type of concrete, beam depth and longitudinal steel ratio. Figures 5.12 and 5.13 show the variation of normalized shear load (V_{nz}) and normalized ultimate shear stress (v_{nz}) of SCC/NC beams, having varying depths and longitudinal steel ratios. In general, SCC beams exhibited lower V_{nz} compared to NC beams for all beam depths (ranging from 150 to 750 mm) and for both longitudinal steel ratios (1% and 2%) (Fig. 5.12). V_{nz} also increased with the increase of beam depth and longitudinal steel ratios, for both NC and SCC.

The normalized ultimate shear stress (v_{nz}) decreased with the increase of beam depth for both SCC and NC beams (Fig. 5.13). When the beam depth increased from 150 to 750 mm, the normalized shear stress of beams with 1% steel reinforcement decreased by 32% for SCC compared to 23% for NC. Similarly, when the beam depth increased from 150 to 750 mm, the normalized shear stress of beams with 2% steel reinforcement decreased by 22% for SCC compared to 20% for NC.

Higher shear resistance of NC beams compared to their SCC counterparts was observed in beams having larger depths and lower longitudinal steel reinforcement ratio (Figs. 5.12 and 5.13). The maximum difference in shear resistance was observed in 1NC750 beam which showed 17% higher V_{nz} compared to its SCC counterpart 1SCC750.

The portion of the shear transfer through aggregate interlock, which normally represents up to 50 % of the total shear transfer, is greatly affected by the coarse aggregate content. In this

study, NC contains 25% more coarse aggregate than SCC. Hence, the reduction in coarse aggregate content in SCC beams is believed to be the main reason for lower ultimate shear resistance in SCC beams than the NC beams.

Figure 5.14 shows the variation of the percentage ratio $r_L (=100 \times V_{nz-NC}/V_{nz-SCC})$ of normalized ultimate shear load of a NC beam (V_{nz-NC}) to that of a SCC beam (V_{nz-SCC}) with beam depth and longitudinal steel ratio. In general, the ratio r_L increased with the increase of beam depth and the rate of increase was much higher for beams containing 1% longitudinal reinforcement, compared to those with 2%. Beams containing 1% reinforcement showed higher r_L compared with those containing 2% reinforcement, irrespective of beam depth. For an increase of steel ratio from 1% to 2%, the ratio r_L increased from 2% to 3% for 150 mm deep beams compared with corresponding 5% to 17% for 750 mm deep beams. This indicates that SCC beams have lower shear strength compared to NC beams and the lowering of strength increases with the increase of beam depth and with the decrease of reinforcement ratio. However, for shallow beams (for example, beam depth of 150 mm), the influence of type of concrete and reinforcement ratio on the shear strength seems to be negligible for the range of beams tested in this study.

As mentioned before, the shear is transferred in a cracked beam through the aggregate interlock in the lower cracked part of the beam (tension zone), resistance of un-cracked concrete in compression zone, and dowel action of the longitudinal steel. For beams having higher longitudinal steel reinforcement, the post-cracking shear resistance through the dowel action, and the un-cracked concrete in compression zone, are higher compared to beams having lower longitudinal steel reinforcement. The portion of the shear transfer through aggregate interlock in post-cracking stage is less for beams with higher reinforcement ratio which is beneficial for SCC because of its weaker aggregate interlock mechanism due to the presence of lower coarse aggregate. This explains why beams containing 1% reinforcement showed higher r_L compared to those with 2%.

Higher shear resistance of NC beams compared to SCC beams with the increase of beam depth (as evident from the increase of r_L with the increase of beam depth in Fig. 5-14) can also be attributed to the development of longer and relatively wider cracks in deeper beams. This means a higher portion of post-crackling shear transfer through aggregate interlock is warranted compared to shallow beams (MacGregor and Bartlett). As SCC generates lower shear resistance

through aggregate interlock, the overall shear resistance of an SCC beam decreases with the increase of the beam depth, compared to its NC counterpart.

5.1.5 Performance of Code-based shear prediction of SCC beams

The ultimate shear resistances of experimental SCC/NC beams without shear reinforcements are calculated based on Code-based equations. In this study, performance of ACI and CSA based design equations is studied.

As per ACI (2005), the ultimate shear resistance (V_u) of beams without shear reinforcements at diagonal (inclined) cracking (where M_f occurs simultaneously with V_f at a section) can be obtained by:

$$V_u = 0.16\sqrt{f'_c} b d + 17\rho_w \frac{V_f d}{M_f} b d \leq 0.29\sqrt{f'_c} b d \quad (5.3)$$

Where:

V_f is the factored shear force at section

M_f is the factored moment at section

b is the beam width

d is the effective depth of beam cross-section

As per CSA specification (2004), the shear resistance (V_u) for beams without shear reinforcements can be obtained as (general method):

$$V_u = \beta\sqrt{f'_c} b d_v \quad (5.4)$$

The factor β can be calculated as:

$$\beta = \frac{520}{(1 + 1500\varepsilon_x)(1000 + S_{ze})} \quad \text{and} \quad S_{ze} = \frac{35S_z}{15 + a_g} \leq 0.85S_z \quad (5.5)$$

Where:

d_v is effective shear depth which can be taken as the greater of $0.9d$ or $0.72h$

ε_x is the longitudinal strain at mid-depth of the member due to factored loads which can be

derived as $\varepsilon_x = \frac{M_f/d_v + V_f}{2E_s A_s}$

E_s is the modulus of elasticity of non-prestressed reinforcement

$S_z (= d_v)$ is the crack spacing parameter dependent on crack control characteristics of longitudinal reinforcement

A_s is the area of non-prestressed tension reinforcement in the beam

a_g is the maximum size of aggregate in concrete

Table 5.3 presents the ultimate shear load derived from experiments and Code-based predictions. Figures 5.15 through 5.18 compare the performance of Code-based equations (ACI - Eq. 5.3 and CSA- Eq. 5.4) in predicting the ultimate shear load (V_u) of SCC/NC beams having 1% and 2% ρ_w and no shear reinforcements. CSA (Eq. 5.4) under predicted the ultimate shear strength of SCC/NC beams irrespective of beam depth (150 to 750 mm) and longitudinal reinforcement ratio (1% and 2%) as the ratio of experimental to CSA predictions ranged between 0.54 and 0.81 with a mean value of 0.68 (Table 5.2 and Figs. 5.15-5.18). In general, CSA is more conservative than ACI (its conservativeness increases with the increase of beam depth) and can be used safely for the prediction of ultimate shear resistance of both SCC and NC beams, as confirmed from this study.

ACI equation is found to safely predict the ultimate shear strength of NC beams with 2% reinforcement (ratio ranges between 0.56 and 0.95). The ratio of ACI predicted to experimental values for NC beams with 1% reinforcement started with 0.59 for 150 mm beam depth and increased to 1.03 for the 750 mm beam depth. ACI equation may not be safe for NC beams with larger depth and low longitudinal reinforcement.

The ratio of the ACI predicted to the experimental values ranges between 0.63 (for 150 mm beam depth) and 1.23 (750 mm beam depth) for SCC beams with 1% reinforcement and between 0.58 (for 150 mm beam depth) and 1.02 (for 750 mm beam depth) for beams with 2% reinforcement. The ACI equation is found to be conservative for SCC beams up to a beam depth of 363 mm (for beams with 1% longitudinal reinforcement) and 500 mm (for beams with 2% longitudinal reinforcement), while it over predicts the shear strength of deeper beams.

5.2 Cracking and deflection characteristics of large-scale SCC beams

5.2.1 Experimental and theoretical analyses of crack width

The current Canadian Code and early ACI 318 provisions handle the crack width based on Gergely and Lutz equation (Gergely and Lutz 1973) presented as Equation 5.6:

$$w = 11 \times 10^{-6} \beta f_s \sqrt[3]{d_c A} = 11 \times 10^{-6} \beta z \quad (5.6)$$

where

$$z = f_s (d_c A)^{1/3}$$

w = crack width in mm

β = distance from the neutral axis to the bottom fiber divided by the distance to the centre of tensile reinforcement

f_s = stress in the longitudinal reinforcement in MPa

d_c = distance from the extreme tension fiber to the centre of the reinforcing bar located closest to it in mm

A = effective tension area of concrete surrounding the tension reinforcement and having the same centroid as that reinforcement, divided by the number of bars or wires in mm^2

Equation 1 was derived statistically from the maximum crack widths at flexural tension surface of members, based on the data obtained from a number of investigations (Gergely and Lutz 1973), and was intended to predict the "maximum crack width". It should be noted that, because of the large scatter in the crack widths data, 10% of the measured crack widths used to derive Eq. 5.6 exceeded 1.5 times the values given by the equation, while 2% were less than 0.5 times the calculated width (MacGregor and Bartlett 2000).

Table 5.3 compares the experimental and calculated (predicted) crack widths from Eq. 1 for both NC and SCC beams with 1% and 2% ρ_w . Crack widths are predicted at three load levels: 50%, 75% and 100% of the failure load. There is an overall agreement between NC and SCC beams in terms of crack widths. The difference in the experimental crack width values between SCC and NC was more pronounced at 100% compared to 50% of failure load. The average difference between SCC and NC in all experimental crack widths was about 0.05 mm.

Figures 5.19 and 5.20 show the percentage ratio of the calculated (predicted) crack widths to the experimental values for both NC and SCC beams. The investigation found that the calculated crack width values were close to those obtained from the experiments on both the 1% or 2% ρ_w NC and SCC beams when applying up to 50% of the failure load. As the applied load increases (75% to 100% of the failure load), the calculated crack widths significantly exceed the experimental values.

The close results between the calculated and the experimental crack width, up to around 50% of the failure load, can be attributed to the fact that fine flexural cracks formed in the mid span (as explained earlier) open wider as the load increases up to around 50% of the failure load.

Widening of these cracks is reduced or stopped with further increase in load (> 50% of the failure load), due to the formation of new diagonal cracks formed away from the mid span.

Up to 50% of the load, the maximum crack width was predominantly governed by flexural (F) cracks (Table 5.3). Beyond 50% of the failure load, crack width is governed by the interaction of diagonal and flexural cracks. Eq. 5.6 seems to provide good prediction when crack width is governed by flexural cracks resulting from flexural failure of beams. As in practice RC, beams are designed for flexure rather than shear failure.

For the case of experimental beams (designed for shear failure), the shear failure resulting from diagonal cracks did not allow flexural cracks to grow wider (as is the case for a flexural mode of failure) causing calculated crack widths significantly higher than the experimental values.

The variation of the ratio " β " used in Eq. 5.6 with beam depth and ρ_w is shown in Fig. 5.21. The value of β is relatively high in shallow (small size) beams ($\beta = 1.93$ in 2NC150), while it is found lower in deeper (large size) beams ($\beta = 1.21$ in 1NC750). The Canadian Code limits the value of z in Eq. 5.6 to 30000 N/mm, for interior exposure, and 25000 N/mm, for exterior exposure (CSA A23.3. 2004). This limitation was established assuming a constant value of 1.2 for β , in order to limit the critical crack width to 0.40 and 0.33 mm for interior and exterior exposure, respectively (MacGregor and Barlett 2000).

As per Figure 5.21, the mean value of β for beams having 1% ρ_w and beam depth greater than 250 mm is 1.21, which closely matches the value ($\beta = 1.2$) assumed in A23.3. For beams having 2% ρ_w and beam depth greater than 250mm, the experimental mean value of β is found to be 1.29 (higher than 1.2). This leads to a lower estimation of z values than those obtained from CSA A23.3, in order to obtain critical crack widths of 0.40 and 0.33 mm for interior and exterior exposure, respectively. For beams with less than 250 mm depth, the assumption of a constant value of β (= 1.2), as per in CSA A23.3, is found to be significantly lower than the values obtained from experiments.

5.2.2 Experimental load-deflection response and strength characteristics

5.2.2.1 Experimental load-deflection response

The load-central deflection responses of SCC and NC beams (shown in Figs. 5.22 through 5.41) showed a similar trend of variation with an overall agreement. The load and

deflection were recorded at first flexural and diagonal crack, as well as at various load levels (50%, 75% and 100% of failure load). Load-deflection responses are associated with a change in stiffness due to the formation of a first flexural crack, diagonal crack and subsequent development and propagation of both types of cracks. The first flexural cracking load is marked by the first step or slope change in load-central deflection response (Figs. 5.22 through 5.41), as well as load-longitudinal bar strain curves. For SCC/NC, beams with 1% ρ_w showed higher deflection compared to those with 2% ρ_w . The presence of several peaks in the load-deflection response of some beams could be related to the formation of additional relatively wide and extended diagonal cracks before failure while the presence of single peak reflects the formation of a single failure diagonal crack.

Table 5.4 summarizes the total experimental load at first flexural crack as well as the total load and deflection at first diagonal crack and at failure. The first cracking loads for both NC and SCC are more or less the same and also, the effect of ρ_w (between 1% and 2%) in the two concrete mixtures was found to be insignificant.

Table 5.5 represents the longitudinal steel strains at mid-span and central deflections at three stages of loading (50%, 75%, and 100% of the failure load). In general, strain in longitudinal steel, at different load levels, decreases with the increase in beam depth and decreases with the increase of ρ_w . The longitudinal steel strain development in both SCC and NC beams are found to be similar. Longitudinal steel in all the beams, except 1NC150 and 1SCC150, did not reach yielding, as the beams were designed to fail in shear.

5.2.2.2 Post-cracking shear resistance and ductility

The ultimate shear resistance of concrete (V_u), in such beams, is the sum of shears derived due to (ASCE-ACI Committee 445 1998): (i) un-cracked concrete at the development of first shear (diagonal) crack (V_d), or un-cracked portions of cracked members, (ii) aggregate interlock between two slip surfaces (in a prominent diagonal crack) in the cracked portion of the beam whose contribution to the shear resistance is dependent on the crack width and the jaggedness of the slip surfaces; and (iii) dowel action of the longitudinal steel reinforcement which resists part of the shear displacement, depending on the relative stiffness of the portion of the bar crossing the crack. The mechanisms of aggregate interlock and dowel action play significant roles in the increase of shear resistance from V_d to V_u . To characterize the

performance of SCC and NC, it is important to analyze the post cracking shear resistance of concrete beams due to aggregate interlock and dowel action, which can be described by % ratio of V_u to V_d ($=100V_u/V_d$) as shown in Figure 5.42.

As the beams depth increases from 150 mm (shallow beam) to 750 mm (deep beam), the % ratio of V_u to V_d in SCC beams decreases from 298% to 147% and from 304 to 154 % in 1% ρ_w and 2% ρ_w beams, respectively. In NC beams, this ratio decreases from 308% to 174% and from 336% to 186% with 1% ρ_w and 2% ρ_w , respectively. This supports the development of lower post cracking shear resistance in SCC, due to lesser aggregate interlock which is a consequence of the presence of 25% lower coarse aggregate compared to NC. The influence of increase in longitudinal reinforcement on post-diagonal cracking shear resistance is minimal.

Figure 5.43 presents the post cracking shear ductility expressed as % ratio of deflection at peak (failure) load (δ_u) to first diagonal crack deflection (δ_d) ($= 100 \delta_u / \delta_d$). As the beam's depth increases from 150 mm (shallow beam) to 750 mm (deep beam), the % ratio of δ_u to δ_d in SCC beams decreases from 416% to 188% and from 571% to 165 % in 1% ρ_w and 2% ρ_w beams, respectively. In NC beams, however, this ratio decreases from 580% to 307% and from 735% to 227% with 1% ρ_w and 2% ρ_w , respectively. This indicates that post cracking shear ductility of NC beams is higher, compared to their SCC counterparts. The difference between SCC and NC is more pronounced in beams with lower steel ratio (ρ_w). The shear ductility also increases with the increase of longitudinal reinforcement in both SCC and NC beams.

Shear design of beams should take into account the consequences of such reduced post cracking shear resistance and ductility of SCC mixture that contains lower amount of coarse aggregate compared to NC.

5.2.3 Theoretical formulations of load-deflection response

ACI and Euro Code-based procedures are used to calculate load-central deflection of SCC/NC beams. Based on ACI Code (ACI Committee 318 2005), the mid span deflection is computed by the usual method for elastic deflection, taking into consideration the effect of cracking and reinforcement on member stiffness. The elastic formula used to calculate the total deflection in this study is as follows:

$$\Delta = \frac{PL^3}{48E_c I_e} + \frac{VQ}{I_e tG} * \frac{L}{2} \quad (5.7)$$

Where:

Δ = total deflection due to flexure and shear in mm

P = applied load, in N

L = effective beam span in mm

V = applied shear load in N

t = beam width in mm

Q = first moment of area about the neutral axis of the beam in mm^3 , G = shear modulus in MPa

E_c = modulus of elasticity of concrete determined by ACI Code (ACI Committee 318 2005) clause 8.6.2 in MPa

I_e = effective moment of inertia of the beam section in mm^4

The value of I_e is calculated based on ACI Code equation (ACI Committee 318 2005) as follows:

$$I_e = I_{cr} + (I_g - I_{cr}) \left[\frac{M_{cr}}{M_a} \right]^3 \leq I_g \quad (5.8)$$

Where:

I_{cr} = moment of inertia of cracked section transformed to concrete

I_g = moment of inertia of gross concrete section about centroidal axis, neglecting reinforcement

M_{cr} = cracking moment

M_a = maximum moment in member at load stage at which deflection is computed

Based on Euro Code (EC2 1992), the mid-span deflection is computed using the beam flexural curvature as follows:

$$\Delta = 0.0833L^2 \left(\frac{1}{r} \right) \quad (5.9)$$

The flexural curvature of the beam " $\frac{1}{r}$ " is calculated from:

$$\frac{1}{r} = \zeta \frac{M}{E_e I_c} + (1 - \zeta) \frac{M}{E_e I_u} \quad (5.10)$$

Where:

M = mid-span moment in member at load stage (P) at which deflection is computed

I_c = moment of inertia of the cracked section

I_u = moment of inertia of the un-cracked section

Effective elastic modulus, E_e and ζ are calculated from:

$$E_e = \frac{E_{c28}}{(1+\varphi)} \quad \text{and} \quad E_{c28} = 1.05 \left(22 \left[\frac{f_{cm}}{10} \right]^{0.3} \right) \quad (5.11)$$

$$\zeta = 1 - 0.5 \left(\frac{M_{cr}}{M} \right) \quad \text{and} \quad \zeta = 0 \quad \text{for un-cracked situation} \quad (5.12)$$

Where:

$$f_{cm} = 8 + f_{ck}$$

f_{ck} = characteristic compressive cylinder strength of concrete at 28 days

φ = creep coefficient at relevant loading time and duration

The values of cracking moment (M_{cr}) associated with the first flexural crack can be calculated based on various Codes. As per ACI (ACI Committee 318 2005):

$$M_{cr} = \frac{f_r I_g}{y_t} \quad (5.13)$$

where:

$$f_r = 0.62276 \sqrt{f'_c} \quad \text{for normal weight concrete}$$

y_t is the distance from centroidal axis of the gross section

I_g is the second moment of area of the gross section (the steel bars are not considered)

As per CSA (CSA A23.3. 2004):

$$M_{cr} = \frac{f_r I_g}{y_t} \quad (5.14)$$

Where:

$$f_r = 0.6 \lambda \sqrt{f'_c} \quad \text{for normal weight concrete}$$

λ is taken equal to 1 for normal density concrete

y_t is the distance from centroidal axis of the gross section to the extreme tension fiber

I_g is the second moment of area of the gross section (the steel bars are not considered)

As per Australian Standard (AS 3600 1988):

$$M_{cr} = Z f_{cf} \quad (5.15)$$

Where:

$$f_{cf} \text{ is the characteristic flexural tensile strength of the concrete} = 0.6 \sqrt{f'_c}$$

Z is the section modulus of the uncracked section, referred to the extreme fiber at which cracking occurs

As per Euro Code (EC2 1992):

$$M_{cr} = f_{ctm} I_u (h - x_u) \quad (5.16)$$

Where:

f_{ctm} is the mean value of axial tensile strength of concrete = $0.3 f_{ck}^{0.67}$

f_{ck} is the characteristic compressive cylinder strength of the concrete at 28 days. f_{ck} is defined as the value of concrete strength which is exceeded by 95% of the control specimens.

I_u is the second moment of area of the uncracked section

x_u is the distance from centroidal axis of the section to the extreme tension fiber

h is the height of the cross section of the beam

As per CSA specification (CSA A23.3, 2004), the shear resistance (V_u) for beams without shear reinforcements can be obtained as:

$$V_u = \alpha \sqrt{f_c'} b d_v \quad (5.17)$$

The factor α can be calculated as:

$$\alpha = \frac{520}{(1 + 1500 \varepsilon_x)(1000 + S_{ze})} \quad \text{and} \quad S_{ze} = \frac{35 S_z}{15 + a_g} \leq 0.85 S_z \quad (5.18)$$

Where:

b is the beam width, d_v is effective shear depth which can be taken as the greater of $0.9d$ or $0.72h$

ε_x is the longitudinal strain at mid-depth of the member due to factored loads which can be

derived as $\varepsilon_x = \frac{M_f / d_v + V_f}{2 E_s A_s}$

E_s is the modulus of elasticity of non-prestressed reinforcement

$S_z (= d_v)$ is the crack spacing parameter dependent on crack control characteristics of longitudinal reinforcement

a_g is the maximum size of aggregate in concrete

V_f is the factored shear force at section

M_f is the factored moment at section

b is the beam width

A_s is the area of non-prestressed tension reinforcement in the beam

5.2.4 Comparison of experimental and theoretical shear load /moment

Eqs. 5.13-16 are used to calculate the cracking moment (M_{cr}) and hence, the first cracking load of the experimental beams. It should be noted that the tested beams were subjected to three-point loading where the maximum moment occurs in a localized region under the applied load at midspan. With four-point loading, the maximum moment occurs over a greater length of the midspan region and hence, the moment at first cracking is reduced compared to that of three points loading. Figures 5.44-5.45 shows the percentage ratio of the calculated first flexural load values obtained from ACI, CSA, AU, and EC2 Codes to experimental values for each of the NC and SCC beams. The calculated values from Codes are found very close to the experimental values for small size (shallow beams up to 200 mm depth) beams and significantly differ for large size beams. Both ACI and CSA predictions yield lower values compared to experiments while both AU and EC2 yield higher values, especially in large size beams. This is attributed to the fact that both ACI and CSA Codes neglect the presence of longitudinal reinforcement, while both AU and EC2 take into account the effect of longitudinal reinforcement in the calculation of the second moment of area of the un-cracked section.

Table 5.5 compares the performance of Code-based equation (CSA- Eq. 5.17) in predicting the ultimate shear load (V_u) of SCC/NC beams having 1% and 2% ρ_w and no shear reinforcements. CSA-based equation under predicted the ultimate shear strength of SCC/NC beams irrespective of beam depth (150 to 750 mm) and longitudinal reinforcement ratio (1% and 2%), as the ratio of experimental to CSA prediction ranges between 0.54 and 0.81 with a mean value of 0.68. In general, CSA-based equation is conservative (its conservativeness increases with the increase of beam depth) and can be used safely for the prediction of ultimate shear resistance of both SCC and NC beams.

5.2.5 Comparison of experimental and theoretical load-deflection response

Figures 5.22-5.41 compares a typical load versus mid span deflection responses of tested beams, obtained from experiments and various Code-based equations (using ACI Eq. 5.7 and

EC2 Eq. 5.9). M_{cr} , calculated from Eq. 5.13, is used for the calculation of mid span (central) deflection using ACI Eq. 5.7, while M_{cr} , calculated from Eq. 5.16, is used for EC2 Eq. 5.9.

The point of slope change in load-deflection curves, based on both ACI and EC2, represents first flexural cracking load calculated using the un-cracked moment of inertia of the beam's cross-section. The post-cracking part of the theoretical response is based on the cracked moment of inertia (both ACI and EC2). In general, experimental deflection values are found reasonably close to the calculated values from both ACI and EC2. However, in some circumstances close to the peak load, experimental deflection values are significantly higher than calculated values (for 1NC150, 2NC150, 2SCC150, 2SCC250, 1SCC750 beams). This can be associated with the sudden shear failure due to the formation of a dominant diagonal crack (typical for the shear dominated failure) causing large deflection at failure. ACI predicted deflections are higher compared with EC2 due to the incorporation of shear deformation in Eq. 5.7. Over all, both ACI and EC2 are conservative in predicting deflection at peak (failure) load for SCC/NC beams and can be used for the calculation of deflection for shear dominated failure, for serviceability point of view. It should be noted that reinforced concrete beams are designed for flexure failure, rather than shear in practical circumstances. Hence, ACI and EC2 equations will perform better in predicting deflection for flexural dominated failure compared with a shear dominated one.

Table 5-1: Cracking loads and crack characteristics of experimental SCC/NC beams

Beam designation	Total applied load , P (kN)			Ratio (%)		No. of crack at failure	Max. crack height (mm)	Max. crack width at failure (mm)
	at first flexural crack (P_f)	at first diagonal crack (P_d)	at failure (P_u)	$100P_f/P_u$	$100P_d/P_u$			
1SCC150	32	49	146	22	34	6	116	3
1NC150	32	50	154	21	32	5	119	2
2SCC150	33	53	161	21	33	6	116	1
2NC150	33	50	168	20	30	6	114	3
1SCC250	58	74	228	25	32	6	189	10
1NC250	60	82	243	25	34	5	182	8
2SCC250	60	83	252	24	33	7	182	3
2NC250	54	85	269	20	32	6	184	2
1SCC363	90	141	298	30	47	8	251	8
1NC363	90	135	330	27	41	6	270	14
2SCC363	96	146	325	30	45	7	248	2.5
2NC363	94	132	349	27	38	5	251	3
1SCC500	109	200	348	31	57	10	362	12
1NC500	120	190	403	30	47	8	358	12
2SCC500	120	240	438	27	55	9	352	10
2NC500	135	205	456	30	45	8	356	5
1SCC750	180	320	471	38	68	11	495	20
1NC750	188	325	567	33	57	12	518	27
2SCC750	222	390	601	37	65	12	435	8
2NC750	205	350	650	32	54	9	446	12

Table 5-2: Shear resistance of SCC/NC beams from experiments and Code-based predictions

Beam designation	Experimental			Code-based prediction		Comparison (Ratio)	
	Ultimate shear load (V_u) kN	Normalized ultimate shear load (V_{nz})	Normalized ultimate shear stress (v_{nz})	Ultimate shear load ACI (kN)	Ultimate shear load CSA (kN)	Ultimate shear (ACI / Exp.)	Ultimate shear (CSA / Exp.)
1SCC150	74	11.0	0.18	46	42	0.63	0.57
1NC150	78	11.3	0.19	46	42	0.59	0.54
2SCC150	81	12.1	0.20	47	47	0.58	0.58
2NC150	85	12.4	0.21	47	47	0.56	0.56
1SCC250	116	17.3	0.17	92	78	0.80	0.67
1NC250	123	18.0	0.18	92	78	0.75	0.63
2SCC250	128	19.1	0.19	96	89	0.75	0.70
2NC250	136	19.9	0.20	96	89	0.70	0.65
1SCC363	153	22.8	0.16	142	112	0.93	0.73
1NC363	169	24.6	0.17	142	112	0.84	0.66
2SCC363	166	24.8	0.17	150	130	0.90	0.78
2NC363	178	26.0	0.18	150	130	0.84	0.73
1SCC500	181	27.0	0.14	206	147	1.14	0.81
1NC500	209	30.4	0.15	206	147	0.99	0.71
2SCC500	226	33.7	0.17	219	172	0.97	0.76
2NC500	235	34.3	0.17	219	172	0.93	0.73
1SCC750	250	37.3	0.12	307	195	1.23	0.78
1NC750	298	43.5	0.15	307	195	1.03	0.65
2SCC750	315	47.0	0.16	321	225	1.02	0.71
2NC750	340	49.6	0.17	321	225	0.95	0.66

Table 5-3: Calculated and experimental crack widths for SCC and NC beams

Beam designation	Number of cracks at different % of failure load level			Calculated crack width at different % failure load level (mm)			Experimental maximum crack width at different % of failure load (mm)					
	Load level			Load level			Load level and crack type					
	50%	75%	100%	50%	75%	100%	50%	*	75%	*	100%	*
1NC150	3	3	7	0.28	0.49	0.69	0.20	F	0.22	F	0.40	D
1SCC150	3	5	9	0.32	0.48	0.67	0.20	F	0.22	F	0.50	D
2NC150	4	6	7	0.20	0.33	0.50	0.14	FD	0.20	D	0.20	D
2SCC150	3	6	11	0.26	0.42	0.52	0.18	FD	0.18	FD	0.18	FD
1NC250	5	5	8	0.19	0.29	0.37	0.20	F	0.30	F	0.30	F
1SCC250	3	4	7	0.21	0.31	0.36	0.18	F	0.20	F	0.20	F
2NC250	3	4	7	0.18	0.27	0.33	0.18	F	0.28	F	0.28	F
2SCC250	5	7	11	0.17	0.24	0.31	0.12	FD	0.14	FD	0.14	FD
1NC363	4	5	10	0.20	0.28	0.37	0.16	F	0.20	F	0.20	D
1SCC363	3	4	7	0.17	0.28	0.35	0.18	F	0.22	F	0.22	F
2NC363	4	5	10	0.18	0.24	0.30	0.16	F	0.20	F	0.20	F
2SCC363	5	8	11	0.12	0.22	0.28	0.10	F	0.12	FD	0.12	FD
1NC500	5	7	11	0.16	0.23	0.29	0.18	F	0.30	F	0.30	F
1SCC500	4	10	14	0.15	0.22	0.27	0.16	F	0.22	F	0.22	F
2NC500	4	8	11	0.10	0.18	0.24	0.12	F	0.14	FD	0.14	FD
2SCC500	6	8	14	0.11	0.18	0.23	0.10	F	0.14	FD	0.14	FD
1NC750	7	12	23	0.14	0.22	0.30	0.18	F	0.24	F	0.24	F
1SCC750	3	9	16	0.13	0.20	0.28	0.16	F	0.20	F	0.20	F
2NC750	6	8	14	0.13	0.19	0.27	0.14	F	0.18	F	0.18	F
2SCC750	5	10	16	0.11	0.18	0.25	0.10	F	0.12	F	0.12	F

* F=flexural failure

D=diagonal failure

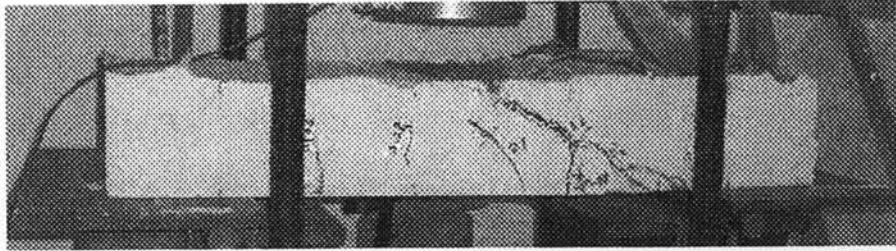
FD=flexural diagonal failure

Table 5-4: Strength-deflection results of SCC and NC beams with 1% and 2% ρ_w

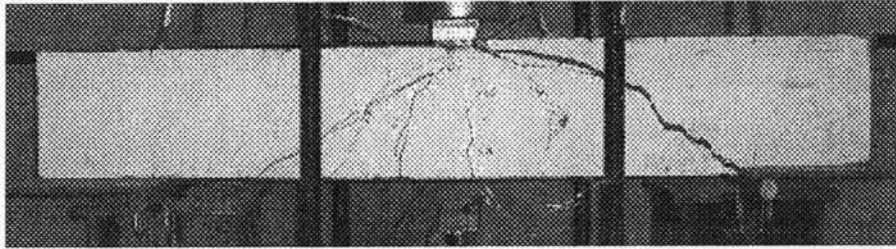
Beam designation	Total load kN			Central deflection mm		Ultimate shear load (V_u) kN	Normalized	
	At first flexural crack (P_f)	At first diagonal crack (P_d)	At failure (P_u)	At first diagonal crack (δ_d)	At failure (δ_u)		Ultimate shear load, (V_{unz}) kN.MPa ^{-1/2}	Ultimate shear stress, (v_{unz}) kN.mm ⁻² MPa ^{-1/2}
1SCC150	32	49	146	0.65	2.5	74	11	0.183
1NC150	32	50	154	0.56	3.25	78	11	0.189
2SCC150	33	53	161	0.56	3.2	81	12	0.202
2NC150	33	50	168	0.34	2.5	85	12	0.206
1SCC250	58	74	228	0.64	2.66	116	17	0.173
1NC250	60	82	243	0.81	2.79	123	18	0.180
2SCC250	60	83	252	0.58	3.08	128	19	0.191
2NC250	54	85	269	0.62	2.06	136	20	0.199
1SCC363	90	141	298	0.97	2.77	153	23	0.157
1NC363	90	135	330	0.77	3.2	169	25	0.170
2SCC363	96	146	325	0.72	1.9	166	25	0.171
2NC363	94	132	349	0.77	2.23	178	26	0.179
1SCC500	109	200	348	1.35	2.9	181	27	0.135
1NC500	120	190	403	1.09	3.35	209	30	0.152
2SCC500	120	240	438	1.15	2.4	226	34	0.169
2NC500	135	205	456	0.95	2.7	235	34	0.172
1SCC750	180	320	471	1.81	3.4	250	37	0.125
1NC750	188	325	567	0.91	3.67	298	44	0.145
2SCC750	222	390	601	1.58	2.6	315	47	0.157
2NC750	205	350	650	0.97	2.2	340	50	0.165

Table 5-5: Central deflection and longitudinal steel strain development in SCC/NC beams

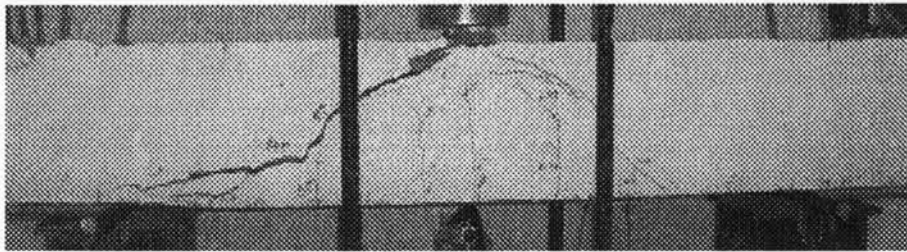
Beam designation	Longitudinal steel strain (ϵ_s) micro-strain			Central deflection at various load levels (mm)			Ultimate shear load CSA (kN)	Ratio of ultimate shear load (CSA / Exp.)
	50%	75%	100%	50%	75%	100%		
1SCC150	1018	1503	2100	1.1	1.6	2.5	42	0.57
1NC150	881	1548	2180	0.92	1.75	3.25	42	0.54
2SCC150	775	1240	1550	0.95	1.45	3.2	47	0.58
2NC150	600	990	1500	0.7	1.1	2.5	47	0.56
1SCC250	990	1468	1700	1.25	1.97	2.66	78	0.67
1NC250	920	1380	1755	1.34	2.03	2.79	78	0.63
2SCC250	626	920	1180	0.93	1.4	3.08	89	0.70
2NC250	687	1006	1250	1.04	1.52	2.06	89	0.65
1SCC363	700	1120	1400	1	2.1	2.77	112	0.73
1NC363	825	1125	1500	1.22	2	3.2	112	0.66
2SCC363	429	780	1000	0.7	1.3	1.9	130	0.78
2NC363	639	869	1070	1.15	1.66	2.23	130	0.73
1SCC500	722	1037	1280	1.3	1.9	2.9	147	0.81
1NC500	760	1100	1380	1.43	2.1	3.35	147	0.71
2SCC500	457	749	970	0.9	1.6	2.4	172	0.76
2NC500	422	763	1030	1.1	1.6	2.7	172	0.73
1SCC750	572	915	1260	1.03	2	3.4	195	0.78
1NC750	642	1006	1340	0.95	1.61	2.6	195	0.65
2SCC750	395	666	920	1.13	1.75	2.6	225	0.71
2NC750	475	721	1000	1.06	1.6	2.2	225	0.66



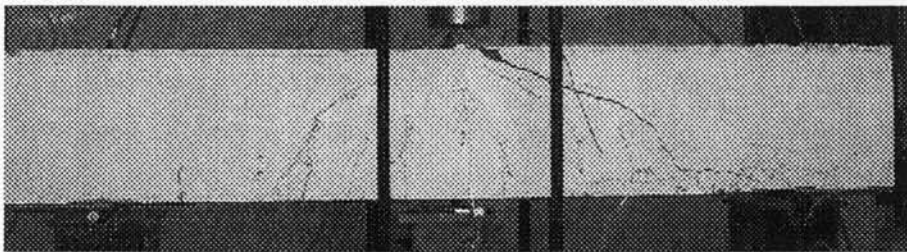
150 mm high beam



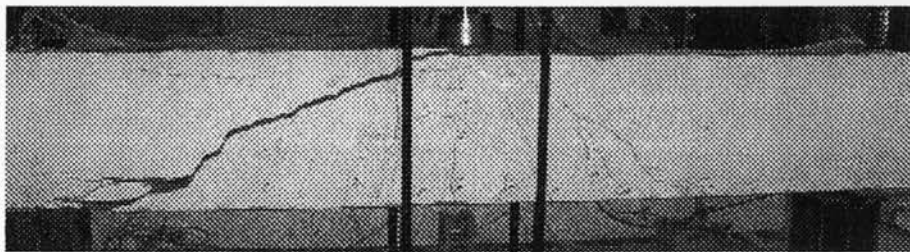
250 mm high beam



363 mm high beam



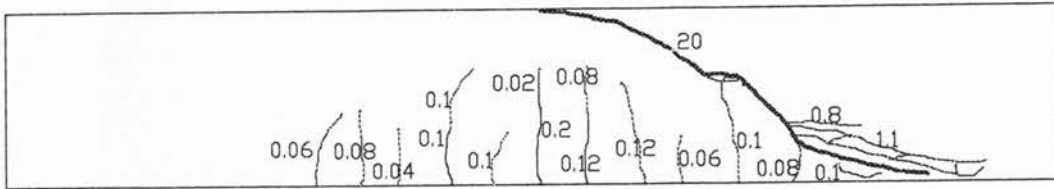
500 mm high beam



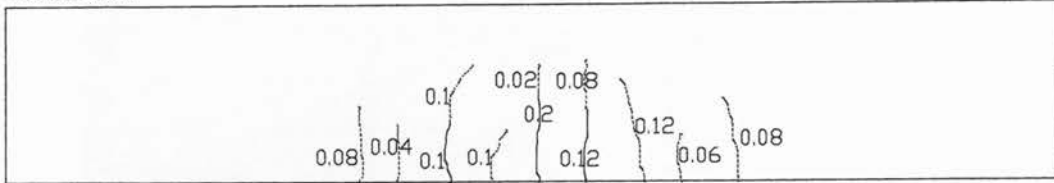
750 mm high beam

Figure 5-1: Typical failure modes of SCC/NC beams of various sizes

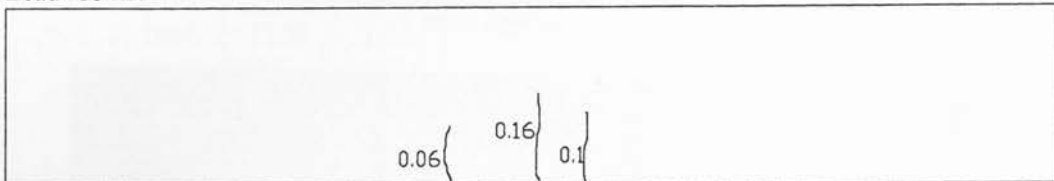
Final Load 471 kN



Load 346kN

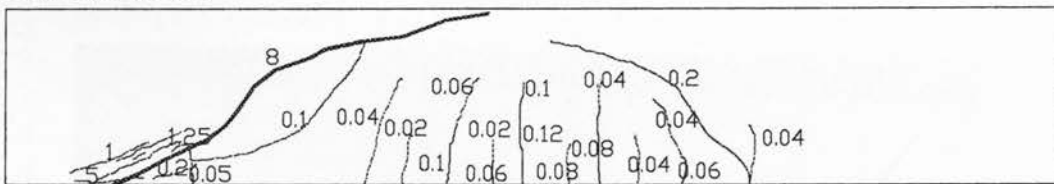


Load 233 kN

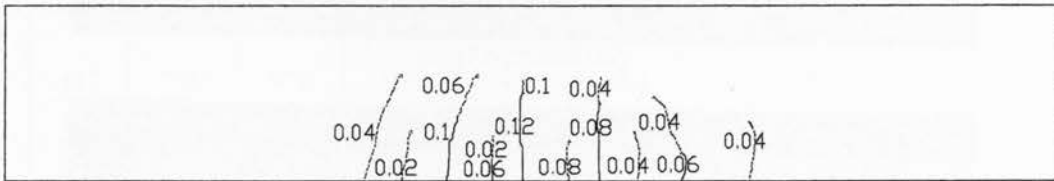


ISCC750

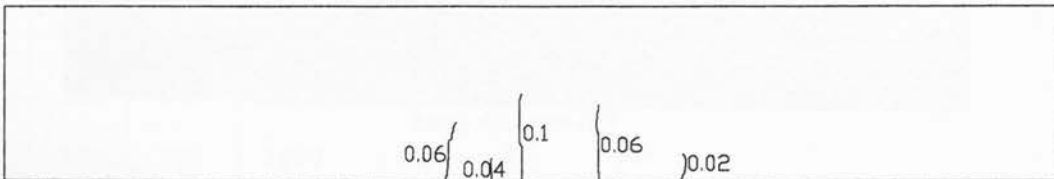
Final Load 601 kN



Load 435 kN



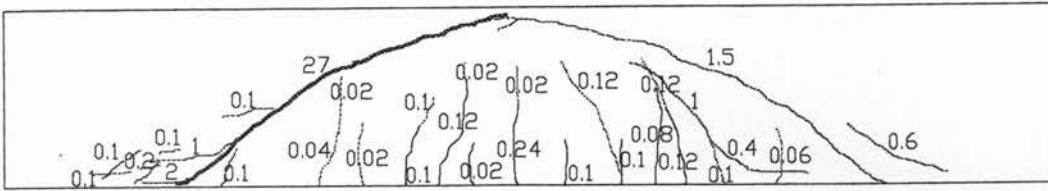
Load 288 kN



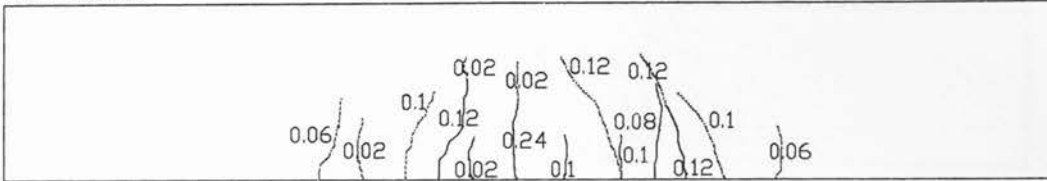
2SCC750

Figure 5-2: Crack development and crack widths (in mm) for 1% and 2% ρ_w 750 mm SCC beams at different load levels (50%, 75%, and 100% of failure load)

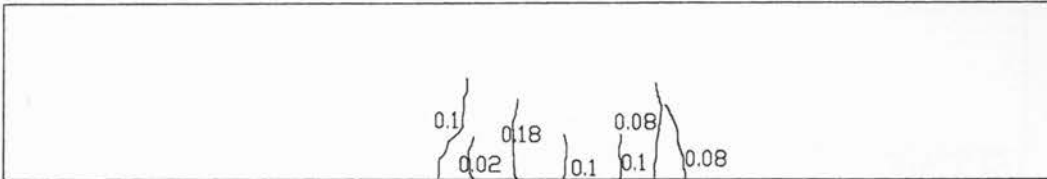
Final Load 567 kN



Load 435 kN

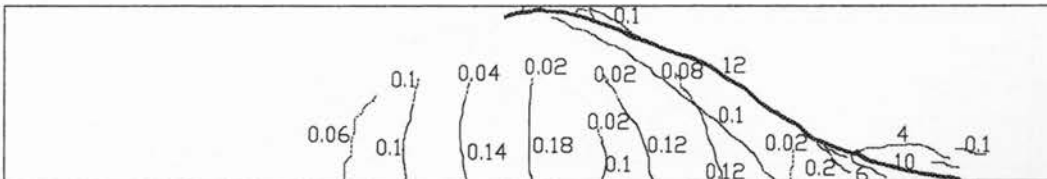


Load 325 kN

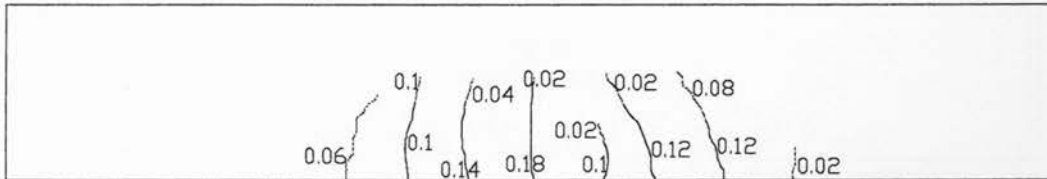


1NC750

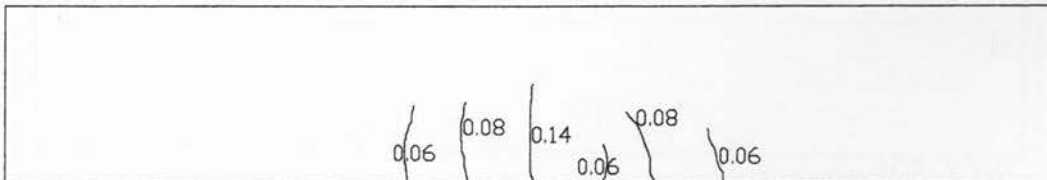
Final Load 650 kN



Load 520 kN



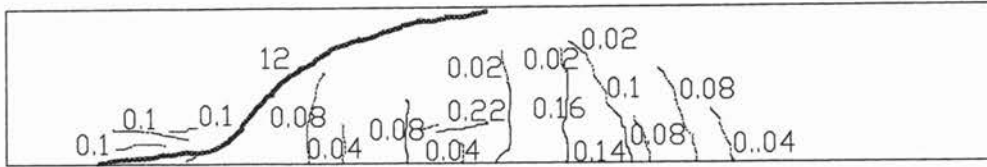
Load 380 kN



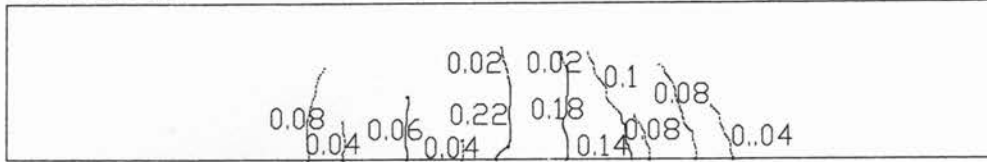
2NC750

Figure 5-3: Crack development and crack widths (in mm) for 1% and 2% ρ_w 750 mm NC beams at different load levels (50%, 75%, and 100% of failure load)

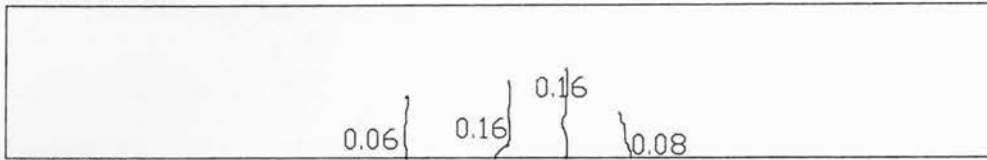
Final Load 348 kN



Load 280 kN

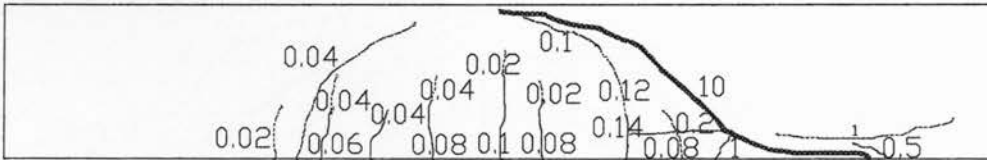


Load 200 kN

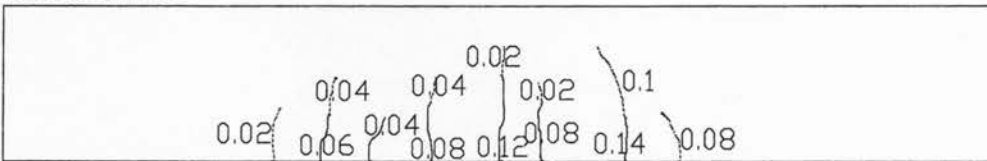


1SCC500

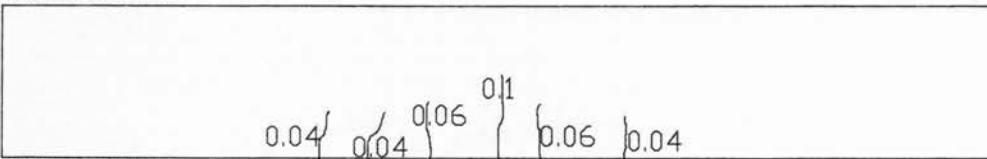
Final Load 438 kN



Load 350 kN



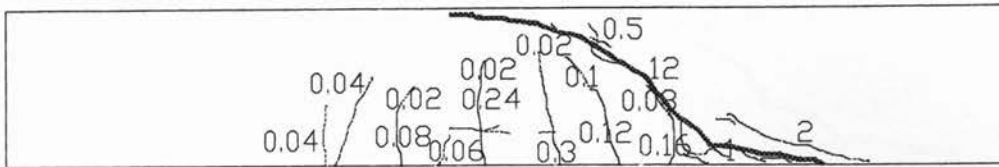
Load 210 kN



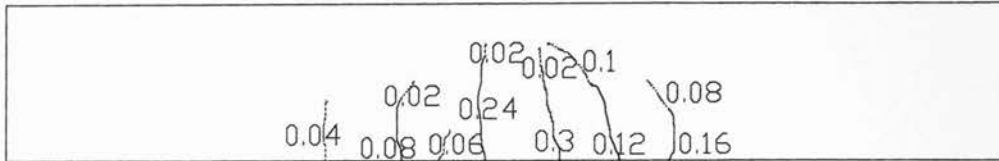
2SCC500

Figure 5-4: Crack development and crack widths (in mm) for 1% and 2% ρ_w 500 mm SCC beams at different load levels (50%, 75%, and 100% of failure load)

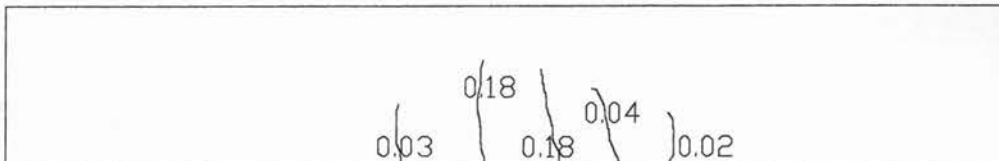
Final Load 403 kN



Load 300 kN

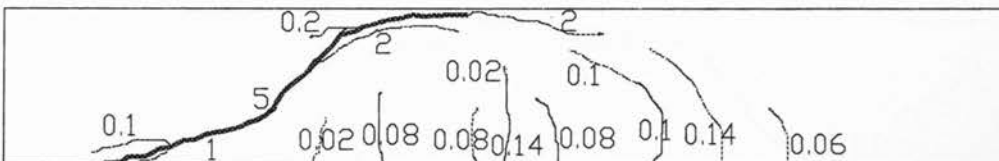


Load 230 kN

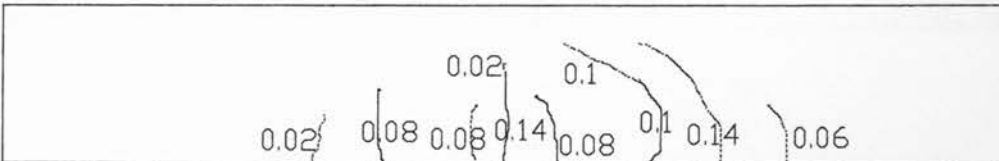


INC500

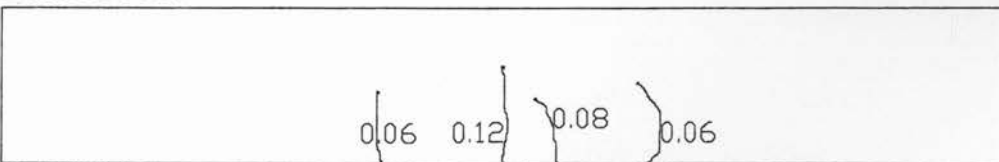
Final Load 456 kN



Load 330 kN



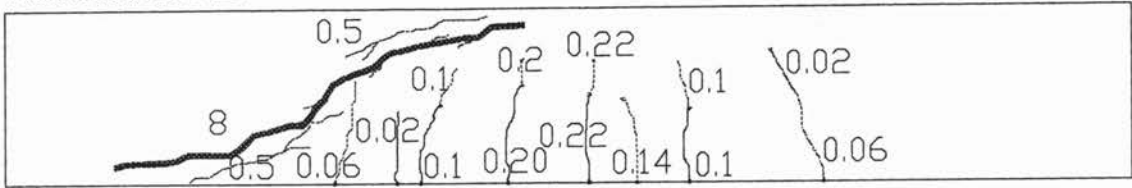
Load 235 kN



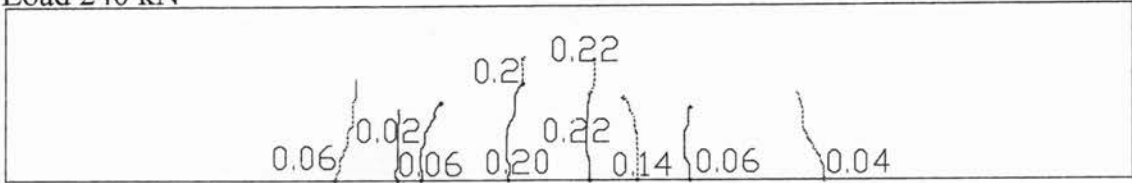
2NC500

Figure 5-5: Crack development and crack widths (in mm) for 1% and 2% ρ_w 500 mm NC beams at different load levels (50%, 75%, and 100% of failure load)

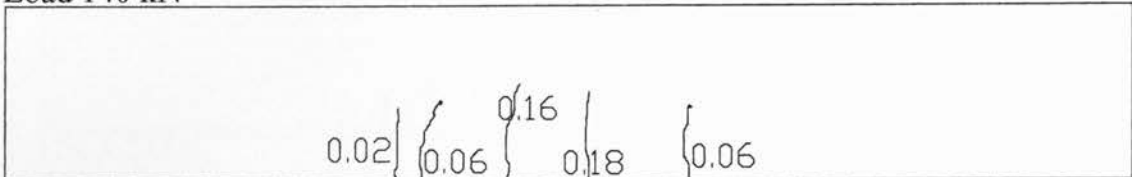
Final load 298 kN



Load 240 kN

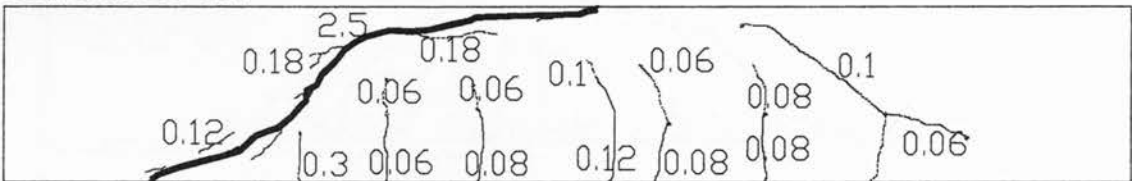


Load 140 kN

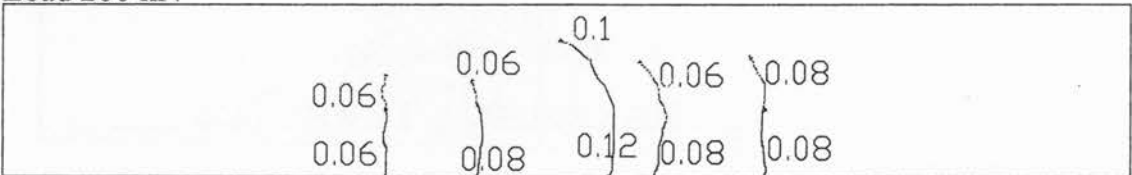


1SCC363

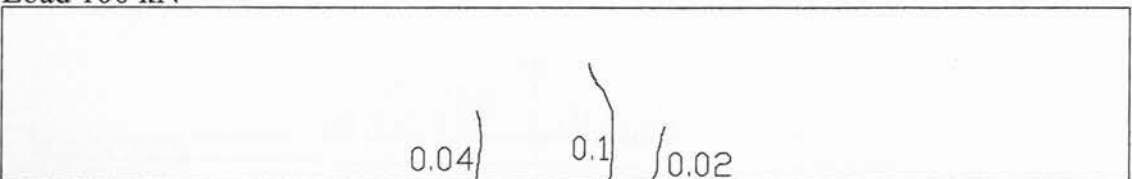
Final load 325 kN



Load 260 kN



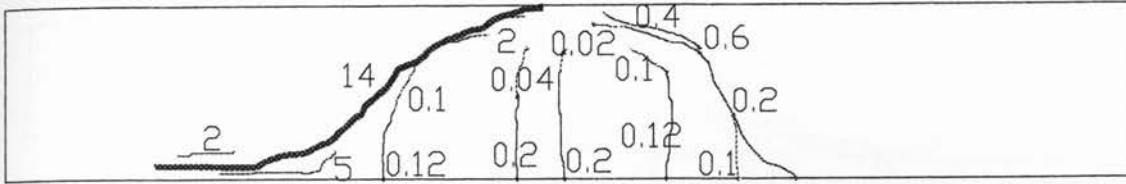
Load 160 kN



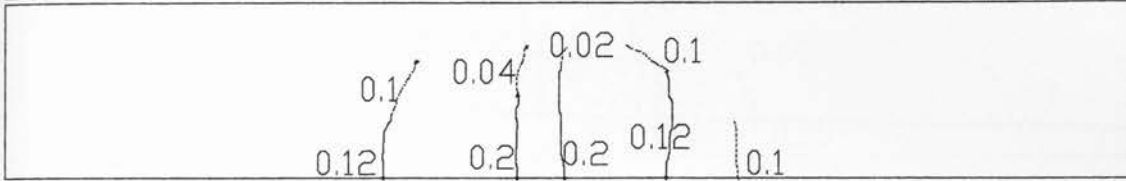
2SCC363

Figure 5-6: Crack development and crack widths (in mm) for 1% and 2% ρ_w 363 mm SCC beams at different load levels (50%, 75%, and 100% of failure load)

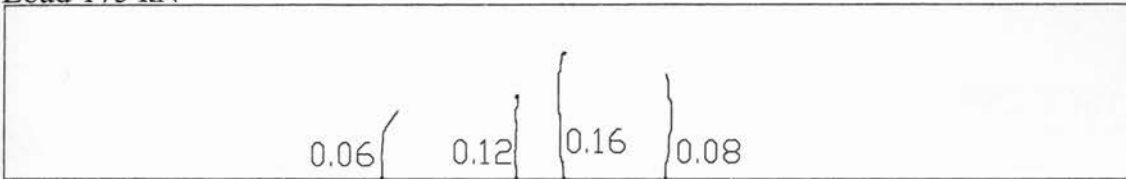
Final load 330 kN



Load 265 kN

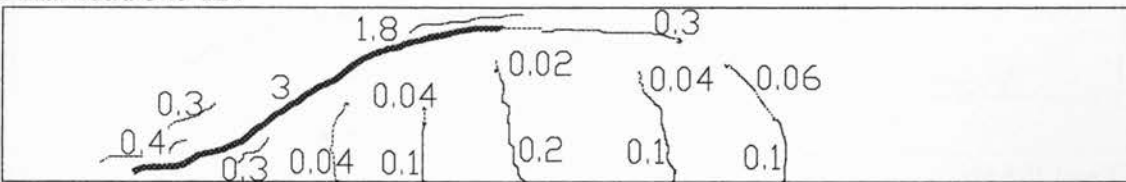


Load 175 kN

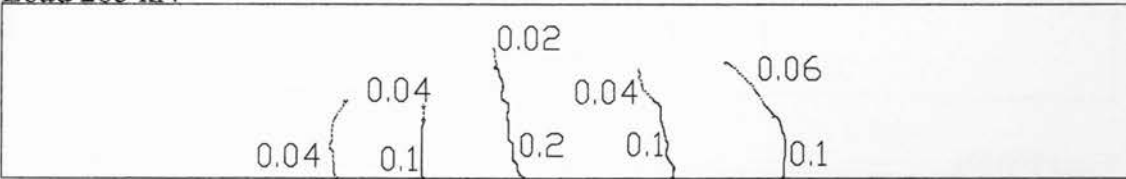


INC363

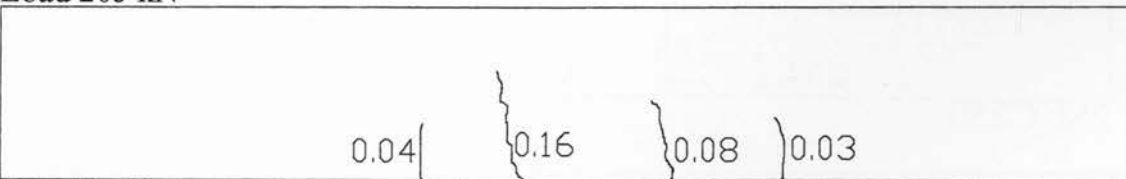
Final load 349 kN



Load 285 kN



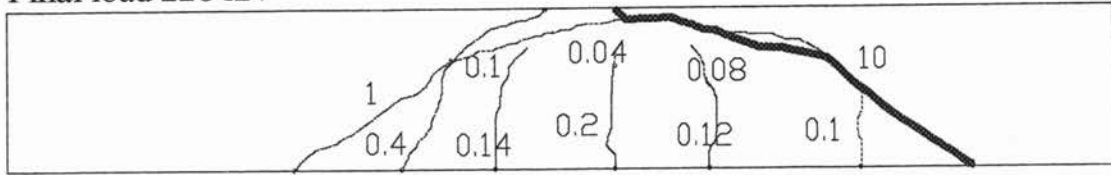
Load 205 kN



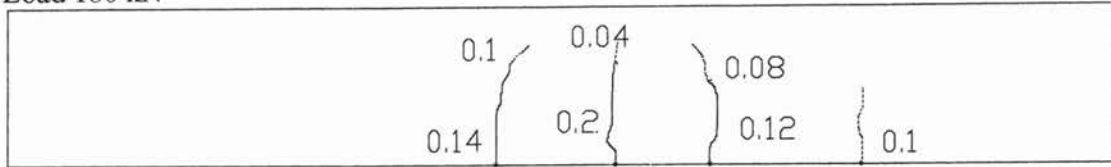
2NC363

Figure 5-7: Crack development and crack widths (in mm) for 1% and 2% ρ_w 363 mm NC beams at different load levels (50%, 75%, and 100% of failure load)

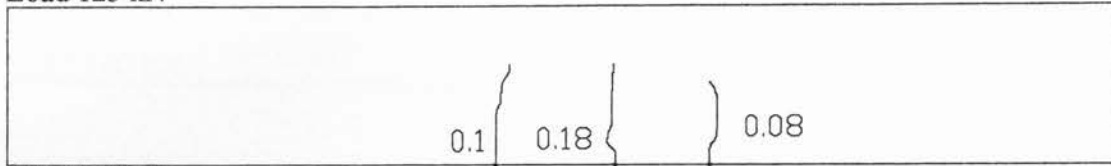
Final load 228 kN



Load 180 kN

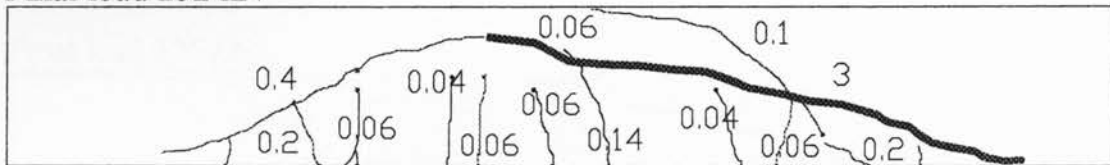


Load 125 kN

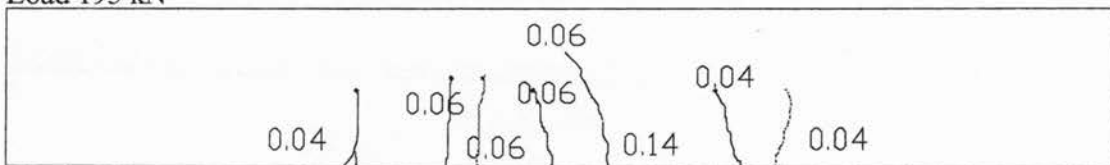


ISCC250

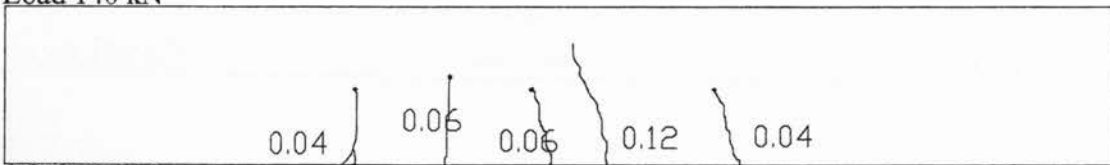
Final load 252 kN



Load 195 kN



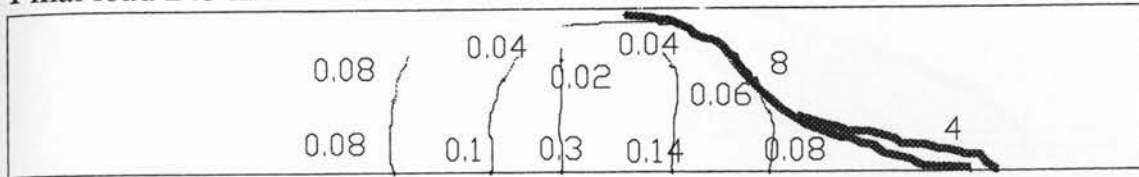
Load 140 kN



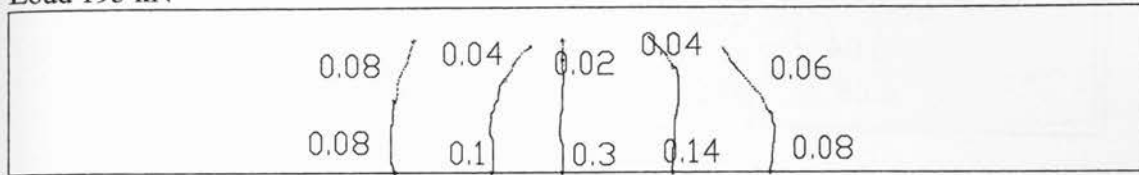
2SCC250

Figure 5-8: Crack development and crack widths (in mm) for 1% and 2% ρ_w 250 mm SSC beams at different load levels (50%, 75%, and 100% of failure load)

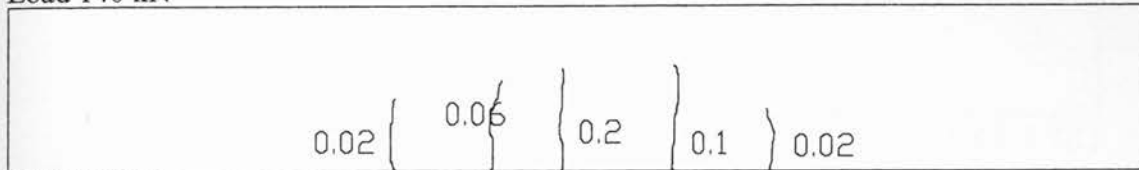
Final load 243 kN



Load 195 kN

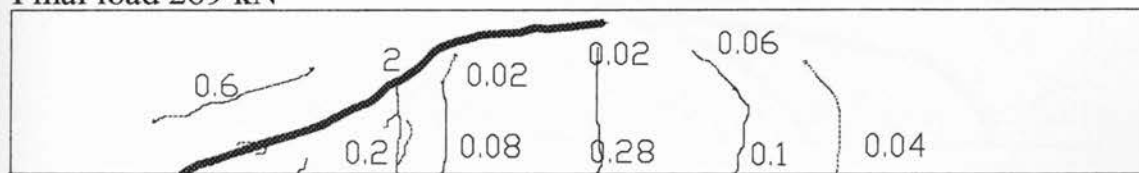


Load 140 kN

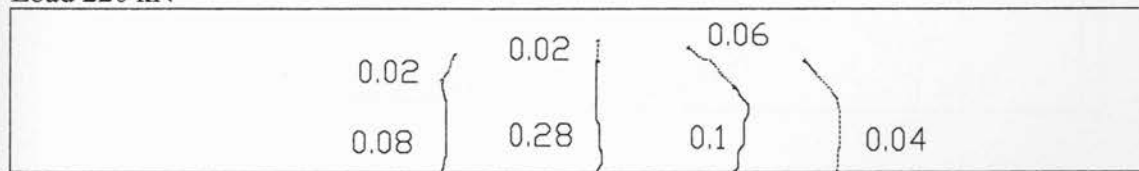


INC250

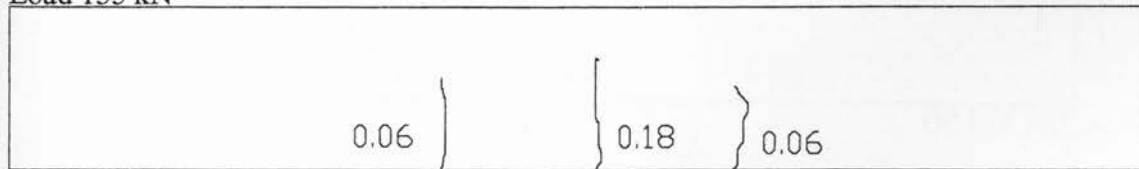
Final load 269 kN



Load 220 kN

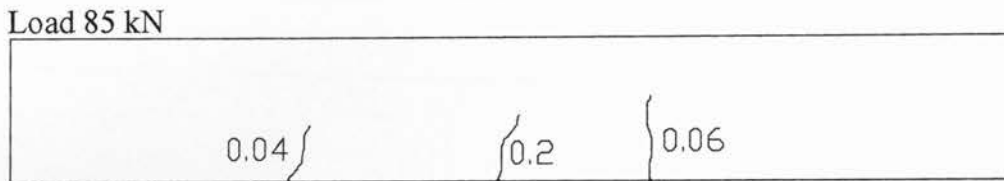
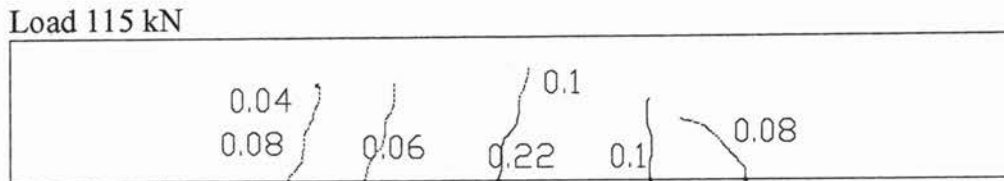
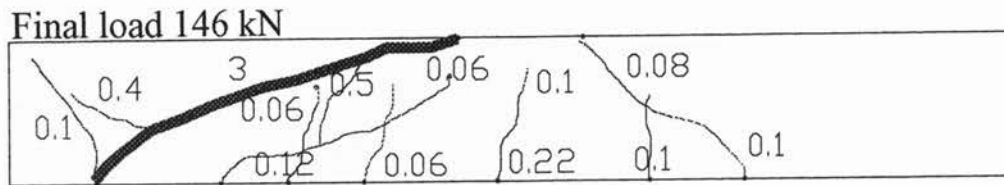


Load 155 kN

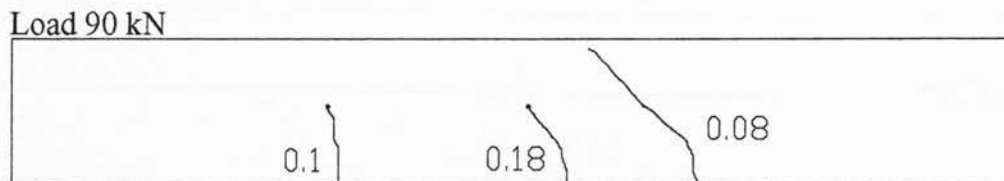
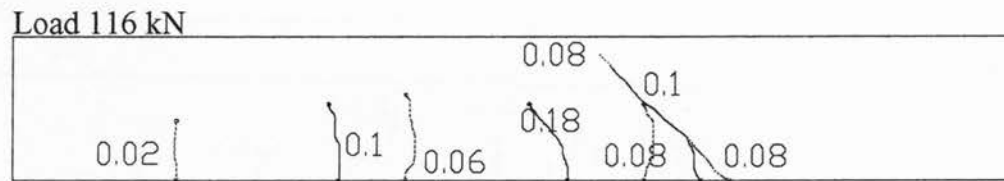
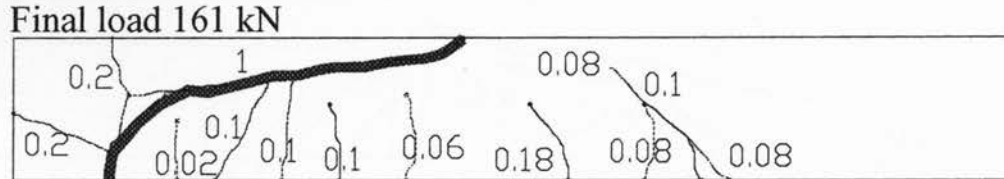


2NC250

Figure 5-9: Crack development and crack widths (in mm) for 1% and 2% ρ_w 250 mm NC beams at different load levels (50%, 75%, and 100% of failure load)



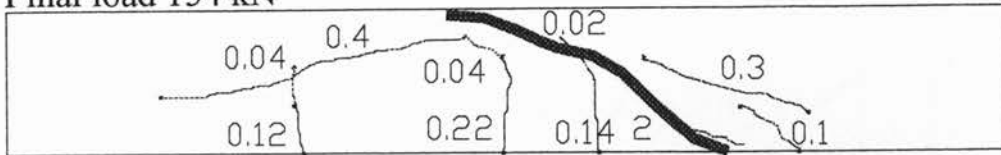
1SCC150



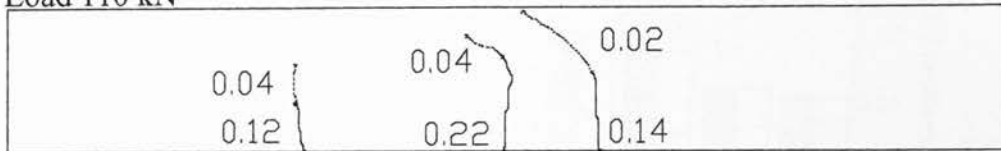
2SCC150

Figure 5-10: Crack development and crack widths (in mm) for 1% and 2% ρ_w 150 mm depth SCC beams at different load levels (50%, 75%, and 100% of failure load)

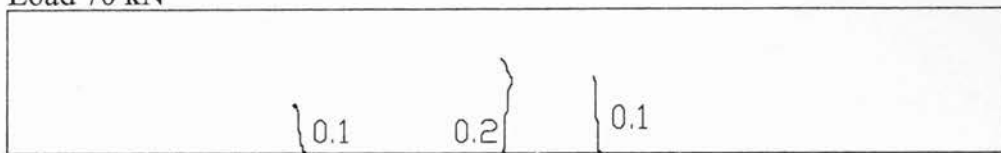
Final load 154 kN



Load 110 kN

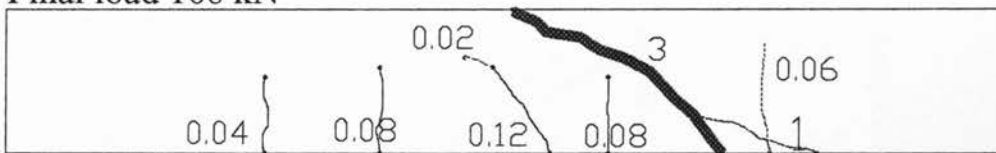


Load 70 kN

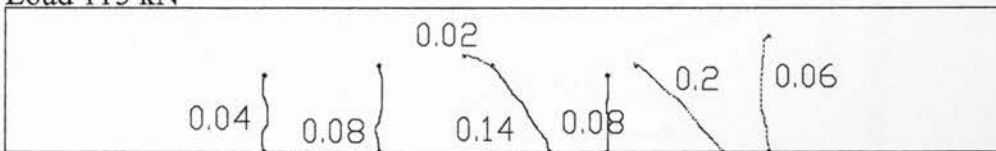


INC150

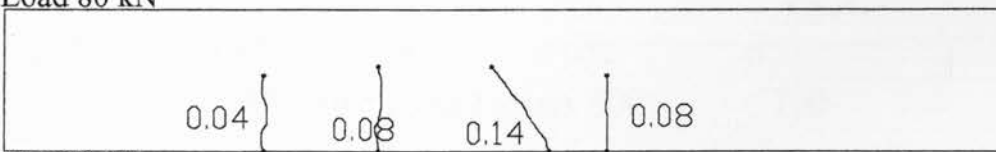
Final load 168 kN



Load 115 kN



Load 80 kN



2NC150

Figure 5-11: Crack development and crack widths (in mm) for 1% and 2% ρ_w 150 mm depth SCC beams at different load levels (50%, 75%, and 100% of failure load)

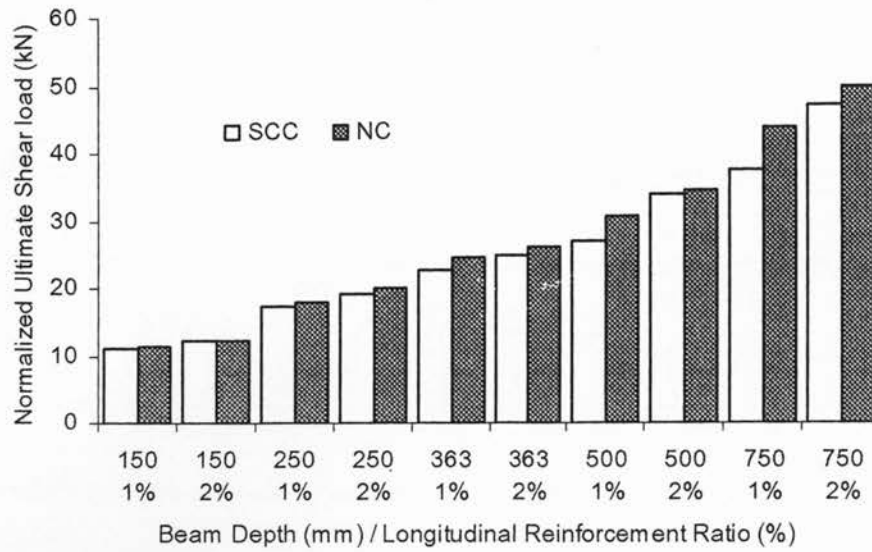


Figure 5-12: Normalized ultimate shear load (V_{nz}) for both SCC and NC beams

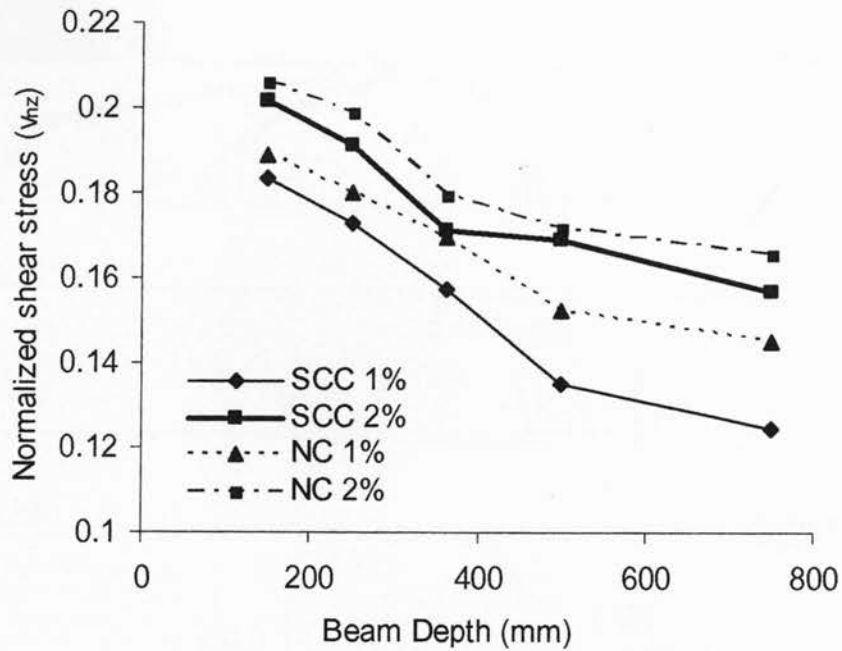


Figure 5-13: Effect of beam depth on normalized shear stress (v_{nz}) for both SCC and NC beams

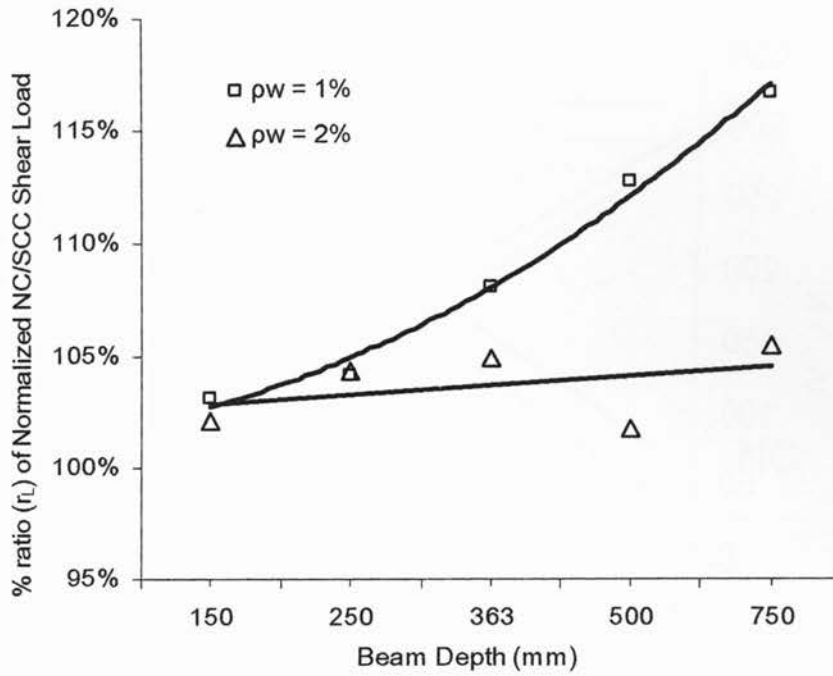


Figure 5-14: Percentage ratio (r_L) of normalized ultimate shear loads ($r_L = 100 * U_{NZ-NC} / U_{NZ-SCC}$)

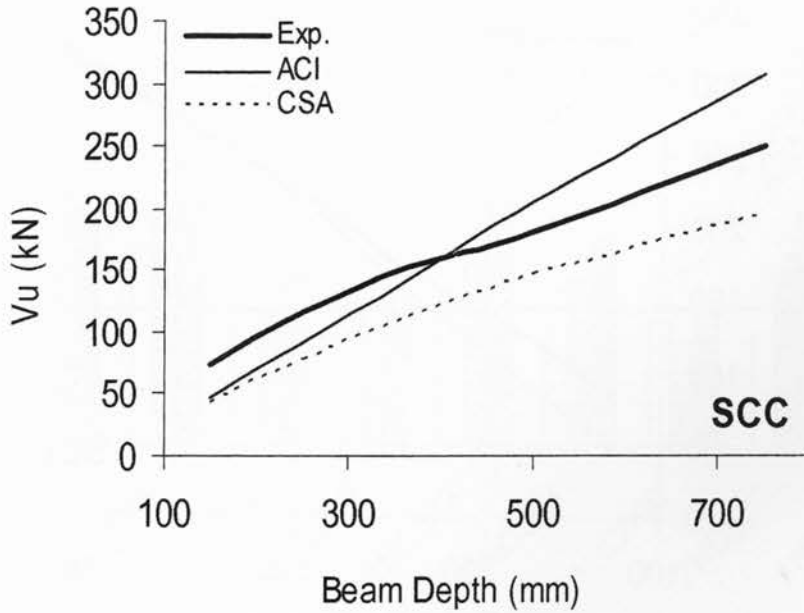


Figure 5-15: Ultimate shear strength (V_u)- experiments and Code predictions (SCC beams with $1\% \rho_w$)

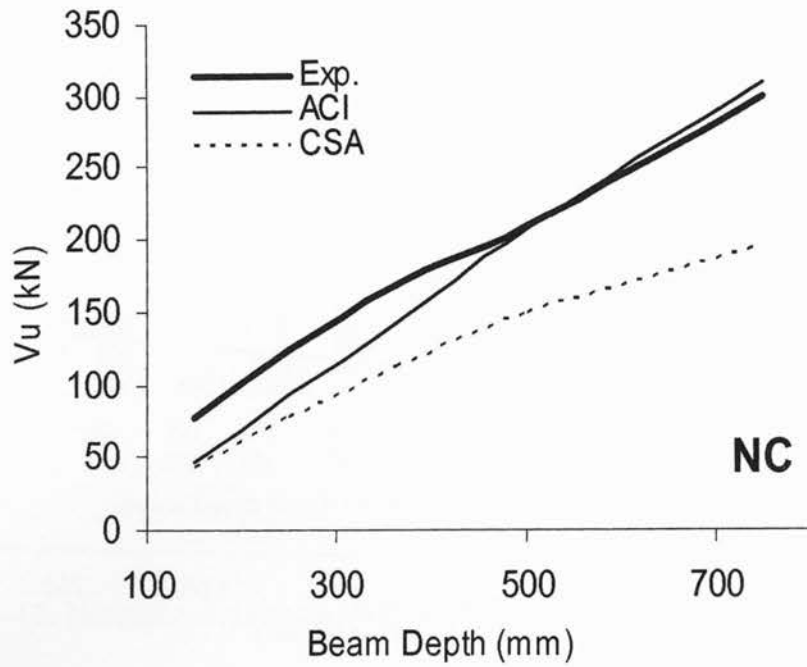


Figure 5-16: Ultimate shear strength (V_u)- experiments and Code predictions (NC beams with 1% ρ_w)

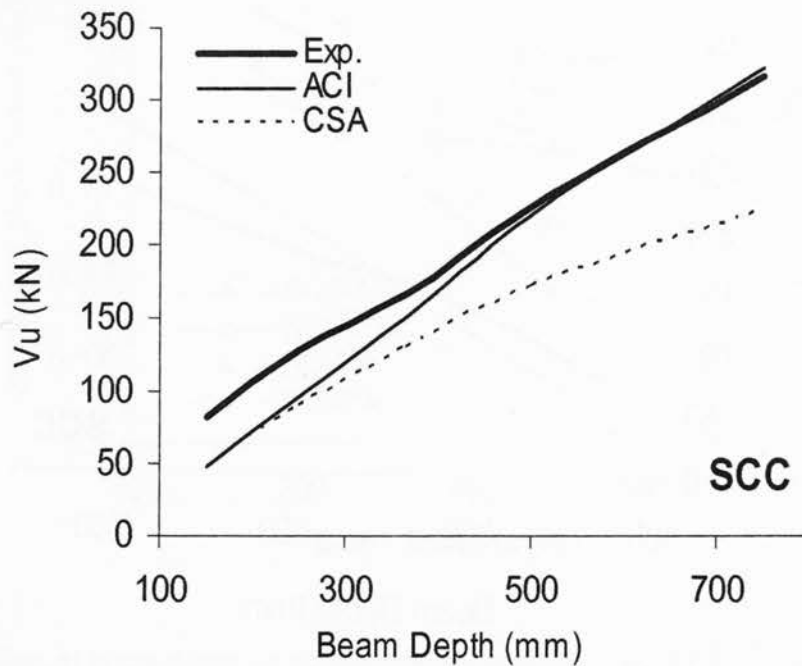


Figure 5-17: Ultimate shear strength (V_u) - experiments and Code predictions (SCC beams with 2% ρ_w)

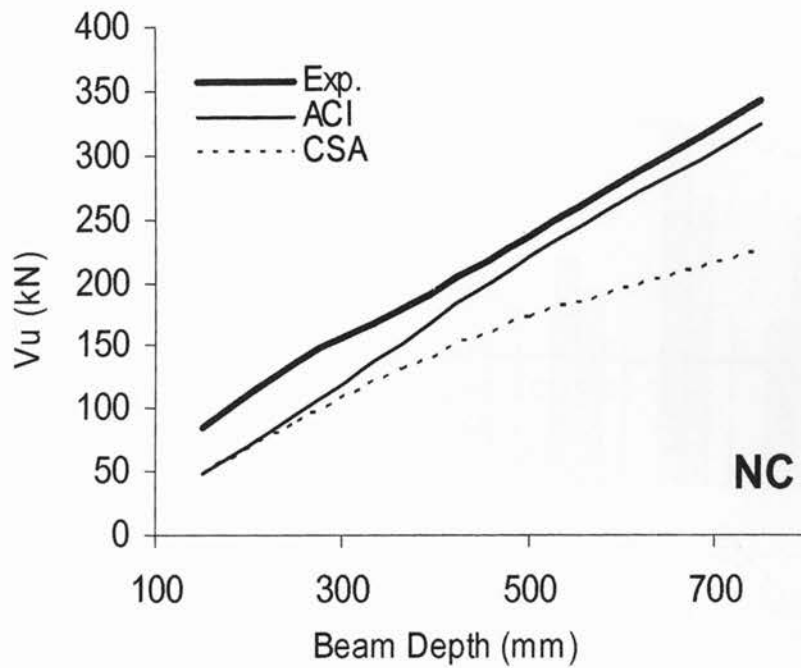


Figure 5-18: Ultimate shear strength (V_u) - experiments and Code predictions (NC beams with 2% ρ_w)

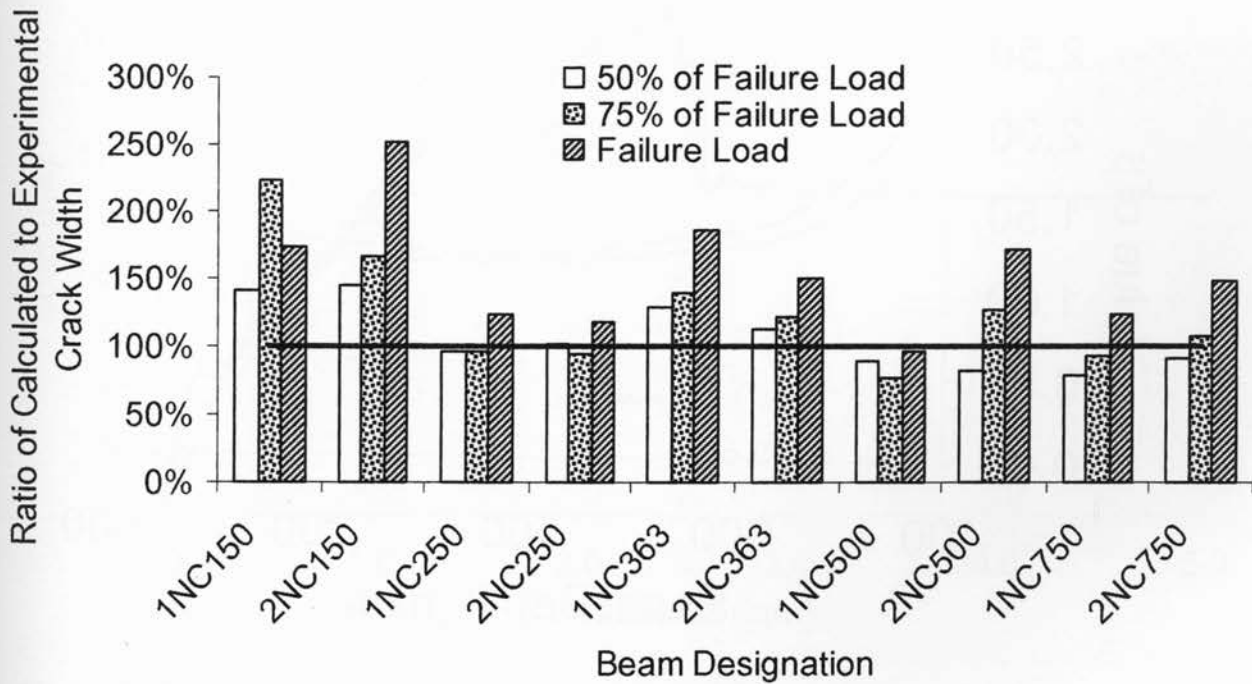


Figure 5-19: Calculated / experimental crack widths for NC in both 1% and 2% ρ_w

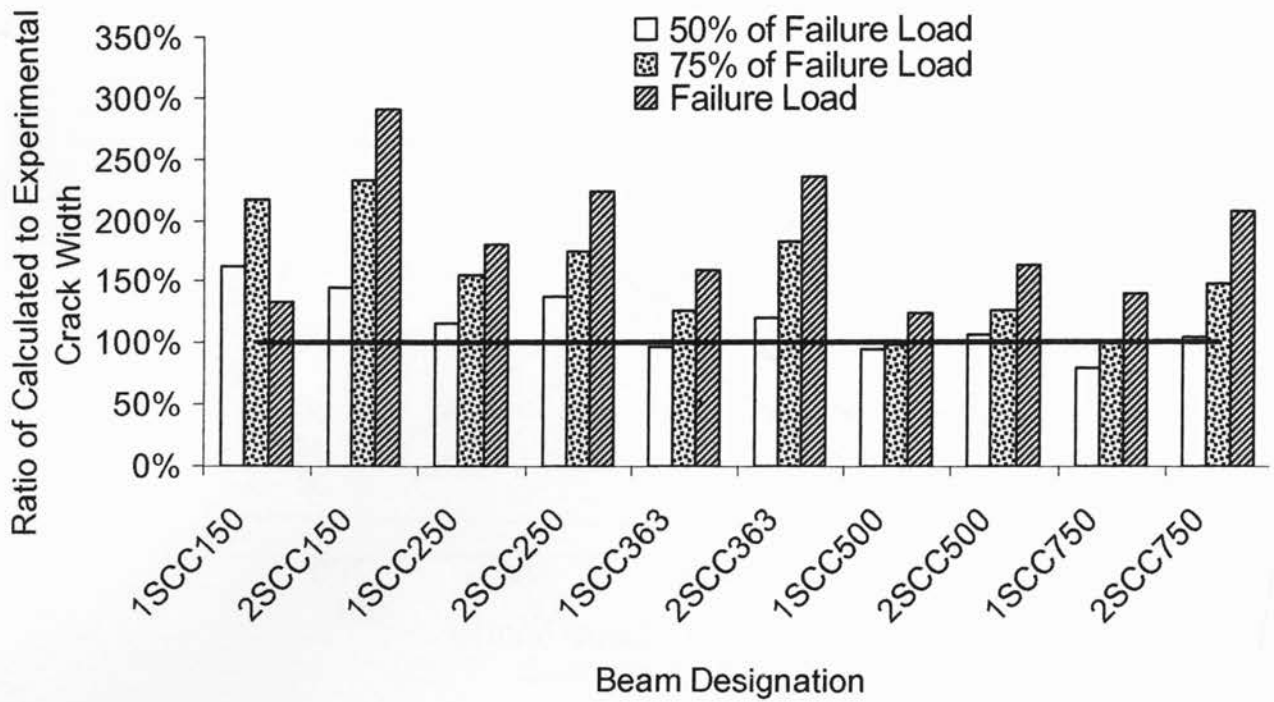


Figure 5-20: Calculated / experimental crack widths for SCC in both 1% and 2% ρ_w

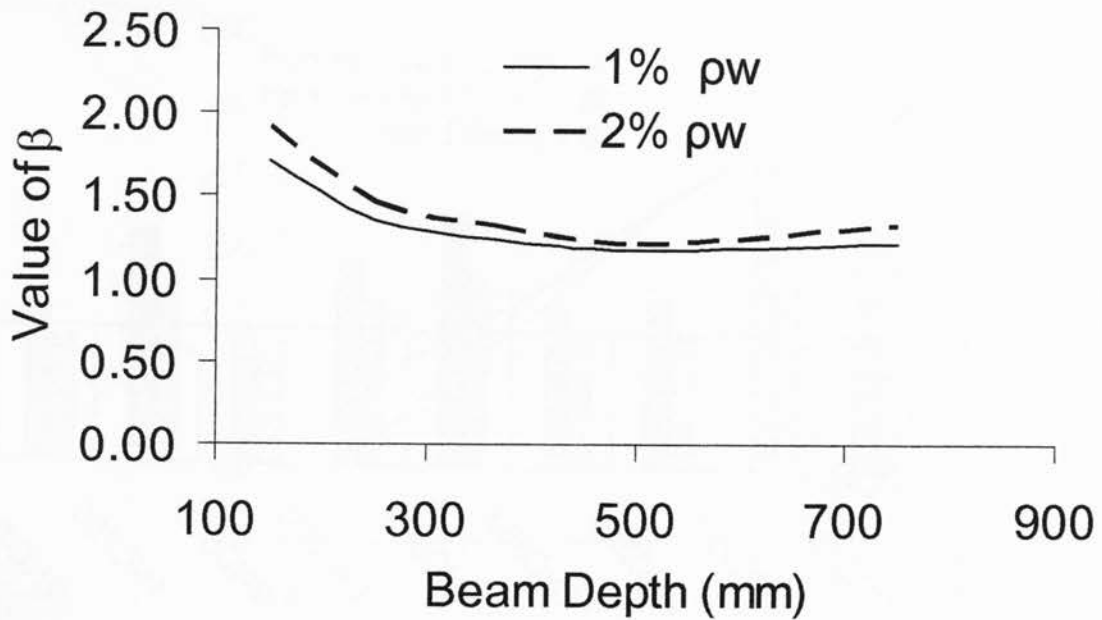


Figure 5-21: β as a function of beam depth and ρ_w

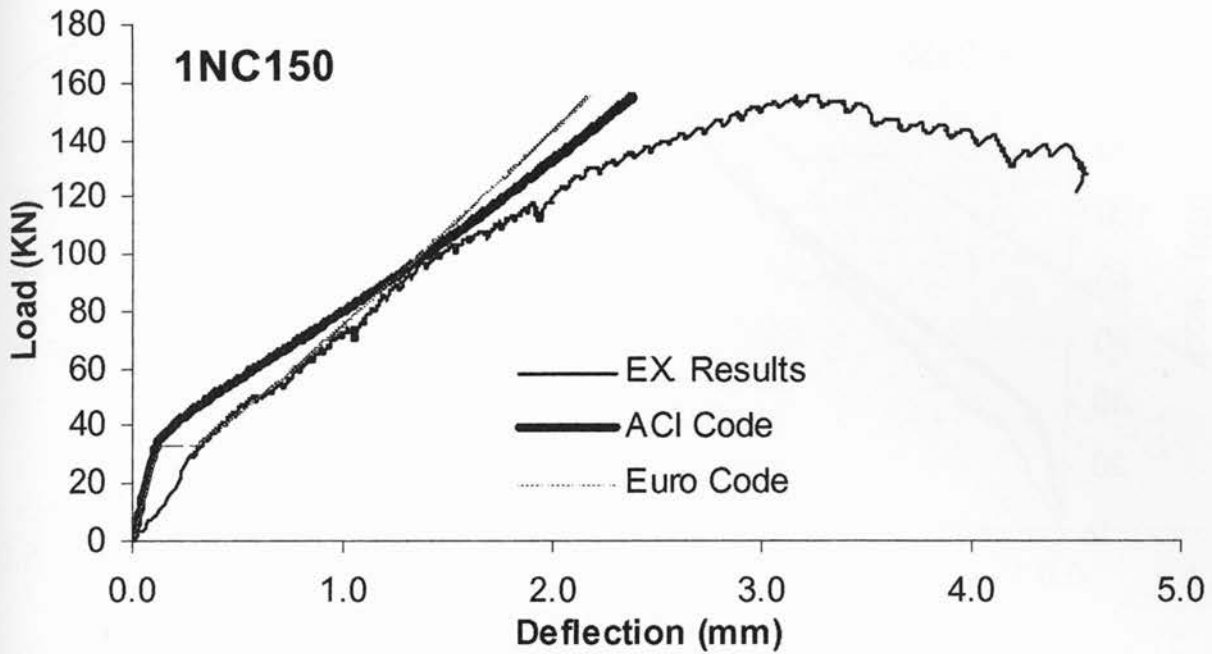


Figure 5-22: Comparison of experimental and Code-based load-mid span deflection responses (1NC150)

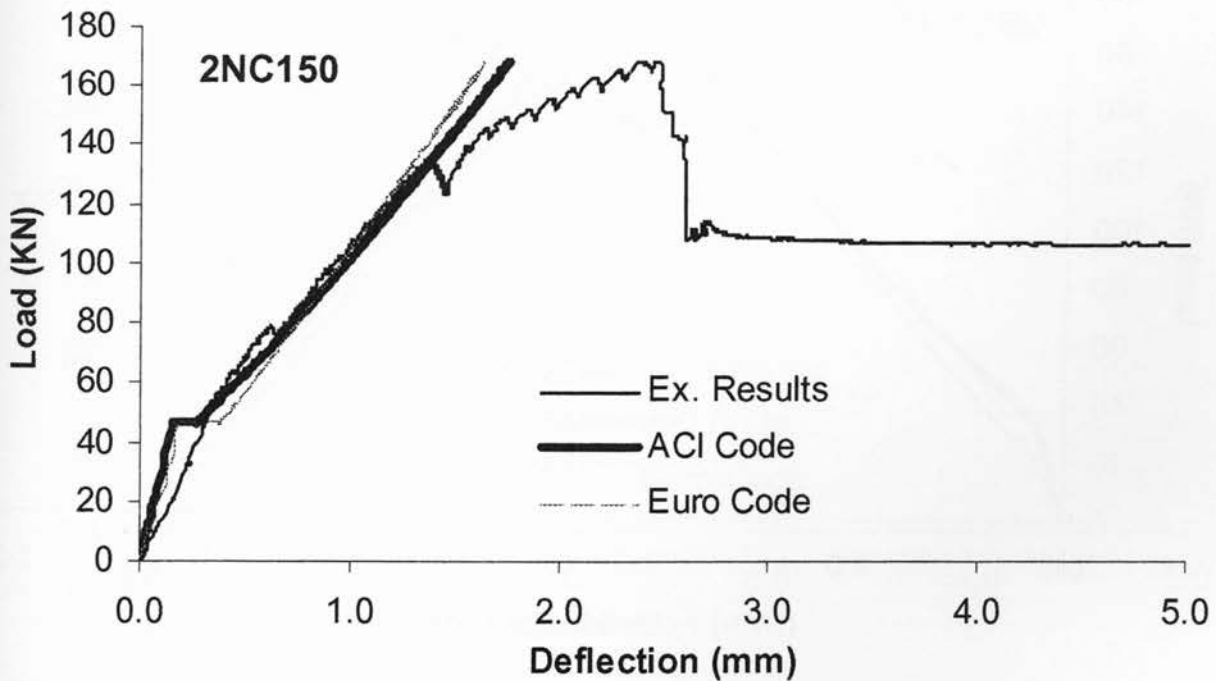


Figure 5-23: Comparison of experimental and Code-based load-mid span deflection responses (2NC150)

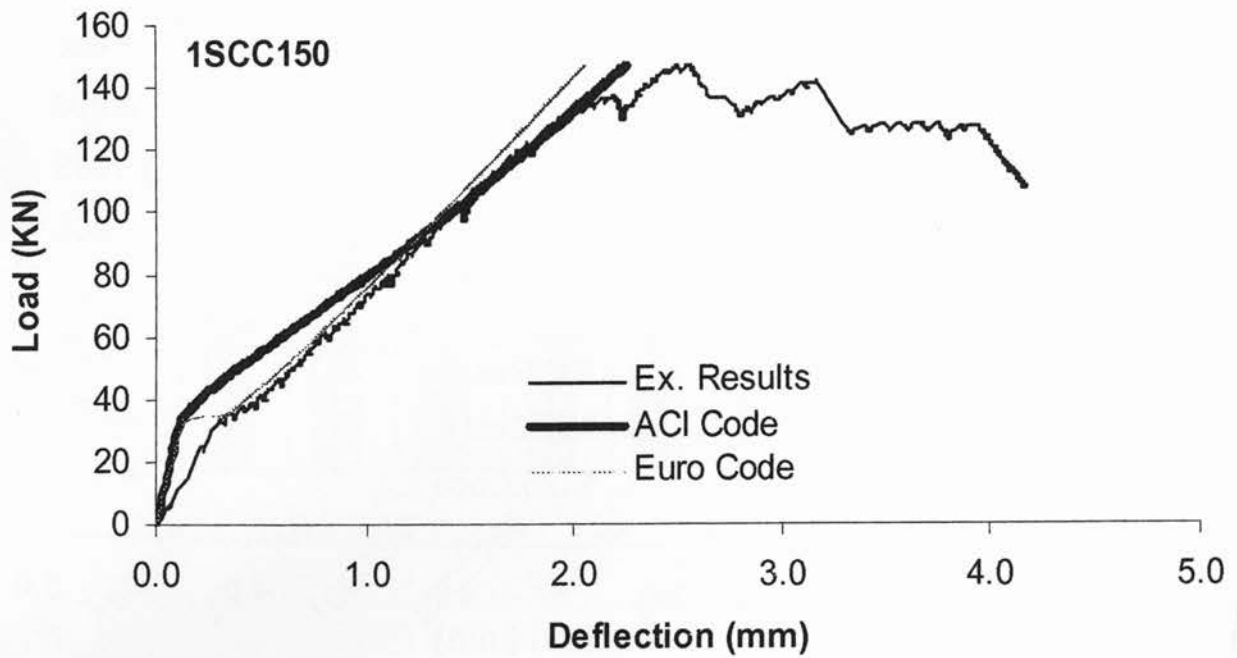


Figure 5-24: Comparison of experimental and Code-based load-mid span deflection responses (1SCC150)

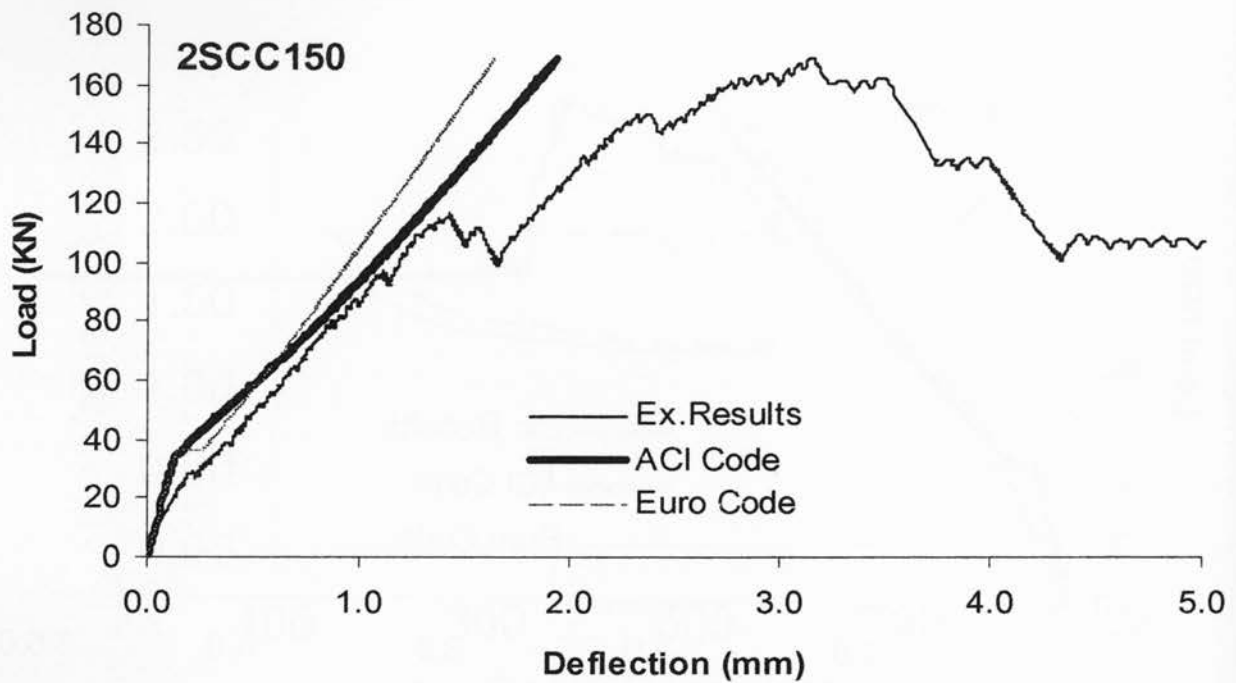


Figure 5-25: Comparison of experimental and Code-based load-mid span deflection responses (2SCC150)

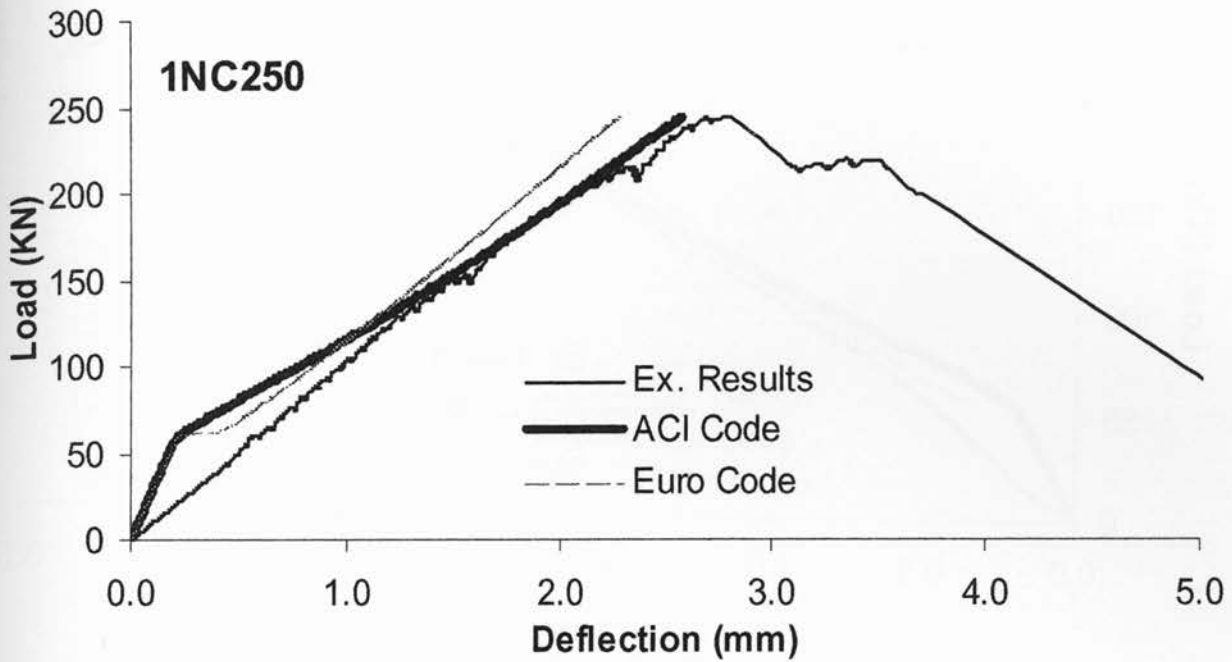


Figure 5-26: Comparison of experimental and Code-based load-mid span deflection responses (1NC250)

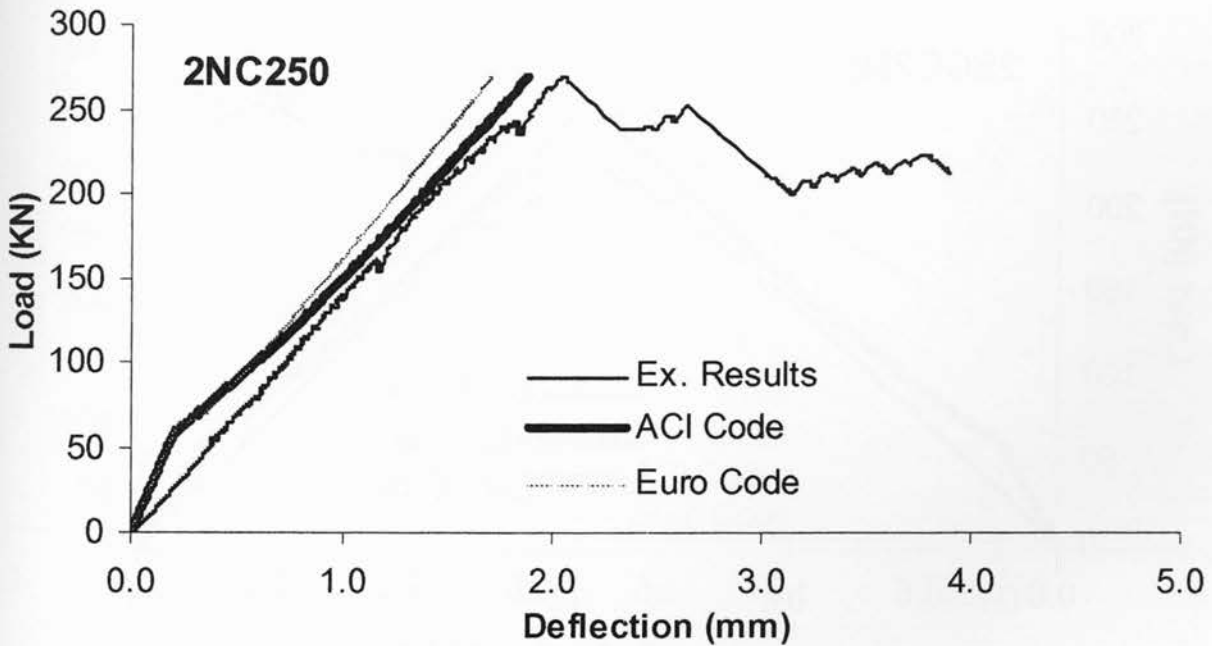


Figure 5-27: Comparison of experimental and Code-based load-mid span deflection responses (2NC250)

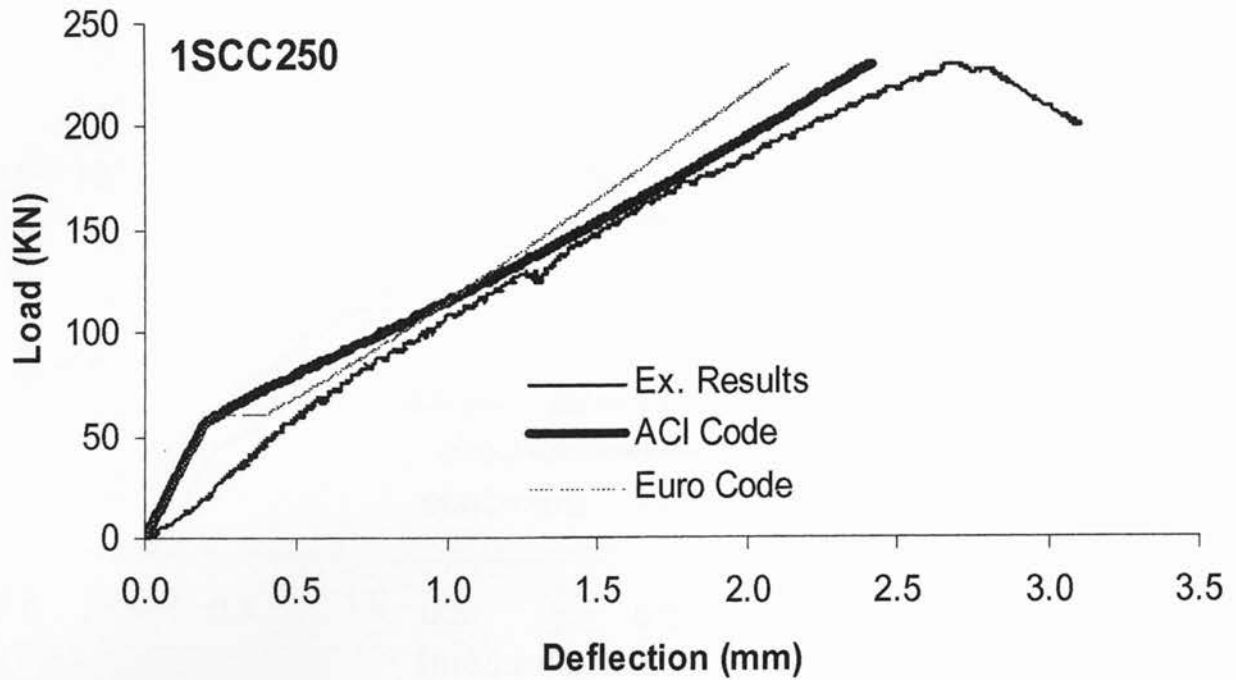


Figure 5-28: Comparison of experimental and Code-based load-mid span deflection responses (1SCC250)

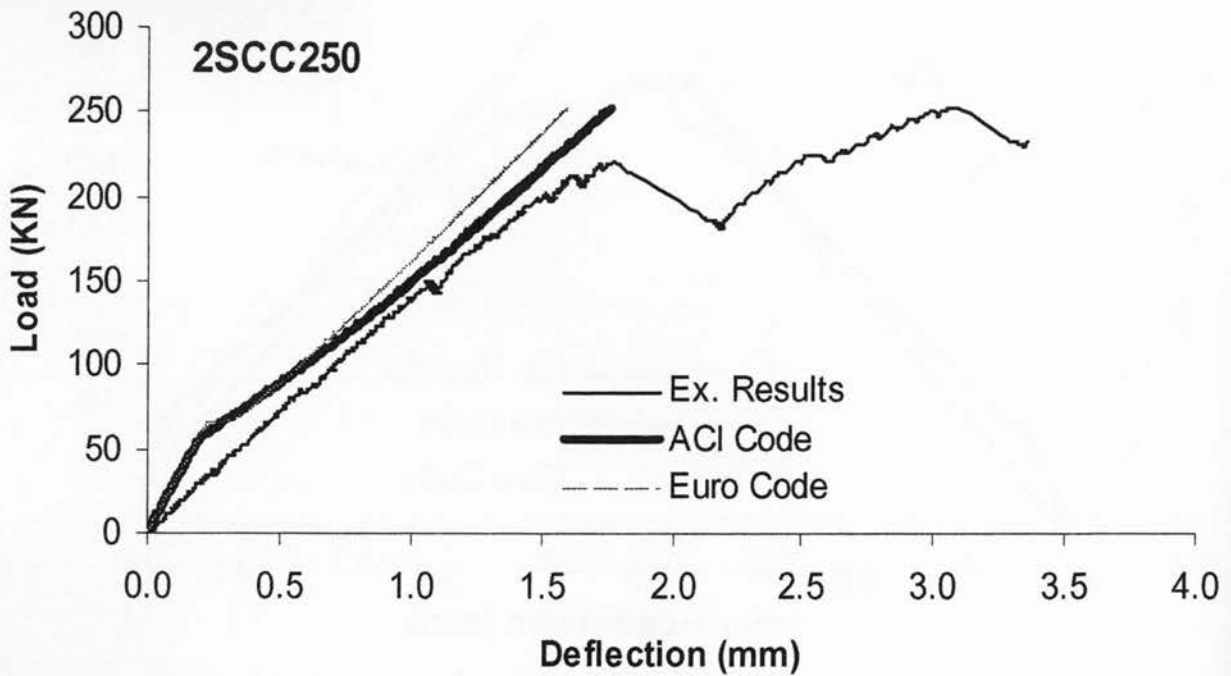


Figure 5-29: Comparison of experimental and Code-based load-mid span deflection responses (2SCC250)

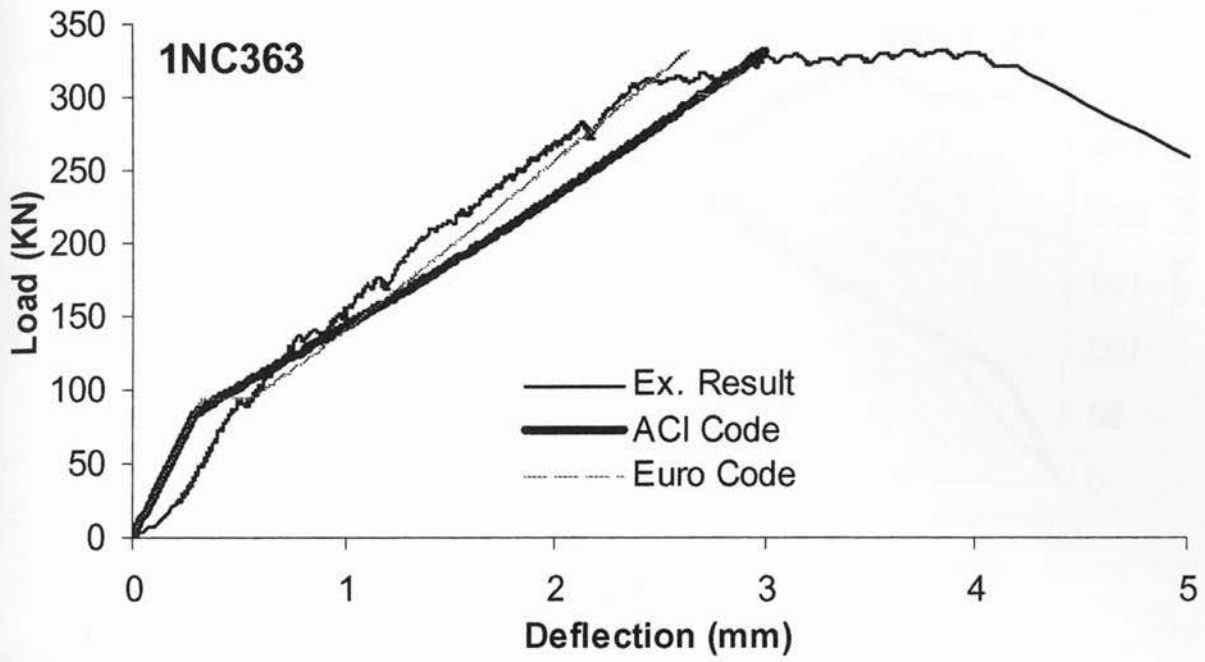


Figure 5-30: Comparison of experimental and Code-based load-mid span deflection responses (1NC363)

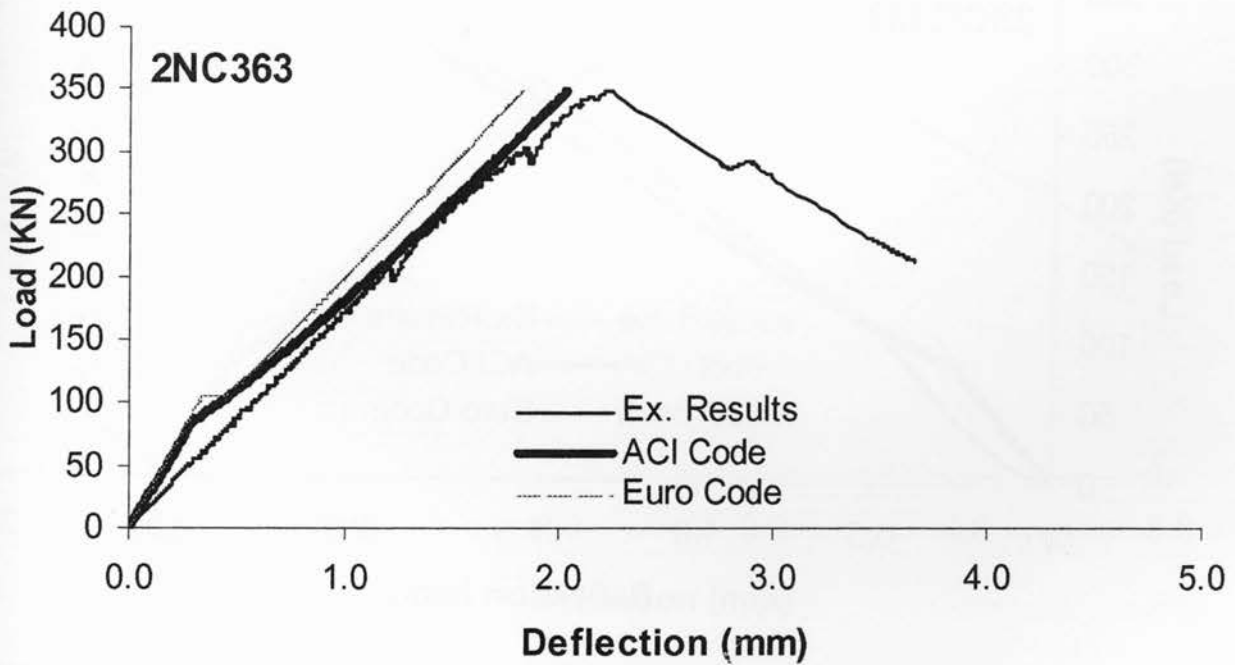


Figure 5-31: Comparison of experimental and Code-based load-mid span deflection responses (2NC363)

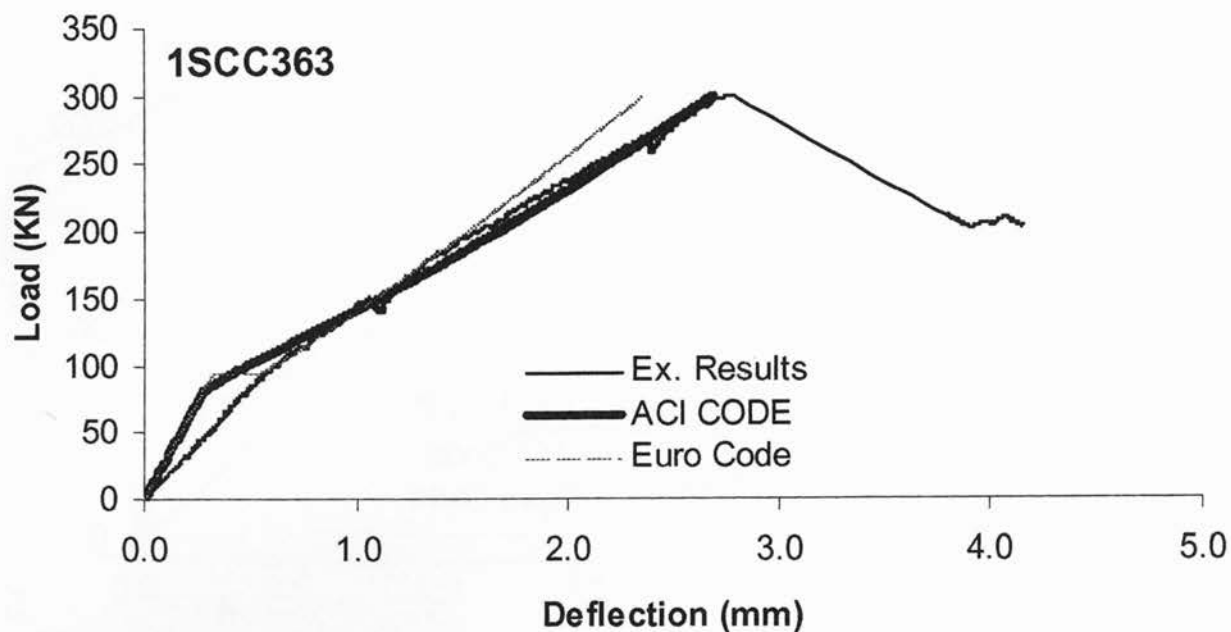


Figure 5-32: Comparison of experimental and Code-based load-mid span deflection responses (1SCC363)

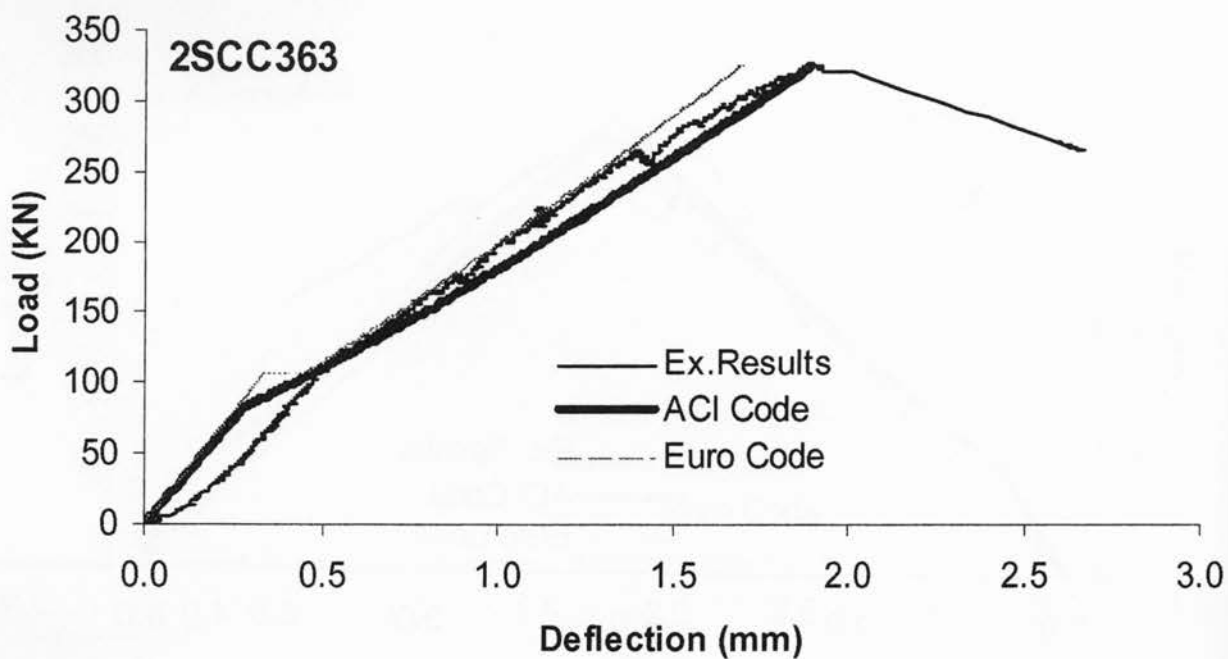


Figure 5-33: Comparison of experimental and Code-based load-mid span deflection responses (2SCC363)

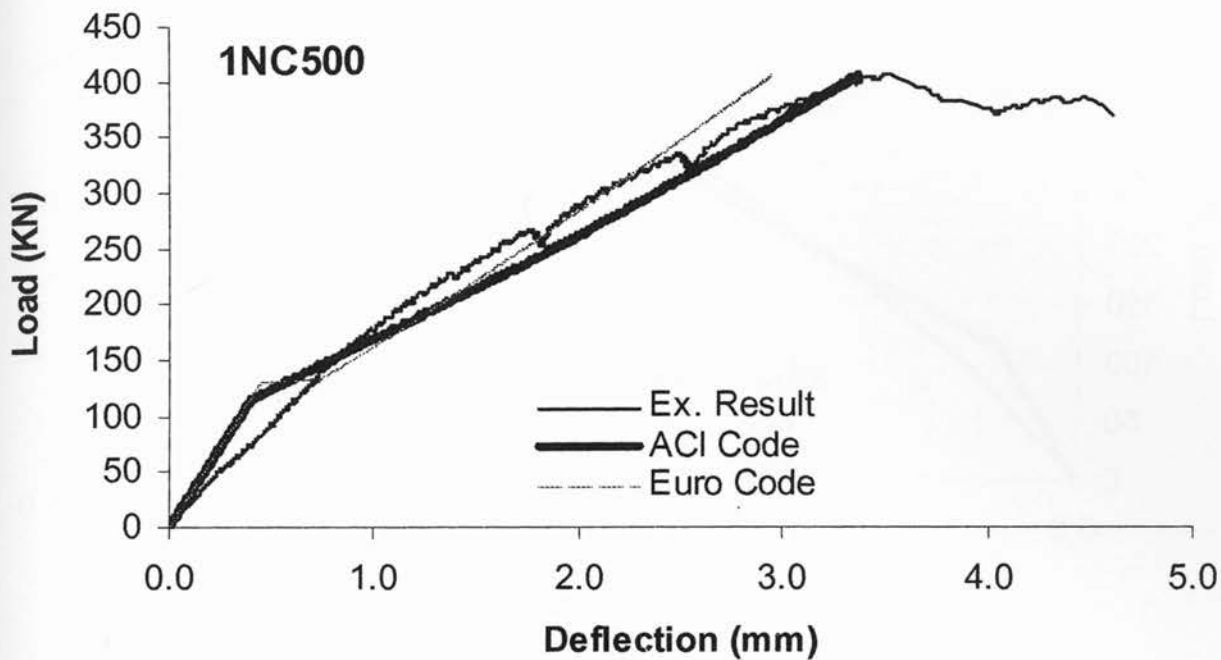


Figure 5-34: Comparison of experimental and Code-based load-mid span deflection responses (1NC500)

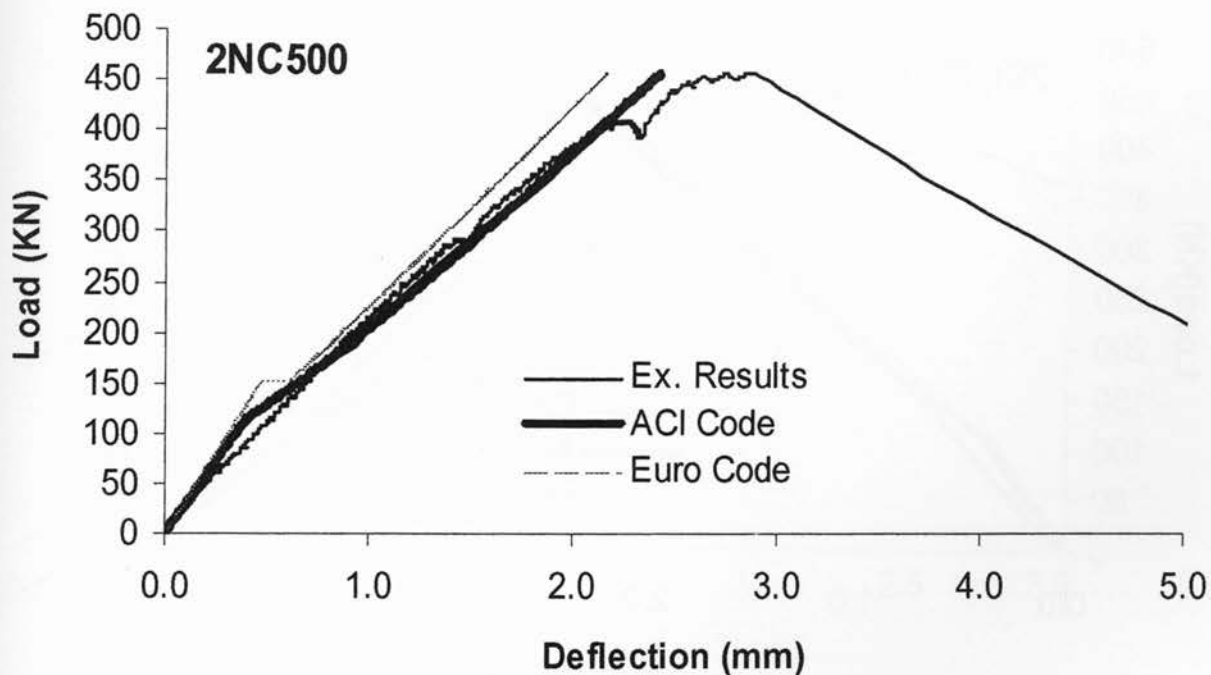


Figure 5-35: Comparison of experimental and Code-based load-mid span deflection responses (2NC500)

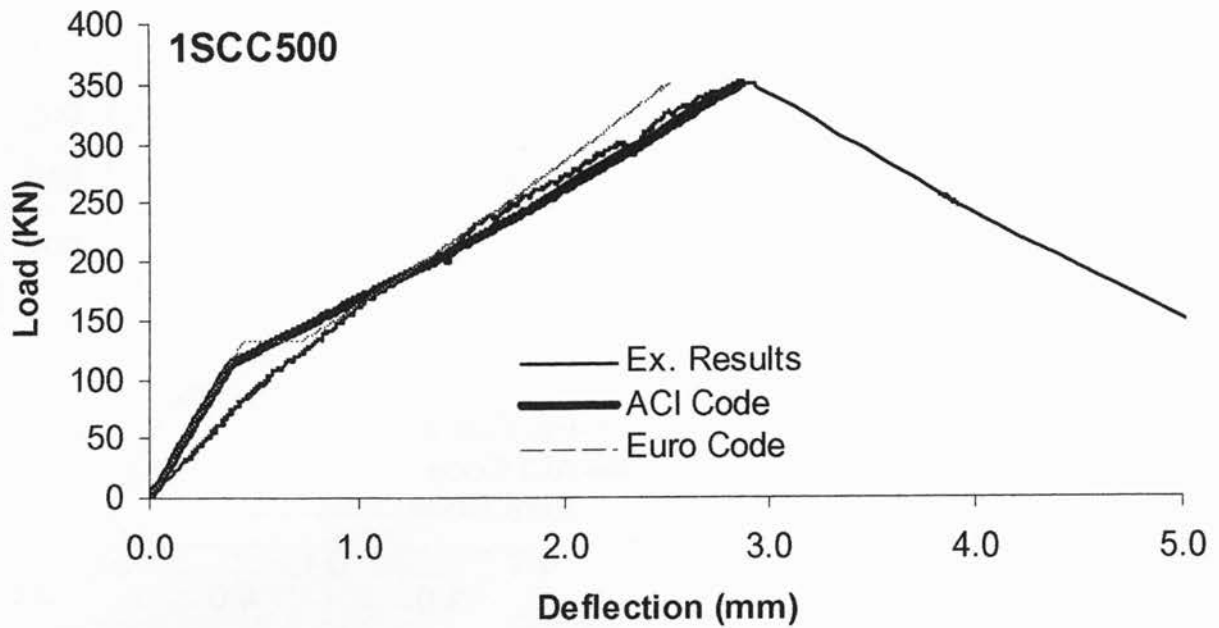


Figure 5-36: Comparison of experimental and Code-based load-mid span deflection responses (1SCC500)

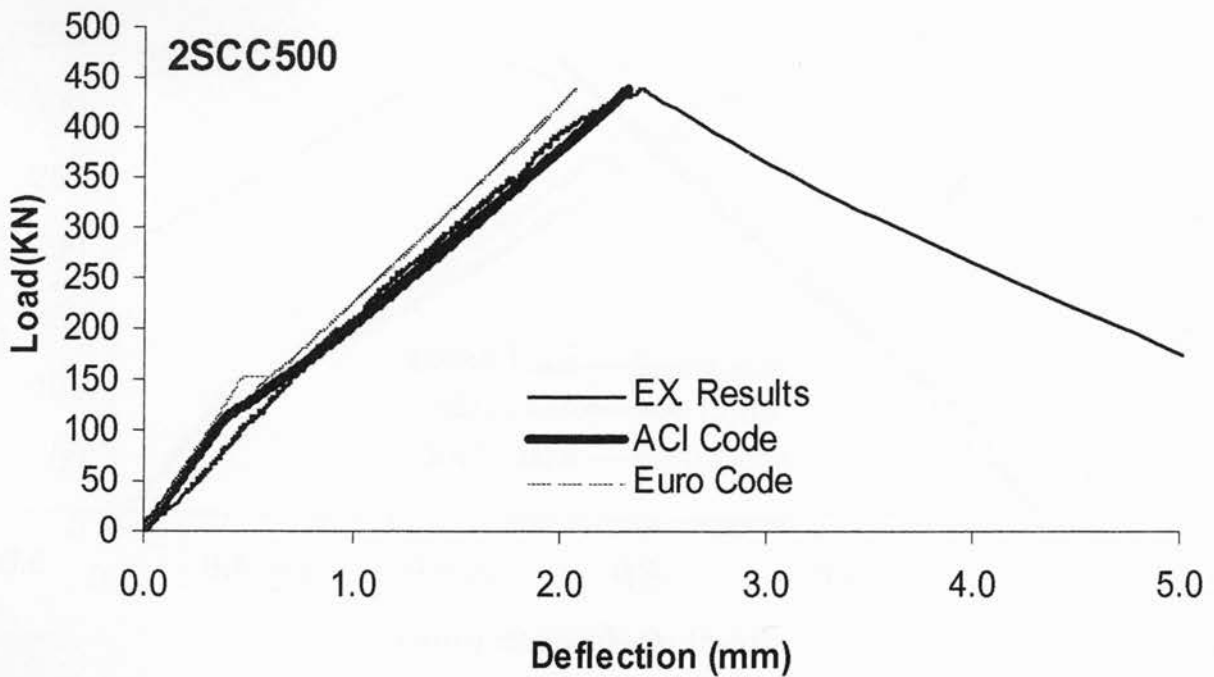


Figure 5-37: Comparison of experimental and Code-based load-mid span deflection responses (2SCC500)

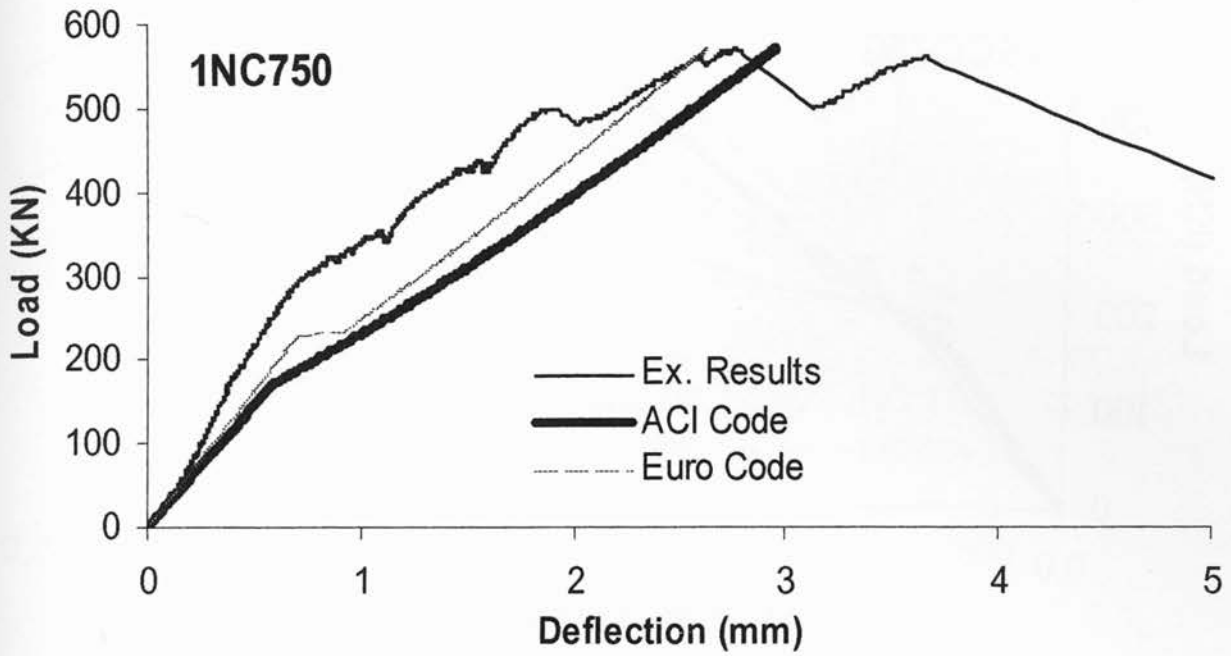


Figure 5-38: Comparison of experimental and Code-based load-mid span deflection responses (1NC750)

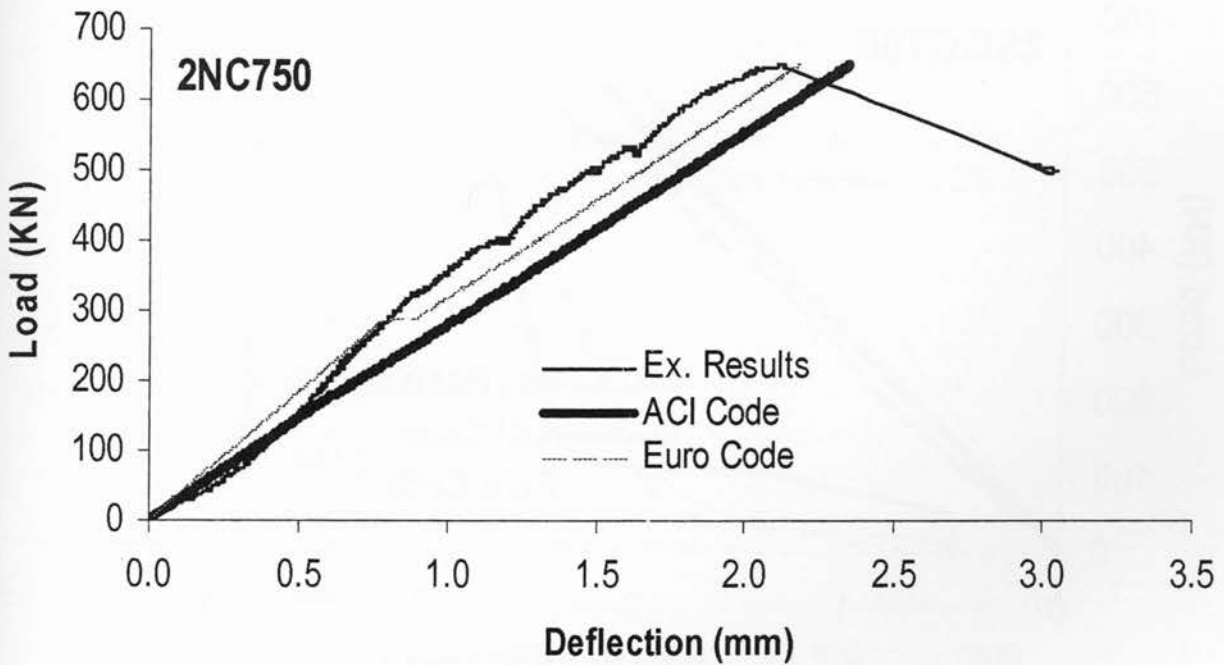


Figure 5-39: Comparison of experimental and Code-based load-mid span deflection responses (2NC750)

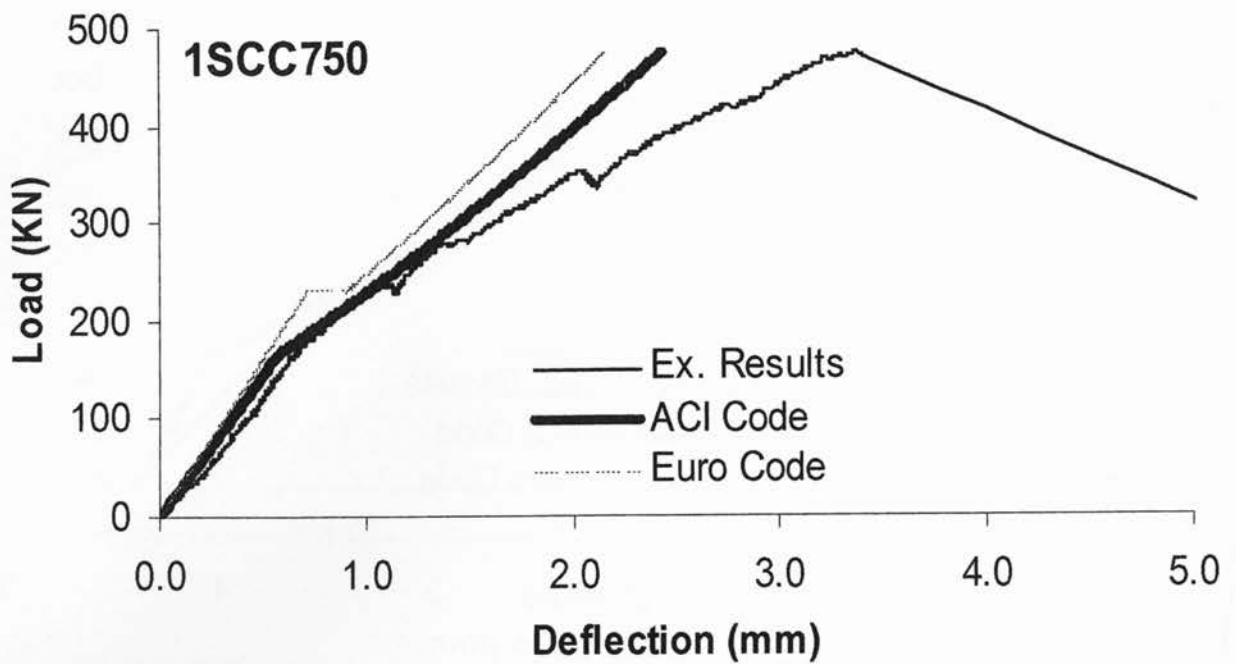


Figure 5-40: Comparison of experimental and Code-based load-mid span deflection responses (1SCC750)

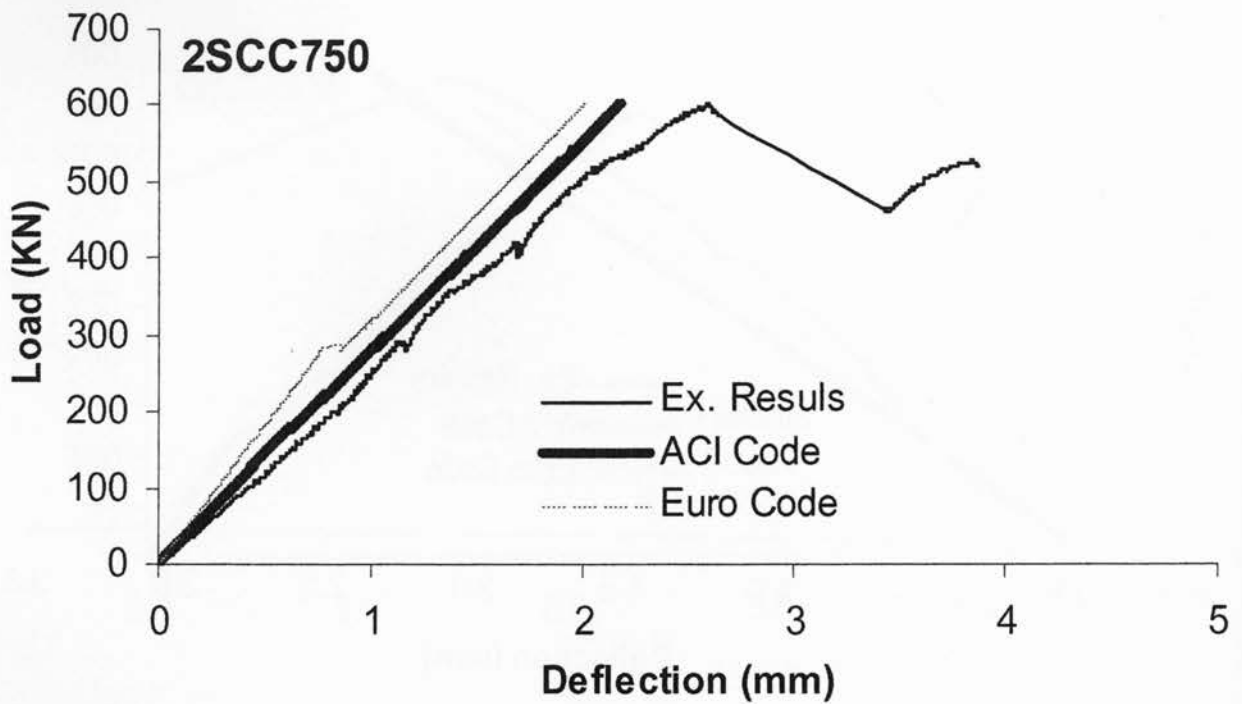


Figure 5-41: Comparison of experimental and Code-based load-mid span deflection responses (2SCC750)

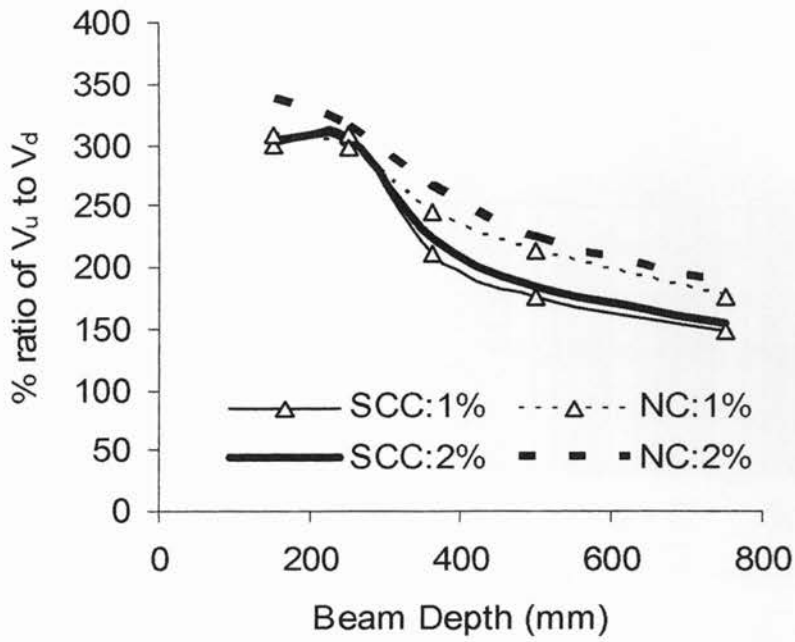


Figure 5-42: Post cracking shear resistance of SCC/NC beams

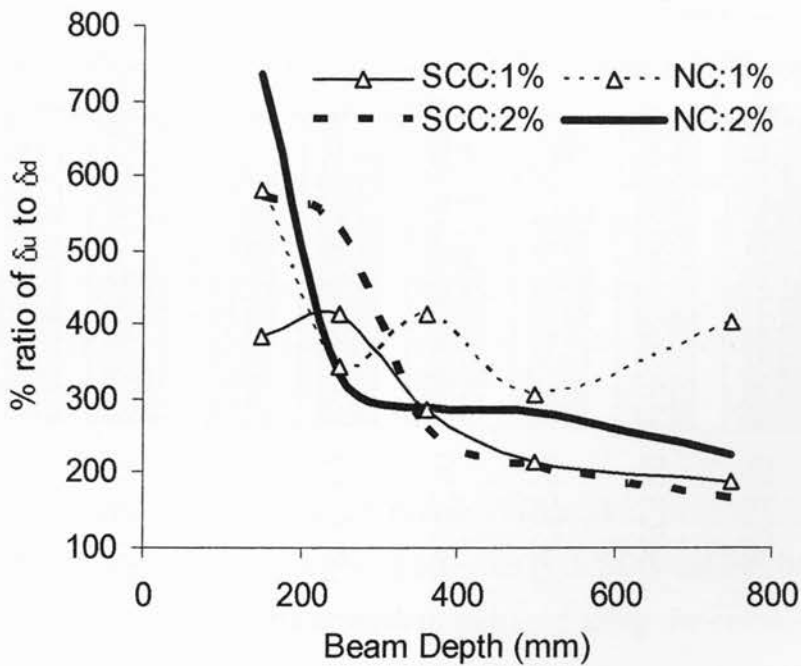


Figure 5-43: Post cracking shear ductility of SCC/NC beams

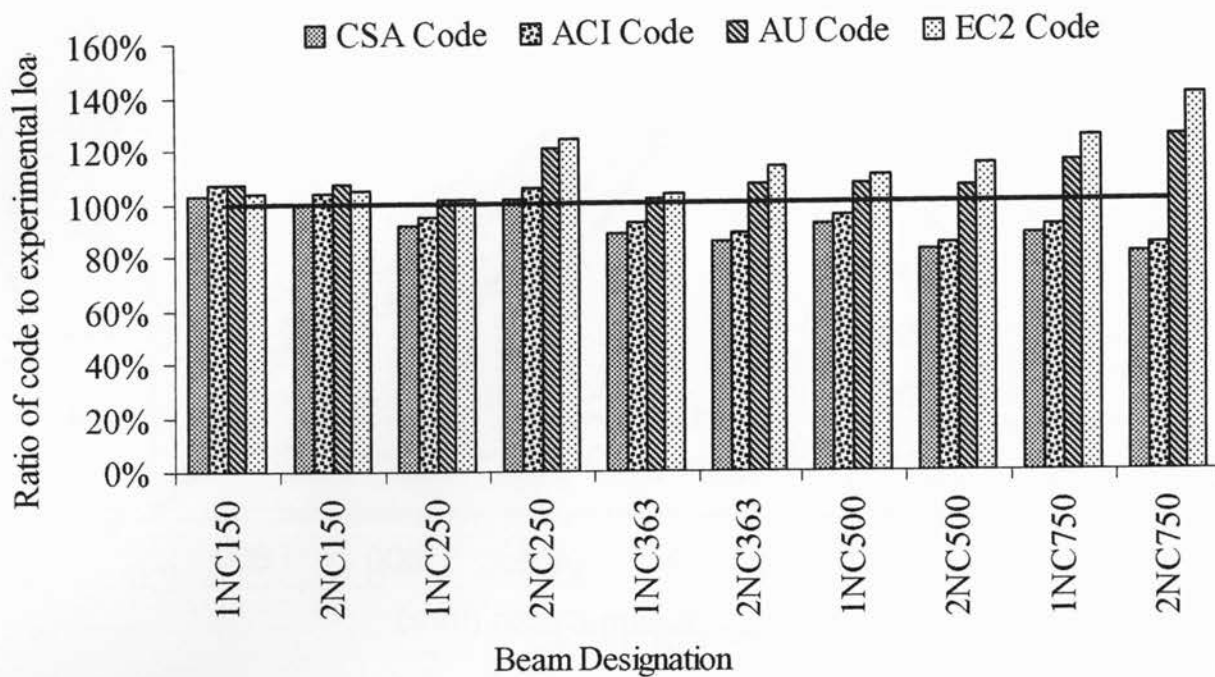


Figure 5-44: Ratio of Code to experimental first cracking load for NC in both 1% and 2% ρ_w

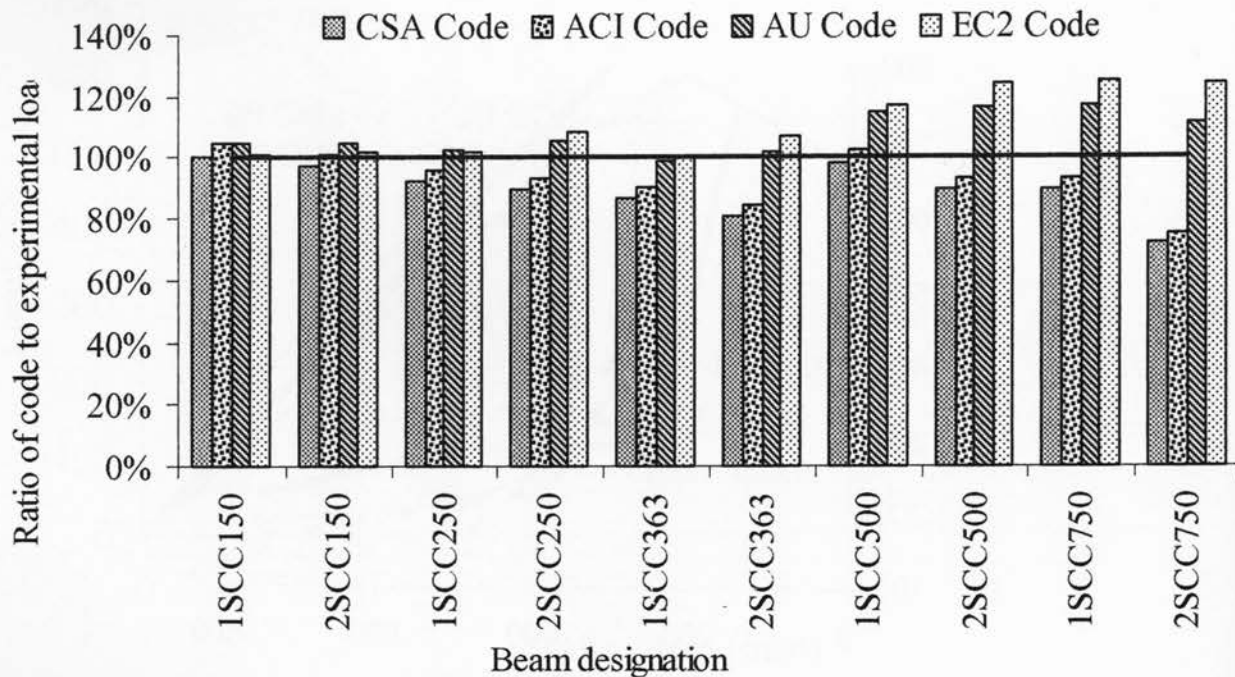


Figure 5-45: Ratio of Code to experimental first cracking load for NC in both 1% and 2% ρ_w

6 Bond Resistance - Results and Discussion

6.1 General observation

Visual observation through transparent formwork showed that the SCC properly filled the forms with ease of movement around reinforcing bars. In general, casting SCC beam was continuous, much faster and easier with less labor effort, compared to casting NC beam which consumed lots of effort and time during vibration and surface finishing. In addition, the electrical vibrator faced difficulty to reach some areas among the heavy reinforcement when casting NC beam. No indication of bleeding at the surface of the two beams was observed during casting, this is because the two mixtures were high quality concretes (Table 4.1).

According to the visual observation through the transparent formwork during casting, SCC mixture flowed under its own weight fast and easy between the dense reinforcements without any materials blockage even in the narrow areas (Fig. 6.1). SCC reached the far end of the beam (4 meter length of travel) within 5 seconds from the beginning of casting.

The level of SCC mixture during the whole time of casting was not horizontal along the beam length but rather slightly inclined (Fig. 6.1) because of the higher viscosity of SCC. Hence, at the end of casting some effort was required to level the top surface of SCC beam. After formwork removal, SCC beam showed smoother and finer surface with less surface pitting compared to NC specimen.

The results of the pull out tests for both SCC and NC beams showed pull out failure of embedded bars (Fig. 6.2) without cracks or spalling of concrete cover. There was no indication of splitting failure in any of the tested bars. This type of failure is attributed to the heavy confinement due to the great cover and the presence of heavy reinforcements around the embedded bars (CEB-FIP).

6.2 Effect of concrete age on bond and compressive strength

Table 6.1 presents the results of the bond stress in both SCC and NC beams at all tested ages (1, 3, 7, 14 and 28 days). The bond stress was averaged along the embedded length of the bar using the following equation:

$$u = \frac{P}{\pi d_b l} \quad (6.1)$$

where p is the applied load, d_b is the nominal diameter and l is the embedded length

Figures 6.3 and 6.4 represent the development of the bond stress with age in both SCC and NC beams at the three heights (150, 510, and 870 mm from the bottom). The slope of the bond stress-age relationship in both SCC and NC beams was very steep before 7 days then becomes constant and almost horizontal after 7 days. This result indicates that the bond stress developed very fast at early age (up to 7 days) and then stagnated with very slow development up to 28 days.

In attempt to verify the uniformity of the compressive strength of the tested specimens, Schmidt hammer and core tests were taken at different locations along the length and the height of the pullout specimen. The results of those tests were very close indicating insignificant variation of compressive strengths along the specimen's height and length. Figure 6.5 compares the development of the compressive strength in both SCC and NC mixtures. The compressive strength development was fast within the first 7 days followed by a slower rate up to 28 days. Figures 6.3, to 6.5 show that the development of bond stress with age (especially in early age) was faster than the development of compressive strength in both SCC and NC mixtures. These results are in agreement with the finding of other researchers (Chan 2003 and Khayat 1998). Also, no significant differences were noted between SCC and NC mixtures in terms of bond stress or compressive strength development with age. It should be noted that the two mixtures were designed to obtain the same compressive strength and had the same type of materials; the only differences were the mix proportions and the use of HRWR to obtain the required flowability of SCC. The amount of slag that acts as a pozzolanic material which could influence the development of compressive strength (ACI Committee 233, 1995) with age was not significantly different in both mixtures (only 35 kg/m^3 difference). Therefore, the two mixtures did not show differences in the development of compressive strength with age.

6.3 Effect of mixture type bond stress

In order to analyze and compare the bond stress in SCC and NC beams, the effect of the variation of compressive strength (f_c') has to be taken into account. Since the predicted development length of reinforcing bars calculated by ACI 318 (2005) and CSA A23.3 (2004) is inversely proportioned to the square root of the compressive strength, the bond stress (u) was normalized (Table 6.1) to count for the difference in compressive strength as follows:

$$u_{nz} = \frac{u}{\sqrt{f'_c}} \quad (6.2)$$

where u_{nz} is the normalized bond stress.

Figure 6.6 presents the normalized bond stress with age in both SCC and NC beams at different heights. The normalized bond stresses are found to be not equal in all ages (especially at early ages). This observation may indicate that the bond stress is not necessarily proportioned to the compressive strength at early ages and if such a correlation between the bond stress and the compressive strength was valid at all ages, Fig. 6.6 would have shown a horizontal line relationship. The reason behind such findings can be attributed to the difference between the development of compressive strength and the development of bond stress with age as indicated earlier.

Figure 6.6 also compares the normalized bond stress in SCC and NC beams at different ages. The normalized bond stress is found to be slightly higher in SCC than that in NC at 3, 7, 14 and 28 days. At the age of 1 day, the difference of normalized bond stress between SCC and NC is hardly recognized. The reason for that could be related to the incomplete development of bond stress at early age. The ratio of the normalized bond stress of SCC to that of NC (u_{ns}/u_{nn}) was higher in top bars and late tested ages compared to bottom bars and early tested ages. For example, the average value of u_{ns}/u_{nn} was 1.077 in top bars at late ages (14 and 28 days) compared to 1.029 in bottom bars at early ages (3 and 7 days). The maximum u_{ns}/u_{nn} was detected at 14 days in the top bars which was 1.085.

It should be noted that in this investigation the bond stress of SCC was slightly higher than that of NC; this finding was somehow different from other researchers' findings (Chan et al. 2003, Khayat 1998) which showed significant increase of bond stress in SCC mixtures compared to that in NC mixtures. The two mixtures in this investigation were designed to obtain high compressive strength; both had slag cement as a pozzolanic material and low water cement ratios (Table 4.1). Therefore, the two mixtures are considered to be high quality concrete and the effect of bleeding, segregation and surface settlement (that could affect the bond stress) was reduced by the superior characteristics of high quality concrete to resist those phenomena's (Aïtcin and Neville 1993, Larbi 1993).

6.4 Comparison between experimental and predicted bond stresses

The provision of both ACI (2005) and CSA (2004) Code-based equations accounts for the developmental length (l_d) of deformed bars only. The minimum required bond stress can then be calculated based on the calculated development length as follows:

$$u = \frac{f_y A_b}{l_d \pi d_b} \quad (6.3)$$

where A_b is the area of the tested bar, l_d and d_b are the embedded length and the diameter of the tested bar, respectively.

According to ACI Code provision (2005), the development of deformed bars in tension can be calculated in SI units as follows:

$$\frac{l_d}{d_b} = 0.027 \frac{f_y}{\sqrt{f'_c}} \frac{\psi_t \psi_e \psi_s \lambda}{\left(\frac{c_b + k_{tr}}{d_b} \right)} \quad (6.4)$$

where ψ_t is the location factor which can be taken as 1.3 if the horizontal reinforcement is placed such that more than 300-mm of fresh concrete is cast below the development length of the bar and 1.0 in all other cases. Therefore, in this investigation ψ_t was taken as 1.3 for calculating the development length of the top and middle bars while 1.0 for the bottom bars. ψ_e is the bar coating factor which was taken as 1.0 as the tested bars were uncoated. ψ_s reflects the more favorable performance of smaller diameter reinforcement, and ψ_s was taken as 1.0 as the tested bars were 20 mm diameter bars. λ is a factor reflecting the lower tensile strength of lightweight concrete and the resulting reduction of the splitting resistance. λ was taken as 1.0 since the tested concretes were normal density. The term $(C_b + K_{tr})/d_b$ was limited to 2.5 because the splitting failure was not likely to occur but rather pull out failure was expected due to the heavy confinement around the tested bars. In addition, the pull out failure actually occurred and confirmed experimentally in all tested bars (Fig. 6.2).

The Canadian Code presents similar equation to calculate the development length for reinforcing bars. The main difference between the Canadian and ACI Code is the bar diameter factor. In ACI Code, this factor is reduced from 1.0 to 0.8 if the bars are equal or less than 6 mm diameter whereas it is reduced from 1.0 to 0.8 if the bars are equal to or less than 20 mm diameter. Therefore, the predicted values of bond stress calculated by ACI Code are 20% less than that calculated by the Canadian Code (Table 6.1).

From Table 6.1, the predicted values obtained from both ACI and CSA codes are found to be significantly lower than those obtained from experiments. For example, the ACI predicted values are on average 20% of the values obtained from experiments at 28 days. The term $(C_b + K_{tr})/d_b$ in equation 2 represents the contribution of confining reinforcement across potential splitting plan and depends on some factors such as the concrete cover thickness and transverse reinforcement. This term was limited to 2.5 because the increase of cover or transverse reinforcement is unlikely to increase the anchorage capacity. In this investigation, the tested bars were located in extremely high confinement (because of the great cover and presence of heavy reinforcement around each bar) with positions and testing techniques that differ from the actual case of the anchorage in conventional flexural beams. Therefore, the confining effect caused extra anchorage yielding higher bond stresses in experiments compared to those predicted by either ACI or CSA codes.

The ratio of predicted to experimental values of the bond stress was not constant in all test ages. For example this ratio was 0.24, 0.17, 0.20, 0.23, and 0.23 at 1, 3, 7, 14, and 28 days of testing, respectively when using ACI equation to calculate the minimum bond stress in the bottom NC bars. This is because the development of bond strength was not proportional to the development of the square root of compressive strength in the same manner at all ages (as shown before). Therefore, the concrete age factor needs to be considered in both ACI and CSA equations especially if the bond stress is calculated before the age of 14 days.

6.5 Bond stress-slip relationship

The free end slip was measured during each pullout test using LVDT connected to a data-acquisition system. Typical bond stress-slip relationship is shown in Fig. 6.7. The experimental load-free end displacement relationships for all tested bars are presented in Appendix A. The figure shows osculating relationship because the load was applied manually using manual hydraulic jack. In order to obtain clear picture to compare between each test, the data after the peak bond stress were discarded then the curves were refined using six order polynomial trend line as shown in Figures 6.8 through 6.10.

Figures 6.8 through 6.10 show the bond stress-slip relationship at different ages for both SCC and NC beams at different bar heights. Both the bond stress and the stiffness of the bond stress-slip curve (expressed in the slopes of the curves) were higher in SCC beams than that in

NC beams at 7, 14 and 28 days. It could be noted that the difference was more pronounced at late age compared to early age. The relationship for the bond stress-slip at 1 and 3 days is not presented here because of the close results which does not present clear picture for comparison. At late age the bond stress was completely developed and gained its full strength therefore, the results of 28 days showed the best relationship to represent the effect of SCC over NC mixtures in enhancing the bond stress and the stiffness of the bond stress-slip.

The bond stress-slip relationship in this investigation did not show significant difference between SCC and NC mixtures. As the two mixtures provided similar compressive strengths and the quality of the two mixtures was relatively high (high strength and low w/c), the effect of bleeding, segregation and surface settlement that influence the bond stress was reduced as mentioned before.

6.6 Effect of bar location on bond stress

The provision of ACI and CSA codes specifies that the top bars are those which are placed such that more than 300 mm of fresh concrete is cast below them. Therefore, the middle and top bars in this investigation are considered as top bars. Figures 6.3 and 6.4 present the results of the bond stress of the embedded bars at 3 heights from the bottom of the beam (150 mm (bottom bars), 510-mm (middle bars) and 870-mm (top bars)). In both NC and SCC beams, the bond stress was slightly higher in the bottom bars than that in top and middle bars at all ages. For example, the bond strength was 20.5 MPa for bottom bars compared to 19.7 MPa for top bars in the SCC beam at 28 days. Also, the bond strength was 20.6 MPa for bottom bars compared to 18.9 MPa for top bars in the NC beam at 28 days. As expected, the increase of the specimen height resulted in an increase of bleeding, segregation and surface settlement which cause a reduction of the bond stress. No significant difference was detected between the top and middle bars at all ages (Figs. 6.3 and 6.4) which confirms the provision of ACI and CSA codes for treating all bars with more than 300-mm concrete cast below as top bars. Also, no significant difference was detected in the bond stress between the top, middle or bottom bars at 1 and 3 days of testing. This is because the bond stress was not fully developed at early age which was not manifested in terms of difference between the three bar levels.

Figures 6.11 through 6.13 compare the normalized bond strength for SCC and NC in the three bar levels at different ages. The figures show that the normalized bond stress of the top bars

was slightly higher in SCC beams than that in NC beams. Meanwhile no significant difference was detected between the normalized bond strength of the bottom bars of SCC and NC during all ages. For example, the 28-days normalized bond stresses at the top bar were 2.95 and 2.75 for SCC and NC, respectively. The 28-days normalized bond stresses at the bottom bar were 3.05 and 3.00 for SCC and NC, respectively. As mentioned before, the effect of bleeding, segregation and surface settlement was reduced in SCC compared to NC beam especially in top bars but the difference was not pronounced because of the superior performance of the two mixtures.

The stiffness of the bond stress-slip curve was also higher in the bottom bars compared to the top bars in both SCC and NC beams as shown in Figures 6.8-6.10. In additions, the bond stress-slip curve showed similar trends for both SCC and NC beams in the bottom bars while showing higher bond stress and stiffness in top and middle bars for SCC compared to NC.

The ratio of the bond stress of bottom to top bars ($U_{\text{bottom}}/U_{\text{top}}$) is presented in Figs. 6.14 to 6.16. The ratio $U_{\text{bottom}}/U_{\text{top}}$ was higher than 1 at all tested ages. Also, this ratio was lower in the SCC beam compared to the NC beam at all ages which indicates that the top bar factor was reduced in SCC compared to NC. This is attributed to the reduction of bleeding, segregation and surface settlement in SCC compared to NC.

Figures 6.14 through 6.16 also indicate that the ratio of $U_{\text{bottom}}/U_{\text{top}}$ started with high value at zero displacement (slip) followed by a decrease up to a net displacement of about 0.2 mm and then, remained almost constant with the increase of net displacement. This result was clearer at 28 days since the bond strength had gained its full strength at that time. At zero displacements, the bond strength was resisted by the bearing of the ribs against the concrete surface and hence, high bond strength was obtained. With the initiation of net displacement, the concrete behind the ribs began to crush and grind allowing some bar slips. With the increase of loading the concrete behind the ribs become compacted and resisting more pullout load until the highest bond strength obtained (around 1 mm displacement). With further increase of pullout loading The force transfer mechanism changes from rib bearing to friction along the vertical line between the tops of the ribs causing a reduction of the bond strength and hence, affecting the top bar factor (CEB-FIP 200). Therefore, it is prudent to compare the bond strength at displacements less than 0.2 mm since it gives better representation of the bond strength.

Table 6-1: Measured and predicted bond stress for SCC and NC beams at different heights and ages

		SCC			NC		
		Top bar	Middle bar	Bottom bar	Top bar	Middle bar	Bottom bar
1 day	Measured bond stress (u) (MPa)	10.08	10.83	10.62	10.19	10.62	10.83
	Normalized bond stress (u_n)	2.61	2.8	2.74	2.71	2.82	2.88
	Minimum bond stress predicted by ACI (MPa)	2.06	2.06	2.68	2	2	2.6
	Minimum bond stress predicted by CSA (MPa)	2.57	2.57	3.35	2.5	2.5	3.26
3 days	Measured bond stress (u) (MPa)	16.99	16.99	17.52	16.56	16.77	17.3
	Normalized bond stress (u_n)	4.01	4.01	4.14	3.83	3.88	4
	Minimum bond stress predicted by ACI (MPa)	2.25	2.25	2.93	2.3	2.3	2.99
	Minimum bond stress predicted by CSA (MPa)	2.82	2.82	3.66	2.88	2.88	3.74
7 days	Measured bond stress (u) (MPa)	18.26	18.26	19.43	17.83	17.94	19.32
	Normalized bond stress (u_n)	3.3	3.3	3.51	3.17	3.18	3.43
	Minimum bond stress predicted by ACI (MPa)	2.94	2.94	3.83	3	3	3.9
	Minimum bond stress predicted by CSA (MPa)	3.68	3.68	4.78	3.75	3.75	4.87
14 days	Measured bond stress (u) (MPa)	18.37	18.15	19.11	17.62	18.05	19.64
	Normalized bond stress (u_n)	2.97	2.94	3.09	2.74	2.8	3.05
	Minimum bond stress predicted by ACI (MPa)	3.29	3.29	4.28	3.43	3.43	4.46
	Minimum bond stress predicted by CSA (MPa)	4.11	4.11	5.35	4.29	4.29	5.57
28 days	Measured bond stress (u) (MPa)	19.75	20.17	20.49	18.9	19.53	20.59
	Normalized bond stress (u_n)	2.94	3.01	3.05	2.76	2.85	3
	Minimum bond stress predicted by ACI (MPa)	3.57	3.57	4.64	3.65	3.65	4.74
	Minimum bond stress predicted by CSA (MPa)	4.46	4.46	5.8	4.56	4.56	5.93

* Top bar at 870mm from the bottom of the beam
Middle bar at 510mm from the bottom of the beam
Bottom bar at 150mm from the bottom of the beam

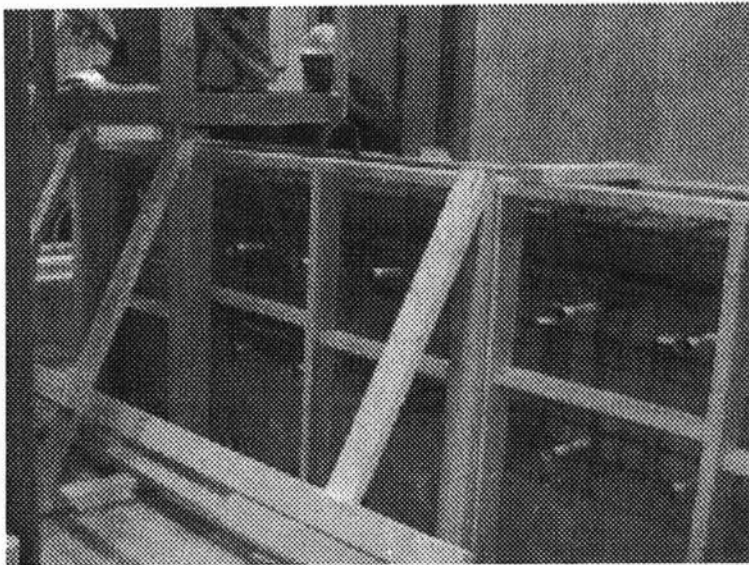


Figure 6-1: SCC beam during casting

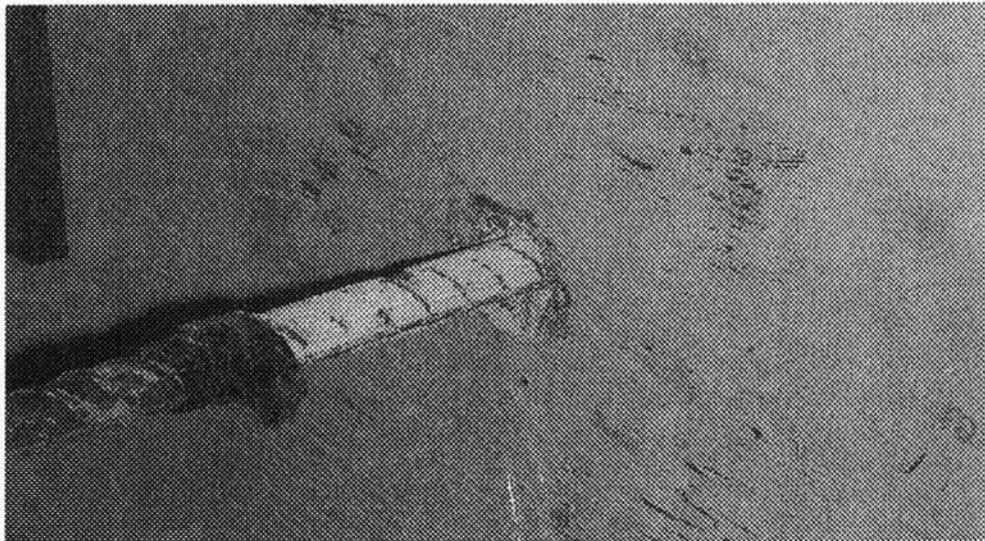


Figure 6-2: Typical pull out failure

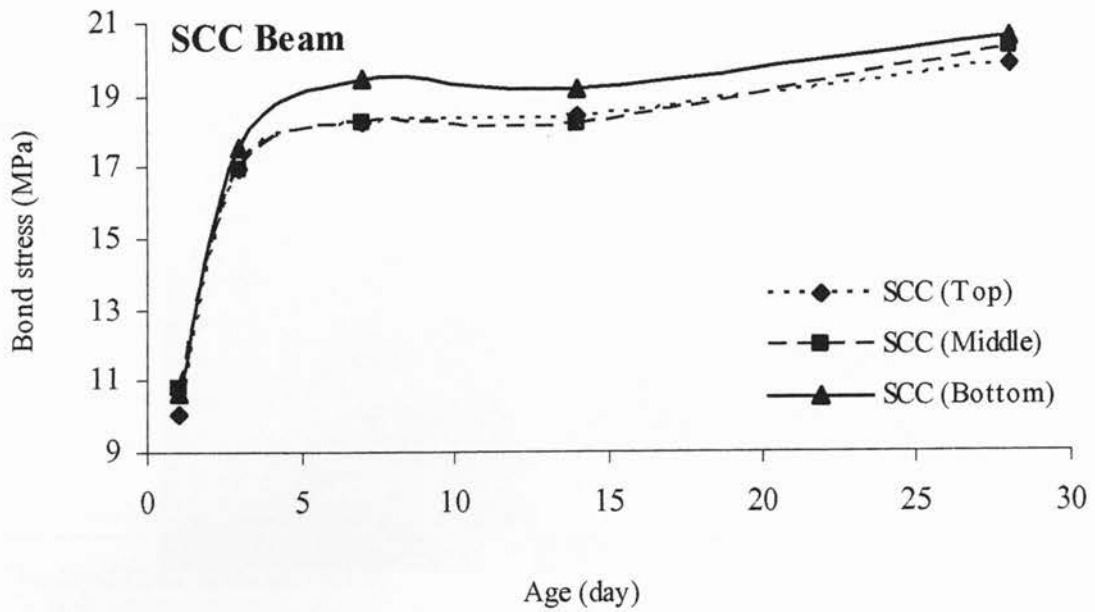


Figure 6-3: Development of bond stress with age for the SCC beam

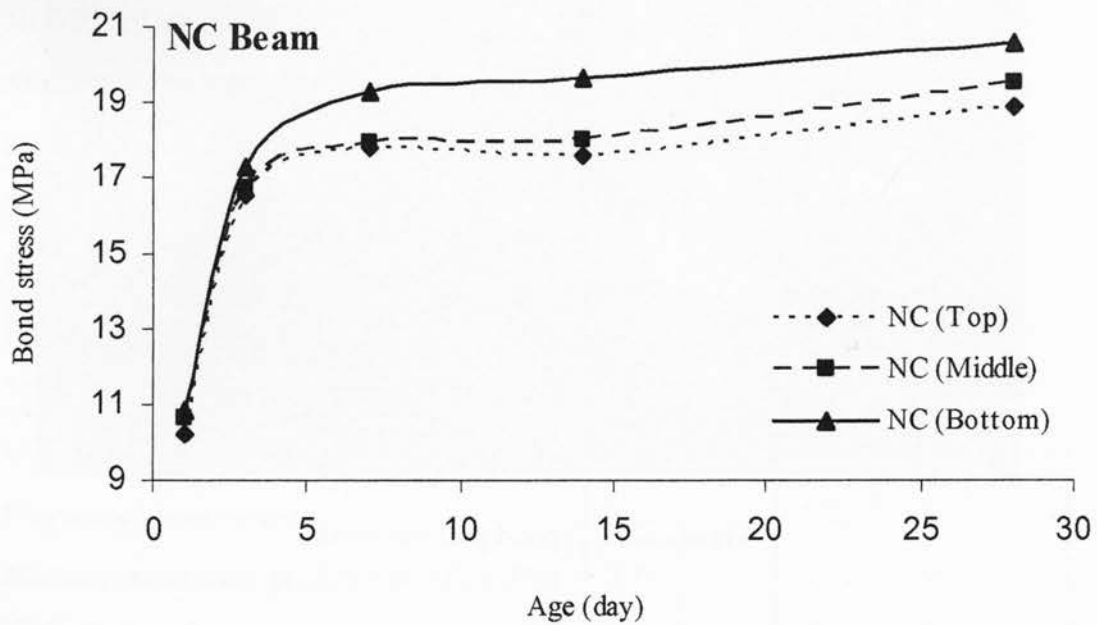


Figure 6-4: Development of bond stress with age for the NC beam

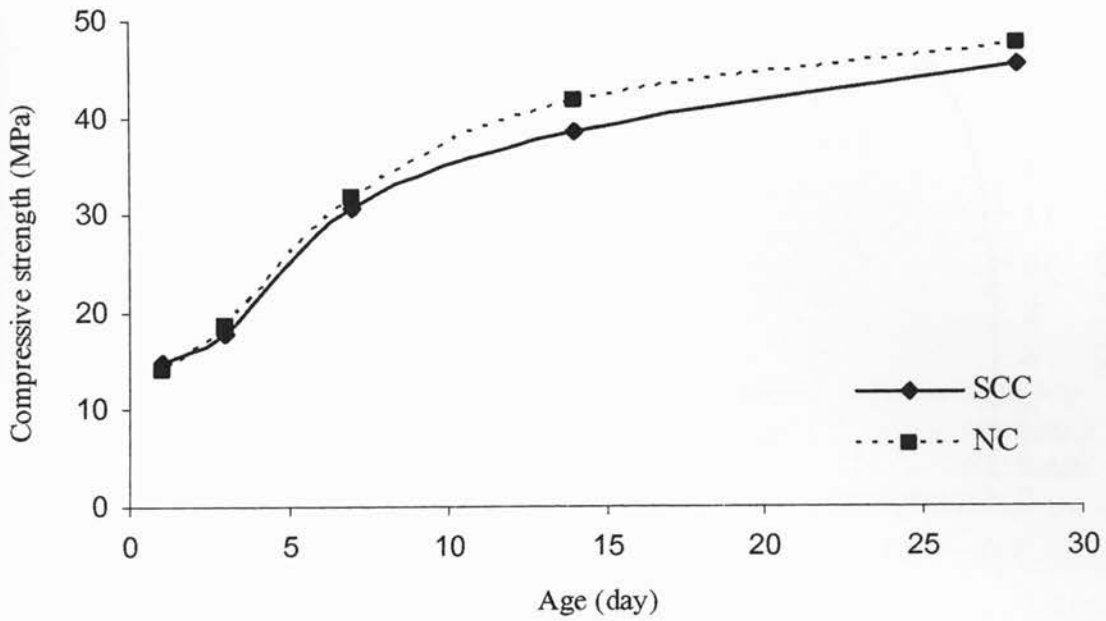


Figure 6-5: Development of compressive strength with age for both SCC and NC beams

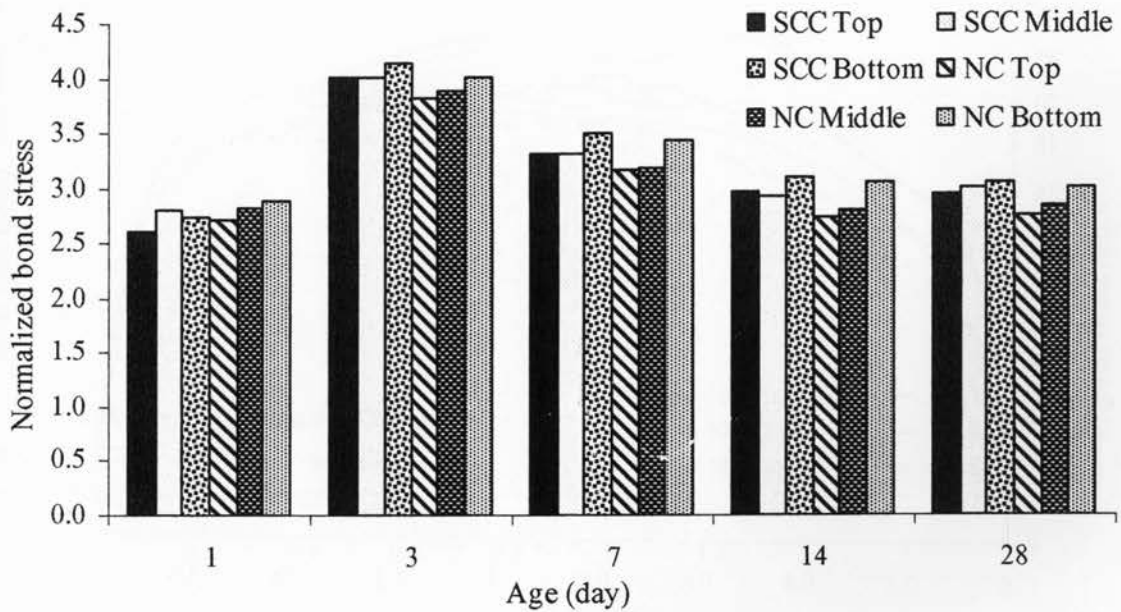


Figure 6-6: Normalized bond stress with age for both SCC and NC beams

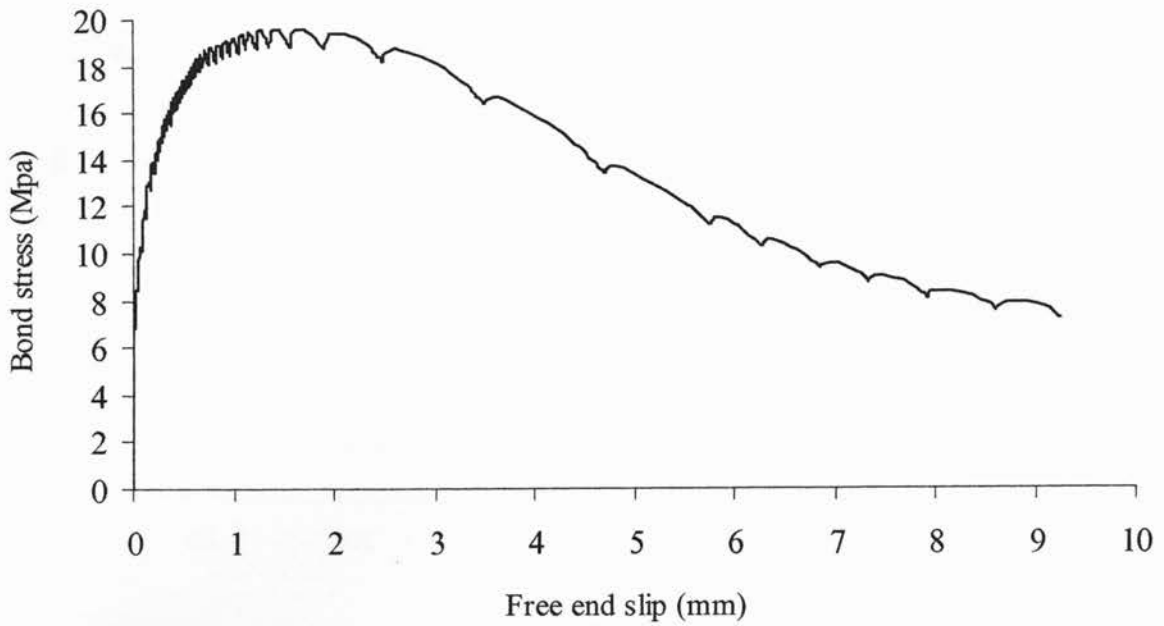


Figure 6-7: Typical bond stress-free end displacement relationship

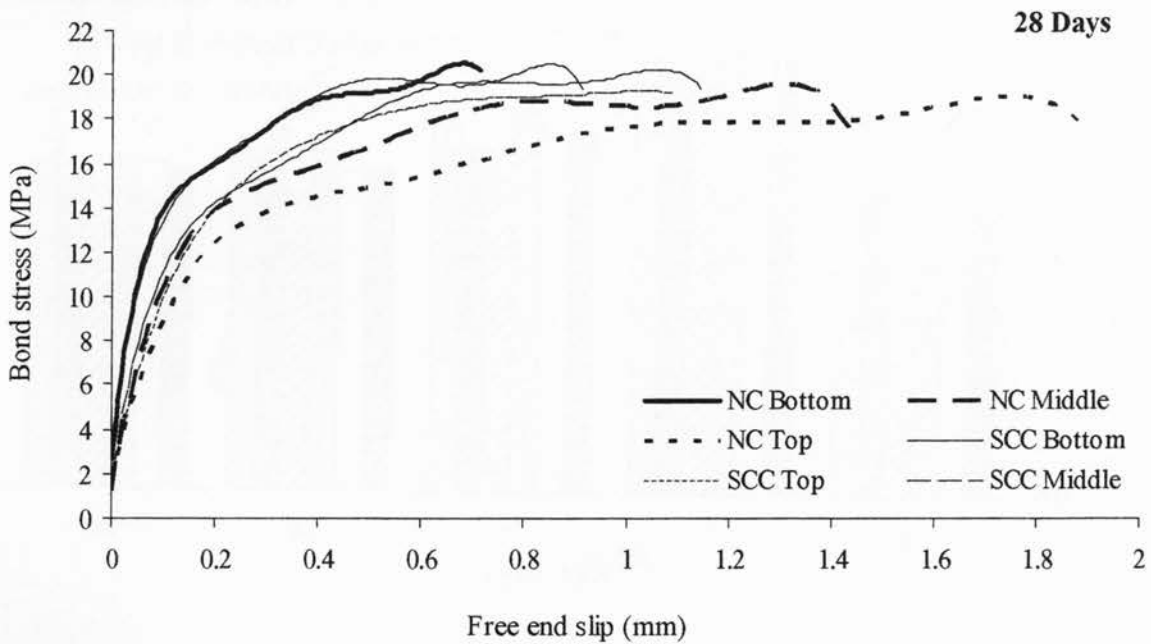


Figure 6-8: Bond stress-free end slip relationship at 28 days for SCC and NC beams at different bar elevations

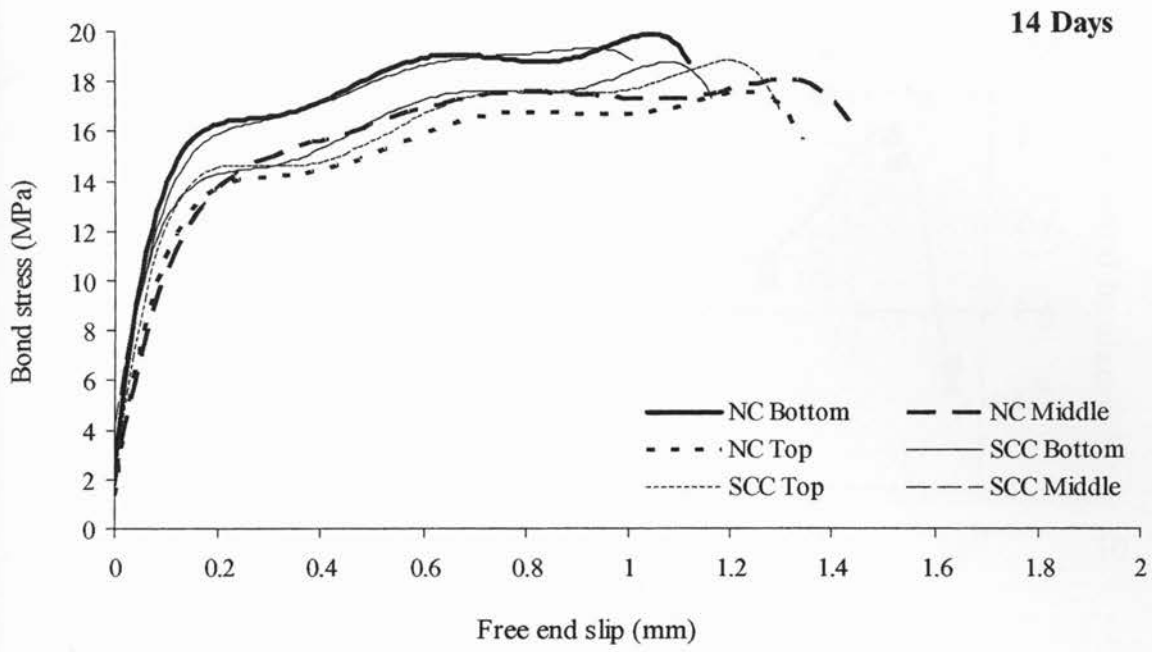


Figure 6-9: Bond stress-free end slip relationship at 14 days for SCC and NC beams at different bar elevations

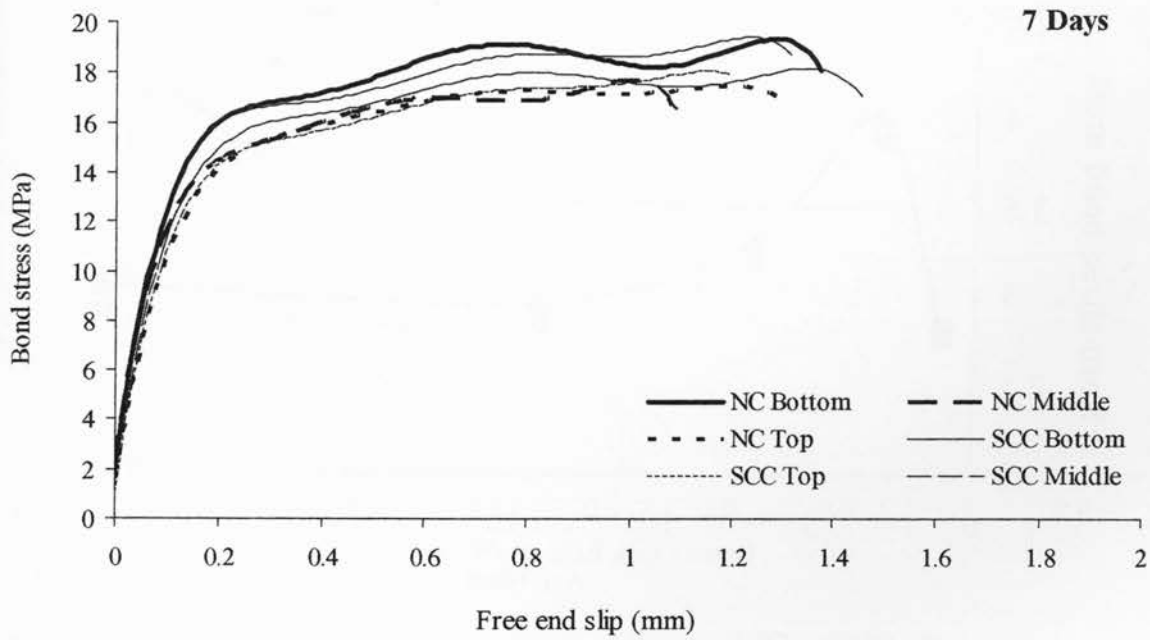


Figure 6-10: Bond stress-free end slip relationship at 7 days for SCC and NC beams at different bar elevations

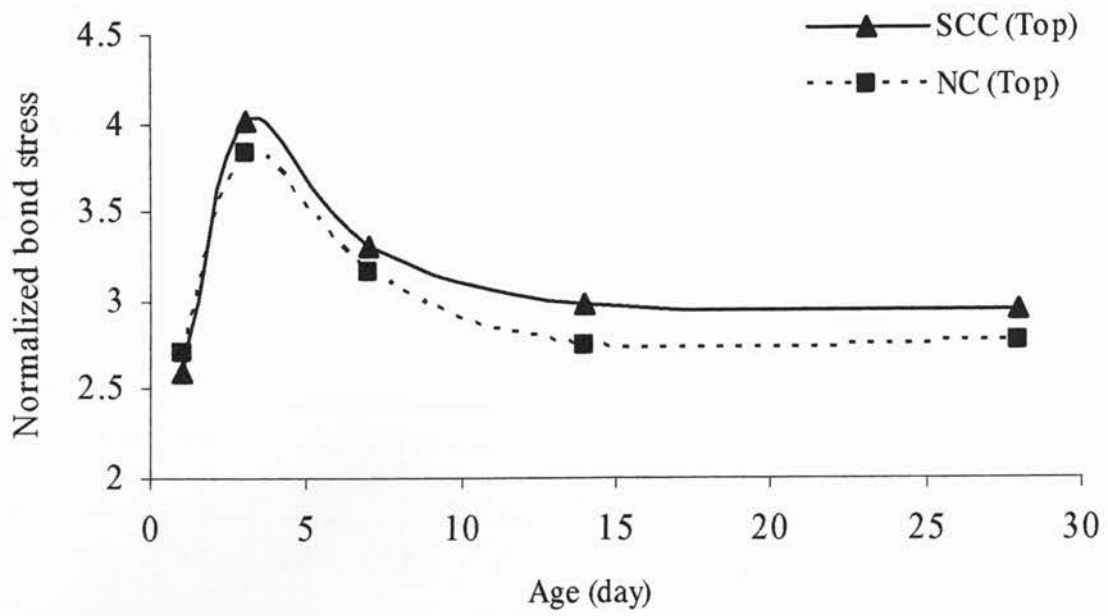


Figure 6-11: Normalized bond stress in SCC and NC beams (top bars)

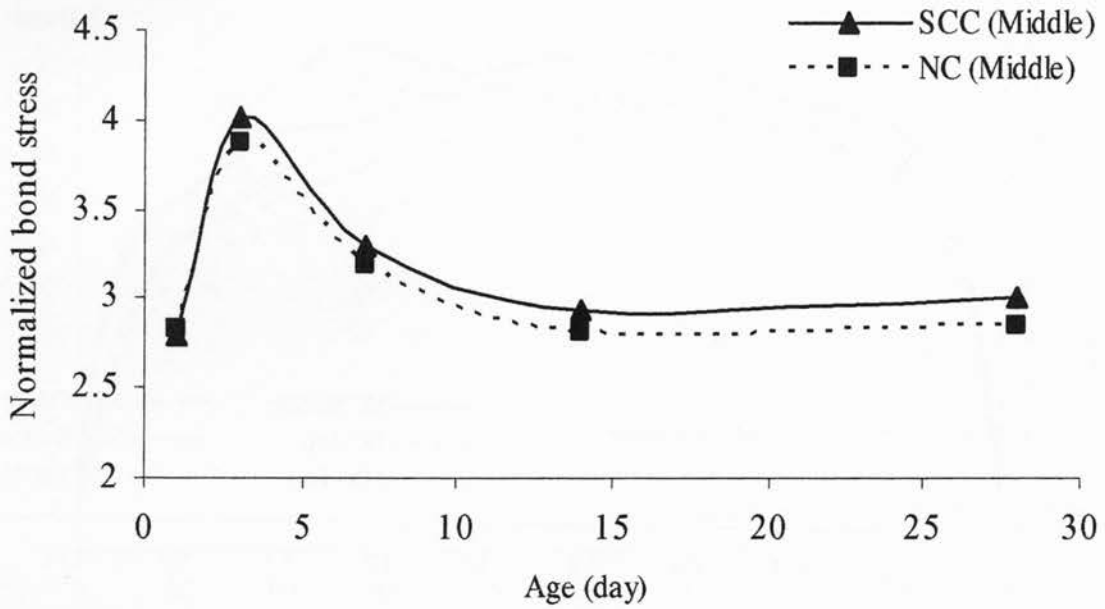


Figure 6-12: Normalized bond stress in SCC and NC beams (middle bars)

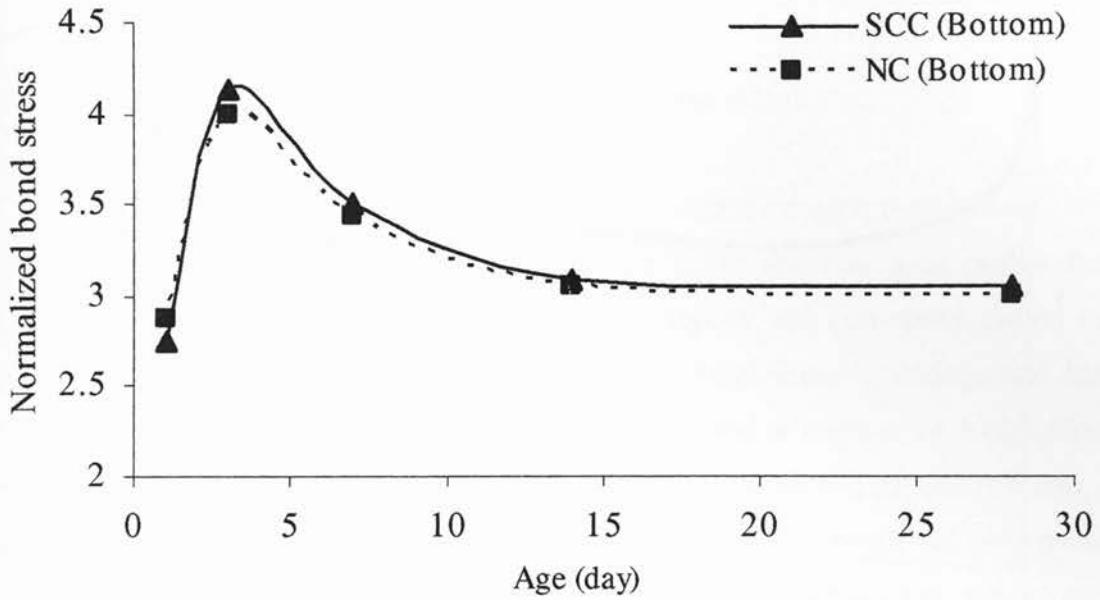


Figure 6-13: Normalized bond stress in SCC and NC beams (bottom bars)

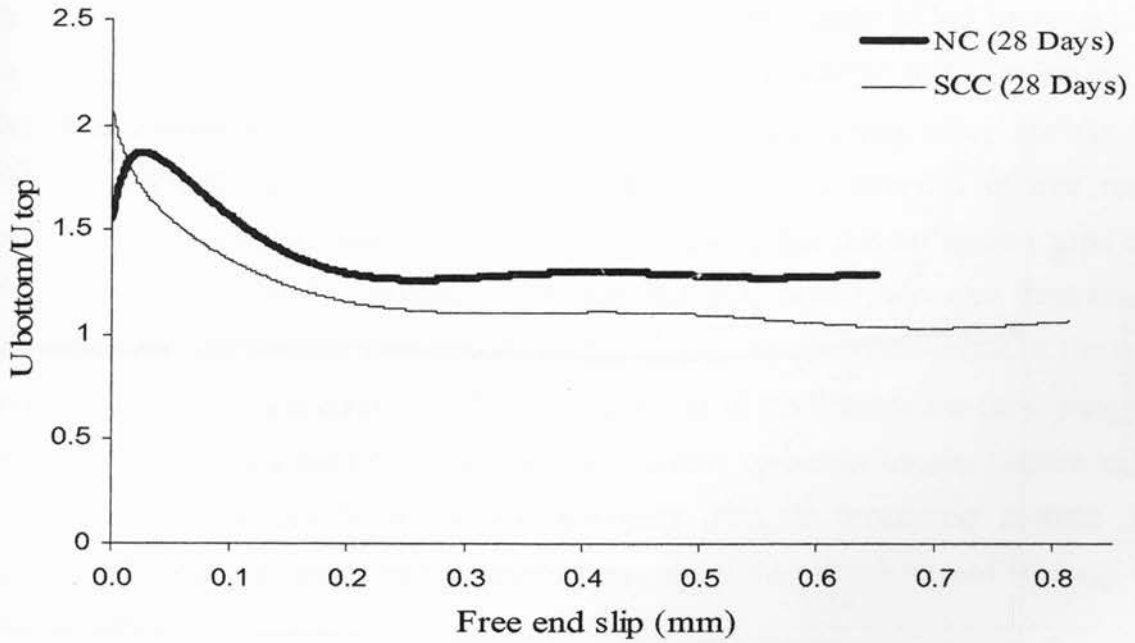


Figure 6-14: Top bar factor at various free end slip for SCC and NC (28 days tested age)

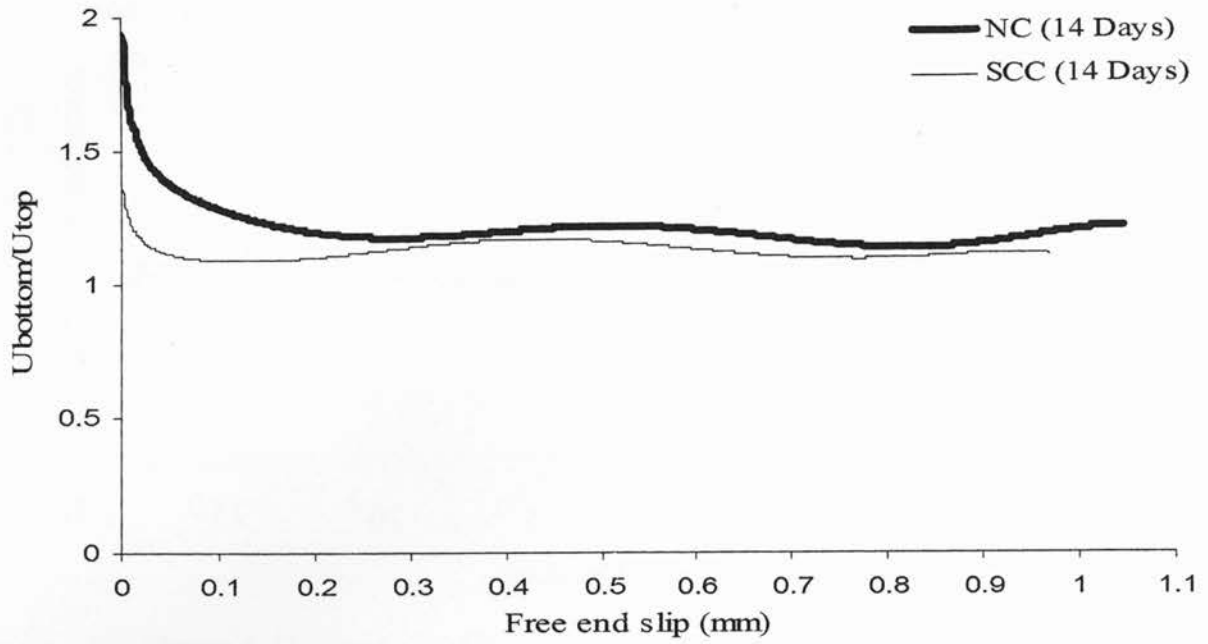


Figure 6-15: Top bar factor at various free end slip for SCC and NC (14 days tested age)

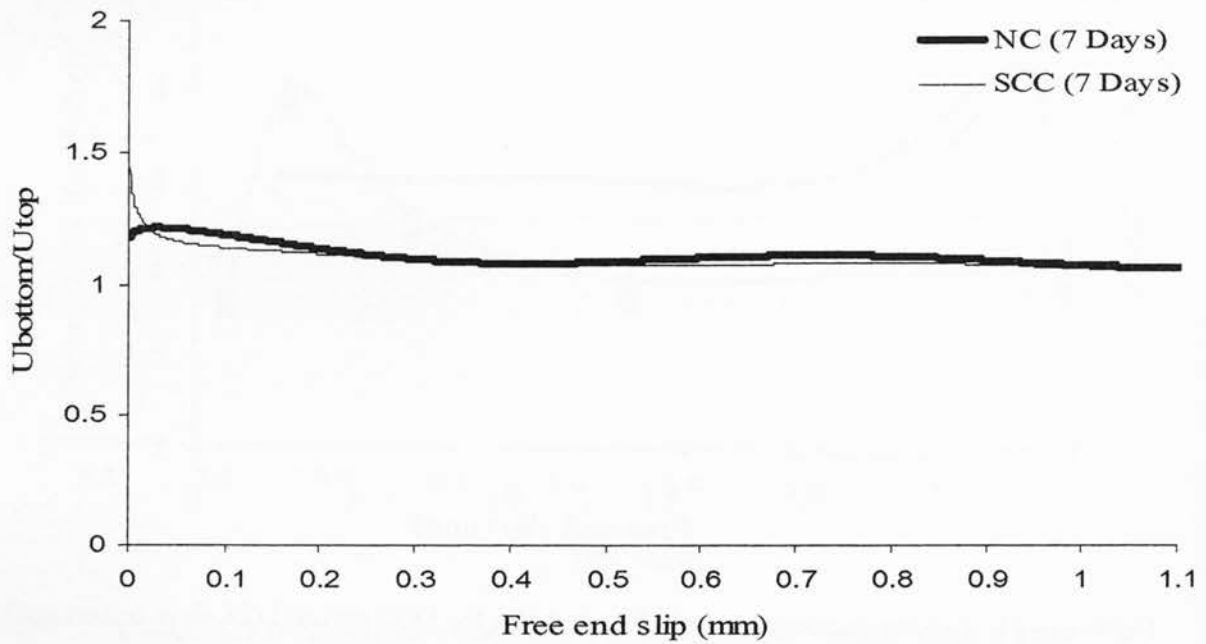


Figure 6-16: Top bar factor at various free end slip for SCC and NC (7 days tested age)

7 Corrosion Resistance - Results and Discussion

7.1 Performance of SCC/NC specimens under corrosion attack

7.1.1 General cracking observation

Figures 7.1 to 7.4 show the crack patterns and widths of each tested beam, after the completion of corrosion stages. SCC beams exhibited fewer and less wide cracks than NC beams, for both moderate and severe corrosion stages (epoxy and non-epoxy coated stirrups beams). For example, SCC-N beam did not have any longitudinal cracking, and had few transverse cracks at stirrup locations, while NC-N beam had a number of longitudinal and transverse cracks. Also, the average crack width for SCC-E beam was around 0.4 mm, while the average crack width for NC-E beam was around 2.4 mm. This result can be attributed to the higher durability and the superior performance of SCC mixture in rebar corrosion resistance due to its dense and enhanced microstructure.

Figures 7.1 to 7.4 also show that the crack patterns and widths were not uniformly distributed in SCC beams, as they were in NC beams. SCC-N beam had only one broken part at the beam's corner, located away from the casting point, while NC-N beam exhibited uniform crack patterns and widths along the beam length. Similarly, SCC-E beam had big spalled cover at the corner of the beam, located away from the casting point, and the crack width at the bottom of the beam was increasing towards the direction of that corner. Meanwhile, NC-E beam showed somehow uniform cracking and had no spalled parts along the beam length. This can be attributed to the fact that SCC beams were cast from one end allowing the concrete to reach the other end under its own weight. The weight of the falling concrete during casting was enough to compact the corner of the beam below the casting point while it did not well compacted at the far end. Corners of beams usually require enough compaction due to the restrain of concrete movement from the formworks in three sides. Therefore, SCC beams showed weak and porous concrete at the corners located far away from the casting points.

The results also indicated that SCC beams were easier to break at the mentioned corners compared to NC beams (which did not break even at corners, having higher crack widths). The reason could be attributed to the fact that the NC mixture contained 25% more of coarse aggregate content than the SCC mixture. The higher volume of coarse aggregate in NC

mixture caused higher crack arresting and prevented the concrete from spalling even at corners with higher crack widths.

7.1.2 Time-dependent corrosion test results

7.1.2.1 Current results

The corrosion rate was monitored during the accelerated corrosion test by a computer-controlled data-acquisition system, which records the current at each one hour interval. Figures 7.5 and 7.6 show the relationship between the current in mA and the immersion time, in days, for SCC/NC beams, with epoxy and non-epoxy coated stirrups tested for severe and moderate corrosion stages, respectively. In general, the current-immersion time relationship for all beams showed an initial decrease in the current followed by a gradual increase. The decrease of the current in the first few days is an indication of the formation of the passive film around the reinforcing steel bar, which protects the steel from corrosion. When depassivation of the steel occurs, corrosion starts and then the rate of corrosion increases significantly (Cornet et al. 1968).

NC beams demonstrated higher current values in the early stages of the test, approximately 1.8 and 0.9 mA in NC-N and NC-E, respectively, compared to SCC beams which demonstrated 0.6 and 0.4 mA in SCC-N and SCC-E, respectively. Also, the current in NC beams was higher than in SCC beams, during the whole test period. The lower current passing through the concrete specimens is an indication of the higher resistivity of the concrete. Permeability of the concrete is the main factor influencing the concrete resistivity (Hope and Alan 1988). The high flowability and superior resistance to bleeding and segregation of SCC beams were thought to be the main factors that improved the permeability and enhanced the quality of concrete, especially below the longitudinal bars.

The point of first increase of the slope, in the time-current curve, indicates the corrosion initiation. Also, the slope of the curve represents the rate of corrosion. NC beams showed earlier corrosion initiation and higher corrosion rate than SCC beams. The corrosion initiation in NC beams started after 3 and 9 days in NC-N and NC-E, respectively, compared to 13 and 30 days in SCC-N and SCC-E beams, respectively. The increase of the corrosion initiation time in epoxy-coated stirrup beams compared to non-epoxy coated stirrup beams was related to the stirrup corrosion, which occurred before longitudinal bar corrosion due to less cover thickness.

SCC beams exhibited a sudden jump in the time-current curve after a relatively steady slope, compared to NC beams which showed relatively gradual increase of the current with the time. The sudden jump in SCC time-current curves was the indication of the concrete cover spalling in SCC beams at the end corners (Figs. 7.1 to 7.4).

7.1.2.2 Half-cell potential measurements

Tables 7.1 through 7.4 demonstrate the results of the half-cell potential test at 25 points along each beam length/perimeter. Figures 7.7 to 7.10 present the average cross sectional readings for each point along the length of the beams. NC showed more negative values compared to SCC in both epoxy and non-epoxy coated stirrup beams (moderate and severe corrosion stages). More negative values in NC beams indicated higher probability of corrosion for NC beams than SCC beams. This expectation was verified and confirmed at the end of the test by the other tests results.

Neither the SCC nor the NC beams showed significant differences in the half-cell readings around the beams' cross sectionals compared to along the beams' lengths (Tables 7.1-7.4). In addition, the readings along the length of the beams for both SCC and NC were depending on the cover thickness, regardless of whether the steel underneath was epoxy or non- epoxy coated. For example, points 1, 3 and 5 for any beam which were located below stirrups (either epoxy or non-epoxy coated) that had 30 mm cover thickness, showed more negative values than point 2 and 4 which were not at stirrup locations and had 40 mm cover thickness. This result matched other researchers' results (Klinghoffer 1995), indicating that the concrete cover is a big factor in determining the half-cell potential reading. Also, point 3 which was located at the middle of any beam, showed less negative value compared to points 1 and 5. This is because point 3 was located below one stirrup only, compared to points 1 and 5 which were below 3 stirrups.

In both epoxy (E) and non-epoxy (N) coated stirrup beams, the readings along the length of the SCC beams were varied based on the distance from the casting point, while the reading along the length of NC beams did not show any significant differences between the two ends of the beam (Figs. 7.7-7.10). The curves for point 1 and 5 in NC-N and NC-E beams were close to each other, indicating no significant differences between the two ends of the beam, while the curves for these two points were shifted away in SCC-N and SCC-E

beams, indicating significant difference between the two beam ends. This result could be an indication of the less-good quality of concrete and the higher probability of corrosion at points far away from casting points, in SCC beams.

Figures 7.7 through 7.10 also showed that the readings of half-cell potential tests presented closed values at the late testing age (high degree of corrosion), compared to at the early testing age (initial corrosion stage). This result indicates that the used half-cell potential test can only represent the probability of corrosion for un-corroded beams, while the test might not give a good indication for already corroded beams.

7.1.3 After corrosion test results

7.1.3.1 Results of chloride content, mass loss and rebar's diameter reduction

Each beam was checked at 25 points/locations along the beam's length/perimeter (Fig 4.20). After the completion of the two corrosion stages, the chloride ion content, measurements of crack widths, rebar mass loss and the reduction of the rebar diameter were taken at each location. The chloride ion contents were taken by collecting concrete powder from each location using an electrical drill. The rebar mass loss and diameter reduction were measured by taking the bars and stirrups out of the beam. Bars were cleaned from the corrosion products and then cut into 5 segments located around each of the 25 points.

Tables 7.5 through 7.8, and Figs. 7.11 through 7.16, present the results of the chloride ion content, crack width, mass loss and diameter reduction at each point located on the beam length/perimeter. In general, the chloride ion content near the rebar surface, at all the points on NC-N and NC-E beams, were higher compared with those of SCC-N and SCC-E tested points. This result confirms the findings of the half-cell and the current monitoring results which indicated the superior performance of SCC mixture in protecting the steel bars from corrosion. The chloride ion content was also increased, with the increase of the corrosion level (Figs. 7.11-7.16). The corrosion level was indicated by the rebar mass loss or diameter reduction, or by the crack width located close to the tested points. This finding is similar to that found by other researchers (Rasheeduzzafar et al. 1992, Amleh and Mirza 1999). Tables 7.5-7.8 indicate that in both NC-N and SCC-N, the chloride ion content was higher at points located below stirrups than at points located below longitudinal bars, where the concrete cover is bigger. This result also confirms other researcher's results [Amleh and Mirza 1999,

Montemor et al. 2002], which indicate that the chloride concentration decreases from the concrete surface to the interior, in the vicinity of the steel rebar.

Figures 7.12, 7.14, and 7.16 revealed the lesser quality of the SCC beams at points located far away from the casting point (point 1), compared to better quality of concrete below the casting point (point 5). Each of the chloride ion content, crack width, rebar mass loss and reduction of bar diameter, were high at the beam's corner located far away from the casting point, compared to the corner located below the casting point. This result explains the spalling of the concrete cover at the mentioned corners, and matched the results of the half-cell potential test, during the corrosion-time monitoring.

SCC-N demonstrated no longitudinal cracks, rebar mass loss or diameter reduction at any of its points, while NC-N showed a number of cracks and significant rebar mass loss and diameter reduction. Also, SCC-E beam had fewer crack widths, less rebar mass loss and less diameter reduction in most of its points compared to NC-E beam. This also helps to prove the superior effect of SCC mixture in rebar corrosion protection.

The crack width increased with the increase of the corrosion level, in all beam types (Figs. 7.11-7.16). The corrosion products accumulate around the bar surface occupying more space and exert pressure on the concrete cover, causing cracking. The crack widths increased with the increase of rebar mass loss, except for the middle part of the external bar of NC-E beam (Fig. 7.11), which showed lower crack width at relatively high mass loss. This is due to the fact that the entire bar was corroded and diminished at this point.

7.1.4 Comparison of theoretical and actual corrosion mass loss

The corrosion mass loss was computed using Faraday's Equation 4.1, based on the amount of electrical energy sent through the bar. The calculated mass loss was compared with the actual mass loss, for each of the tested beams, after computing the total actual metal loss in the longitudinal bars and stirrups (Fig. 7.17). The results show that the actual mass loss was less than the theoretical mass loss, for all tested beams. The percentages of actual to theoretical mass losses were 97%, 91%, 83% and 74% in NC-N, SCC-N, NC-E and SCC-E beams, respectively. As indicated from previous studies (Auyeung et al. 2000, Spainhour and Wootton 2006), when current passing through a bar is suspended in a salt solution, the correlation between actual and predicted mass loss is almost perfect. On the other hand, for

bars embedded in concrete, the mass loss based on Faraday's law overestimated the actual mass. This is attributed to the fact that some of the passing currents do not contribute to corrosion, but are consumed while passing through the concrete cover.

The results also indicated that the percentage of actual to theoretical mass loss was higher in NC, compared to SCC, for all tested beams. This is because NC beams corroded faster and developed earlier cracks than SCC beams. These cracks decrease the concrete resistance, resulting in corrosion that is closer to predicted levels (Auyeung et al. 2000, Spainhour and Wootton 2006).

7.1.5 Results of the small concrete cylinders samples

After evaluating the results of the full-scale tested beams and confirming the superior performance of SCC compared to NC, it was essential to examine their performance in small concrete cylinders. This would manifest the effect of bleeding and segregation on durability degradation, as well as facilitate the investigation of the effect of different types of HRWR (used in SCC) on the protection of rebar corrosion.

The accelerated corrosion test for the concrete cylinders was terminated after 25 days when all samples had completely corroded. Figure 7.18 demonstrates one corroded concrete cylinder from each concrete type. As concluded from the current-time measurements, the corrosion initiation time, in all concrete types, was very close. Also the rate of corrosion, after corrosion initiation, was similar in the four concrete mixtures. The corrosion initiation time in SCC and NC mixtures (same mixtures used in the full-scale concrete beams), commenced after 13 days of the test, while the other two SCC mixtures (with different HRWR) exhibited corrosion initiation time 2 and 3 days earlier.

The crack pattern and crack widths were also similar in the four concrete mixtures. All concrete cylinders exhibited one longitudinal crack having 1 mm width along the length of the embedded bar (Fig. 7.18).

As expected, bleeding and segregation (associated with large concrete volumes and adopted casting/placing/vibrating techniques) were the factors affecting the concrete performance in the full-scale concrete beams, where SCC showed superior performance over NC. This was not observed in small cylinder specimens, where the bleeding and segregation was minimized and better concrete confinement to the embedded bar was ensured, compared

to the bottom longitudinal bars in the full-scale beams. This is why the small concrete cylinders did not manifest the difference between SCC and NC, in rebar corrosion protection. In addition, the close results of the corrosion performance, in all SCC mixtures, indicate that the HRWR types do not have any chemical effect on corrosion protection.

7.2 Results of testing the strength and cracking of full-scale corroded SCC/NC beams

7.2.1 Ultimate failure load and mode of failure

In order to evaluate the performance of SCC and NC beams before and after corrosion, the ultimate failure load (P_u) was normalized to count for the difference in compressive strength between SCC and NC. Since the tested beams were designed to fail in shear, and the shear strength is proportional to the square root of the compressive strength of concrete (f'_c), the normalized ultimate failure load (P_{nz}) was calculated as follows:

$$P_{nz} = \frac{P_u}{\sqrt{f'_c}} \quad (7.1)$$

Table 7.9 presents the results of the ultimate failure load for each level of corrosion of the tested beams. Figures 7.19 through 7.25 show each tested beam at failure. At 0 corrosion stage, the NC-0 beam showed 10% higher ultimate failure load than the SCC-0 beam. Both beams failed in shear as expected and the failure occurred suddenly with a loud noise, right after the formation of a dominant diagonal crack, which occurred after the formation of flexure and flexure-shear cracks (Figs. 7.19, 7.20). As mentioned before, SCC mixture contains 25% less coarse aggregate than NC mixture. The 25% less coarse aggregate content in SCC was the main reason for its lower ultimate failure load compared to its NC counterpart. The shear transfer, due to the aggregate interlock mechanism, decreases with the reduction of coarse aggregate content in the concrete medium.

At the first corrosion stage, NC-1 beam also exhibited higher ultimate failure load than SCC-1 beam (15% higher in normalized ultimate failure load). Both beams failed in shear, and the failure mode and cracking performance of the two beams was similar to that in the zero corrosion stage. No significant reduction of the ultimate failure load was observed due to the corrosion in this stage. The difference of the normalized ultimate failure load was 1% for SCC-1 and SCC-0, and 5% for NC-1 and NC-0.

The dowel action of the longitudinal bars (which depends on the bar diameter) contributes up to 25% of the beams shear capacity (Taylor 1974). At the end of this corrosion stage, NC-1 beam developed 7.68% actual mass loss of the longitudinal bars, while SCC-1 beam developed 1.48%. Both of these percentages were not high enough to obtain significant reduction of the bar diameter and to reduce the bars dowel action, flexural capacity or the longitudinal bar's anchorage bond strength. In addition, the pre-developed corrosion cracks, in both NC-1 and SCC-1 beams, had no effect on the flexural or shear cracks that developed during loading. The corrosion cracks in NC-1 beam were longitudinal cracks along the bar length and formed separately from the loading cracks. Also, the corrosion cracks and cover spalling in SCC-1 beam were developed at the beam's corner away from the support and had no interference with the cracks developed during loading. Therefore, the shear capacity of the corroded beams was not affected by the level of corrosion at this stage.

At the second corrosion stage, NC-2 beam exhibited 28% higher normalized ultimate failure load than SCC-2 beam. In addition, the normalized ultimate failure loads were reduced by 35% and 22%, compared to un-corroded beams, for both SCC and NC, respectively. Both NC-2 and SCC-2 beams showed differences in failure modes. The NC-2 beam failed due to flexure failure, while the SCC-2 beam failed due to anchored slippage failure (Figs. 7.23-7.25). At the end of this corrosion stage, the percentage of the actual mass loss in NC-2 beam was 24.49% while only 8.13% in SCC-2 beam. The mass loss and the reduction of bar diameter in NC-2 beam was somehow distributed along the bar's length, while SCC-2 beam showed concentrated mass loss and rebar diameter reduction at one end only (located far away from the casting point) (Figs. 7.26-7.27). The high level of corrosion in NC-2 beam, especially at the beam's center, caused significant reduction of rebar diameter, which reduced the capacity of the beam in flexure and resulted in flexural failure, instead of shear failure.

The longitudinal bars, for all beams, were designed to have the exact anchorage length for flexural reinforcing bars, according to A23.3-04 CL.11.3.9.1 (2004). Such design was intended to investigate the effect of the corrosion level in reducing the rebar's developmental length. The requirement for the longitudinal bar's developmental length was sufficient up to 24.49 % of the total mass loss in NC-2 beam while it was not sufficient in SCC-2 beam at 8.13% of the total mass loss. This is due to the fact that the SCC-2 beam exhibited concentrated corrosion and reduction of the bar's length at one end of the beam only, near the anchorage of

the longitudinal bars (Figs. 7.24-7.25). This concentration in corrosion significantly reduced the rebar-concrete bond strength and caused slippage of the longitudinal bars at that area.

7.2.2 Load cracking observations

7.2.2.1 Non-corroded and first degree corroded beams

As mentioned earlier, both non-corroded and first degree corroded SCC and NC beams failed in shear. The cracking behavior for those beams, under applied load, generally started with fine flexural cracks at the beam's mid span. With further increase of loading, new flexural cracks formed away from the mid-span and with additional load, either those later cracks started to curve toward the loading point or new diagonal cracks began to form separately in locations farther away from the mid span (Figs. 7.28-7.33). In both SCC and NC beams, the cracks extended up to 50% of the beam height when the load level reached 50% of the failure load, and up to 70% of the beam height when the load reached 75% of the failure load. The angle for the early curved cracks was around 55° , while the angle for the failure diagonal cracks was around 35° .

The first flexural cracks occurred in all beams at around the same load level as the tensile strength for both SCC and NC were very close. The first diagonal cracks in the SCC beams occurred at around 48% of the failure load, while the first diagonal cracks in the NC beams occurred at around 40% of the failure load. This observation supports the development of lower post diagonal cracking shear resistance in SCC due to lesser aggregate interlock, as a consequence of the presence of 25% lower coarse aggregate compared to NC.

SCC beams exhibited slightly fewer diagonal cracks at smaller angles compared to NC beams. In addition, NC beams failed after occurrence of two big diagonal cracks in both sides of the beam, while SCC beams failed after the occurrence of only one big diagonal crack, at one of the beam sides (Figs. 7.28-7.31). No differences were detected between SCC and NC beams in terms of crack widths, crack heights, or failure modes. The failure of all SCC and NC beams was noisy and accompanied with huge explosion.

7.2.2.2 Second degree corroded beams

The high degree of corrosion in SCC and NC beams that occurred in this stage greatly affected the bottom longitudinal bars, and changed the cracking performance, as well as the

failure modes. The NC-2 beam developed two vertical cracks at the middle of the beam during loading; the width of these cracks was increasing with the increase of the applied load until flexural failure occurred. The corrosion in the NC-2 beam was distributed along the beam's length in two of the three bottom bars and concentrated mostly at the middle of the third bar (Fig. 7.26). As a consequence, the flexural capacity of the beam was significantly reduced compared to the shear capacity, and the beam failed in bending.

The SCC beam developed one shallow vertical crack at the beam mid-span and this crack sustained until failure, without any significant increase in width. The failure of this beam occurred suddenly due to anchor slippage at one end only, forming one crack as indicated in Figs. 7.24 and 7.33. The severe corrosion that accumulated at one end in the SCC-2 beam caused reduction of the bar length and bond strength, which resulted in anchorage slippage failure.

The development of fewer cracks under loading in second degree corroded beams, compared to their un-corroded and first degree corroded counterparts, is believed to be related to the change of the failure mode, which eliminated the development of shear and shear-bending cracks. In addition, the development of fewer cracks in the second corrosion stage could also be related to the existence of the wide and deep horizontal crack (resulted from corrosion), which somehow separated the lower part of the beam and obstructed the transfer of the stress from the top to the lower fiber of the beam.

7.2.3 Crack width calculation

The crack widths under loading, for both NC and SCC beams in the three levels of corrosion, were measured and compared to the calculated crack widths for the un-corroded beams (Table 7.10). Both calculated and experimental crack widths were detected at three load stages, 50%, 75% and 100% of the expected failure load of the un-corroded beams. The crack widths were calculated as per section 5.2.1

As can be seen from Table 7.10, the load-cracking width performance of the un-corroded and the first degree corroded NC and SCC beams was different than that of the second degree corroded beams. The calculated crack width values for NC-0,1 and SCC-0,1 beams were close to those obtained from experiments with up to 50% of the un-corroded beam's failure load. As the applied load increased (75% to 100% of failure load), the calculated crack width significantly exceeded the experimental values. As mentioned earlier, NC-0,1 and SCC-0,1 beams failed in

shear after developing flexural cracks. The similarity in results, between the calculated and the experimental crack widths up to around 50% of the failure load, can be attributed to the fact that the fine flexural cracks formed in the mid span open wider with the increase of loading, up to around 50% of the failure load. However, the widening of these cracks was reduced/stopped with further increase in load (> 50% of the failure load), due to the formation of new diagonal cracks formed away from the mid span. Up to 50% of the load, the maximum crack width was predominantly governed by flexural (F) cracks (Table 7.10). Beyond 50% of the failure load, crack width was governed by the interaction of diagonal and flexural cracks.

The NC-2 beam exhibited one main flexural crack at the beam's mid-span and this crack continued to widen up to the failure load (flexural failure). The crack width for this beam at 50% of NC-0 failure load was 80% higher than the calculated value while at 75% of NC-0 failure load, the experimental crack width significantly exceeded the calculated value (Table 7.10). The 80% increase of the experimental value at 50% load stage can be related to the increase of the longitudinal bar stress, due to the reduction of the bar diameter resulting from corrosion. Also at 75% of NC-0 failure load, NC-2 beam reached 95% of its ultimate load (due to the effect of corrosion). At this load level, the longitudinal bars exhibited very high elongation before failure, which resulted in a significant difference between the calculated and the experiment values.

The crack performance of SCC-2 beam was different compared to other beams. For up to 50% of the SCC-0 failure load, SCC-2 beam demonstrated a 0.22 mm flexural crack which was slightly higher than the calculated value (0.17 mm). This crack continued to widen until it reached 0.4 mm before the ultimate load, then one inclined crack occurred right before the failure, due to the longitudinal bar splitting. The crack width showed a slightly higher experimental value than the calculated value for SCC-0 during the load testing because of the increase of longitudinal bars stresses, due to the diameter reduction resulted from corrosion.

In general, Equation 5.6 seems to provide good predictions when crack width is governed by flexural cracks resulting from flexural failure of beams. For the case of experimental beams (designed for shear failure), the shear failure, resulting from diagonal cracks, did not allow flexural cracks to open wider (as is the case for a flexural mode of failure). This caused the calculated crack widths to be significantly higher than the experimental values. In addition, when a significant degree of corrosion occurs, the rebar diameter decreases. This causes an increase in the value of f_s , which is higher than the value considered in Equation 5.6 (because this equation

account for un-corroded bars only), which results in higher crack width values than that calculated by the equation.

7.2.4 Experimental load deflection response

The load-deflection responses for both NC and SCC beams, at various degrees of corrosion, are presented in Figs. 7.34-7.39. Table 7.11 also presents the load and deflection at first flexural and diagonal crack, as well as the deflection at various load levels of the un-corroded beams (50%, 75% and 100% of failure load of the un-corroded beams). No significant differences in deflection performance were observed between NC and SCC beams at zero and first degree of corrosion stages. The load deflection response of the four beams showed similar trends of variation and fairly close load-deflection slopes. The higher deflection was observed at higher failure load regardless of the concrete type.

The first degree of corrosion (1.48% and 7.68% actual rebar mass loss in SCC and NC beams, respectively) did not affect the load-deflection response or the maximum deflection of the beams. In the second degree of corrosion, the load-deflection response of SCC-2 beam was different than the un-corroded and first degree corroded SCC beams. For up to 71% of the maximum failure load of SCC-0, the load-deflection response of SCC-2 showed a similar trend of variation and similar load-deflection slopes to those of SCC-0,1 beams. Beyond 71%, the beam developed an inclined-horizontal crack and failed right after, due to the longitudinal bar splitting.

The performance in terms of the load-deflection response in NC-2 beam was also different from the NC beams at zero and first degree of corrosion. For up to 57% of NC-0 failure load, the load deflection response of NC-2 showed slightly higher slope than that of NC-0,1. The increased slope of the load-deflection curve could be related to the increase of the beam's ductility which resulted from the reduction of the longitudinal bar diameter, due to corrosion especially at mid-span. Beyond 57% of NC-0 failure load, high deflection was developed at a constant load level (Fig. 7.38), the beam then showed gradual development of deflection with the applied load until failure occurred. The load-deflection curve for NC-2 indicated flexural failure of the beam. The high deflection developed after 57% of NC-0 failure load is thought to be related to the high elongation that occurred in the longitudinal bars after yield.

The load deflection curves for NC-2 and SCC-2 beams showed a gradual decrease of loading after the peak load, compared to NC and SCC beams at zero and first degree corrosion which showed a sudden drop of loading after the peak load. This result indicates that the flexural and longitudinal bar splitting failure did not occur suddenly and soundly, as in the case of the shear failure.

7.2.5 Post-cracking shear resistance and ductility

The first flexural cracking load was observed visually and confirmed by marking the first step or slope change in the load-central deflection curve. The first diagonal cracking load was also observed visually and was verified by a sudden jump in the elongation of the diagonal LVDT, mounted on the surface of the beam across the diagonal crack.

In general, the first flexural cracking load in SCC and NC beams were similar. This is because the tensile strength for both mixtures was very close (Table 4.7). The first flexural cracking load slightly increased in first degree corroded beams, and then dropped in second degree corroded beams (especially NC-2 beam). The slight increase of the first flexural cracking load is related to the increase of the tensile strength of the tested beams in the first corrosion stage (Table 4.7). While the drop of the first flexural cracking load in the second corrosion stage was related to the existence of the deep horizontal corrosion cracks (which were bigger in NC-2). These horizontal cracks reduced the effective cross sectional depth of the beams and resulted in a higher tensile stress at the lower bottom fiber, which causes earlier flexural cracks.

The ratio of the failure load to the first diagonal cracking load (P_u/P_d) was higher in NC beams than in SCC beams (Table 7.11). The ratio of P_u/P_d was 244.4% and 255.0% in NC-0 and NC-1, respectively. This compared to 211.3% and 208.5% in SCC-0 and SCC-1, respectively. As mentioned earlier, all beams were designed to fail in shear, the aggregate interlock between two slip surfaces in a prominent diagonal crack contributed up to 50% of shear transfer (Taylor 1974). The lower ratio of P_u/P_d in SCC beams supports the development of lower post cracking shear resistance in SCC. This is due to lesser aggregate interlock as a consequence of the presence of 25% lower coarse aggregate compared to NC.

The post cracking shear ductility, expressed as the ratio of the deflection at failure load to the deflection at first diagonal crack load (δ_f/δ_d), was higher in NC beams compared to SCC beams. The ratio of δ_f/δ_d was 415.6% and 367% in NC-0 and NC-1 beams, respectively,

compared to 285.6% and 300% in SCC-0 and SCC-1 beams, respectively. This result indicates that the post cracking shear ductility is higher in NC beams compared to SCC beams. Shear design of beams should take into account the consequences of such reduced post cracking shear resistance and ductility of SCC compared to its NC counterpart

7.2.6 Comparison between actual and theoretical deflection

As mentioned earlier, the actual deflection was measured by one LVDT placed below the mid-span of each beam. The actual deflection reading was recorded versus the applied load and compared with the values calculated by the ACI and Euro codes. The equations for calculating the mid-span deflection for both ACI and Euro codes are presented in section 5.2.3.

Figures 7.34-7.39 show the applied load versus the actual deflections and theoretical deflections, calculated based on Equations 5.7 and 5.9. The point of slope change in load-deflection curves, based on both ACI and EC2 codes, represent first flexural cracking load, which is calculated using the un-cracked moment of inertia of beam cross-section. The post-cracking part of the theoretical response is based on cracked moment of inertia (both ACI and EC2).

In general, the experimental deflection values for all beams in the three corrosion stages except NC-2 were found to be reasonably close to the calculated values from both ACI and EC2 Code-based equations. However, in some circumstances close to the peak load, experimental deflection values are significantly higher than calculated values (for NC-0, NC-1, and SCC-1 beams). This can be associated with the sudden shear failure, due to the formation of a dominant diagonal crack (typical for the shear dominated failure) causing large deflection at failure. ACI predicted deflections are higher compared with EC2 due to the incorporation of shear deformation in Equation 5.7. Overall, both ACI and EC2 Codes are conservative when predicting deflection at peak (failure) load for SCC/NC beams and can be used for the calculation of deflection for shear dominated failure from a serviceability point of view. It should be noted that reinforced concrete beams are designed for flexure failure rather than for shear, in practical circumstances. Hence, ACI and EC2 Code-based equations will perform better in predicting deflection for flexural dominated failure compared with a shear dominated one.

The experimental deflection of the NC-2 beam was also found reasonably close to the calculated values from both ACI and EC2 Codes, up to 67% of the failure load. Beyond this load

level, NC-2 beam developed high deflection at a relatively constant load (due to the high longitudinal bars elongation after yielding resulting from high corrosion levels) which makes the experimental deflection values significantly higher than the calculated values.

Table 7-1: Half-cell potential readings at 25 points along SCC-E beam length/ perimeter

Point #	1 Day	5 Day	10 Day	25 Day	40 Day	56 Day	71 Day	89 Day	105 Day
	SCC-E								
1-1	-0.226	0.278	0.36	0.362	-0.106	-0.21	-0.301	-0.381	-0.42
1-2	-0.243	0.259	0.325	0.315	-0.141	-0.24	-0.331	-0.401	-0.43
1-3	-0.295	0.24	0.42	0.315	-0.134	-0.19	-0.237	-0.312	-0.356
1-4	-0.26	0.248	0.45	0.197	-0.209	-0.21	-0.198	-0.258	-0.33
1-5	-0.241	0.261	0.472	0.249	-0.181	-0.19	-0.185	-0.237	-0.315
2-1	-0.164	0.473	0.709	0.681	0.033	-0.09	-0.201	-0.255	-0.302
2-2	-0.175	0.458	0.697	0.667	0	-0.13	-0.26	-0.308	-0.39
2-3	-0.176	0.415	0.646	0.6	-0.06	-0.16	-0.251	-0.318	-0.377
2-4	-0.179	0.43	0.658	0.607	0	-0.12	-0.221	-0.275	-0.332
2-5	-0.181	0.448	0.658	0.611	0.018	-0.08	-0.16	-0.201	-0.24
3-1	-0.226	0.363	0.608	0.6	-0.024	-0.16	-0.277	-0.362	-0.416
3-2	-0.251	0.302	0.555	0.553	-0.069	-0.21	-0.341	-0.411	-0.512
3-3	-0.263	0.236	0.436	0.437	-0.103	-0.17	-0.235	-0.321	-0.353
3-4	-0.23	0.254	0.496	0.515	-0.076	-0.16	-0.242	-0.315	-0.363
3-5	-0.262	0.283	0.515	0.538	-0.049	-0.14	-0.221	-0.295	-0.332
4-1	-0.167	0.5	0.685	0.705	0.026	-0.13	-0.275	-0.355	-0.413
4-2	-0.168	0.49	0.677	0.69	-0.027	-0.17	-0.305	-0.401	-0.458
4-3	-0.169	0.49	0.67	0.684	0.089	-0.09	-0.253	-0.322	-0.38
4-4	-0.174	0.49	0.675	0.686	0.224	0.02	-0.197	-0.269	-0.296
4-5	-0.174	0.496	0.674	0.689	0.237	0.05	-0.153	-0.251	-0.23
5-1	-0.237	0.315	0.557	0.566	0.124	-0.07	-0.263	-0.361	-0.395
5-2	-0.245	0.31	0.564	0.564	0.113	-0.09	-0.285	-0.391	-0.428
5-3	-0.271	0.319	0.591	0.582	0.111	-0.1	-0.31	-0.434	-0.465
5-4	-0.257	0.321	0.605	0.62	0.208	-0.03	-0.253	-0.357	-0.38
5-5	-0.251	0.321	0.591	0.622	0.233	0.01	-0.218	-0.311	-0.327

Table 7-2: Half-cell potential readings at 25 points along NC-E beam length/ perimeter

Point #	1 Day	5 Day	10 Day	25 Day	40 Day	56 Day	71 Day	89 Day	105 Day
	NC-E								
1-1	-0.384	-0.237	-0.226	-0.31	-0.274	-0.297	-0.305	-0.32	-0.347
1-2	-0.357	-0.255	-0.243	-0.299	-0.317	-0.323	-0.32	-0.341	-0.364
1-3	-0.374	-0.272	-0.255	-0.281	-0.31	-0.31	-0.295	-0.325	-0.342
1-4	-0.37	-0.261	-0.234	-0.261	-0.341	-0.334	-0.307	-0.327	-0.331
1-5	-0.355	-0.209	-0.202	-0.32	-0.294	-0.299	-0.283	-0.311	-0.371
2-1	-0.229	-0.08	-0.093	-0.259	-0.334	-0.319	-0.28	-0.33	-0.349
2-2	-0.231	-0.121	-0.138	-0.329	-0.386	-0.35	-0.281	-0.324	-0.341
2-3	-0.24	-0.181	-0.192	-0.35	-0.383	-0.393	-0.377	-0.391	-0.401
2-4	-0.213	-0.053	-0.069	-0.274	-0.341	-0.39	-0.403	-0.421	-0.435
2-5	-0.222	-0.019	-0.065	-0.243	-0.286	-0.353	-0.385	-0.411	-0.421
3-1	-0.257	-0.076	-0.103	-0.263	-0.271	-0.284	-0.27	-0.322	-0.332
3-2	-0.302	-0.16	-0.173	-0.31	-0.332	-0.315	-0.27	-0.331	-0.339
3-3	-0.3	-0.205	-0.243	-0.358	-0.391	-0.388	-0.363	-0.421	-0.411
3-4	-0.322	-0.121	-0.149	-0.279	-0.336	-0.353	-0.326	-0.371	-0.379
3-5	-0.27	-0.088	-0.1	-0.252	-0.304	-0.33	-0.337	-0.394	-0.399
4-1	-0.182	-0.09	-0.067	-0.276	-0.28	-0.31	-0.3	-0.319	-0.327
4-2	-0.178	-0.1	-0.097	-0.265	-0.277	-0.281	-0.315	-0.324	-0.335
4-3	-0.177	-0.11	-0.155	-0.29	-0.3	-0.311	-0.306	-0.378	-0.408
4-4	-0.176	0	-0.022	-0.27	-0.31	-0.321	-0.331	-0.401	-0.433
4-5	-0.18	0.01	-0.024	-0.292	-0.33	-0.317	-0.327	-0.392	-0.423
5-1	-0.409	-0.237	-0.281	-0.3	-0.324	-0.315	-0.284	-0.315	-0.34
5-2	-0.466	-0.3	-0.274	-0.32	-0.36	-0.34	-0.305	-0.336	-0.374
5-3	-0.39	-0.248	-0.28	-0.31	-0.326	-0.317	-0.291	-0.331	-0.364
5-4	-0.395	-0.28	-0.255	-0.312	-0.347	-0.345	-0.324	-0.351	-0.391
5-5	-0.357	-0.234	-0.25	-0.291	-0.336	-0.348	-0.343	-0.377	-0.421

Table 7-3: Half-cell potential readings at 25 points along SCC-N beam length/ perimeter

Point #	1 Day	5 Day	10 Day	25 Day	40 Day
	SCC-N				
1-1	-0.326	0.16	0.033	-0.092	-0.236
1-2	-0.367	0.121	-0.055	-0.181	-0.255
1-3	-0.29	0.139	-0.055	-0.18	-0.303
1-4	-0.235	0.125	0.06	-0.1	-0.304
1-5	-0.22	0.145	0	-0.12	-0.301
2-1	-0.18	0.646	0.526	0.527	0.144
2-2	-0.188	0.619	0.51	0.504	0.107
2-3	-0.187	0.602	0.492	0.443	-0.005
2-4	-0.189	0.6	0.5	0.484	0.085
2-5	-0.183	0.61	0.513	0.502	0.121
3-1	-0.284	0.271	0.159	0.087	-0.118
3-2	-0.315	0.243	0.133	0.053	-0.164
3-3	-0.22	0.226	0.116	-0.02	-0.197
3-4	-0.2	0.193	0.091	-0.049	-0.191
3-5	-0.196	0.133	0.091	-0.063	-0.233
4-1	-0.169	0.627	0.559	0.526	0.134
4-2	-0.171	0.61	0.562	0.516	0.113
4-3	-0.171	0.606	0.547	0.502	0.059
4-4	-0.17	0.6	0.551	0.488	0.116
4-5	-0.164	0.622	0.562	0.503	0.136
5-1	-0.179	0.55	0.421	0.187	-0.186
5-2	-0.189	0.525	0.376	0.137	-0.23
5-3	-0.173	0.517	0.32	0.076	-0.21
5-4	-0.173	0.47	0.28	0.029	-0.22
5-5	-0.165	0.408	0.249	0.003	-0.185

Table 7-4: Half-cell potential readings at 25 points along NC-N beam length/ perimeter

Point #	1 Day	5 Days	10 Days	25 Days	40 Days
	NC-N				
1-1	-0.312	-0.413	-0.402	-0.38	-0.374
1-2	-0.337	-0.445	-0.412	-0.396	-0.383
1-3	-0.385	-0.481	-0.42	-0.377	-0.37
1-4	-0.405	-0.44	-0.427	-0.4	-0.42
1-5	-0.39	-0.424	-0.414	-0.414	-0.421
2-1	-0.319	-0.15	-0.169	-0.424	-0.467
2-2	-0.324	-0.13	-0.216	-0.454	-0.491
2-3	-0.325	-0.14	-0.314	-0.432	-0.47
2-4	-0.327	-0.12	-0.175	-0.44	-0.418
2-5	-0.322	-0.11	-0.141	-0.394	-0.4
3-1	-0.357	-0.308	-0.345	-0.411	-0.442
3-2	-0.384	-0.351	-0.375	-0.405	-0.447
3-3	-0.374	-0.36	-0.38	-0.42	-0.446
3-4	-0.35	-0.299	-0.366	-0.405	-0.456
3-5	-0.331	-0.28	-0.366	-0.413	-0.441
4-1	-0.336	-0.174	-0.311	-0.425	-0.519
4-2	-0.339	-0.224	-0.339	-0.447	-0.528
4-3	-0.352	-0.18	-0.32	-0.445	-0.473
4-4	-0.354	-0.25	-0.31	-0.471	-0.49
4-5	-0.337	-0.225	-0.29	-0.463	-0.487
5-1	-0.412	-0.41	-0.455	-0.447	-0.438
5-2	-0.438	-0.49	-0.477	-0.433	-0.441
5-3	-0.413	-0.543	-0.47	-0.373	-0.409
5-4	-0.44	-0.537	-0.502	-0.422	-0.37
5-5	-0.431	-0.519	-0.52	-0.437	-0.39

Table 7-5: Chloride content, rebar mass loss, maximum crack width and the reduction of bar diameter at each point along NC-E beam length/perimeter

Point #	Chloride Ion Content (%)	Stirrups Mass Loss (gm)	Rebars Mass Loss (gm)	Minimum Rebar Diameter (mm)	Maximum Crack Width at Rebars (mm)	Maximum Crack width at Stirrups (mm)
NC-E						
1-1	0.55	0	491.5	14.3	4.1	0
1-2	0.5	0	491.5	14.3	4.7	0
1-3	0.2	0	160.8	21.5	0.14	0
1-4	0.42	0	295.3	19.3	2.6	0
1-5	0.38	0	295.3	19.3	2.3	0
2-1	0.77	0	1173.5	0	5	0
2-2	0.84	0	1173.5	0	5	0
2-3	0.22	0	184.6	22.1	0.16	0
2-4	0.27	0	202.6	21.5	2.4	0
2-5	0.3	0	202.6	21.5	2.1	0
3-1	1.1	200 gm	1475.5	0	5	0
3-2	0.95	localized	1475.5	0	5.2	0
3-3	0.29	corrosion	193.6	20.7	0.16	0
3-4	0.36	in epoxy	259.6	20	2.6	0
3-5	0.41	stirrups	259.6	20	2	0
4-1	0.46	0	483.5	16.3	3.8	0
4-2	0.44	0	483.5	16.3	4.3	0
4-3	0.25	0	186.6	20.8	0.16	0
4-4	0.3	0	223.6	19.8	2.3	0
4-5	0.27	0	223.6	19.8	1.6	0
5-1	0.31	0	375	16.6	2.6	0
5-2	0.45	0	375	16.6	3.1	0
5-3	0.2	0	163.6	21.6	0.14	0
5-4	0.38	0	287.6	19	2.2	0
5-5	0.4	0	287.6	19	1.6	0

Table 7-6: Chloride content, rebar mass loss, maximum crack width and the reduction of bar diameter at each point along SCC-E beam length/perimeter

Point #	Chloride Ion Content (%)	Stirrups Mass Loss (gm)	Rebars Mass Loss (gm)	Minimum Rebar Diameter (mm)	Maximum Crack Width at Rebars (mm)	Maximum Crack width at Stirrups (mm)	Remarks
SCC-E							
1-1	0.61	251 gm	640.3	8.4	1.6	Spalling	Cover spalling & reduction in bars length
1-2	0.68	Localized corrosion in epoxy stirrups	640.3	8.4	2.8	Spalling	
1-3	0.34		239	21.5	0.2	Spalling	
1-4	0.38		262	19	1.4	Spalling	
1-5	0.35		262	19	0	Spalling	
2-1	0.16		0	111.8	21.9	0.2	0
2-2	0.18	0	111.8	21.9	1	0	
2-3	0.13	0	54.9	22.8	0.08	0	
2-4	0.12	0	59.9	22.7	0.4	0	
2-5	0.09	0	59.9	22.7	0	0	
3-1	0.14	0	107.8	21.7	0.18	0	
3-2	0.17	0	107.8	21.7	0.9	0	
3-3	0.15	0	77.9	21.5	0.1	0	
3-4	0.12	0	86.9	21.87	0.6	0	
3-5	0.14	0	86.9	21.8	0	0	
4-1	0.17	0	105.8	22.8	0.14	0	
4-2	0.19	0	105.8	22.8	0.7	0	
4-3	0.13	0	51.9	23.5	0.08	0	
4-4	0.12	0	46.9	22.6	0.3	0	
4-5	0.1	0	46.9	22.6	0	0	
5-1	0.14	0	81.8	23.2	0	0	
5-2	0.16	0	81.8	23.2	0.6	0	
5-3	0.1	0	58.9	23.3	0.08	0	
5-4	0.09	0	42.9	23.3	0.3	0	
5-5	0.10	0.00	42.9	23.30	0.00	0.00	

Table 7-7: Chloride content, rebar mass loss, maximum crack width and the reduction of bar diameter at each point along NC-N beam length/perimeter

Point #	Chloride Ion Content (%)	Stirrups Mass Loss (gm)	Rebars Mass Loss (gm)	Minimum Rebar Diameter (mm)	Maximum Crack Width at Rebars (mm)	Maximum Crack width at Stirrups (mm)
NC-N						
1-1	0.61	371.34	137.5	22.2	0	0
1-2	0.59		137.5	22.2	1.2	0.08
1-3	0.61		127.5	22.2	0.1	0.08
1-4	0.51		124.5	23.2	1	0.08
1-5	0.48		124.5	23.2	0	0
2-1	0.17	0	154.5	21.7	0	0
2-2	0.19	0	154.5	21.7	1.3	0
2-3	0.2	0	158.5	23	0.12	0
2-4	0.15	0	147.5	22.8	1.1	0
2-5	0.18	0	147.5	22.8	0	0
3-1	0.45	116.88	104.5	21	0	0
3-2	0.36		104.5	21	1	0.04
3-3	0.47		110.5	22.4	0.1	0.04
3-4	0.51		147.5	23	1.2	0.06
3-5	0.43		147.5	23	0	0
4-1	0.2	0	130.5	22.2	0	0
4-2	0.18	0	130.5	22.2	1.2	0
4-3	0.15	0	108.5	22.9	0.1	0
4-4	0.17	0	124.5	22.8	1.3	0
4-5	0.16	0	124.5	22.8	0	0
5-1	0.47	523.58	149.5	24.2	0	0
5-2	0.66		149.5	24.2	1.3	0.12
5-3	0.87		113.5	22.6	0.1	0.12
5-4	0.57		83.5	22.4	0.7	0.12
5-5	0.52		83.5	22.4	0	0

Table 7-8: Chloride content, rebar mass loss, maximum crack width and the reduction of bar diameter at each point along SCC-N beam length/perimeter

Point #	Chloride Ion Content (%)	Stirrups Mass Loss (gm)	Rebars Mass Loss (gm)	Minimum Rebar Diameter (mm)	Maximum Crack Width at Rebars (mm)	Maximum Crack width at Stirrups (mm)	Remarks
SCC-N							
1-1	0.7			24.2	0	Spalling	372 = 222 rebar's mass loss and 150 gm reduction of bar length
1-2	0.97			24.2	0	Spalling	
1-3	0.47	324.75	372	24.2	0	0.4	
1-4	0.55			24.2	0	0.04	
1-5	0.4			24.2	0	0	
2-1	0.03	0	0	24.2	0	0	
2-2	0.09	0	0	24.2	0	0	
2-3	0.12	0	0	24.2	0	0	
2-4	0.07	0	0	24.2	0	0	
2-5	0.05	0	0	24.2	0	0	
3-1	0.05		0	24.2	0	0	
3-2	0.11		0	24.2	0	0.06	
3-3	0.18	46	0	24.2	0	0.06	
3-4	0.21		0	24.2	0	0.06	
3-5	0.14		0	24.2	0	0	
4-1	0.08	0	0	24.2	0	0	
4-2	0.05	0	0	24.2	0	0	
4-3	0.11	0	0	24.2	0	0	
4-4	0.1	0	0	24.2	0	0	
4-5	0.09	0	0	24.2	0	0	
5-1	0.05		0	24.2	0	0	
5-2	0.1		0	24.2	0	0.06	
5-3	0.12	139	0	24.2	0	0.06	
5-4	0.16		0	24.2	0	0.06	
5-5	0.2		0	24.2	0	0	

Table 7-9: Ultimate failure load and mode of failure for each level of corrosion

Beam No.	f_c at the time of test MPa	Ultimate failure load (P_u) KN	Normalized ultimate failure load (P_{nz}) KN/(MPa) ^{1/2}	% of actual longitudinal bars mass loss	Time under accelerated corrosion test (Days)	Failure mode	Remarks
SCC-0	45	298	44.42	0	0	Diagonal shear failure	
NC-0	47	330	48.14	0	0	Diagonal shear failure	
SCC-1	53	319	43.82	1.48	48	Diagonal shear failure	Corrosion and cover spalling at only one end of the beams located away from casting point
NC-1	56	380	50.78	7.68	48	Diagonal shear failure	No cover spalling
SCC-2	53	212	29.12	8.13	103	Bond splitting failure	Cover spalling at only one end of the beams located away from casting point
NC-2	56	280	37.42	24.49	103	Bending failure	No cover spalling

Table 7-10: Comparison between calculated and experimental crack widths for uncorroded SCC and NC beams

Beam designation	Crack number (% of failure Load) (mm)			Calculated crack width for 0 corroded beams (% of Failure Load) (mm)			Experimental maximum crack width before failure (% of Failure Load of 0 corroded beam) (mm)					
	50%	75%	100%	50%	75%	100%	50%		75%		100%	
NC-0	4	5	10	0.20	0.28	0.37	0.16	F	0.20	F	0.20	D
NC-1	3	6	11				0.20	F	0.20	F,D	0.26	D
NC-2	2	3	3				0.36	F	15	F	-	
SCC-0	5	8	11	0.17	0.28	0.35	0.18	F	0.22	F	0.22	F
SCC-1	4	7	9				0.20	F	0.22	D	0.22	D
SCC-2	1	2	-				0.22	F	-	-	-	

* governing crack type; F: Flexure crack; D: Diagonal crack; FD: Flexure-diagonal crack

Table 7-11: Strength-deflection results of SCC and NC beams in different corrosion stages

Beam designation	Total load (kN)			P_u/P_d (%)	Deflection in each beam (mm)		δ_f/δ_d (%)	Deflection (% of Failure Load of the uncorroded beams) (mm)		
	at first flexural crack (P_f)	at first diagonal crack (P_d)	at failure (P_u)		at first diagonal crack load (δ_d)	at failure load (δ_f)		50%	75%	100%
SCC-0	90	141	298	211.3%	0.97	2.77	285.6%	1	2.1	2.77
NC-0	90	135	330	244.4%	0.77	3.2	415.6%	1.22	2	3.2
SCC-1	105	153	319	208.5%	1.1	3.3	300.0%	0.9	1.8	2.99
NC-1	103	149	380	255.0%	1.12	4.11	367.0%	1.27	2.34	3.35
SCC-2	97	-	212	-	-	2.01	-	1	-	-
NC-2	75	-	280	-	-	23.28	-	1.35	14.4	-

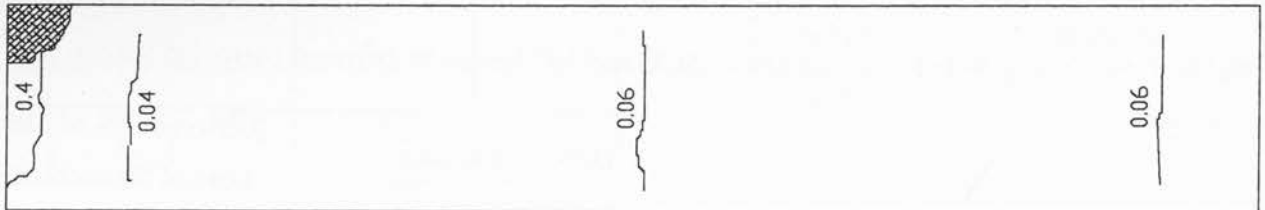
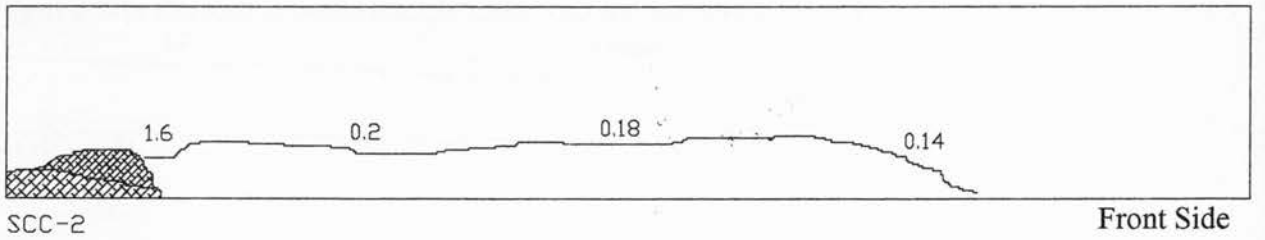
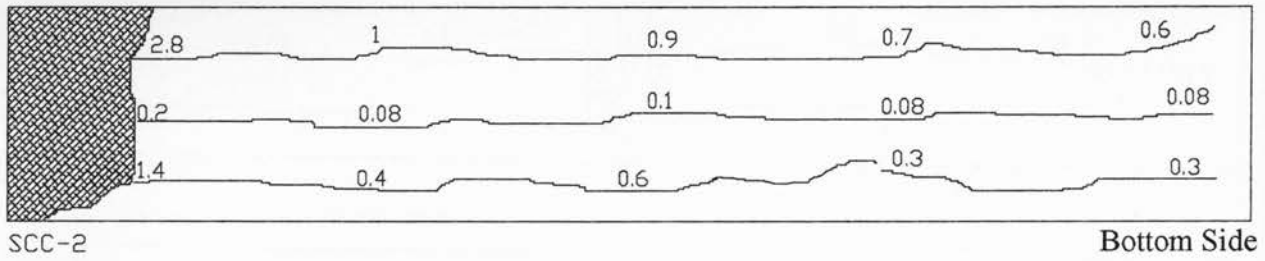
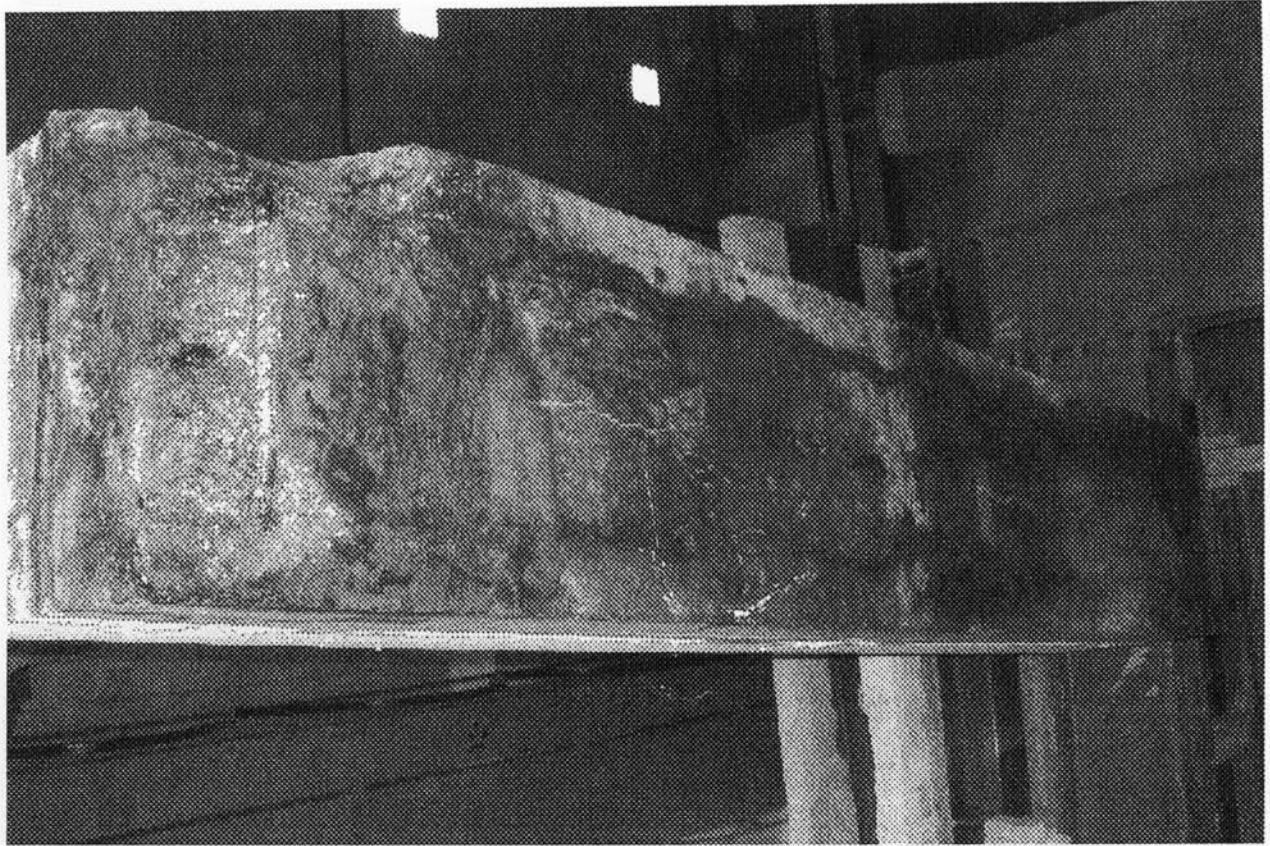
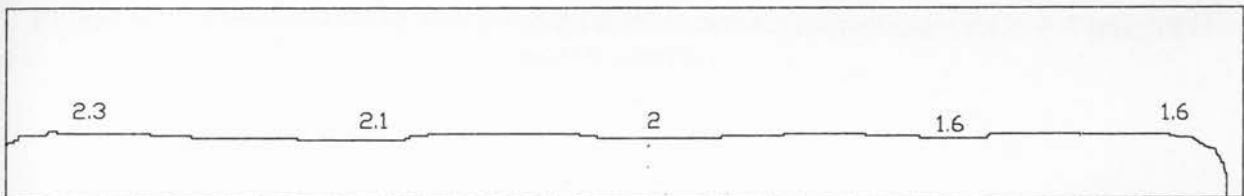
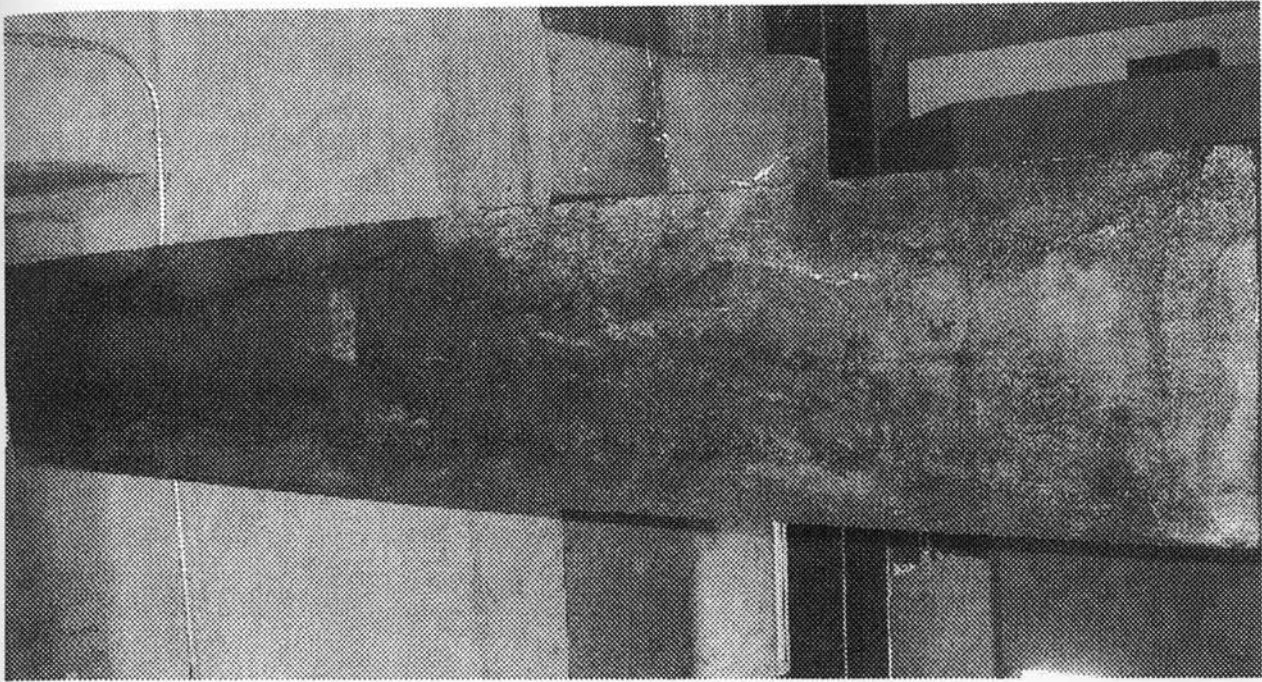


Figure 7-1: Corrosion performance, crack pattern and widths in non-epoxy coated stirrups SCC-1 beam



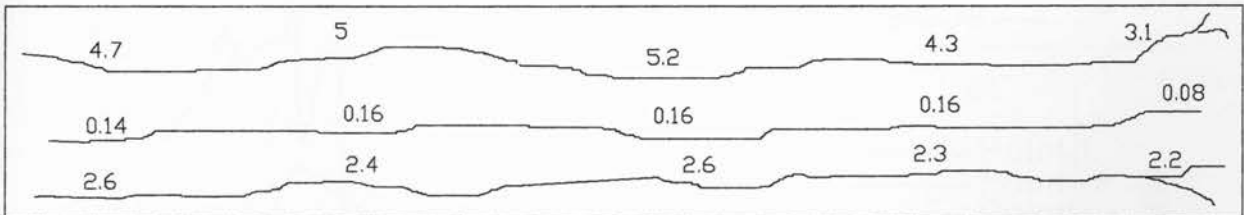
● Concrete cover spalling

Figure 7-3: Corrosion performance, crack pattern and widths in epoxy coated stirrups SCC-2 beam



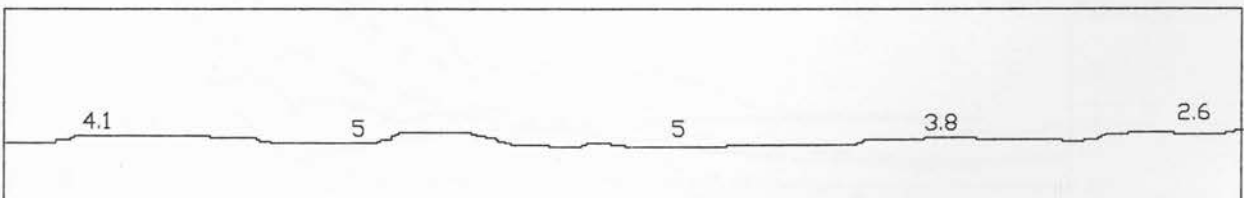
NC-2

Back Side



NC-2

Bottom Side



NC-2

Front Side

Figure 7-4: Corrosion performance, crack pattern and widths in epoxy coated stirrups NC-2 beam

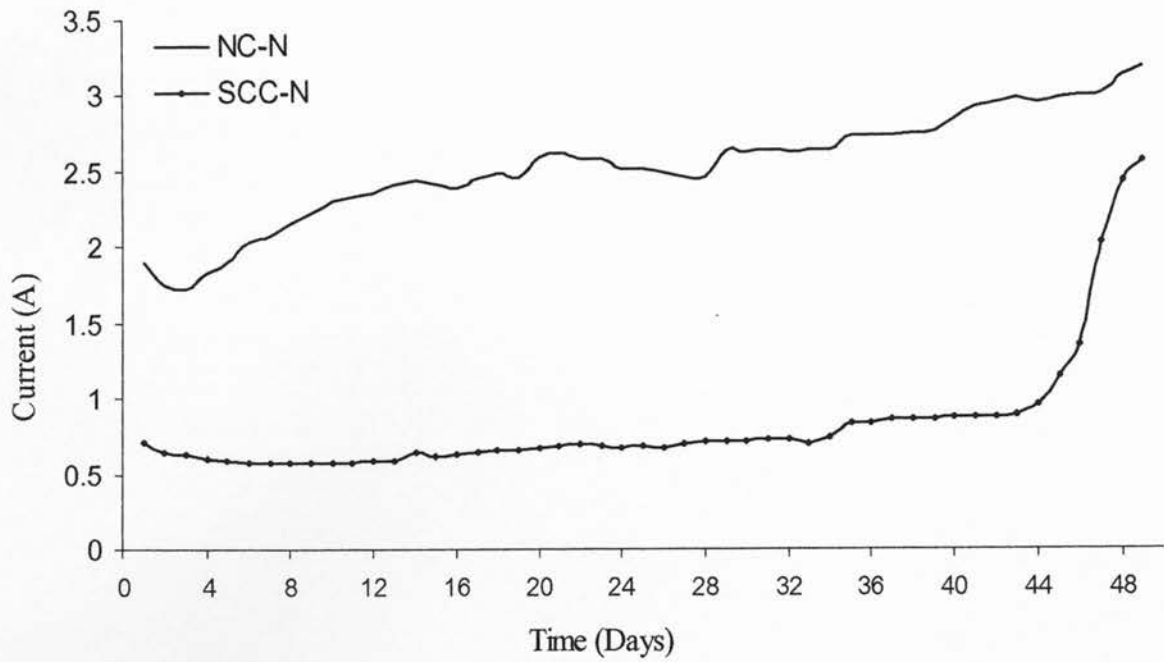


Figure 7-5: Current-time measurements for non-epoxy coated stirrup beams in moderate corrosion stage

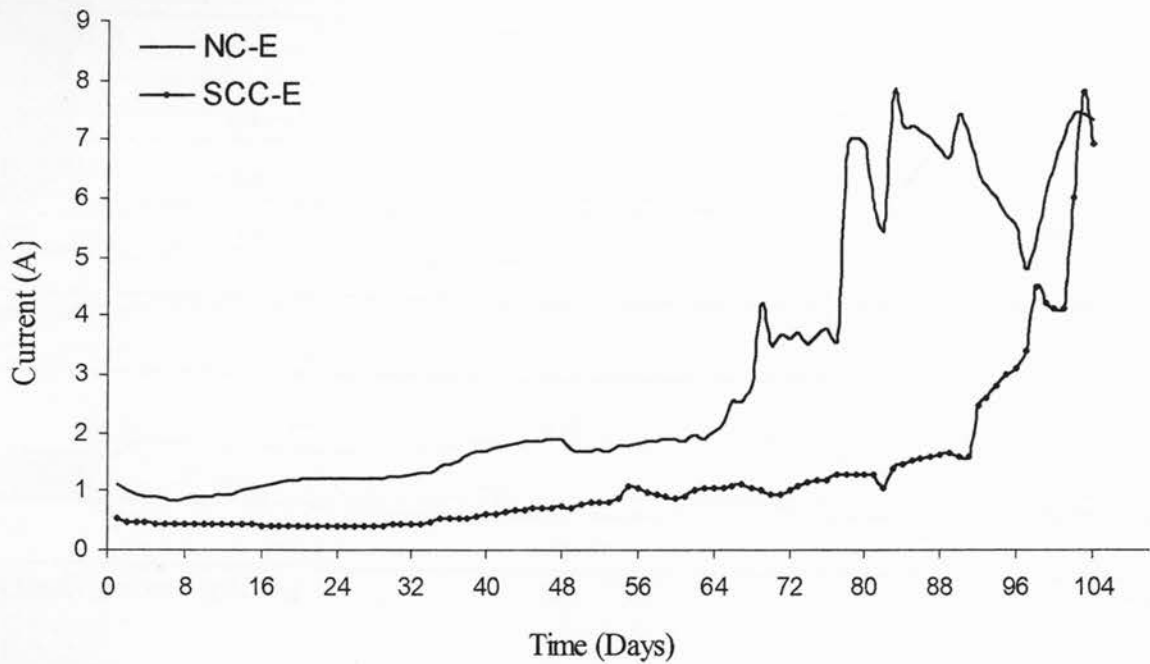


Figure 7-6: Current-time measurements for non-epoxy coated stirrup beams in severe corrosion stage

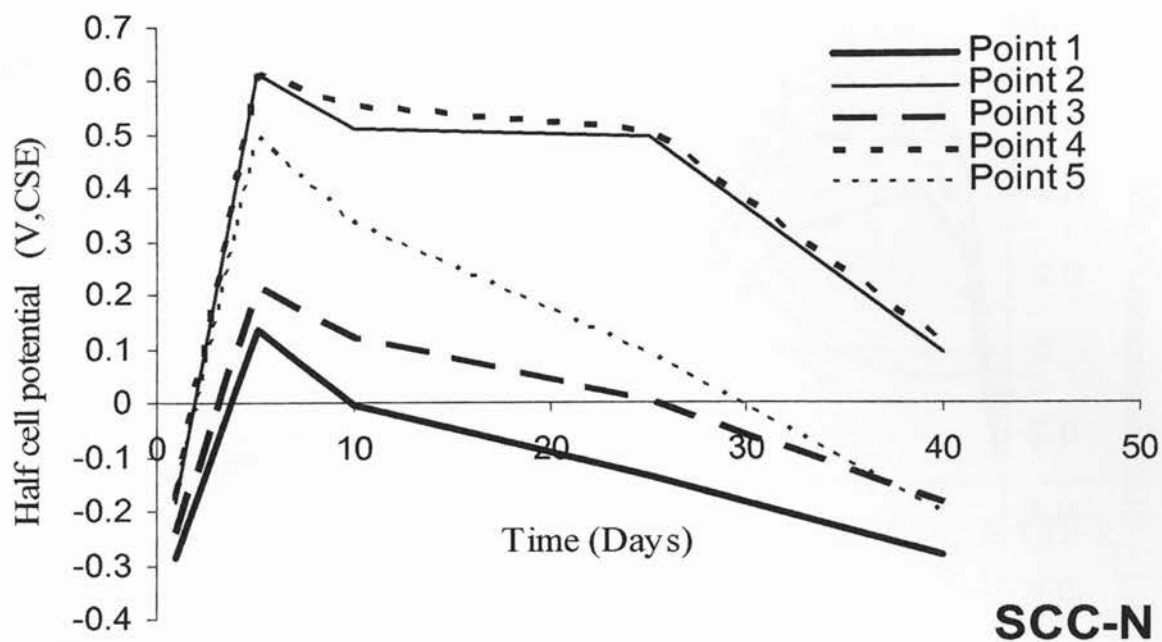


Figure 7-7: Average cross section half-cell reading at each point along SCC-N beam length

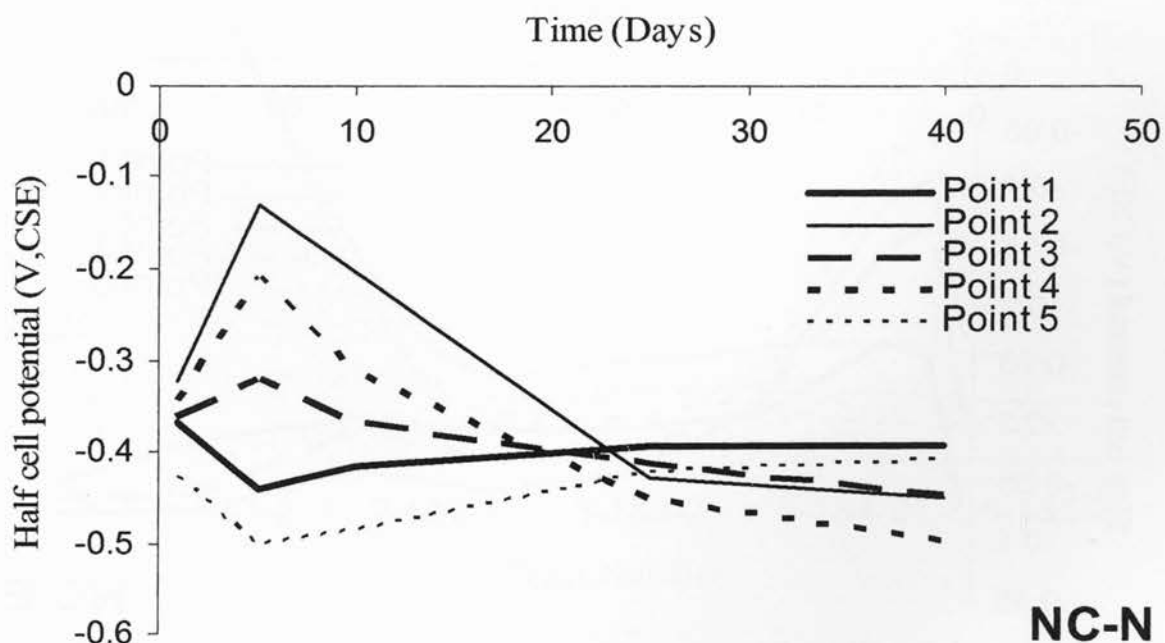


Figure 7-8: Average cross section half-cell reading at each point along NC-N beam length

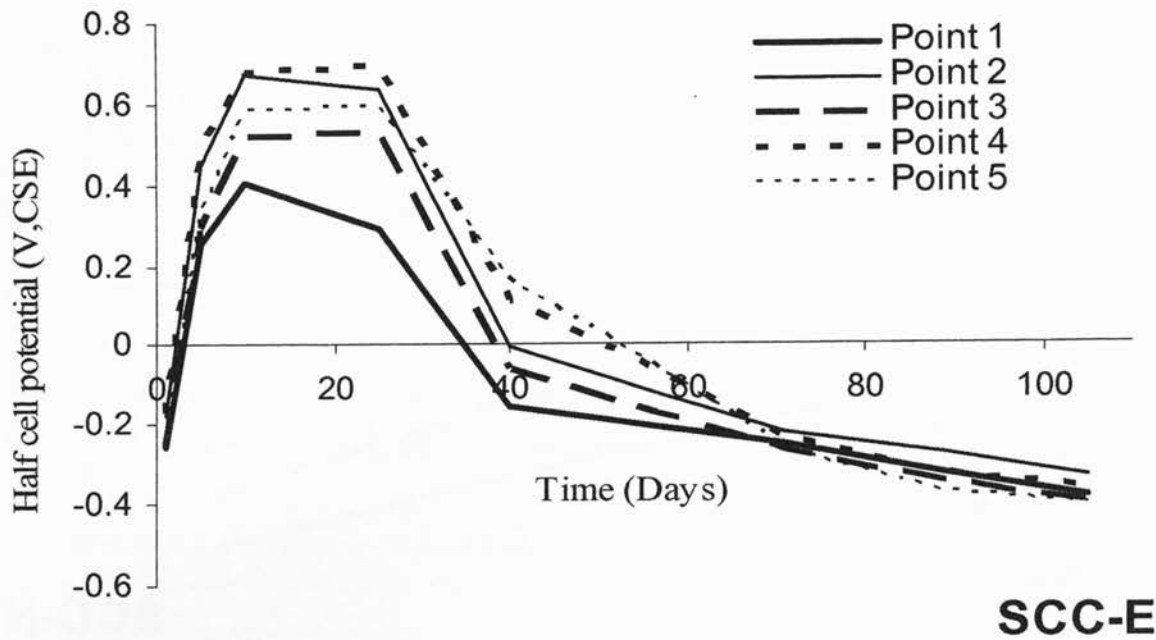


Figure 7-9: Average cross section half-cell reading at each point along SCC-E beam length

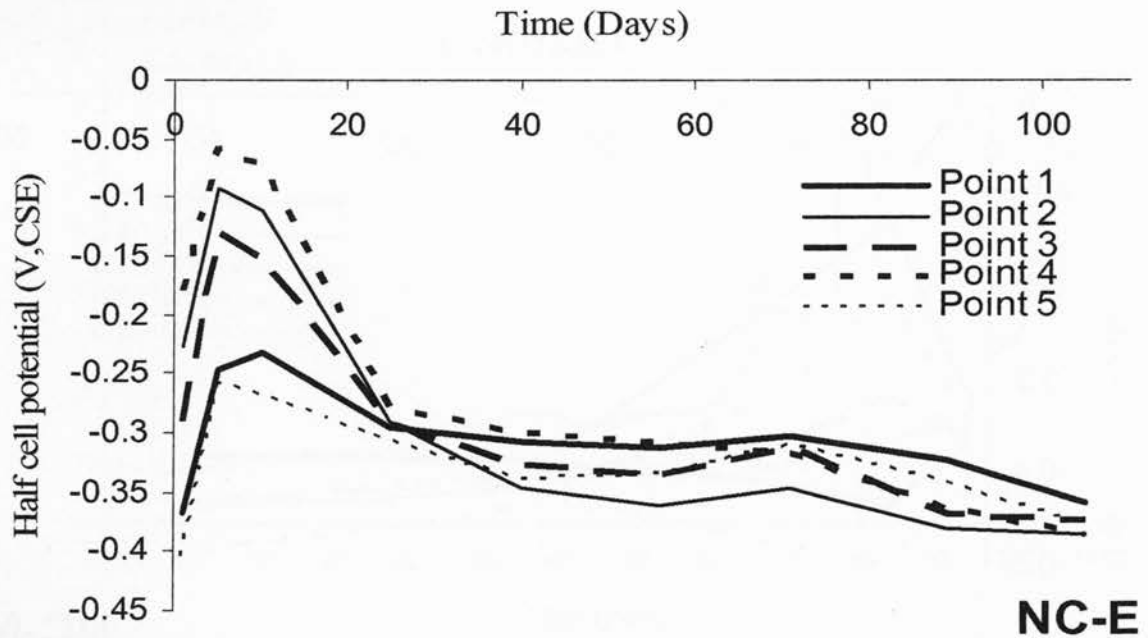


Figure 7-10: Average cross section half-cell reading at each point along NC-E beam length

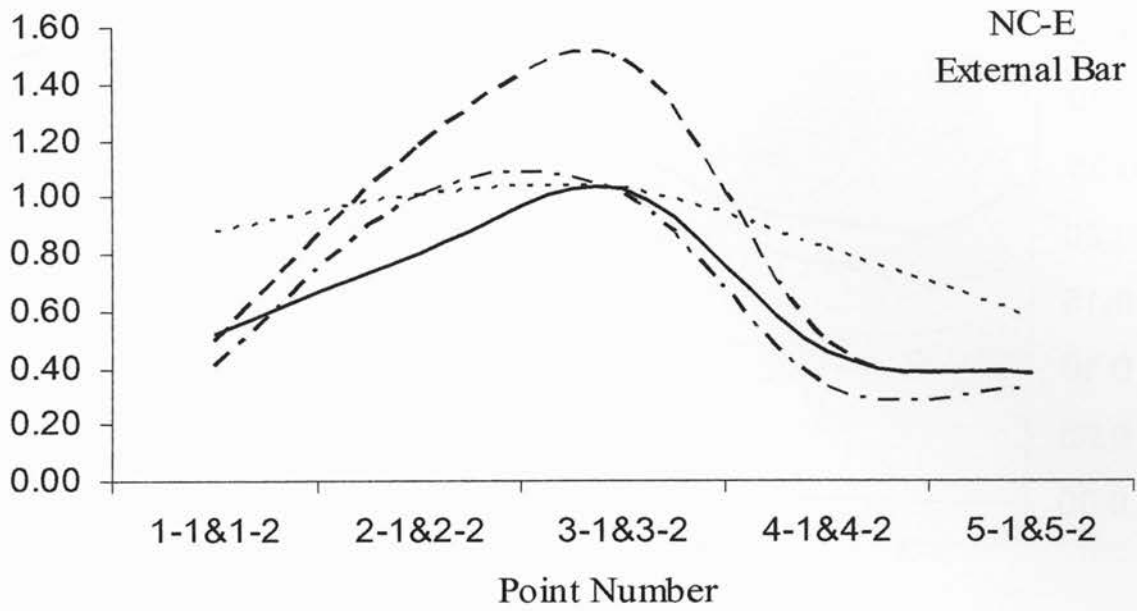


Figure 7-11: Chloride content, rebar mass loss, maximum crack width and the reduction of bar diameter along the front external bars of NC-E

_____ Chloride content (%), Mass loss (Kg), Maximum total crack width (mm),
 - - - - - Reduction of bar diameter (% of the original diameter)

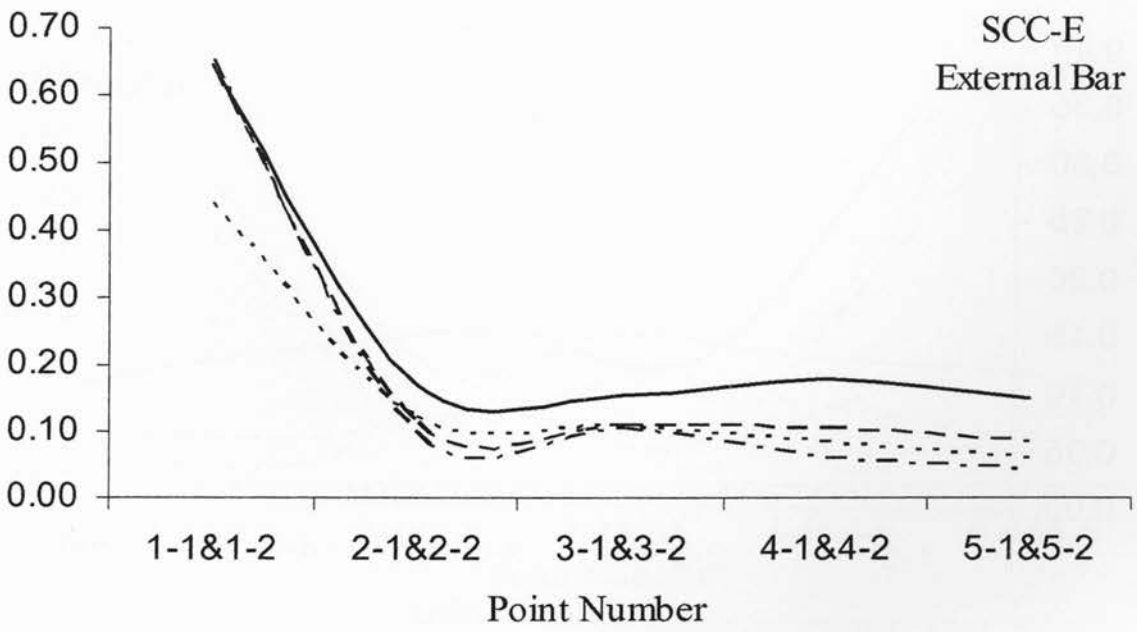


Figure 7-12: Chloride content, rebar mass loss, maximum crack width and the reduction of bar diameter along the front external bars of SCC-E

_____ Chloride content (%), Mass loss (Kg), Maximum total crack width (mm),
 - - - - - Reduction of bar diameter (% of the original diameter)

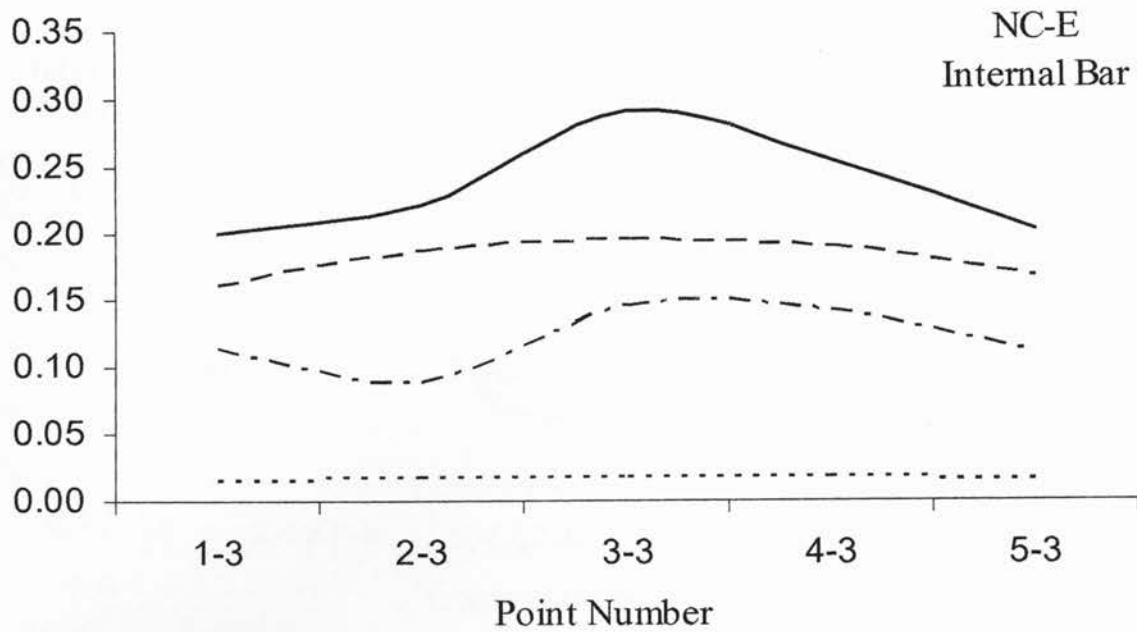


Figure 7-13: Chloride content, rebar mass loss, maximum crack width and the reduction of bar diameter along the internal bar of NC-E

———— Chloride content (%), - - - - - Mass loss (Kg), Maximum total crack width (mm),
 - Reduction of bar diameter (% of the original diameter)

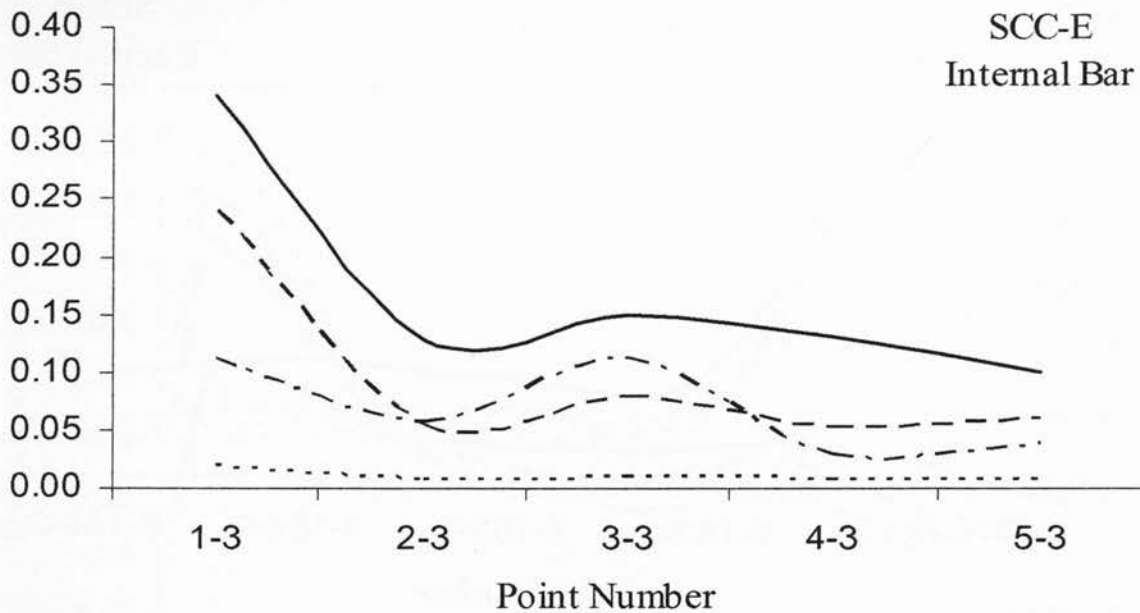


Figure 7-14: Chloride content, rebar mass loss, maximum crack width and the reduction of bar diameter along the internal bars of SCC-E

———— Chloride content (%), - - - - - Mass loss (Kg), Maximum total crack width (mm),
 - Reduction of bar diameter (% of the original diameter)

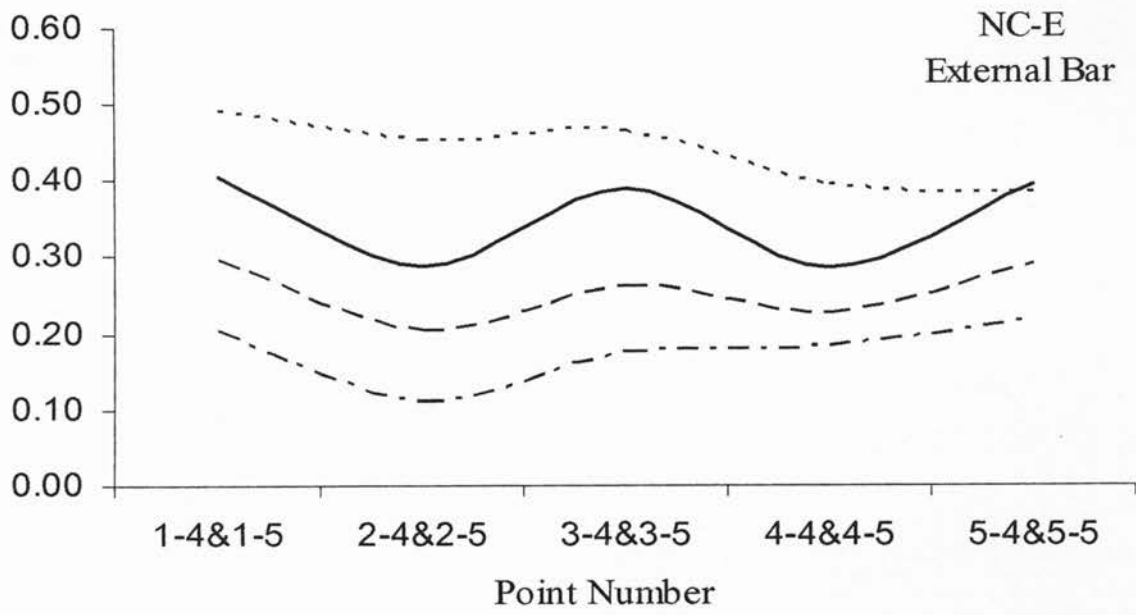


Figure 7-15: Chloride content, rebar mass loss, maximum crack width and the reduction of bar diameter along the back external bars of NC-E

_____ Chloride content (%), Mass loss (Kg), Maximum total crack width (mm),
 - - - - - Reduction of bar diameter (% of the original diameter)

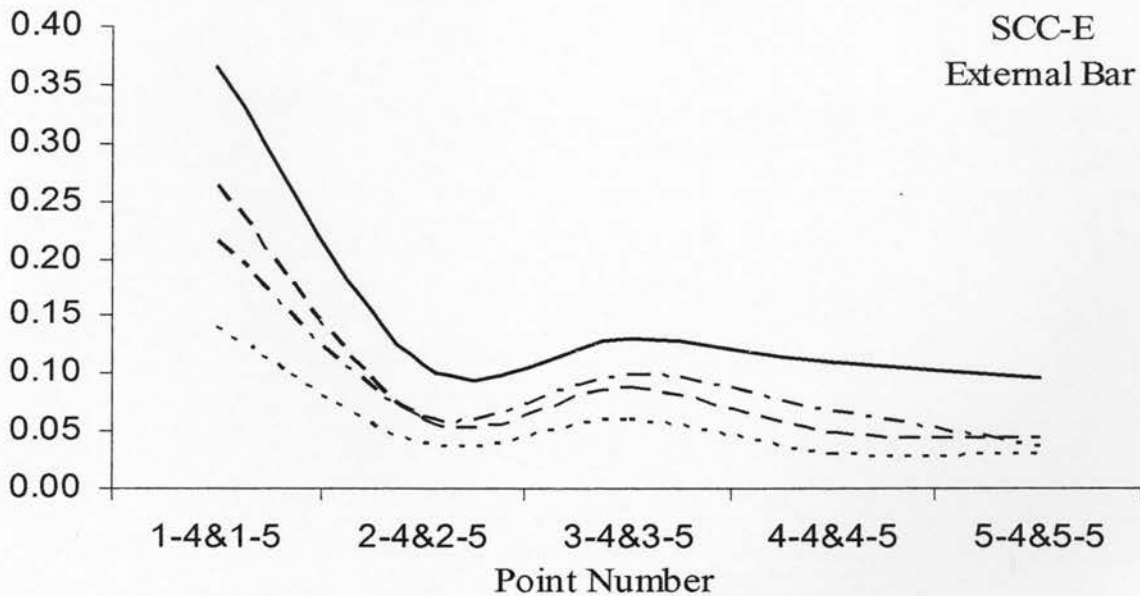


Figure 7-16: Chloride content, rebar mass loss, maximum crack width and the reduction of bar diameter along the back external bar of SCC-E

_____ Chloride content (%), Mass loss (Kg), Maximum total crack width (mm),
 - - - - - Reduction of bar diameter (% of the original diameter)

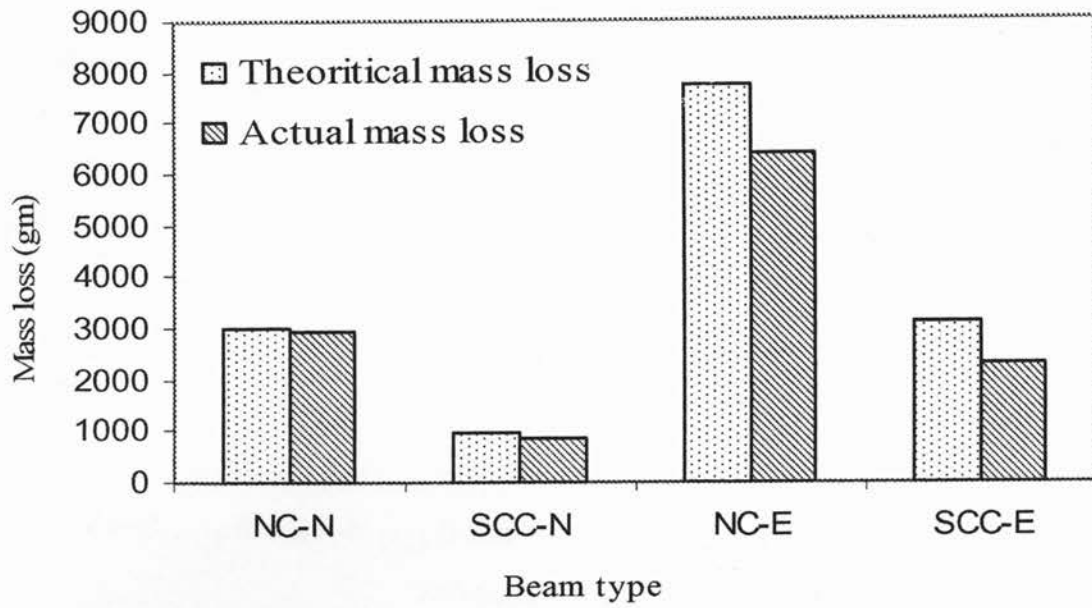


Figure 7-17: Comparison of theoretical and actual mass loss in all tested beams



Figure 7-18: Corrosion performance in the small concrete cylinders

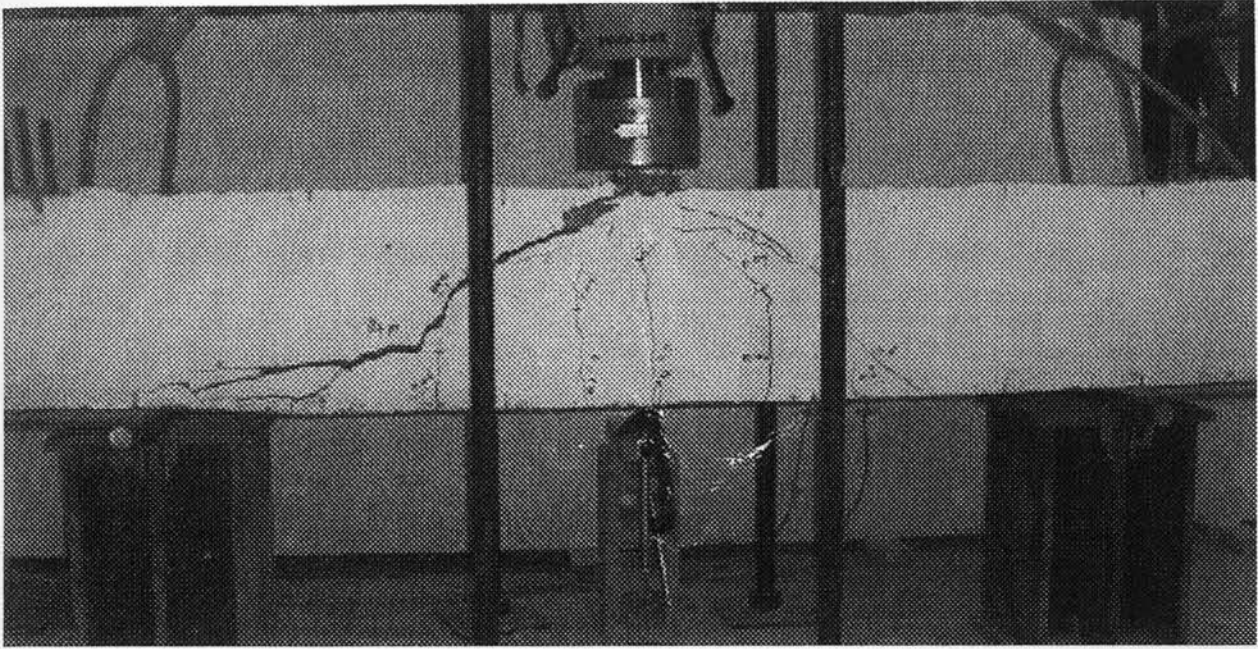


Figure 7-19: Failure of NC-0 beam

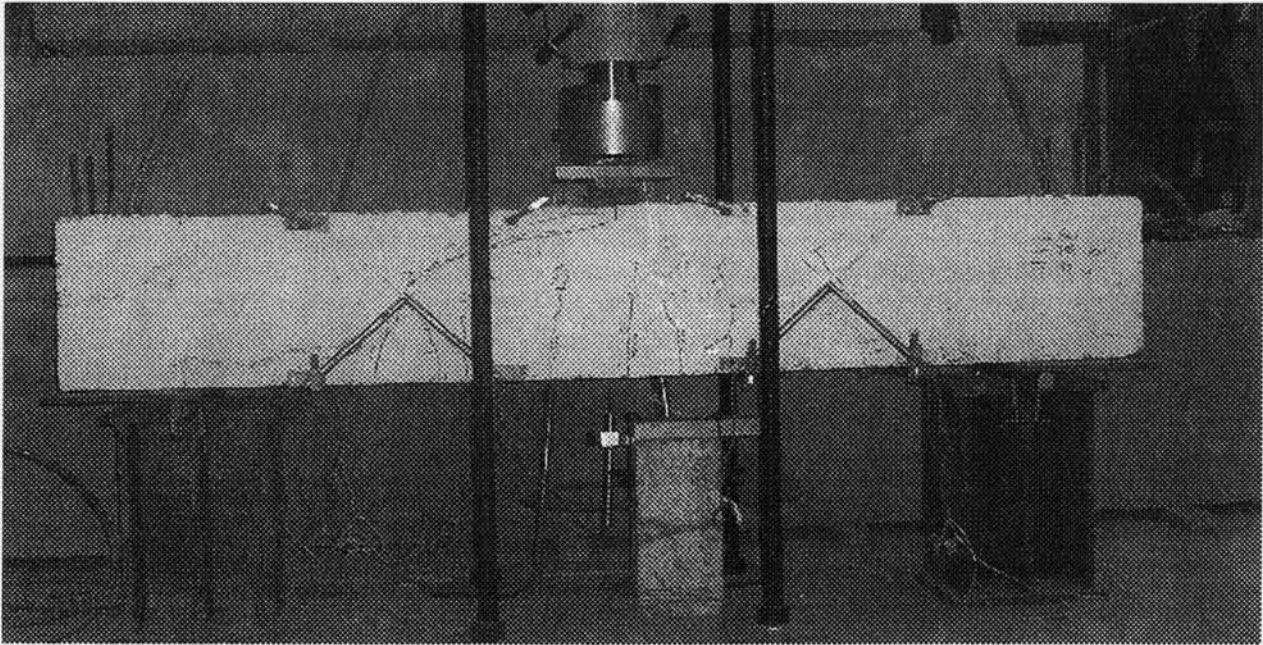


Figure 7-20: Failure of SCC-0 beam

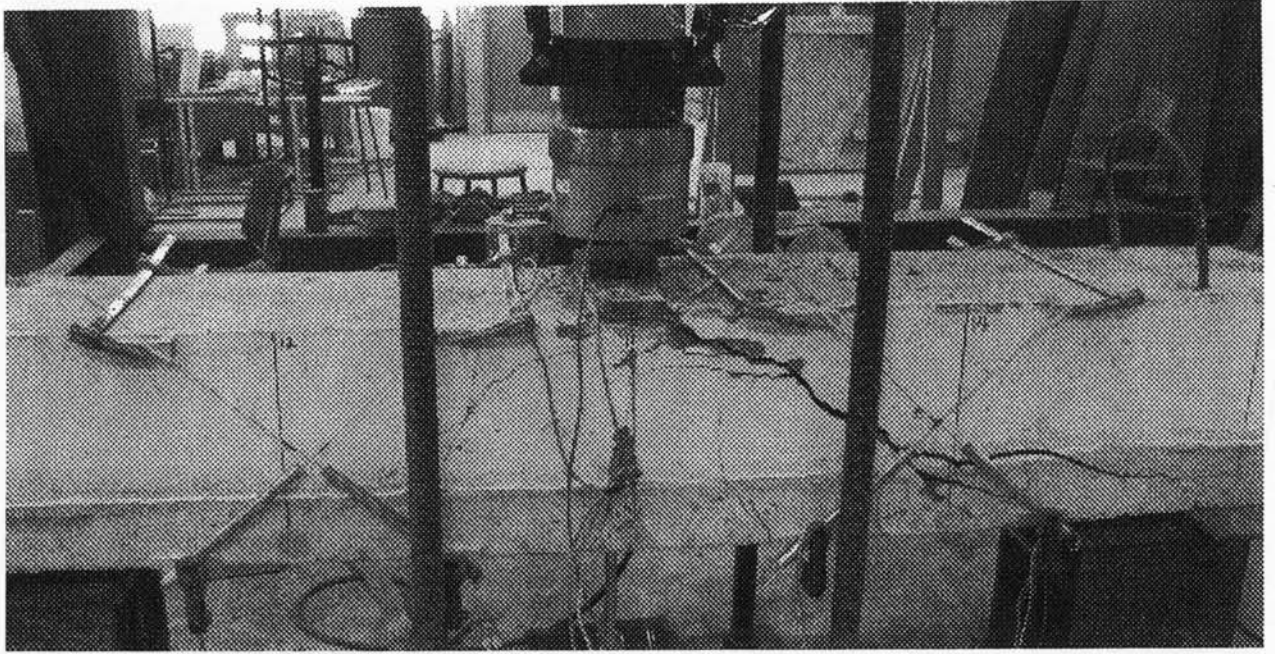


Figure 7-21: Failure of NC-1 beam

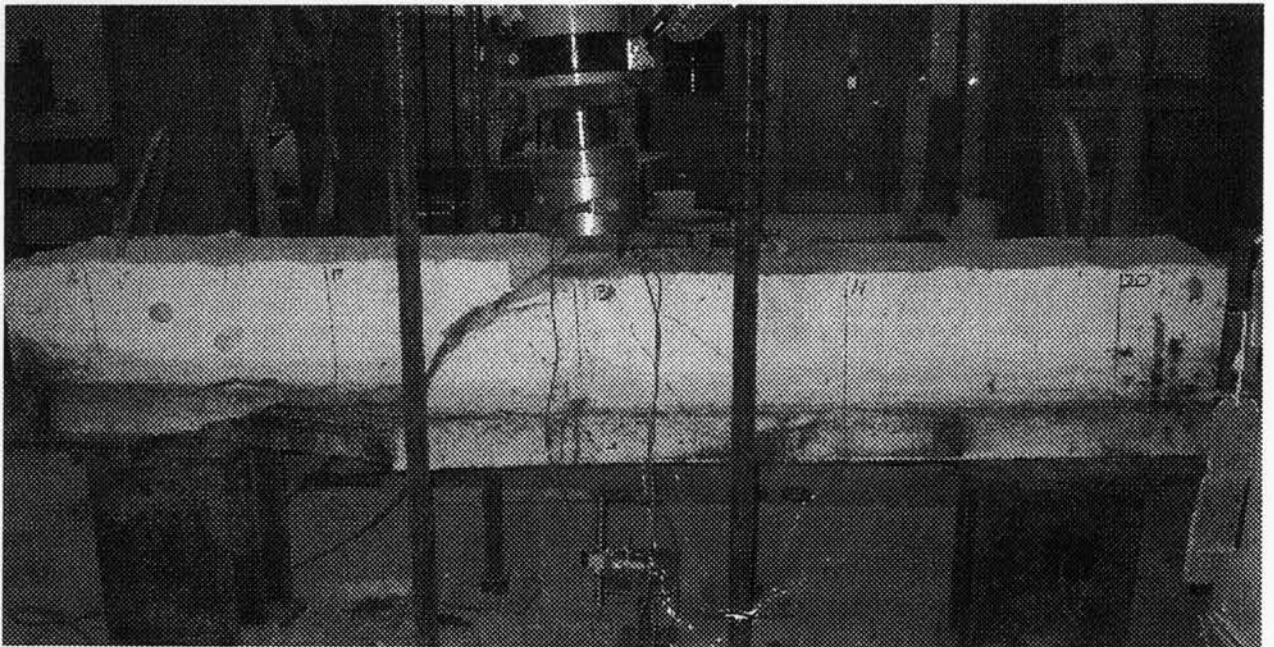


Figure 7-22: Failure of SCC-1 beam

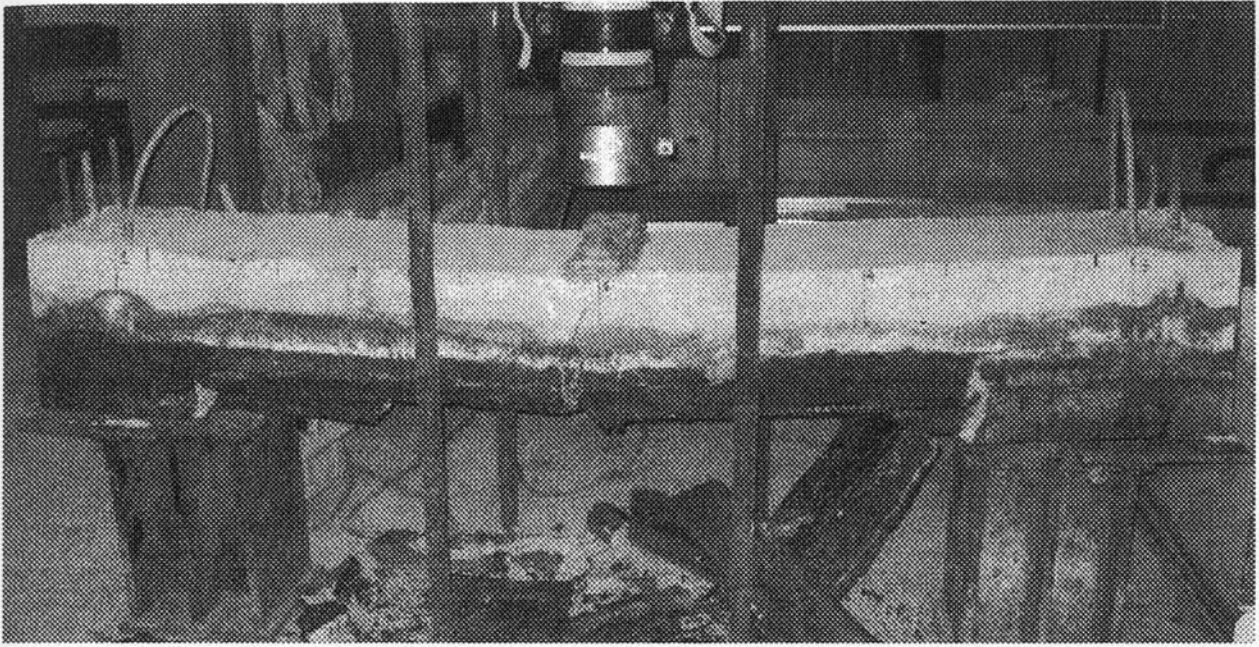


Figure 7-23: Failure of NC-2 beam

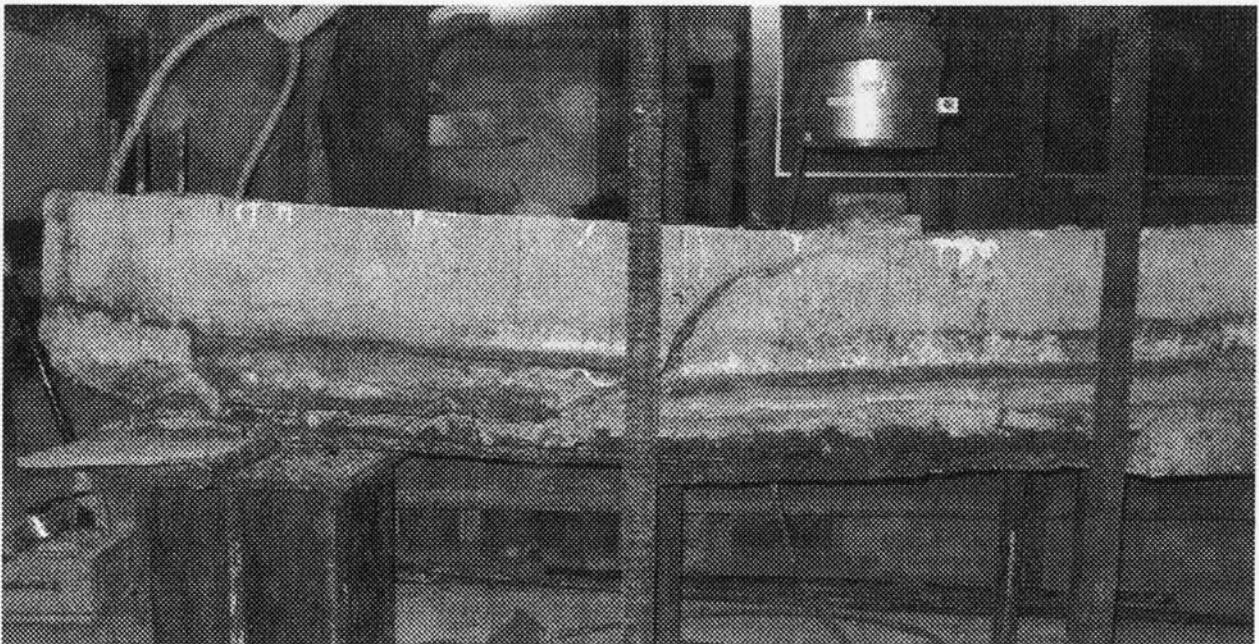


Figure 7-24: Failure of SCC-2 beam

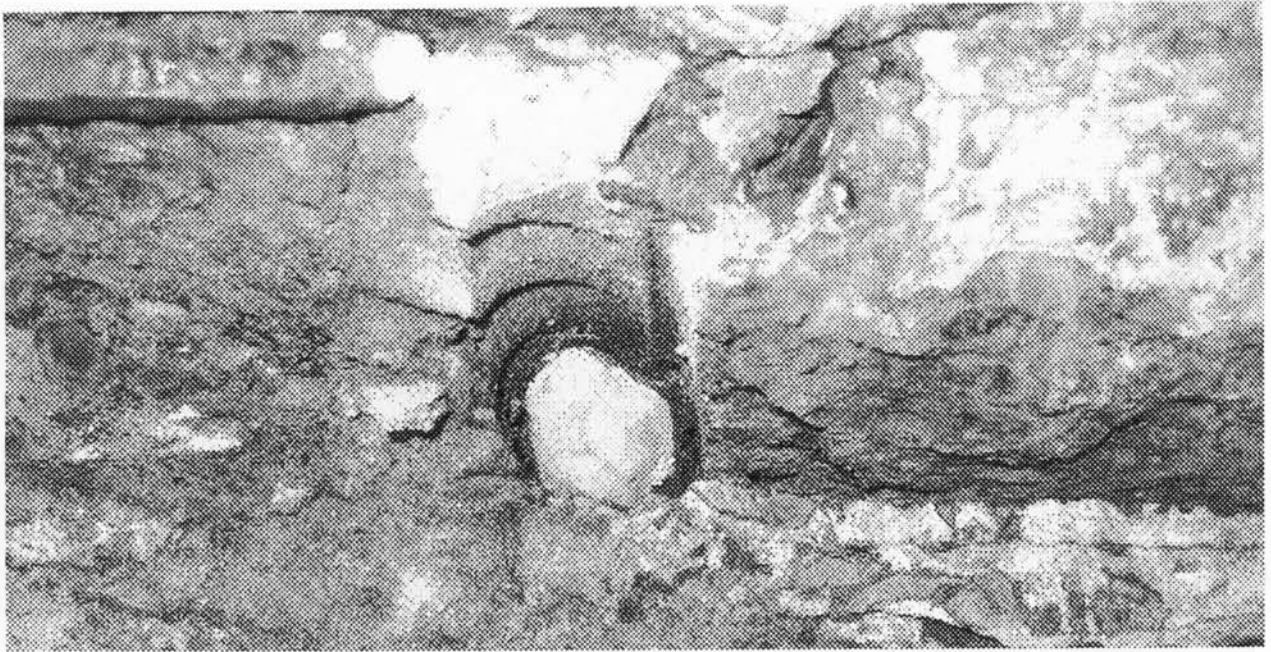


Figure 7-25: SCC-2 Rebar slippage

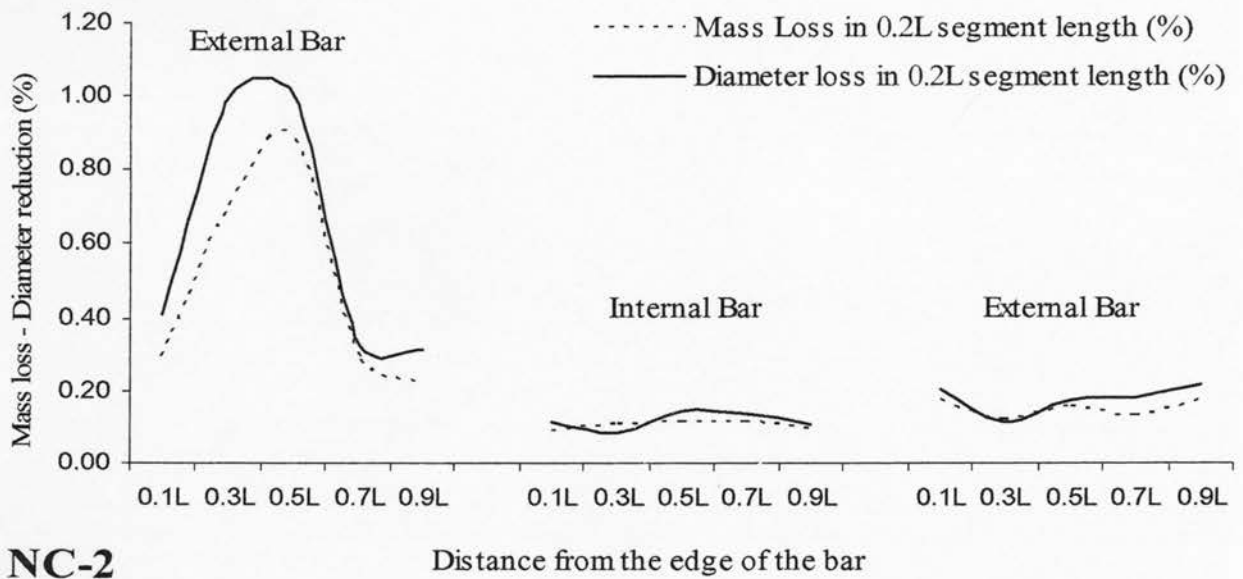


Figure 7-26: Reduction of mass loss and bar diameter in NC-2

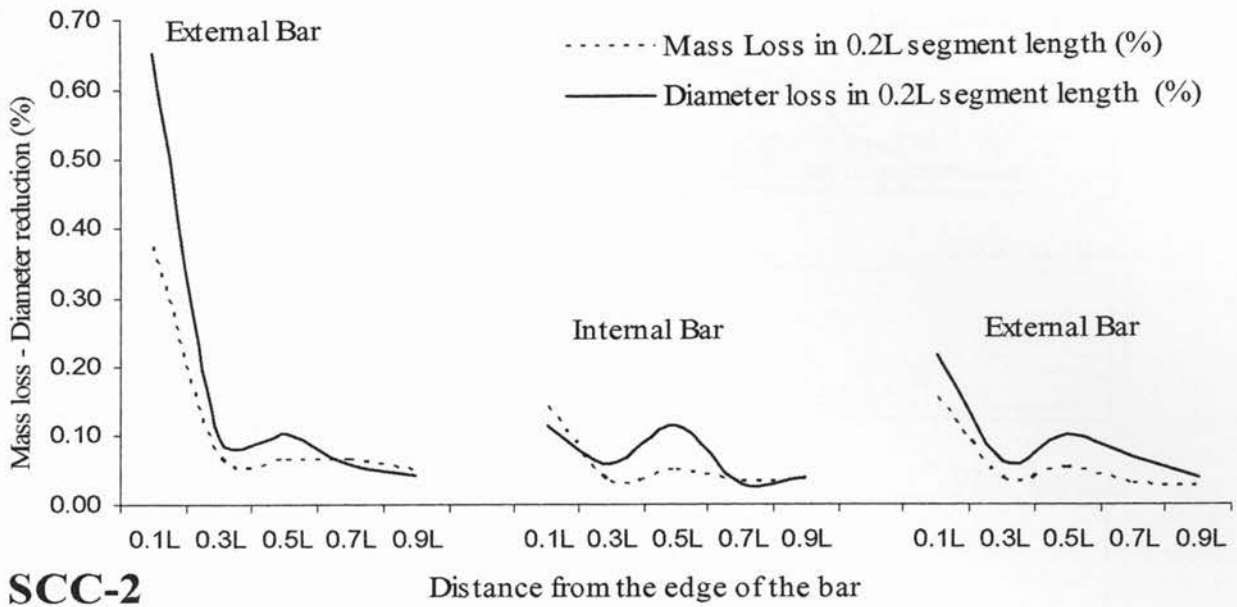


Figure 7-27: Reduction of mass loss and bar diameter in SCC-2

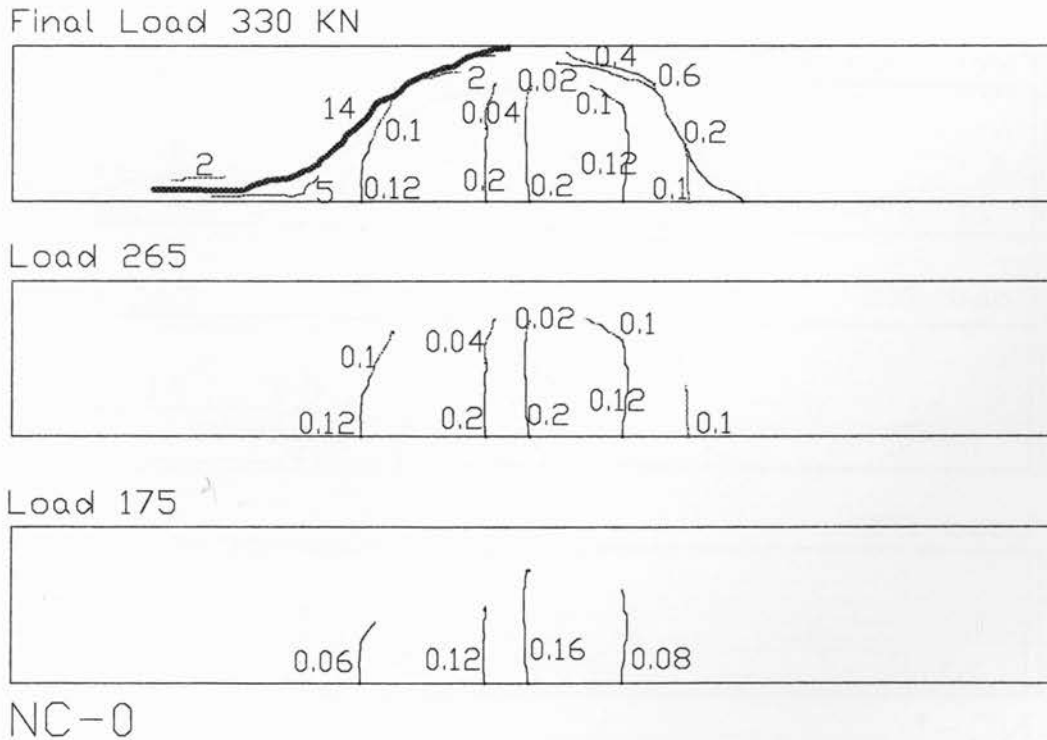
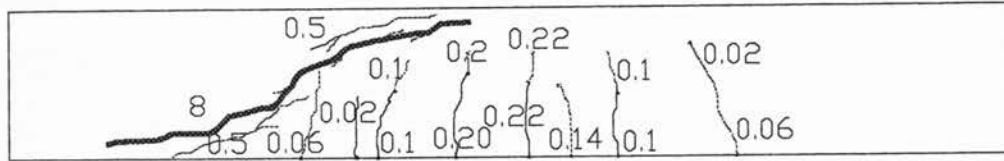
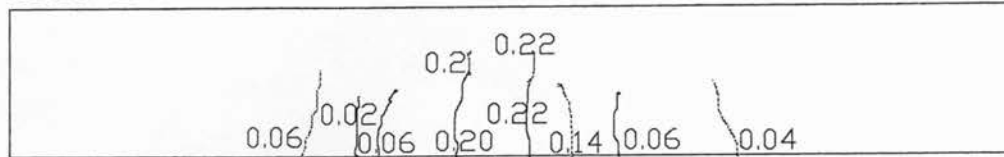


Figure 7-28: NC-0 crack development and crack widths at different load levels (50, 75, and 100% of failure load)

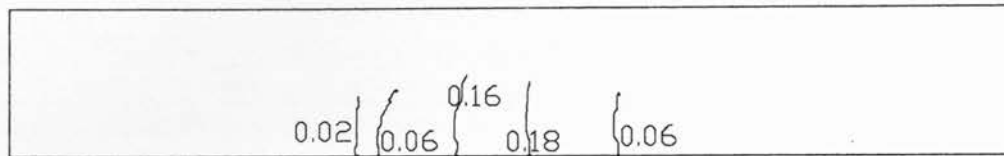
Final Load 298 KN



Load 240



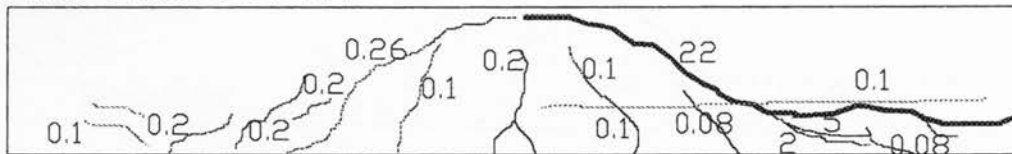
Load 140



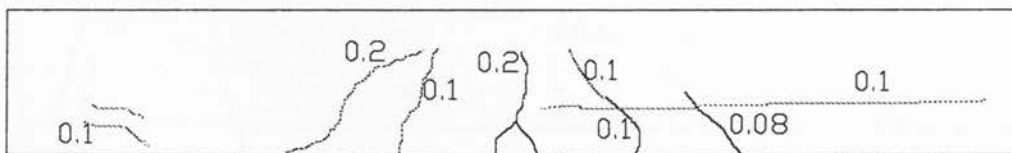
SCC-0

Figure 7-29: SCC crack development and crack widths at different load levels (50, 75, and 100% of failure load)

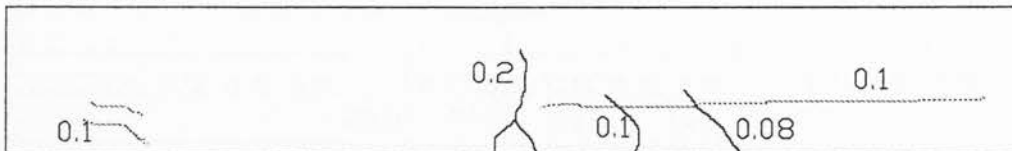
Final Load 380 KN



Load 265



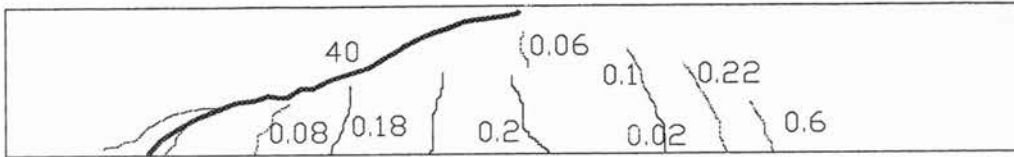
Load 175



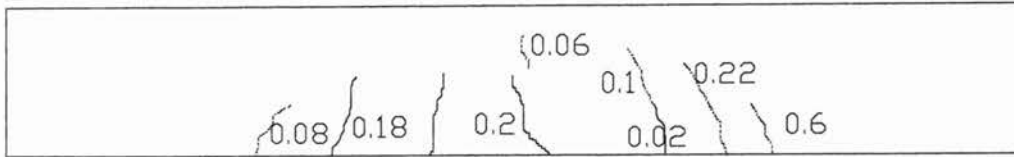
NC-1

Figure 7-30: NC-1 crack development and crack widths at different load levels (50, 75, and 100% of failure load) of uncorroded beam

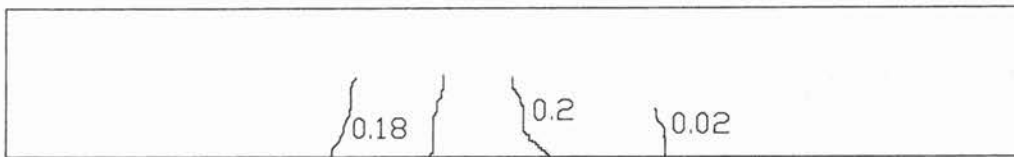
Final Load 319 KN



Load 240



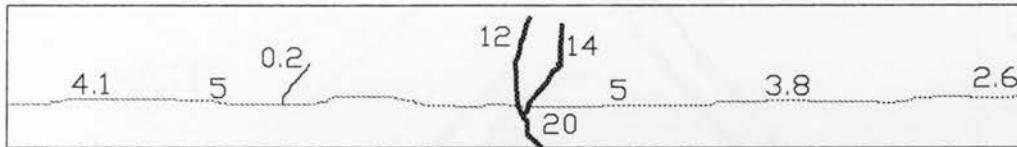
Load 140



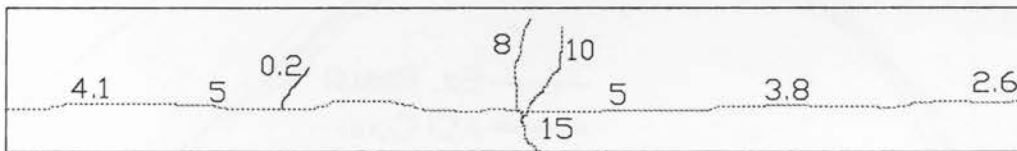
SCC-1

Figure 7-31: SCC-1 crack development and crack widths at different load levels (50, 75, and 100% of failure load) of uncorroded beam

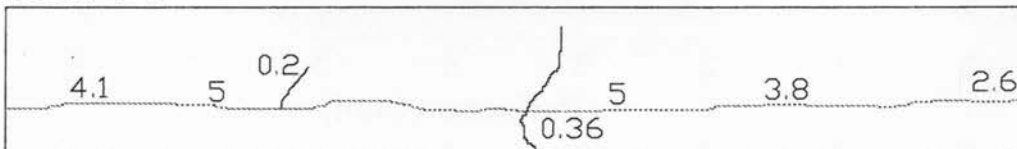
Final Load 280 KN



Load 265



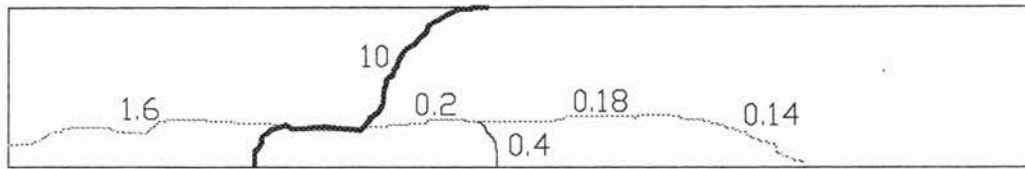
Load 175



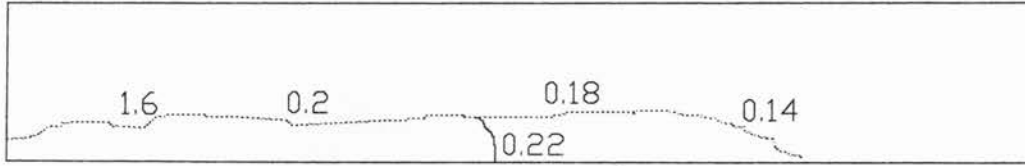
NC-2

Figure 7-32: NC-2 crack development and crack widths at different load levels (50, 75, and 100% of failure load) of uncorroded beam

Final Load 212 KN



Load 140



SCC-2

Figure 7-33: SCC-2 crack development and crack widths at different load levels (50, 75, and 100% of failure load) of uncorroded beam

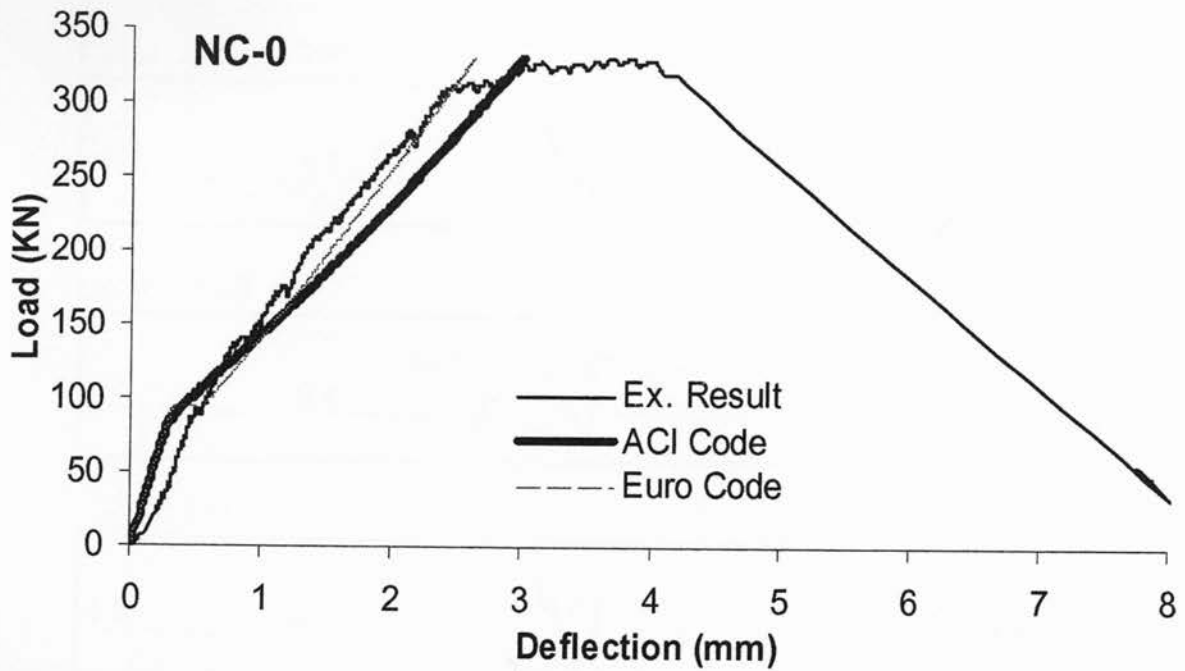


Figure 7-34: Comparison of experimental and Code-based load-mid span deflection response for NC-0

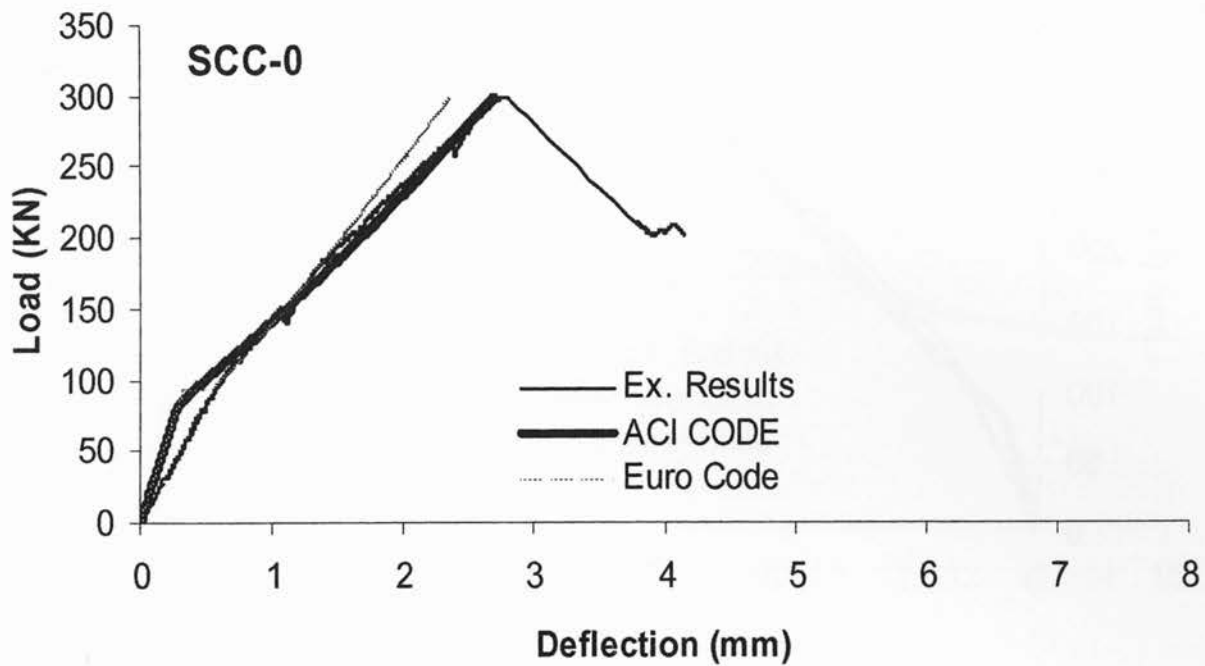


Figure 7-35: Comparison of experimental and Code-based load-mid span deflection response for SCC-0

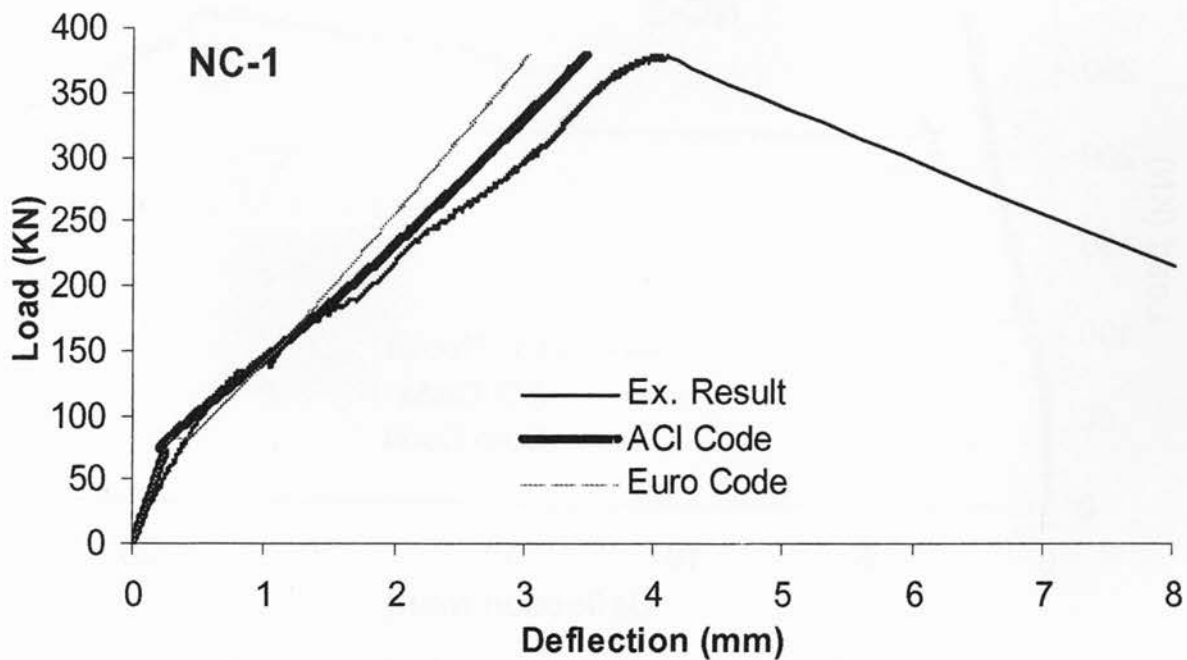


Figure 7-36: Comparison of experimental and Code-based load-mid span deflection response for NC-1

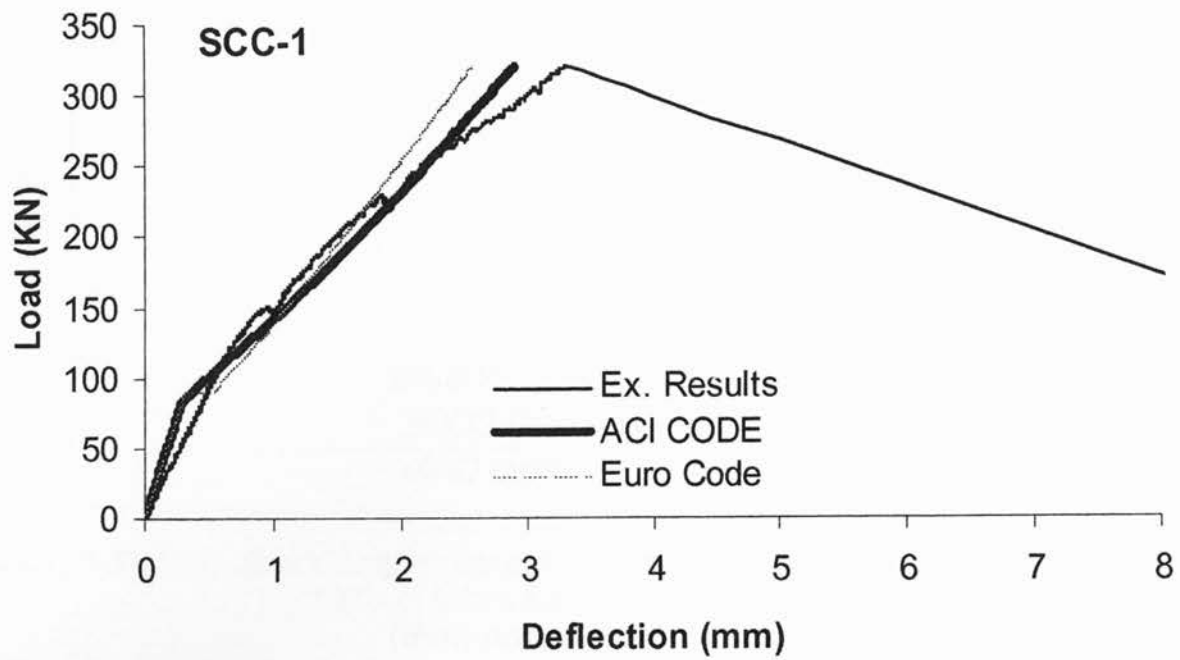


Figure 7-37: Comparison of experimental and Code-based load-mid span deflection response for SCC-1

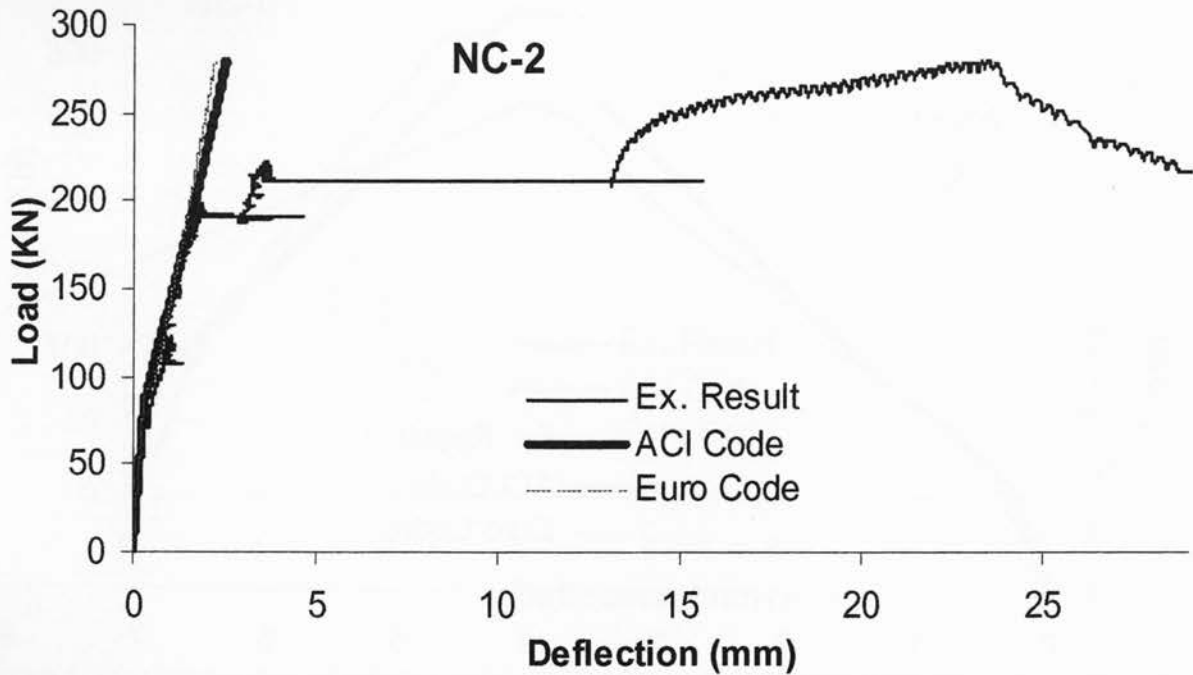


Figure 7-38: Comparison of experimental and Code-based load-mid span deflection response for NC-2

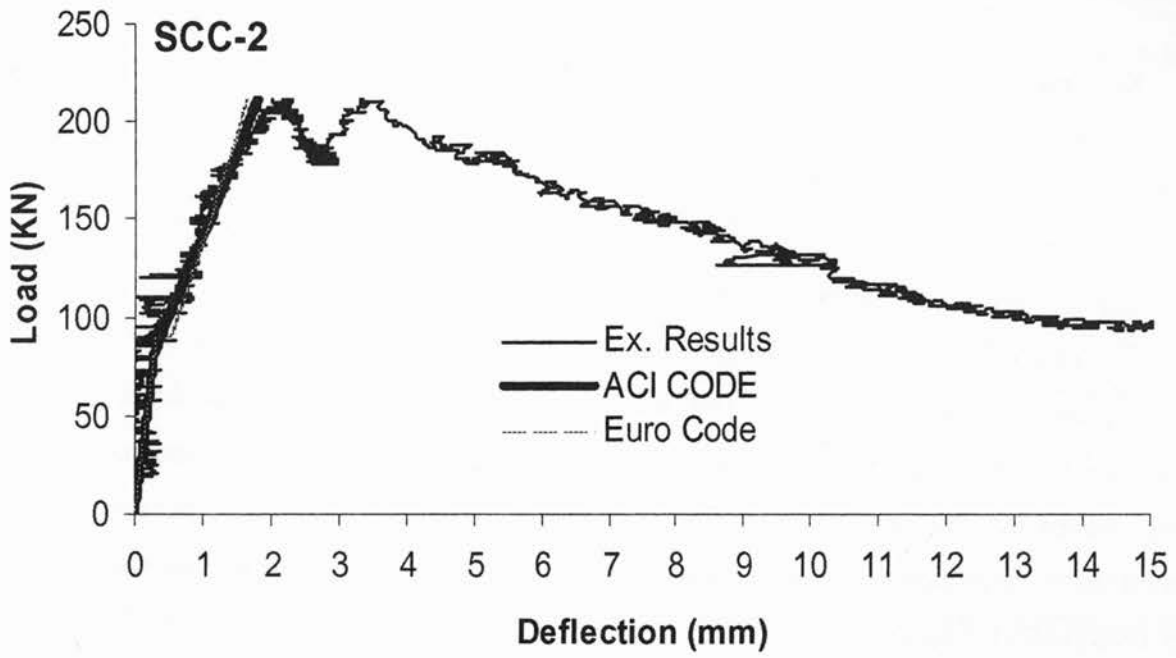


Figure 7-39: Comparison of experimental and Code-based load-mid span deflection response for SCC-2

8 Conclusions and Recommendations

8.1 Summary

The shear resistance, bond characteristics, and corrosion performance of selected SCC mixture were described and compared with those of NC counterparts. The used SCC/NC mixtures had similar ingredients and achieved comparable strength. The selected SCC mixture was mainly characterized by the lower coarse aggregate content compared to NC (approximately NC contains 25% more coarse aggregate content than SCC).

Based on the experimental test results, crack pattern, crack width, crack load, load-deflection response, failure modes and overall shear resistance at failure were critically analyzed using beams having no shear reinforcements. The bond characteristics of deformed bars embedded in large heavily reinforced beams were evaluated based on the concrete age, stress-slip relationship, and the effect of the bar location. The corrosion performance and cracking behavior of full-scale SCC/NC beams were described based on the current measurements, half-cell potential readings, crack pattern and widths, chloride ion content, rebar mass loss and diameter reduction. In addition, the degradation of strength, mid-span deflection, failure load, modes of failure of the corroded beams, were studied. Based on the results presented herein, the following conclusions and recommendations are warranted:

8.2 Conclusions

- Overall, SCC and NC showed similar shear resistance characteristics in the pre-cracking stage. No significant difference was noted between SCC and NC beams in terms of crack widths, crack heights, crack angles or overall failure mode. The ultimate shear load of SCC/NC beams increased with the increase of longitudinal reinforcement, while ultimate shear stress decreased with the increase of beam depth irrespective of either 1% or 2% longitudinal reinforcement ratios, as expected.
- SCC beams showed lower ultimate shear load compared to their NC counterparts and the shear strength reduction was higher in deeper beams with lower longitudinal steel ratios. When the beam depth was increased from 150 to 750 mm, the shear stress of beams with 2% longitudinal reinforcement ratio dropped by 22% (SCC) and 20% (NC) compared to 32% (SCC) and 23% (NC) in beams with 1% reinforcement ratio. NC beam with 750 mm depth and 1% reinforcement ratio showed 17% higher ultimate shear load compared to its

SCC counterparts. Lower shear strength of SCC is attributed to the development of lesser aggregate interlock, as a consequence of the presence of a lower quantity of coarse aggregate compared to NC.

- The post diagonal cracking shear resistance and ductility of SCC beams were also lower compared to NC beams, due to the development of lesser aggregate interlock as a consequence of the presence of a lower quantity of coarse aggregate (in SCC compared to NC). Shear design of beams should take into account the consequences of such reduced post cracking shear resistance and ductility of SCC compared to its NC counterpart.
- Beams with a higher longitudinal steel ratio (2%) generally showed narrower crack widths compared to those with a low longitudinal steel ratio (1%), for both SCC and NC beams tested for shear
- CSA based equations are found to be conservative in predicting the shear strength of both SCC and NC beams irrespective of beam depth or longitudinal reinforcement ratio and the predicted values were generally lower than the experimental values. Although the ACI equation for shear strength is conservative for NC beams with 2% reinforcement ratio irrespective of beam depth, it was not conservative for deeper NC beams with a 1% reinforcement ratio nor for deeper SCC beams with either a 1% or 2% reinforcement ratio. Hence, for deeper beams with comparatively lower longitudinal reinforcements, the ACI equation may not be safe and the risk of over prediction is higher for SCC beams compared to NC beams.
- For SCC/NC, Gergely and Lutz equation predicted reasonably well, the crack width at 50% of the failure load but significantly over predicted the crack widths at 75% and 100% of the failure load.
- For large size beams, both ACI and CSA equations underestimated the first flexural cracking load, while the AS (Australian Standard) and EC2 (Euro Code) equations overestimated this value. However, for shallow beams all four Code-based equations predicted values close to those obtained from experiments.
- Both ACI and EC2 are conservative in predicting deflection at peak (failure) load for SCC/NC beams and can be used for the calculation of deflection in shear dominated beam failure.

- Casting the heavily reinforced large-scale SCC beam was continuous, much faster and easier with less labor required, compared to the NC beam, which consumed lots of effort and time during vibration and surface finishing. In addition, SCC mixture flowed under its own weight quickly and easily between the dense reinforcements, without material blockage even in the very narrow areas. After formwork removal, the SCC beams showed a smoother and finer surface with less surface pitting compared to the NC beams.
- The development of bond stress with age was faster than the development of compressive strength in both the SCC and NC mixtures (especially at early tested ages). Also, no significant differences were noted between the SCC and NC mixtures in terms of bond or compressive strength development with age.
- The normalized bond stress was slightly higher in SCC than in NC at 3, 7, 14 and 28 days. At the one day mark, the difference of normalized bond stress between SCC and NC was hardly recognized because of the incomplete bond development. Also, the ratio of the normalized bond stress of SCC to that of NC (u_{ns}/u_{nn}) was higher in top bars and late tested ages, rather than bottom bars and early tested ages.
- The ACI and CSA Code-based predicted values of bond stress are significantly lower than those obtained from experiments. This was attributed to the nature of the experimental investigation where steel bars are tested under very heavy confinement due to the great cover and the present of heavy reinforcement around the embedded bars that hardly occurred in regular RC beams. The imposed confinement induced extra anchorage capacity to the pullout bars which is not taken into account by either ACI or CSA Code-based equations.
- Both ACI and CSA based predictions of bond stress were not valid in all tested ages (different in early ages than late ages). This is due to the fact that the development of compressive strength was different than the development of bond strength with age. Therefore, the concrete age factor needs to be considered in both ACI and CSA equations, especially if the bond stress is calculated before the age of 14 days.
- The stiffness of the bond stress-slip curve was higher in SCC beams compared to their NC counterparts at 7, 14 and 28 days. The difference was more pronounced at a later age rather than in the earlier ages.

- In both NC and SCC beams, the bond stress was slightly higher in the bottom bars than in the top and middle bars at all ages. The difference was more pronounced at late ages rather than early ages. Also, no significant difference was detected between the top and middle bars at all ages. This is confirming the provision of ACI and CSA codes which says: “for treating all bars with more than 300 mm concrete cast below bars as top bars.”
- The bond stress-slip curve showed similar trends of variation for both SCC and NC beams in the bottom bars. However, higher bond stress and stiffness in top and middle bars was observed in SCC compared to NC.
- Based on overall performance of the full-scale beams that were tested, the SCC mixture exhibited superior rebar corrosion protection compared to its NC counterpart. Distinct advantages of SCC over NC was revealed in terms of corrosion protection from the results of current measurements with time, crack widths and patterns, half-cell potential measurements, chloride ion contents near the bar surface and the rebar mass loss/diameter reduction.
- The cracks in the SCC beams, due to corrosion, were easily propagated and extended compared to NC beams. SCC beams exhibited breaking, and spalling of concrete cover, even at locations which had lower crack widths compared to the NC beams. This is attributed to the presence of a lower volume of coarse aggregate in SCC beams (25% less than NC) causing lower crack arresting capacity that induces concrete spalling, even at locations having lower crack widths.
- The SCC mixture showed non-uniform concrete properties along the length of the full-scale concrete beams when casting from one end, causing poor quality concrete at the far end due to improper compaction and distribution. As a consequence, at corners located away from the casting point, severe corrosion and spalling of concrete cover was observed. The results of half-cell measurements, crack widths, chloride ion contents, rebar mass loss and rebar diameter reduction confirmed such findings. Therefore, when casting SCC beams (especially if the beam is long, shallow and narrow) it is recommended to move the casting point along the beam length to ensure uniform compaction, especially at corners.

- A strong correlation between the predicted rebar mass loss by Faraday's equation and the experiments suggests that theoretical estimates can be used to examine the effect of corrosion over time.
- The types of admixture used in SCC mixtures have no effect on corrosion performance in terms of corrosion initiation, corrosion rate, crack patterns and crack widths.
- The difference between SCC and NC mixtures, in terms of corrosion performance, was only pronounced in large-scale concrete beams, whereas no such difference was observed in small-scale cylinder specimens. This is due to the fact that the effect of bleeding and segregation was reduced/eliminated in small-scale cylinders.
- Up to 7.7% and 1.5% of actual mass loss resulted from accelerated corrosion of the flexural bars in NC and SCC beams, respectively. The maximum load capacity and failure modes of the beams were not affected. When the actual mass loss of the flexural bars of SCC beams reached 8.13% (concentrated more at the support) the ultimate failure load dropped by 35% and the beam failed due to anchorage slippage. Also, when the actual mass loss of the flexural bars of the NC beams reached 24.5% (slightly higher mass loss at the mid-span), the ultimate failure load dropped by 22% and the beam exhibited flexural failure
- Beams at 0 (0% rebar mass loss) and first (10% theoretical rebar mass loss) degree corrosion stages that failed in shear, as it was originally designed for, proved that the SCC mixture has lower shear capacity than the NC mixture. The post diagonal cracking shear resistance and ductility of SCC beams were also lower compared to NC beams. This is due to the development of lesser aggregate interlock as a consequence of the presence of a lower quantity of coarse aggregate (in SCC compared to NC). Shear design of beams should take into account the consequences of such reduced post cracking shear resistance and ductility of SCC, compared to its NC counterpart.
- The SCC-2 beam that was originally designed for enough anchorage length for flexural bars at support, failed due to anchorage slipping when the actual mass loss of flexural bars reached 8.13%. This was due to the concentration of corrosion at the beam supports, which reduced the bond strength in those areas. However, NC-2 beam at second degree corrosion stage reached 24.5% of actual mass loss and was able to resist anchorage

slippage failure. This is because the corrosion in NC-2 beams was not concentrated at supports but rather distributed along the beam's length.

- ACI (ACI Committee 2005) and EC2 (Eurocode 1992) were conservative at predicting un-corroded and corroded SCC/NC beam deflections at peak (failure) load. However, at a high degree of corrosion, where failure of the beam was due to bending (such as NC-2 beam) because of high elongation of the longitudinal bars at yield, experimental deflection was significantly higher than the Code, based on predicted values. In general, both ACI and EC2 can be used for the calculation of deflection in shear dominated beam failure, even at moderate corrosion stages.

8.3 Recommendations

- It is recommended to study the shear strength and cracking performance of lightweight SCC beams made without shear reinforcements especially when SCC mixture has lower coarse aggregate content compared to NC mixture. As mentioned before, the reduction of the aggregate interlock (as a consequence of the presence of lower coarse aggregate content in SCC compared to NC) was the main reason behind the lower shear strength in SCC beams compared to their NC counterparts. The protruded aggregate particles along a diagonal shear crack obstruct the slippage between the two surfaces of the crack causing an increase in the shear resistance. In lightweight concrete, the diagonal cracks are expected to penetrate the lightweight aggregate particles which are normally weaker than the mortar. This of course, can lead to the formation of smooth fractured surfaces and subsequent development of weak aggregate interlock mechanism.
- It is also recommended to investigate the shear strength and cracking behavior of high strength SCC beams made without shear reinforcements and compare the results with those of high strength NC beams. The diagonal shear cracks in high strength concrete are also expected to penetrate the aggregate particles rather than finding a way around it. This is because of the fact that the mortar in high strength concrete could be stronger than the aggregate particles. The fracture surface along the diagonal cracks is expected to be similar to that of lightweight concrete and the development of weak aggregate interlock mechanism due to smooth fracture surfaces is also warranted.

- Further investigation on the effect of SCC casting technique on the uniformity of SCC mixtures is recommended. It was concluded from this investigation that SCC mixture showed non-uniform concrete properties (in terms of corrosion resistance) along the length of the full-scale concrete beams when casting from one end, causing poor quality concrete at the far end due to improper compaction and distribution. Therefore it is important to study the uniformity of SCC mixtures (in terms of durability) when casting from one end only especially if long, shallow and narrow sections are used (such as slabs or long narrow beams). This is because of the fact that the self-compaction capacity of SCC is expected to reduce at points farthest away from the casting point causing non-uniformity along the section length.

References

- Abrishami, H.H., and Mitchell, D. (1993), "Bond Characteristics of Pretensioned Strand", *ACI Materials Journal*, Vol.3, No. 90, June, pp. 228-235.
- ACI 224R-92, (1992), "Control of Cracking in Concrete Structures", *ACI Manual of Concrete Practice*, Part 3, American Concrete Institute, Detroit.
- ACI Committee 233, (1995), "Ground Granulated Blast-Furnace Slag as a Cementitious Constituent in Concrete (ACI 233R-95)", American Concrete Institute, Farmington Hills, Mich., pp.18.
- ACI Committee 318, (1951), "Building Code Requirements for Reinforced Concrete", American Concrete Institute. Detroit.
- ACI Committee 318, (1995), "Building Code Requirements for Structural Concrete", (ACI 318M-95) and Commentary- ACI 318RM-95, American Concrete Institute, Detroit.
- ACI Committee 318, (2005), "Building Code Requirements for Structural Concrete", (ACI 318M-05) and commentary (ACI 318RM-05). American Concrete Institute, Farmington Hills, Mich., pp.151.
- ACI committee 408, (1991), "State Of The Art Report: Bond under Cyclic Loads", *Journal of the American concrete institute*, No. 88-M68, pp. 669-673.
- Ahmad, S.H., Khaloo A.R., and Poveda A., (1986), "Shear Capacity of Reinforced High-Strength Concrete Beams", *ACI Journal*, Vol 83, March-April, pp. 297-305.
- Aitcin, P.C.,and Neville, A.M., (1993), "High Performance Concrete Demystified", *Concrete International*, Vol.15, No.1, pp. 21-26.
- Al-Amoudi, O., Rasheeduzzafar., Maslehuddin, M., and Al-Mana, A., (1993), "Prediction of Long-Term Corrosion Resistance of Plain and Blended Cement Concretes", *ACI Journal*, Vol 6, No.90, pp. 564-570.
- Amleh, L.,and Mirza, S., (1999), "Corrosion Influence on Bond Between Steel and Concrete", *ACI Structural Journal* May- June, Vol 3, No.96, pp. 415-423.
- AS 3600, (1988), "Concrete Structures. Standards Association of Australia", Sydney, Australia.

- ASCE-ACI Committee 445, (1998), "Recent Approaches to Shear Design of Structural Concrete", ASCE Journal of Structural Division, Vol 2, No.124, pp. 1375-1417.
- ASTM A615 / A615M, (2008), "Standard Specification for Deformed and Plain Carbon-Steel Bars for Concrete Reinforcement", American Society for Testing and Materials.
- ASTM C 143/C 143/M, (2001), "Standard Test Method for Slump of Hydraulic-Cement Concrete", American Society for Testing and Materials.
- ASTM C 39/C 39/M, (2001), "Standard Test Method for Compressive Strength of Cylindrical Concrete Specimens", American Society for Testing and Materials.
- ASTM C 494/C 494/M-99a, (2001), "Standard Specification for Chemical Admixtures for Concrete", American Society for Testing and Materials.
- ASTM C 496-96, (2001), "Standard Test Method for Splitting Tensile Strength of Cylindrical Concrete Specimens", American Society for Testing and Materials.
- ASTM C 876, (1991), "Standard Test Method for Half-Cell Potentials of Uncoated Reinforcing Steel in Concrete", Annual Book of ASTM Standards, American Society for Testing and Materials.
- ASTM C1611 / C1611M – 05, (2005), "Standard Test Method for Slump Flow of Self-Consolidating Concrete", American Society for Testing and Materials.
- ASTM G1, (2003), "Standard Practice for Preparing, Cleaning, and Evaluating Corrosion Test Specimens", American Society for Testing and Materials.
- Aitcin, P.C., and Neville, A.M., (1993), "High Performance Concrete Demystified", Concrete International, Vol.15, No.1, pp. 21-26.
- Auyeung, Y., Balaguru, P., and Chung, L., (2000), "Bond Behavior of Corroded Reinforcement Bars", ACI Materials Journal, Vol 2, No.97, pp. 214-220.
- Avery, T., (2004), "Self-Compacting Concrete Powerful Tool for Complicated Pours", concrete monthly, news from the cement and concrete industries
- Barnes, P., Ghos, A., and Mackay, A.L., (1980), "Cement Tubules – Another Look", Cement and Concrete Research, Vol.10, No.5, pp. 639-645.
- Bazant, Z.P., and Kazemi, M.I., (1991), "Size Effect on Diagonal Shear Failure of Beams Without Stirrups", ACI Journal, Vol.88, No.3 pp. 268-276.

- Bazant, Z.P., Kim, J.K., (1984), "Size Effect in Shear Failure of Longitudinally Reinforced Beams", ACI Journal, Vol.81, pp. 456-468.
- Bentz, E.C., (2005), "Empirical Modeling of Reinforced Concrete Shear Strength Size Effect For Members without Stirrups", ACI Structural Journal, Vol.102, pp. 232-241.
- Berke, N.S., Cornman, C.R., Jeknavorian, A. A., Knight, G.F., and Wallevik, O., (2002), "The Effective Use of Superplasticizers and Viscosity-Modifying Agents in Self-Consolidating Concrete", Conference proceedings: First North American Conference on the Design and Use of Self-Compacting Concrete, Nov. 12-13, Center for Advanced Cement Based Materials, pp. 173-178.
- Bentur, A., Diamond, S., and Berke, N. S., (1997), "Steel Corrosion in Concrete: Fundamentals and Civil Engineering Practice", E & FN Spon, London, pp. 201.
- Bonen, D., and Shah, S., (2005), "Fresh and Hardened Properties of Self-Consolidating Concrete", Progress in structure engineering and materials, Vol. 7, No.1 pp.14-26.
- Bouzoubaâ, N., and Lachemi, M., (2001), "Self-Compacting Concrete Incorporating High Volumes of Class F Fly Ash: Preliminary Results", Cem Concr Res, Vol.3, No.31 pp. 413-420.
- Brettmann, B., Darwin, D., and Dohaney, R.C., (1986), "Bond of Reinforcement to Superplasticized Concrete", ACI Journal, pp.98-107
- Bui, V., Akkaya, Y., and Shah, S., (2002), "Rheological Model for Self-Consolidating Concrete", ACI Journal, Vol.6, No.99, pp. 549-559.
- Building and civil engineering structures, BS EN 1992-1-1, (1992), British Standards Institute, London.
- Cairns, J., and Abdullah, R., (1994), "Fundamental Tests on the Effect of an Epoxy Coating on Bond Strength", ACI Journal /July- August No. 91-M32, pp. 331-338.
- Carrasquillo, R.L., Nilson, A.H., and Slate, P.O., (1981), "Properties of High Strength Concrete Subject to Short-Term Loads", ACI Structural Journal, Vol.78, No.3, May-June, pp. 171-178.
- CEB-FIP, (2000), "Bond of Reinforcement in Concrete", Bulletin No. 10, International Federation for Structural Concrete, pp. 427.

- Chan, Y. W., Chen, Y.S., and Liu, Y.S., (2003), "Development of Bond Strength of Reinforcement Steel in Self- Consolidating Concrete", ACI Structural Journal, Vol.100, No.4, pp.490-498.
- Chan, Y.W., Chen, Y.G., and Liu, Y.S., (2003), "Effect of Consolidation on Bond of Reinforcement in Concrete of Different Workabilities", ACI Journal, Title no.100-M35, pp.294-301.
- Chan, Y. W., and Li, V.C., (1997), "Age Effect on The Characteristics of Fiber/Cement Interfacial Bond", Journal of Materials Science, Vol. 32, No.19, pp. 5287-5292
- Chana, P.S.,(1987), "Investigation of the Mechanism of Shear Failure of Reinforced Concrete Beams", Mag of Concrete Research, Vol.39, No.141, pp. 196-204
- Choi, O.C., and Lee, W.S., (2002), "Interfacial Bond Analysis of Deformed Bars to Concrete", ACI journal, No. 99-S75, pp. 750-755.
- Cladera, A., and Mari, A.R., (2005), "Experimental Study on High-Strength Concrete Beams Failing In Shear ",engineering structures, Vol. 27, No.10, pp. 1519-1527
- Collins, M.P., Mitchell, D., Adebar, A., Vecchio, F.J.A., (1996), 'General Shear Design Method', ACI Structural Journal, Vol.1, No.93pp. 36-45.
- Collins, M.P., and Mitchell, D., (1991), "Prestressed Concrete Structures", Prentice Hall, Englewood Cliffs, N.J.
- Collins, M.P., and Kuchma, D., (1997), "How Safe Are Our Large, Lightly Reinforced Concrete Beams, Slabs and Footings", Paper published in Concrete Canada Compendium for Technology Transfer Day: The Specifications and Use of HPC, University of Toronto, October 1,pp. 87-116.
- Collins, M.P., and Mitchell, D., (1997), "Prestressed Concrete Structures", Response Publications, Canada, pp. 766.
- Collins, M.P., Mitchell, D., Adebar, P., and Vecchio, F.J., (1996), "General Shear Design Method", ACI St. J., Vol.93, No.1, pp. 36-45.
- Cornet, I., Ishikawa, T., and Bresler, B., (1968), "The Mechanism of Steel Corrosion in Concrete Structure", Materials Protection, Vol.3, No.7, pp. 44-47.
- CSA Committee A23.3, (2004), "Design of Concrete Structures", Canadian Standards Association, Rexdale, Ontario.

- Dakhil, F. H., Cady, P. D., and Carrier, R. E., (1975), "Cracking of Fresh Concrete as Related to Reinforcement", ACI journal Proceedings, Vol. 72, No. 8, pp. 421-428.
- Darwin, D., and Ebeneze, K.G., (1993), "Effect of Deformation Height and Spacing on Bond Strength of Reinforcing Bars", ACI Structural Journal, Vol. 90, No.6, Nov-Dec, pp. 646-657.
- David, W., (1941), "Bond Stress in Concrete Pullout Specimens", American Concrete Institute, Vol.13, No.1, September, pp. 37-50.
- Domone, P.L., (2007), "A Review of the Hardened Mechanical Properties of Self-Compacting Concrete", Cem Concr Comp, Vol.29, pp. 1-12.
- Edwards, A.D., and Jannopoulos, P.J., (1978), "Local Bond Stress-Slip Relationship under Repeated Loading", magazine of Concrete research, Vol.103, No.30, pp. 62-72.
- EFNARC standards, (2002), "Specification and Guidelines for Self-Compacting Concrete", ISBN 0953973344
- Elzanaty, A.H., Nilson A.H., and Slate, P.O.,(1986), "Shear Capacity of Reinforced Concrete Beams Using High-Strength Concrete ", ACI Journal, Vol.83, March-April, pp. 290-296.
- Eurocode 2 (EC2), (1992), 'Design of concrete structures – Part 1-1: General – Common Rules for Building and Civil Engineering Structures, BS EN 1-1, British Standards Institute, London.
- Fenwick, R.C., and Paulay, T., (1968), "Mechanisms of Shear Resistance of Concrete Beams", Journal of the Structural Division, ASCE, Vol.94, No. ST10, pp. 2325-2350.
- Ferguson, P.M., (1966), "Bond Stress: The State of Art", Report by ACI committee 408, ACI Journal, Vol.11, No.63, pp. 408. 1-408.22.
- Ferguson, P.M., Turpin R.D.,and Thompson, J.N., (1954), "Minimum Bar Spacing as Function of Bond and Shear Strength", ACI Journal, Vol.10, No.50,pp. 869-88.
- Gergely, P., and Lutz, L.A., (1973), "Maximum Crack Width in Reinforced Concrete Flexural Member", ACI Publication SP-20, American Concrete Institute, Detroit, Special Publication January 1, pp. 87-117.
- Ghezal, A., Khayat, K.H., and Beaupre, D., (2002), 'Effect of High-Range Water Reducer-Viscosity Enhancing Admixture Combination on Rheological Properties of Concrete Equivalent Mortar', Conference proceedings: First North American Conference

on the Design and Use of Self-Compacting Concrete, Nov. 12-13, Center for Advanced Cement Based Materials, pp. 159-166

- Grunewald, S., and Walraven, J., (2001), "Parameter-Study on The Influence of Steel Fibers And Coarse Aggregate Content On The Fresh Properties of Self-Compacting Concrete", Cement and Concrete Research, Vol.6, pp. 1793-1798.
- Hall, R., (2004), "Self-Consolidating Concrete, A Primer for Ready-Mix Applications", CE news, for the business of civil engineering
- Haque, M. N., and Kayyali, O. A., (1995), "Aspects of Chloride Ion Determination in Concrete", ACI Mater J, Vol.5, No.92, pp. 532-541.
- Hope, B., and Alan, K., (1988), "Corrosion of Steel in Concrete Made With Slag Cement", ACI Journal , Vol.5, No.84, pp. 525-531
- Hoshino, M., (1988), "Difference of The W/C Ratio, Porosity and Microscopical Aspect between the Upper Boundary Paste and The Lower Boundary Paste of The Aggregate in Concrete", Materials and structures Vol.21, No.125, pp.336-340.
- Hoshino, M., (1989), "Relationships between Bleeding, Coarse Aggregate, and Specimen Height of Concrete", ACI Materials Journal, Vol. 86, No.2, pp. 185-190.
- Hossain, K.M.A, and M. Lachemi, M., (2004), "Use of Volcanic Debris and Industrial Wastes in the Development of Self-Consolidating Concrete for Sustainable Construction", Proce. of the 5th Structural Specialty Conference of the Canadian Society for Civil Engineering, Saskatoon, Canada, June 2-5.
- Hughes, D.C., (1985), "Structure of Hardened Cement Paste", Magazine of Concrete Research, Vol.37, No.133, pp. 227-233.
- Hussain, S., and Rasheeduzzafar., (1994), "Corrosion Resistance Performance of Fly Ash Blended Cement Concrete", ACI Journal 1994, Vol.3, No.91, pp. 264-272.
- Jennings, H.M., (1983), "The Developing Microstructure in Portland Cement" Advances in Cement Technology, S.N. Ghosh, Ed., Pergamon, New York, pp. 349-396.
- Kani, G.N.J., (1966), "Basic Facts Concerning Shear Failure", ACI Journal, Vol.63, June, pp. 675-692.
- Kani, G.N.J., (1967), "How Safe are our Large Reinforced Concrete Beams", ACI Journal, Vol.64, March, pp. 128-141.

- Kani, M.W., Huggins, M.W., and Wittkopp, R.W., (1979), 'Kani on Shear in Reinforced Concrete', University of Toronto Press, Toronto, Ontario, pp. 225.
- Khayat, K., (2000), "Optimization and Performance of Air-Entrained, Self-Consolidating Concrete", ACI Journal Vol. 97, No. 5.
- Khayat, K.H., Paultre, P., and Tremblay, S., (2001), "Structural Performance and in-Place Properties of Self-Consolidating Concrete Used for Casting Highly Reinforced Columns", ACI Materials Journal, Vol.5, No.98, pp. 371-378.
- Khayat, K.H., Tremblay, S., Paultre, P., (1999), "Structural Response of Self-Consolidating Concrete Columns", In: Skarendahl A, Petersson O, editors. Proceedings of the RILEM Symposium on Self-Compacting Concrete. RILEM Publications S.A.R.L.: Stockholm, pp. 291-306.
- Khayat, K., (1999), "Workability, Testing, and Performance of Self-Consolidating Concrete", ACI Materials Journal, Vol.96 No.3, May-June, pp.346-353.
- Khayat, K.H., (1998), "Use of Viscosity-Modifying Admixture to Reduce Top-Bar Effect of Anchored Bars Cast with Fluid Concrete", ACI Materials Journal, pp. 158-167.
- Khayat, K.H., Manai, K., and Trudel, A., (1996), "In Situ Mechanical Properties of Wall Elements cast using Self Consolidating Concrete", ACI Materials Journal, December, Vol.6, No.94, pp. 491-500.
- Khayat, K. H., Assaad, J., and Daczko, J., (2004), "Comparison of Field-Oriented Test Methods to Assess Dynamic Stability of Self-Consolidating Concrete", ACI Materials Journal, Vol.101, No.2, Mar.-Apr, pp. 168-176.
- Kim, J.K., and Park, Y.D., (1994), "Shear Strength of Reinforced High Strength Concrete Beams without Web Reinforcement", Magazine of Concrete Research, Vol.46 No. 166, March, pp. 7-16.
- Kim, J.K., Trejo, D., and Hueste, M.D., (2007), "Shear Characteristics of Self-Consolidating Concrete for Precast Prestressed Concrete Members", ACI Publication SP-247-5, American Concrete Institute, Detroit, Special Publication September 1, pp. 53-63.
- Kimura, H., and Jirsa, J., (1992), "Effects of Bar Deformation and Concrete Strength on Bond of Reinforcing Steel to Concrete", PMFSEL Report No. 92-4, Phil M. Ferguson Structural Engineering Laboratory, University of Texas at Austin.

- Klinghoffer, O., (1995), "In Situ Monitoring of Reinforcement Corrosion by Means of Electrochemical Methods", Nordic Seminar, February.
- Kong, F. K., and Evans, R. H., (1987), "Reinforced and Prestressed Concrete", Van Nostrand Reinhold (UK) Co. Ltd.
- Kong, P.Y.L., and Rangan, B.V., (1998), "Shear Strength of High-Performance Concrete Beams", ACI Structural Journal, Vol.95, No. 6, Nov.-Dec. pp. 677-688.
- Kreijger, P.C., (1987), "The Skins of Concrete – Research Needs", Magazine of Concrete Research, Vol.39, No.140 pp. 122-123.
- Lachemi, M., Hossain, K.M.A., Lambros, V., and Bouzoubaâ, N., (2003), "Development of Cost-Effective Self-Compacting Concrete Incorporating Fly Ash, Slag Cement or Viscosity Modifying Admixtures", ACI Materials Journal, Vol.5, No.100, pp. 419-425.
- Lachemi, M., Hossain, K.M.A., Lambros, V., Nkinamubanzi, P.C., and Bouzoubaâ, N., (2004), "Self-Compacting Concrete Incorporating New Viscosity Modifying Admixtures", Cem Concr Res, Vol.6, No.24, pp. 917-926.
- Lachemi, M., Hossain, K.M.A., and Lambros, V., (2005), "Shear Resistance of Self-Consolidating Concrete Beams - Experimental Investigations", Canadian Journal of Civil Engineering, Vol.6, No.32, pp. 1103-1113.
- Lachemi, M., Hossain, K.M.A., Patel, R., Shehata, M., and Bouzoubaâ, N., (2007), "Prediction of Flow Behaviour of High Volume Fly Ash Self-Consolidating Concrete from the Rheology of Paste and Mortar", Magazine of Concrete Research, Vol.7, No.59, pp. 517-528.
- Larbi, J.A., (1993), "Microstructure of the Interfacial Zone Around Aggregate Particles in Concrete", Heron, Vol.38, No.1, pp. 69.
- Lea, F. M., (1971), "The Chemistry of Cement and Concrete", Chemical publishing, Inc.
- Leroy, A., Lutz, and Gergely, P., (1967), "Mechanics of Bonds and Slip of Deformed Bars in Concrete", ACI Journal, No. 64-62, pp. 711-721.
- Lessard, M., Talbot, C., Phelan, W.S., Baker, D., (2002), "Self-Consolidating Concrete Solves Challenging Placement Problems at the Pearson International Airport in Toronto, Canada", 1st North American Conference on the Design and Use of Self-Consolidating Concrete (SCC). Rosemont, Illinois, pp. 12-13.

- Lessard, M., Sarkar, S.L., Ksinsik, D.W., and Aitcin P.C., (1992), "Long-Term Behavior of Silica Fume Concrete International", Vol. 14, No.4, pp. 25-30.
- Lutz, L.A., Gergely, P., Winter, G., (1966), "Mechanics of Bond and Slip of Deformed Reinforcing Bars in Concrete", Research Report No. 324, Department of Civil Engineering, Cornell University, Ithaca, New York.
- MacGregor, J., Bartlett, F., (2000), "Reinforced Concrete, Mechanisms and Design", First Canadian Edition, Prentice Hall Canada Inc., Scarborough, Ontario, pp.1042.
- MacGregor, J.C., (1992), "Reinforced Concrete: Mechanics and Design", 2nd ed., Prentice Hall, Englewood Cliff, N.J., PP. 848.
- MacGregor, J.G., and Gergely, P., (1977), "Suggested Revisions to ACI Building Code Clauses Dealing with Shear in Beams", ACIJ. Vol. 74, No.10, Oct. 1977, pp. 493-500.
- Maslehuddin, M., Ibrahim, A., Al Sulaimani, G.J., Abdulaziz, A., and Sahe, l A.N., (1990), "Effect of Rusting of Reinforcing Steel on its Mechanical Properties and Bond With Concrete", ACI Journal ,No. 87-M53, pp. 496-500.
- Maso, J.C., (1980), "The Bond Between Aggregates and Hydrated Cement paste", proceedings of the 7th International Congress on the Chemistry of Cement, Paris, Vol.1, pp., VII/I-VII/15.
- McCurrich, L.H., (1986), "Reduction in Permeability and Chloride Diffusion with Superplasticizers", Concrete, Vol. 20, No. 8, pp. 9-10.
- Mehta, P.K., (1981), "Studies on Blended Portland cement Containing Santorin Earth," Cement and Concrete Research, Vol.11, No.4, pp. 507-518.
- Mehta, P.K., (1986), "Concrete Structure, properties and Materials", prentice Hall Inc., New Jersey, Chapters 2 and 6.
- Mehta, P.K., (1980), "Durability of Concrete in Marine Environment", A Review, performance of Concrete in Marine Environment, ACI SP-65, V.M.Malhotra, Ed., pp. 1-20.
- Mehta, P.K., (1993), "Concrete Structure, Properties, and Materials", Prentice-Hall, Inc., Englewood Cliffs, N.J.07632
- Midgley, H.G., and Illston, J.M., (1983), "Stone Comments on the Microstructure of Hardened Cement pastes", Cement and Concrete Research,

- Mindess, S., Young, F., and Darwin, D., (2003), "Concrete Second Edition", Prentice Hall, Upper Saddle River, NJ, pp. 644.
- Morita, S., and Kaku, T., (1979), "Splitting Bond Failures of Large Deformed Reinforcing Bars", ACI Journal, Vol.1, No. 76, pp. 93-110.
- Montemor, M.F., Cunha, M.P., Ferreira, M.G., and Simoes, A.M., (2002), "Corrosion Behavior of Rebars in Fly Ash Mortar Exposed to Carbon Dioxide and Chlorides", Cement Concr Comp, Vol.24, pp. 45-53.
- Monteiro, P.J.M., Maso, J.C., and Ollivier, J.P., (1985), "The Aggregate-Mortar Interface", Cement and Concrete Research, Vol.15, No. 6, pp. 953-958.
- Nehdi, M., Pardhan, M., and Koshowski, S., (2004), "Durability of Self-Consolidating Concrete Incorporating High Volume Replacement Composite Cement", Cement and Concrete Research, pp. 2103-2112.
- Neville, A. M., (1996), "Properties of Concrete", John Wiley & sons, Inc., pp.256-258.
- Neville, A.M., (1981), "Properties of Concrete", 3rd Edition, Pitman Publishing Ltd., London, Chapter
- Nielsen, A., (1985), "Durability," Beton Bogen (The Concrete book), Edited by Aa. D. Herholdt, Chr. F.P. Justesen, P. Nepper-Christensen, and A. Nieleesen, Aalborg, Portland, pp. 200-43.
- Oberholster, R.E, (1986), "Pore Structure, Permeability and Diffusivity of Hardened Cement Paste and Concrete in Relation to Durability: Status and Prospects", Proceedings of the 8th International Congress on the Chemistry of Cement, Brazil, Vol.1, pp. 324-335.
- Okamura, H., and Ouchi, M., (1999), "Self -Compacting Concrete. Development, Present Use and Future", Proceedings 1st International RILEM Symposium on Self-Compacting Concrete, Stockholm, Sweden, September, pp.3-14.
- Okamura, H., and Ozawa, K., (1995), "Mix Design for Self-Compacting Concrete", Concrete Library of Japanese Society of Civil Engineers, No.25, June, pp.107-120.
- Ouchi, M., et al., (2003), "Applications of Self-Compacting Concrete in Japan, Europe and the United States", United States Department of Transportation - Federal Highway Administration - Infrastructure.

- Ozawa, K., Sakata, N., and Iwai, M., (1994), "Evaluation of Self-Compactibility of Fresh Concrete Using Funnel Test", *Proce. Of JSCE*, Vol.23, pp. 490.
- Park, R., and Paulay, T., (1975), "Reinforced Concrete Structures", John Wiley and Sons, New York.
- Patel, R., Hossain, K.M.A., Shehata, M., and Lachemi, M., (2004), "Development of Statistical Models for the Mix Design of High Volume Fly Ash Self-Compacting Concrete", *ACI Materials Journal*, Vol.4, No.101, pp. 294-302.
- Peer, L.B.B., (1990), "Water Flow into Unsaturated Concrete", Phd. Dissertation, University of Cambridge, London.
- Persson, B.,(2001), "A Comparison between Mechanical Properties of Self-Compacting Concrete and the Corresponding Properties of Normal Concrete", *Cement and Concrete Research*, Vol.31,pp. 193-198
- Persson, B.,(2003), "Internal Frost Resistance and Salt Frost Scaling of Self-Compacting Concrete", *Cement and Concrete Research*, Vol.33, pp. 373-379
- Ping, X., Beaudoin, J.J and Brousseau, R., (1991), "Flat Aggregate-Portland Cement Paste Interfaces I.Electrical Conductivity Models", *Cement and Concrete Research*, Vol. 21, No. 4, pp. 515-522.
- Rasheeduzzafar, Al-Saadoun S. S., and Al-Gahtani, A. S., (1992), "Reinforcement Corrosion-Resisting Characteristics of Silica-Fume Blended-Cement Concrete", *ACI Journal* , Vol.4, No.89, pp. 337-344
- Rasheeduzzafar, Ehtesham, H.S, and Al-Saadoun, S.S., (1992), "Effect of Tricalcium Aluminate Content of Cement on Chloride Binding and Corrosion of Reinforcing Steel in Concrete", *ACI Material Journal* Jan- Feb, Vol.1, No.89, pp. 3-13.
- Rehm G., (1968), "The basic principles of the bond between steel and concrete", *Cement and Concrete Association*, Translation No.134, London, pp.66.
- Rehm, G., (1961), "Uber Die Grunlagen Des Verbundes Zwischen Stahl Und Beton", *Deutscher Ausschuss für Stahlbeton*, Heft 138, Wilhelm Ernest und Sohn, Berlin
- Robberts, J., and Marshall, V., (2005), "Analysis and Design of Concrete Structure", Vol 1: Fundamentals

- Sarkar, S.L. and Aitcin, P.C., (1987), "Comparative Study of the Microstructures of Normal and Very High-Strength Concrete Cement", *Concrete and Aggregates*, Board Vol.32, 1953, pp. 285-297.
- Scrivener, K.L., (1989), "The Microstructure of Concrete" *Materials Science of Concrete I*, J.P. Skalny, Ed., The American Ceramic Society Inc., pp. 127-161.
- Scrivener, K.L., (1984), "The Development of Microstructure during the Hydration of Portland Cement", Ph.D. Thesis, University of London.
- Scrivener, K.L., And Gartner, E.M., (1987), "Microstructural Gradients in Cement Paste Around Aggregate Particles", *Bonding in Cementitious Composites*, S. Mindess and S.P.Shah, Ed., *Materials Research Society Symposium Proceedings*, Vol. 114, pp.77-85.
- Scrivener, K.L., And Pratt, P.L., (1987), "The Characterization and Quantification of Cement and Concrete Microstructures", *Pore Structure and Material Properties*, J.C. Maso, Ed., *Proceeding of the 1st International Congress by RILEM*. Vol. I, pp.61-68
- Shioya, T., (1989), "Shear Properties of Large Reinforced Concrete Members ", *Special Report of Institute of Technology, Shimizu Corporation*, No. 25, Feb.
- Sonebi, M., Batros, P., Zhu, W., Gibbs, J., and Tamimi, A., (2000), "Properties of Harden Concrete", Task 4, final report (2000). *Advance concrete masonry center*, University of Paisley, Scotland, UK, pp. 6-73
- Sonebi, M., Tamimi, A., and Bartos, P., (2003), "Performance and Cracking Behavior of Reinforced Beams Cast with Self-Consolidating Concrete", *ACI Journal*, Title no. 100-M57, November-December.
- Sonebi. M., Zhu,W., and Gibbs.J., (2001), " Bond of Reinforcement in Self- Compacting Concrete", *Concrete and Masonry Centre*, University of Paisley.
- Soretz, S., and Holzenbein, H., (1979), "Rib Dimension Influence on Bond and Bendability", *ACI journal. Proceedings* Vol. 76, pp. 87-91.
- Soroka, I., (1979), "Portland Cement Paste and Concrete," *Macmillan Press*, London.
- Spainhour, L.K., and Wootton, I.A., (2006), 'Corrosion Process and Abatement in Reinforced Concrete Wrapped by Fiber Reinforced Polymer', *Transportation research board 85th annual meeting*.
- Stanik, B., (1998),"The Influence of Concrete Strength, Distribution of Longitudinal Reinforcement, Amount of Transverse Reinforcement and Member Size on Shear

Strength of Reinforced Concrete Members", M.A.Sc. Thesis, University of Toronto, Department of Civil Engineering, pp. 711.

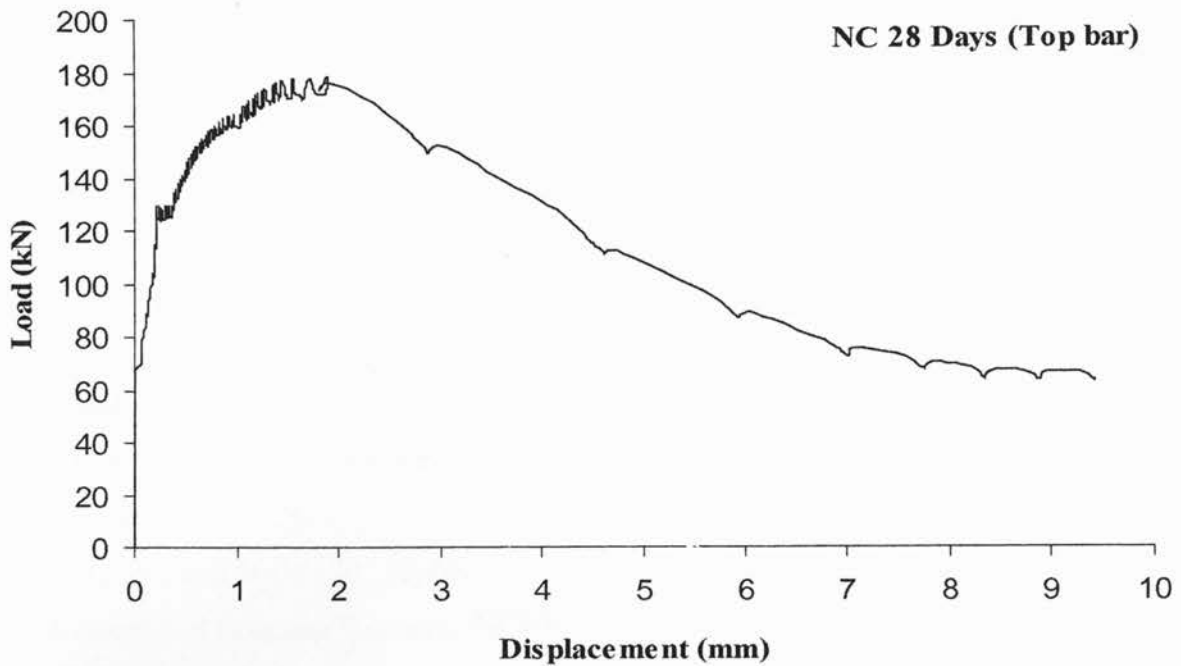
- Stratfull, R.F., (1957), "The Corrosion of Steel in a Reinforced Concrete Bridge", Vol. 13, pp 173-179.
- Tachibana, M. S., (1999), "Flexural Strength of Concrete Beams with Corroding Reinforcement", ACI Structural Journal, Vol 96, No.1, Jan.-Feb. pp. 149-158.
- Tachibana, Y., Maeda, K. I., and Kajikawa, M., (1990), "Mechanical Behavior of RC Beams Damaged by Corrosion of Reinforcement", Third International Symposium on Corrosion of Reinforcement in Concrete Construction, UK, pp. 178-187.
- Taylor, H.P.J., (1970), "Investigation of Forces Carried across Cracks in Reinforced Concrete Beams in Shear by Interlock of Aggregate" TRA 42.447, Cement and Concrete Association, London, pp. 22.
- Taylor, H.P.J., (1974), "The Fundamental Behavior of Reinforced Concrete Beams in Bending and Shear", ACI SP-42, Detroit, pp. 43-77.
- Taylor, H.F.W., (1990), "Cement Chemistry", Academic press Ltd., California, Chapters 5, 6 & 7.
- Tompos, E.J., and Frosch, R.J., (2002), "Influence of Beam Size, Longitudinal Reinforcement, and Stirrup Effectiveness on Concrete Shear Strength", ACI Journal, Vol.5, No.99, pp. 559-567.
- Tompos, E., and Frosch, R., (2003), "Influence of Beam Size, Longitudinal Reinforcement, and Stirrup Effectiveness on Concrete Shear Strength", ACI structural Journal, Vol.99 No.5, pp 559-567.
- Uomoto, T., Tsuji, K., and Kakizawa, T., (1984), "Deterioration Mechanism of Concrete Structures Caused by Corrosion of Reinforcing Bars", Transactions of Japan Concrete Institute, Vol 6, pp. 163-170.
- Walraven, J., and Lehwalter, N., (1994), "Size Effects in short beams loaded in shear", ACI structural Journal, Vol.91 No.5, pp 585-593.
- Walraven, J.C., (1981), "Fundamental Analysis of Aggregate Interlock", Journal of the Structural Division, ASCE, Vol.107, No. 11, pp. 2245-2270.

- Welch, G.B. and Patten, B.J.F., (1967), "Reduction in Concrete-Steel Bond with Horizontally Embedded Reinforcement", UNCIV Report No R-8, university of New South Wales, pp 26.
- Yang, K., et al., (2003), "Shear Characteristics of High-Strength Concrete Deep Beams Without Shear Reinforcements", Engineering Structures, pp 1343-1352.
- Yurugi, M., Sakata, N., Iwai, M., and Sakai, G., (1993), "Mix Proportion for Highly Workable Concrete", Proceedings of Concrete 2000, Dundee, pp. 579-589.
- Zararis, P.D., and Papadakis. , (2001), "GC. Diagonal Shear Failure and Size Effect in RC Beams without Web Reinforcement", ASCE Journal of Structural Division, Vol. 7, No.127, pp. 733-741.
- Zhu, W., and Bartos, P., (2003), "Permeation Properties of Self-Compacting Concrete", Cement and Concrete Research, pp. 921-926.
- Zhu, W., Gibbs, J.C., and Bartos, P.J.M., (2001), "Uniformity of In Situ Properties of Self-Compacting Concrete in Full-Scale Structural Elements," Cement and Concrete Composites, Vol.23, pp. 57-64.

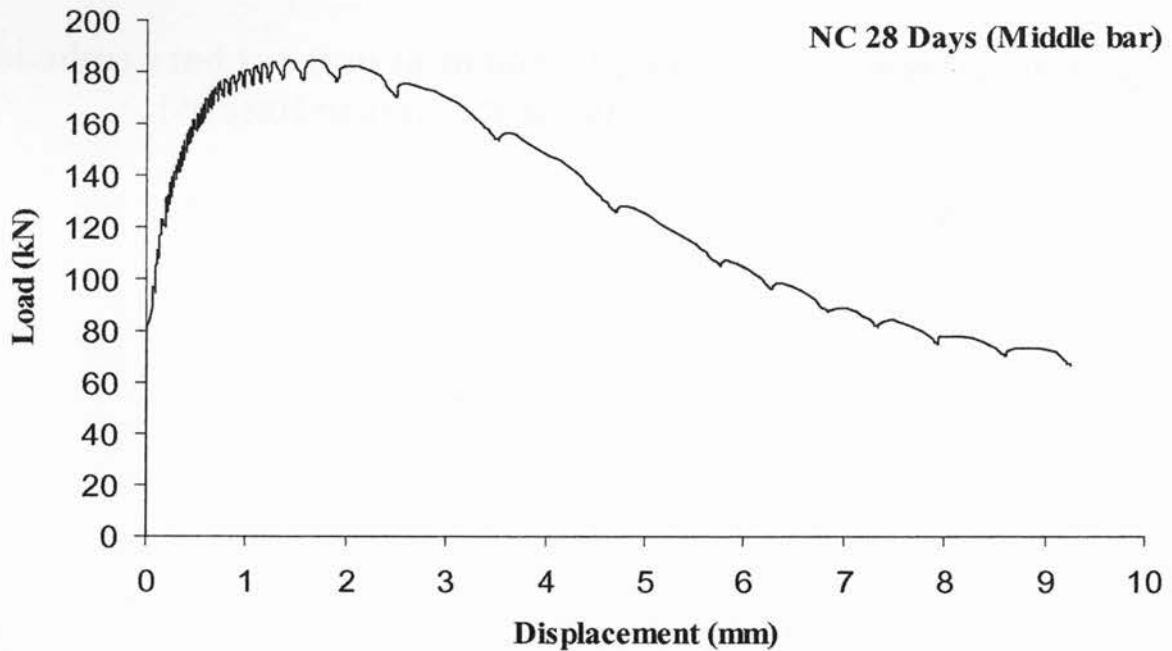
Appendices

Appendix A

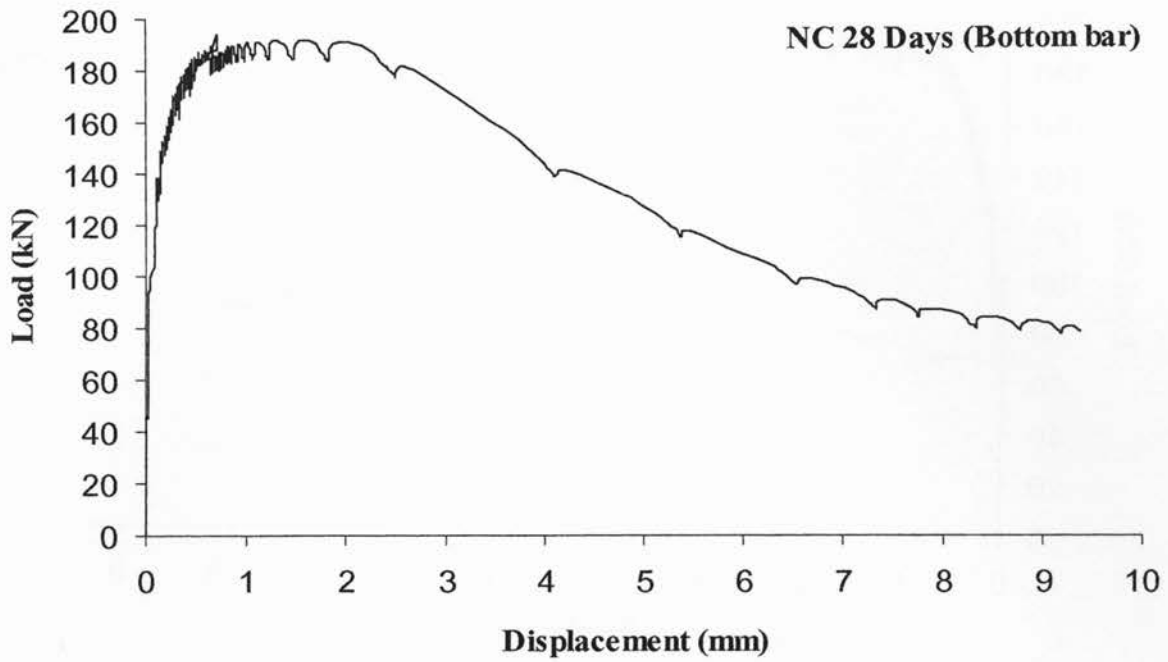
Experimental load-free end displacement of pull out bars embedded in SCC/NC beams (Bond Resistance Results)



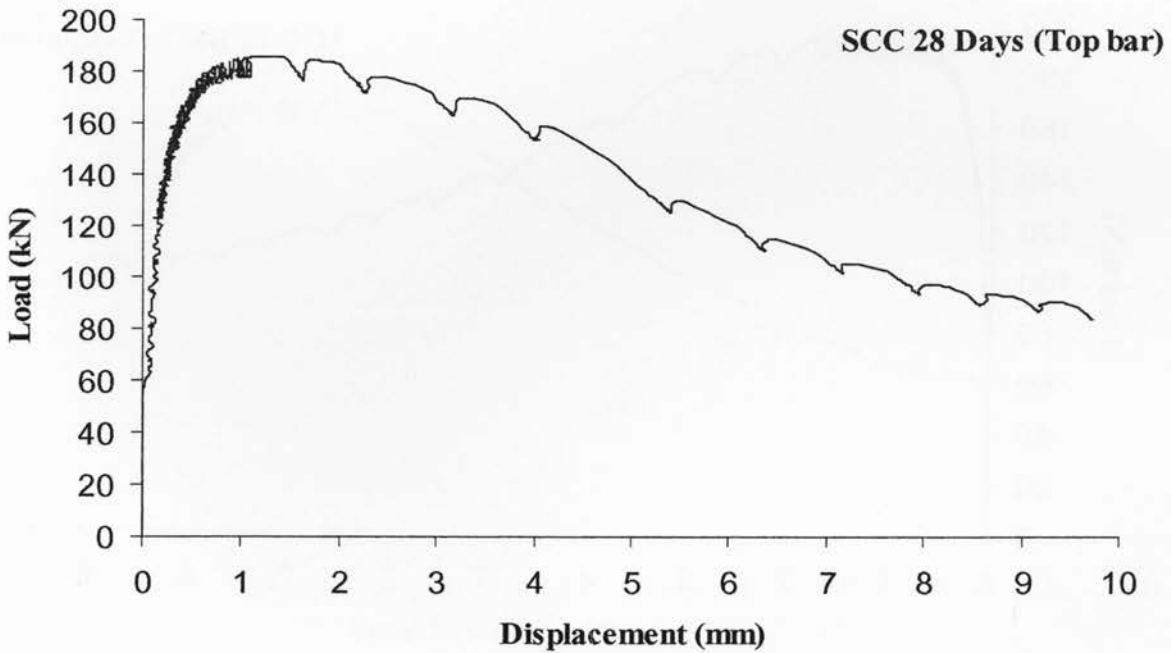
A 1: Experimental load-free end displacement (top bar embedded in the NC beam at 28 days tested age) [Bond stress (MPa) = 0.106 Load (kN)]



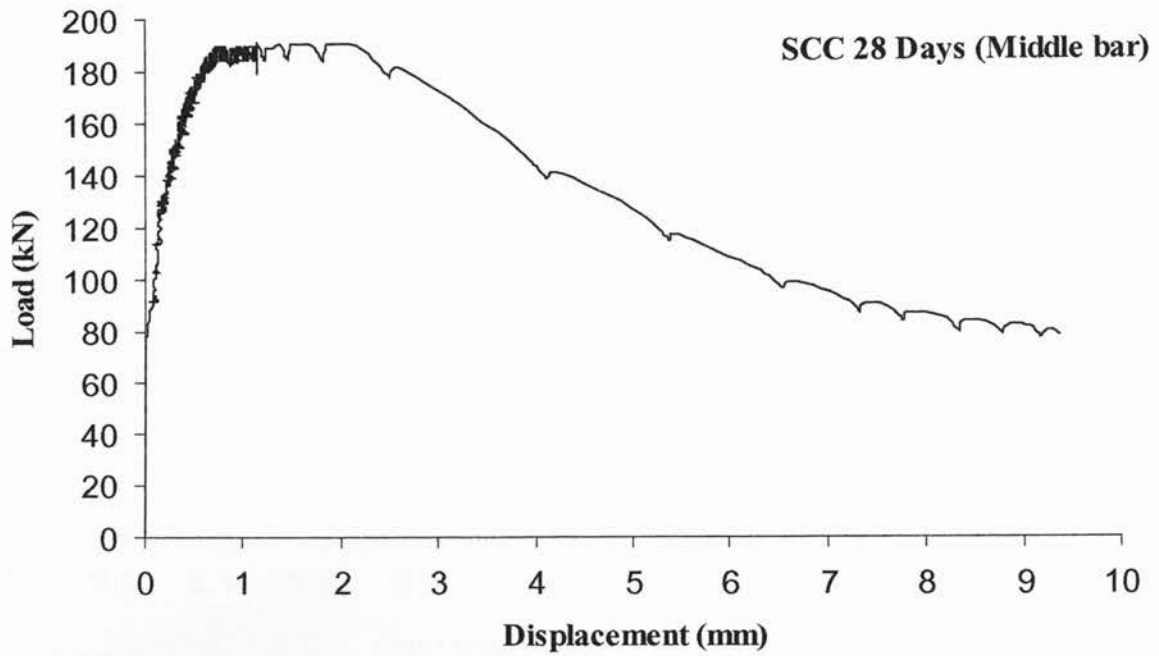
A 2: Experimental load-free end displacement (middle bar embedded in the NC beam at 28 days tested age) [Bond stress (MPa) = 0.106 Load (kN)]



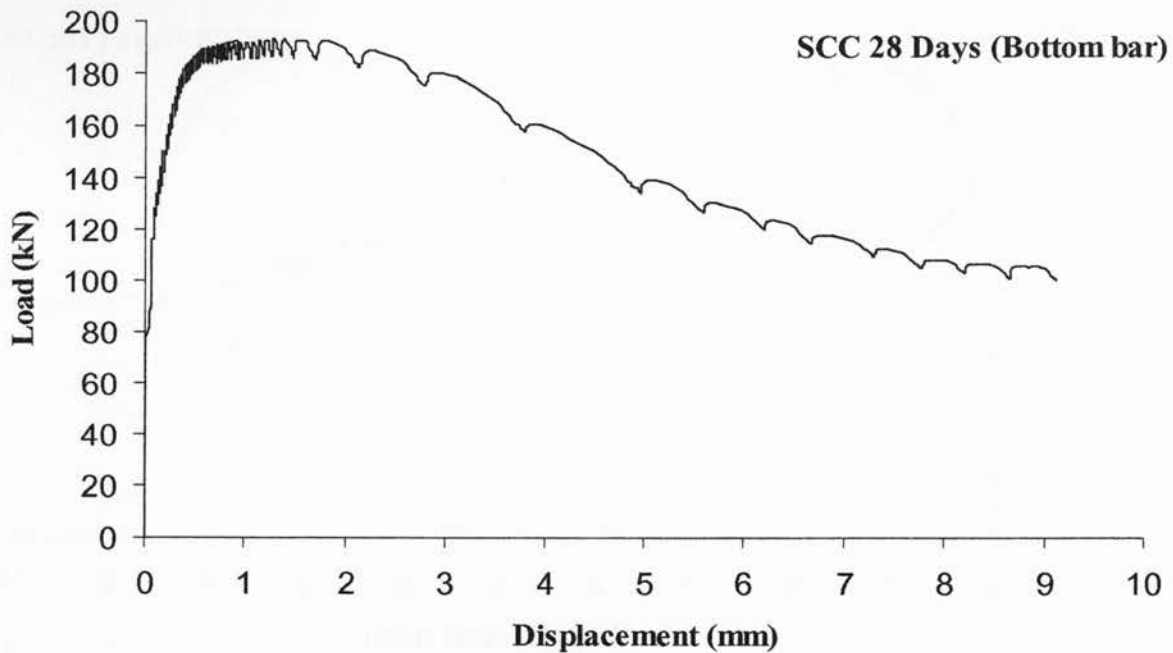
A 3: Experimental load-free end displacement (bottom bar embedded in the NC beam at 28 days tested age) [Bond stress (MPa) = 0.106 Load (kN)]



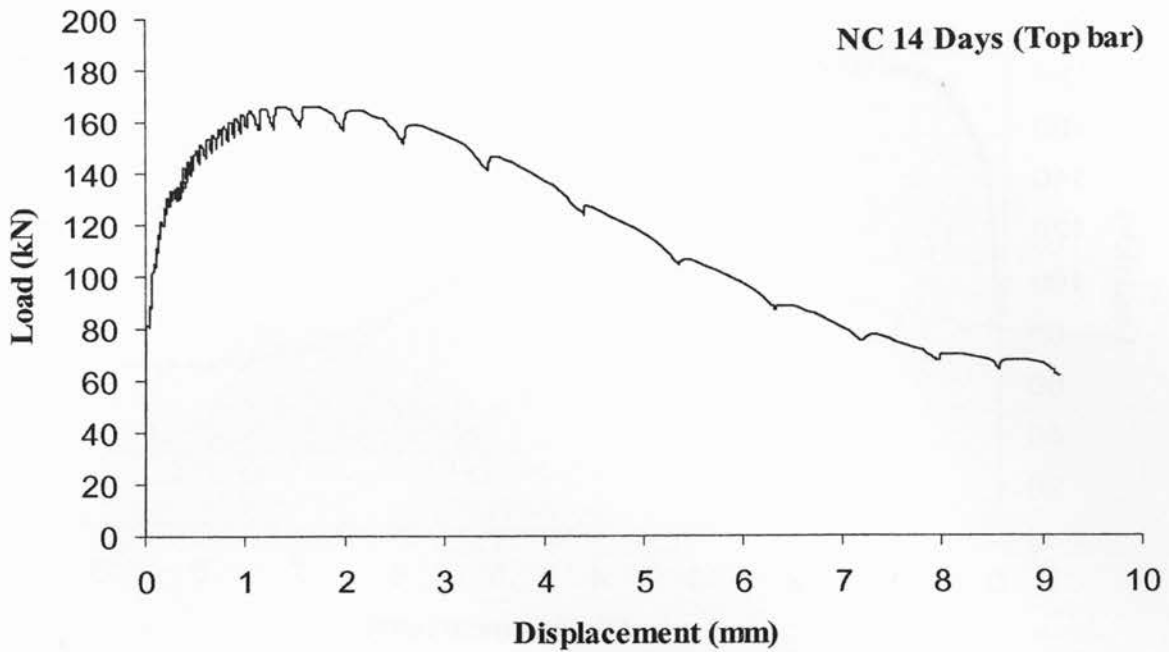
A 4: Experimental load-free end displacement (top bar embedded in the SCC beam at 28 days tested age) [Bond stress (MPa) = 0.106 Load (kN)]



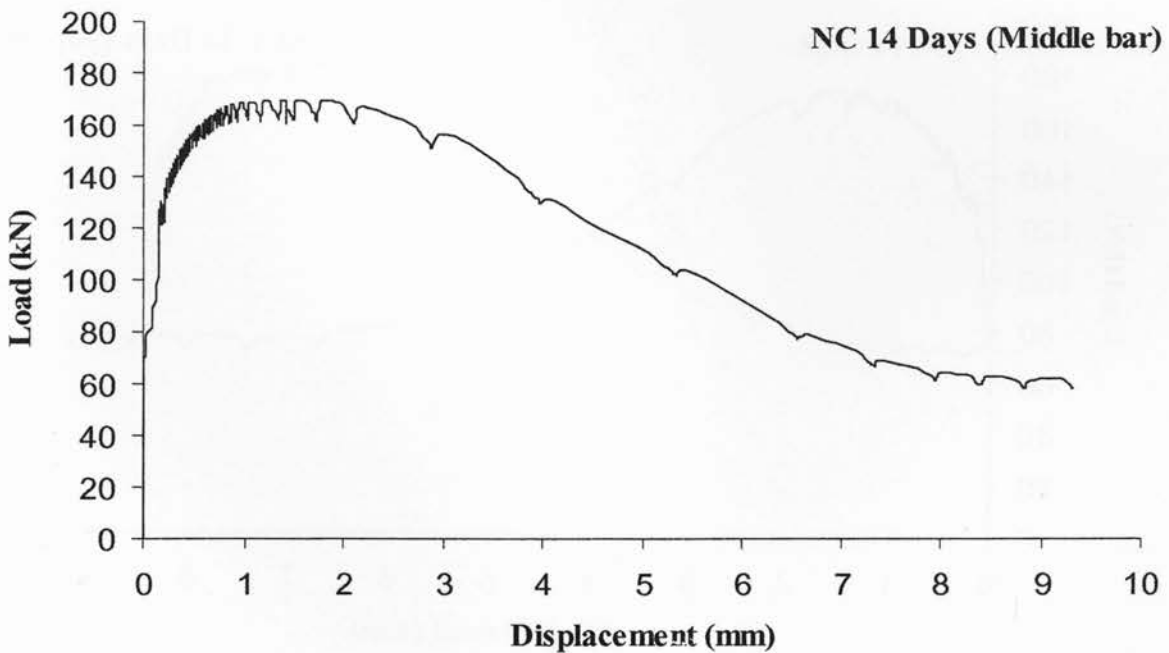
A 5: Experimental load-free end displacement (middle bar embedded in the SCC beam at 28 days tested age) [Bond stress (MPa) = 0.106 Load (kN)]



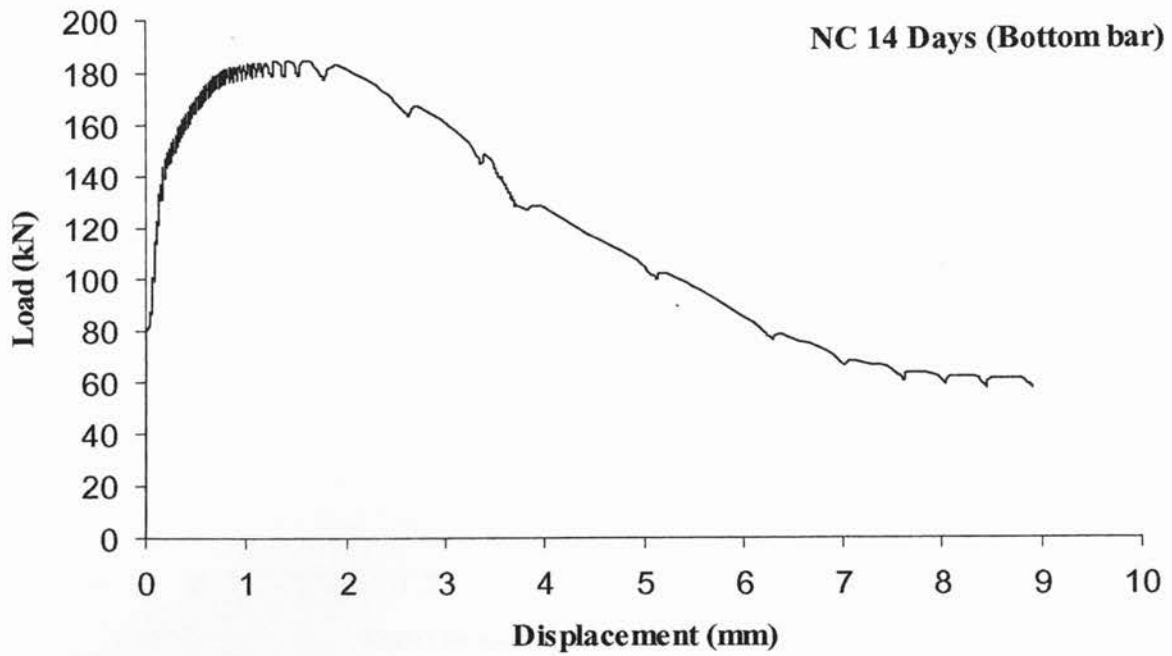
A 6: Experimental load-free end displacement (bottom bar embedded in the SCC beam at 28 days tested age) [Bond stress (MPa) = 0.106 Load (kN)]



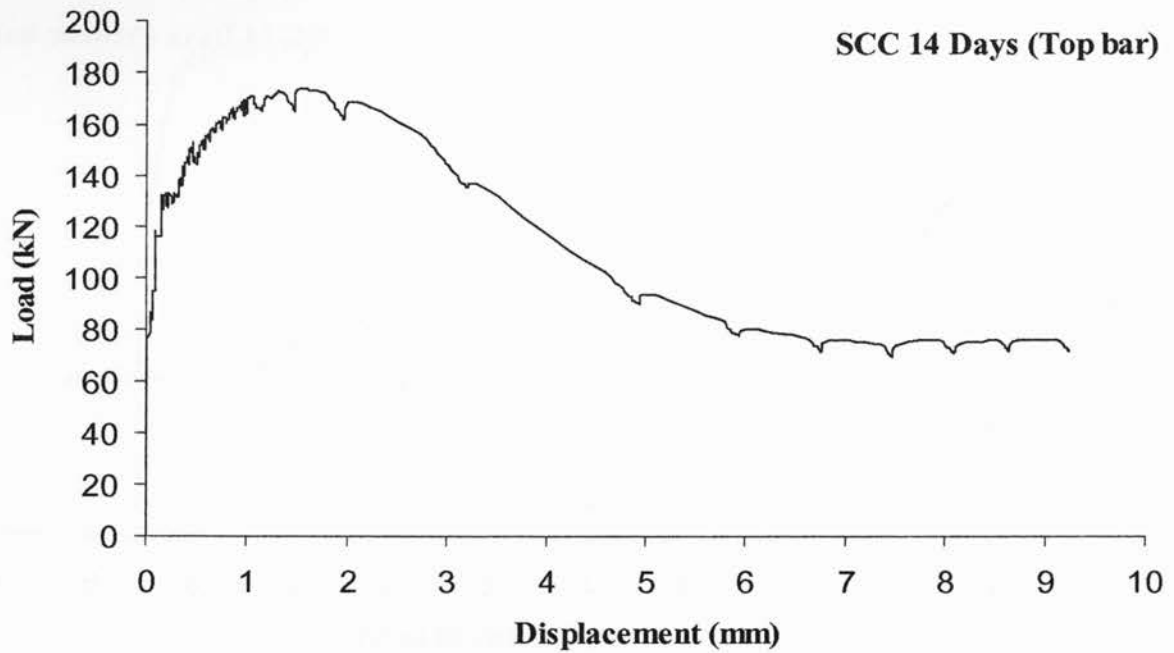
A 7: Experimental load-free end displacement (top bar embedded in the NC beam at 14 days tested age) [Bond stress (MPa) = 0.106 Load (kN)]



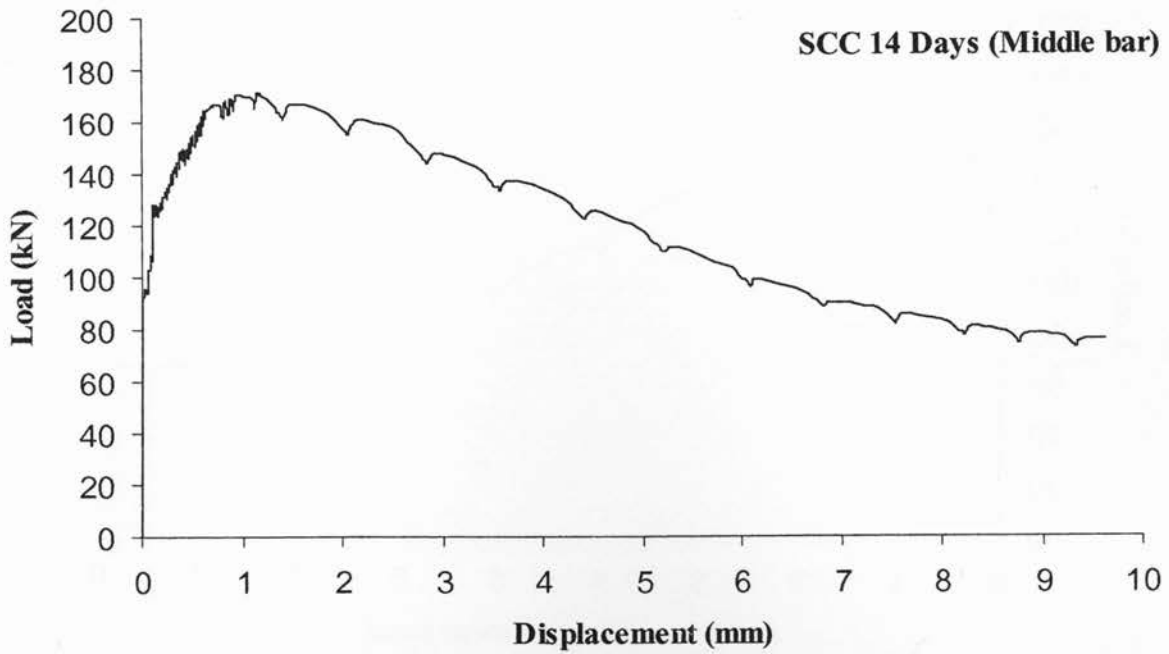
A 8: Experimental load-free end displacement (middle bar embedded in the NC beam at 14 days tested age) [Bond stress (MPa) = 0.106 Load (kN)]



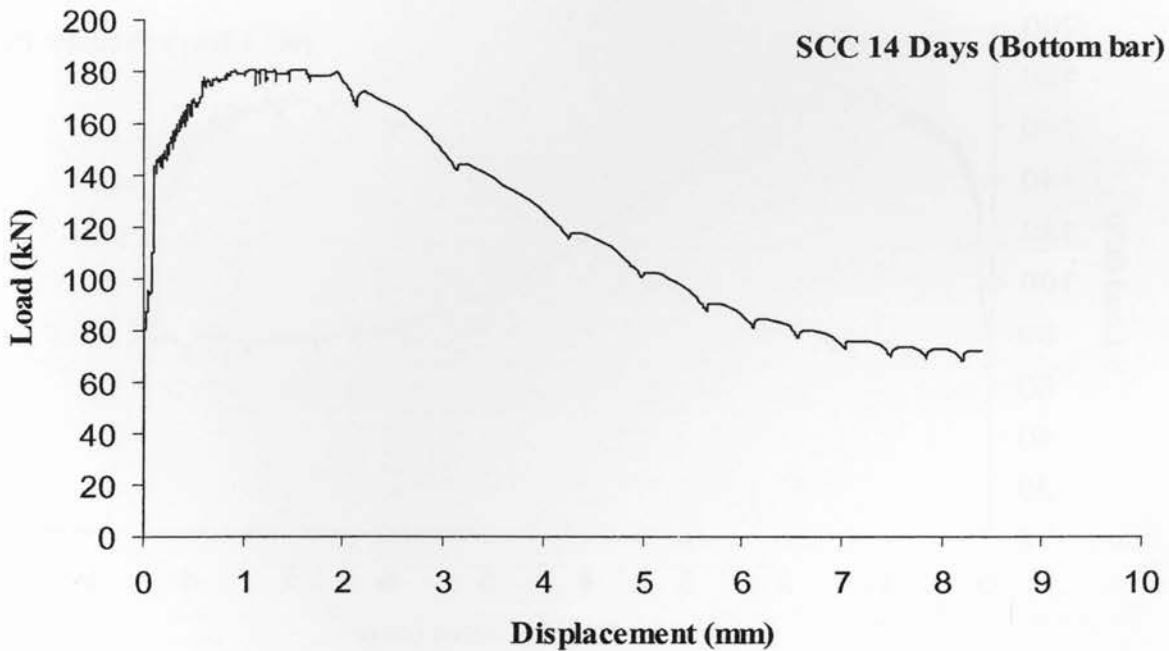
A 9: Experimental load-free end displacement (bottom bar embedded in the NC beam at 14 days tested age) [Bond stress (MPa) = 0.106 Load (kN)]



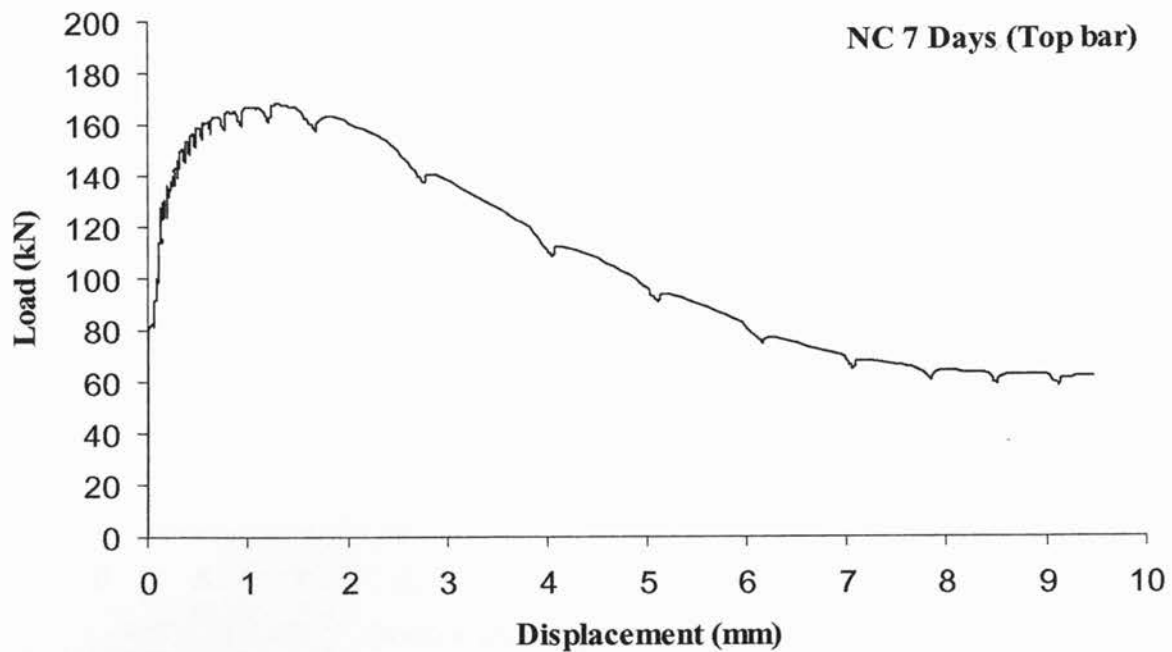
A 10: Experimental load-free end displacement (top bar embedded in the SCC beam at 14 days tested age) [Bond stress (MPa) = 0.106 Load (kN)]



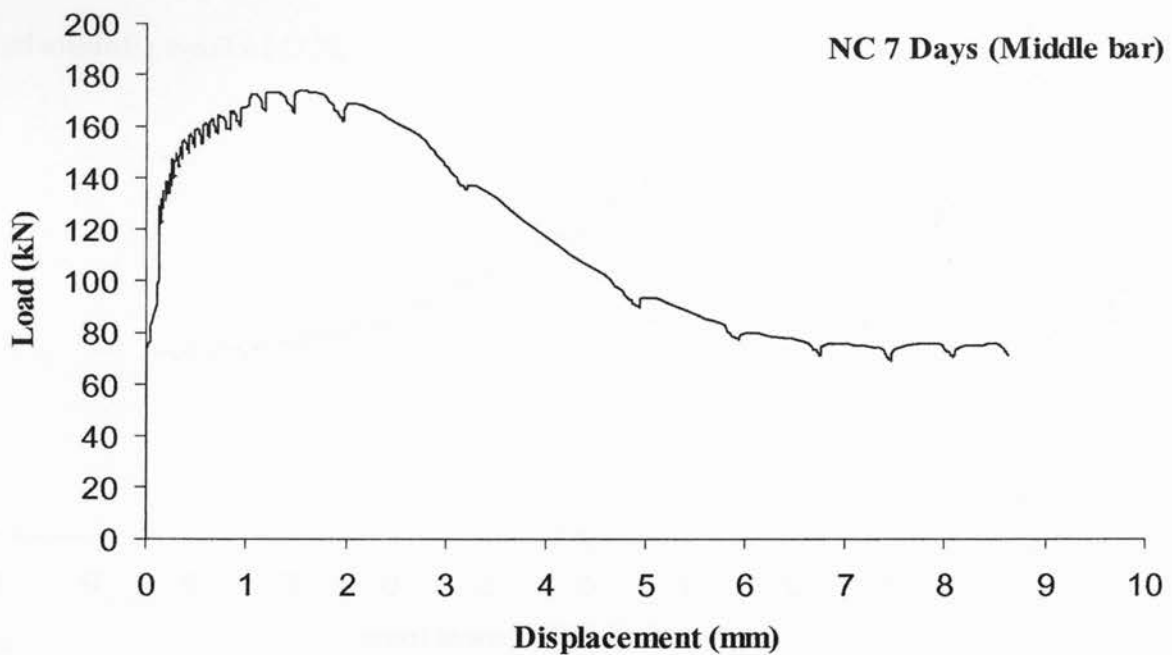
A 11: Experimental load-free end displacement (middle bar embedded in the SCC beam at 14 days tested age) [Bond stress (MPa) = 0.106 Load (kN)]



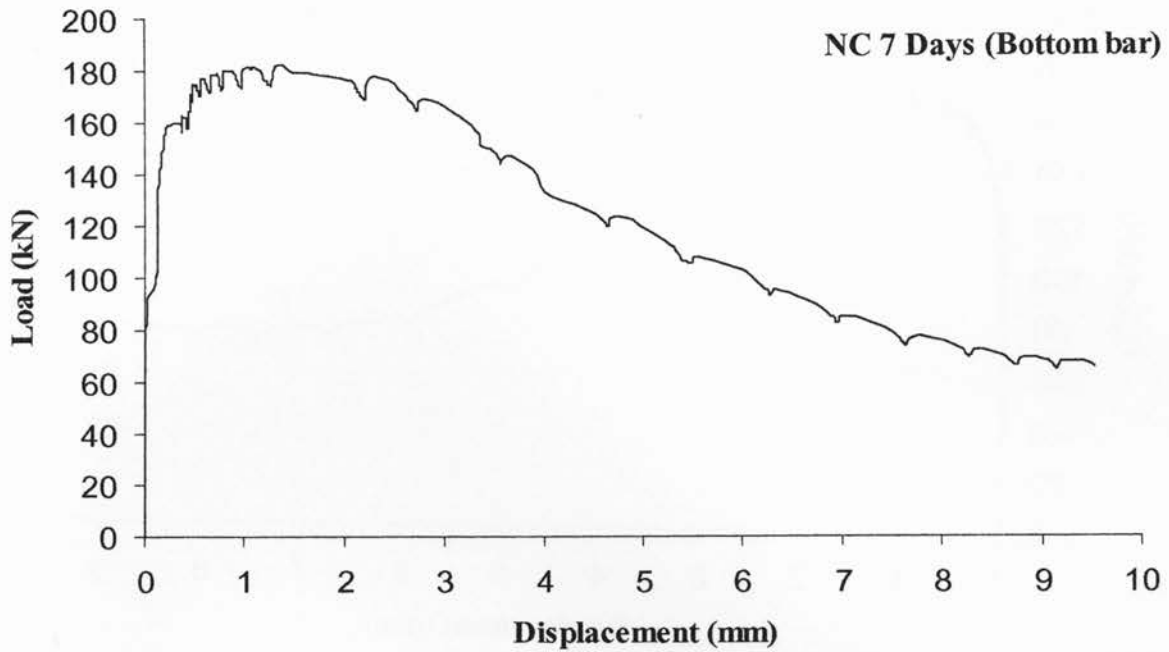
A 12: Experimental load-free end displacement (bottom bar embedded in the SCC beam at 14 days tested age) [Bond stress (MPa) = 0.106 Load (kN)]



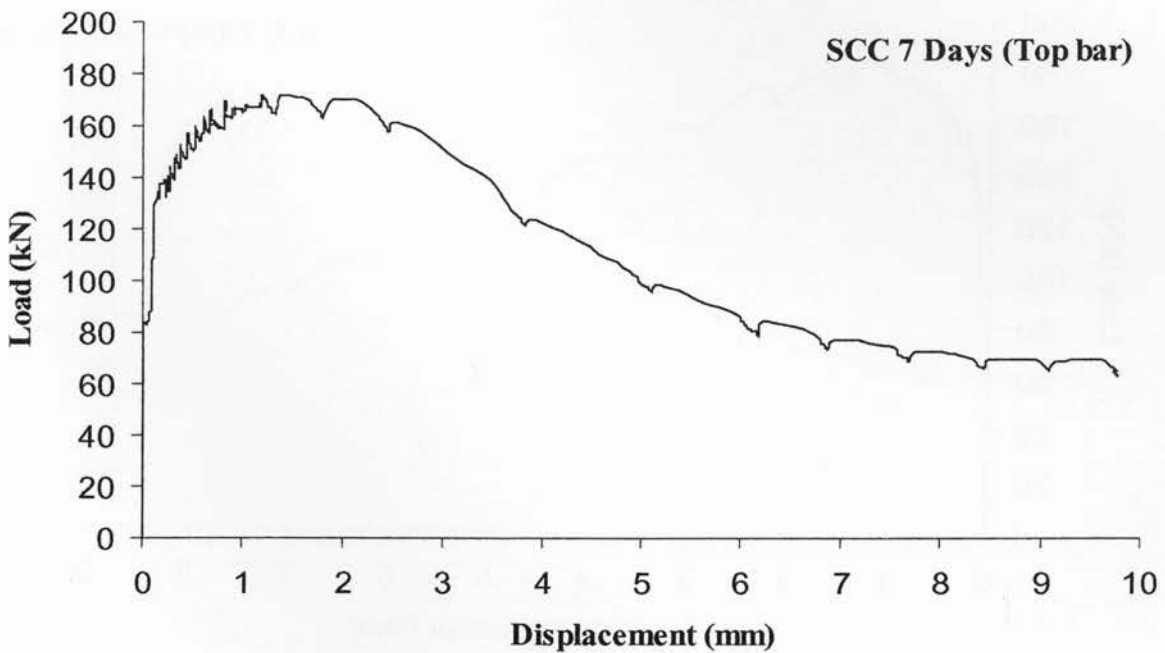
A 13: Experimental load-free end displacement (top bar embedded in the NC beam at 7 days tested age) [Bond stress (MPa) = 0.106 Load (kN)]



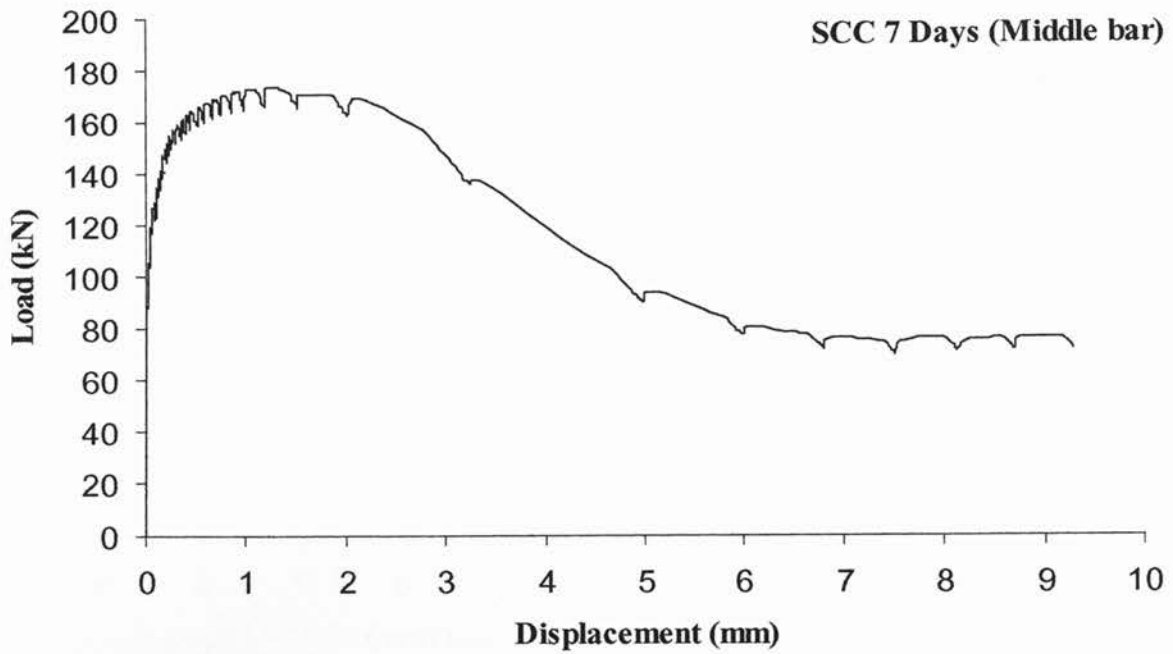
A 14: Experimental load-free end displacement (middle bar embedded in the NC beam at 7 days tested age) [Bond stress (MPa) = 0.106 Load (kN)]



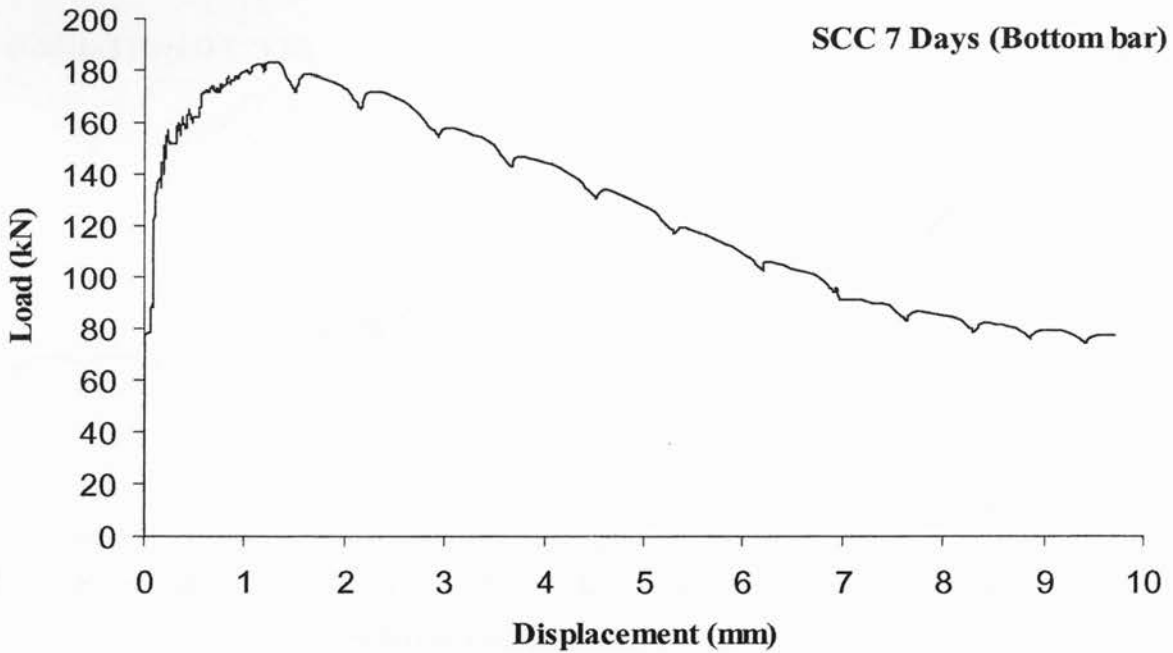
A 15: Experimental load-free end displacement (bottom bar embedded in the NC beam at 7 days tested age) [Bond stress (MPa) = 0.106 Load (kN)]



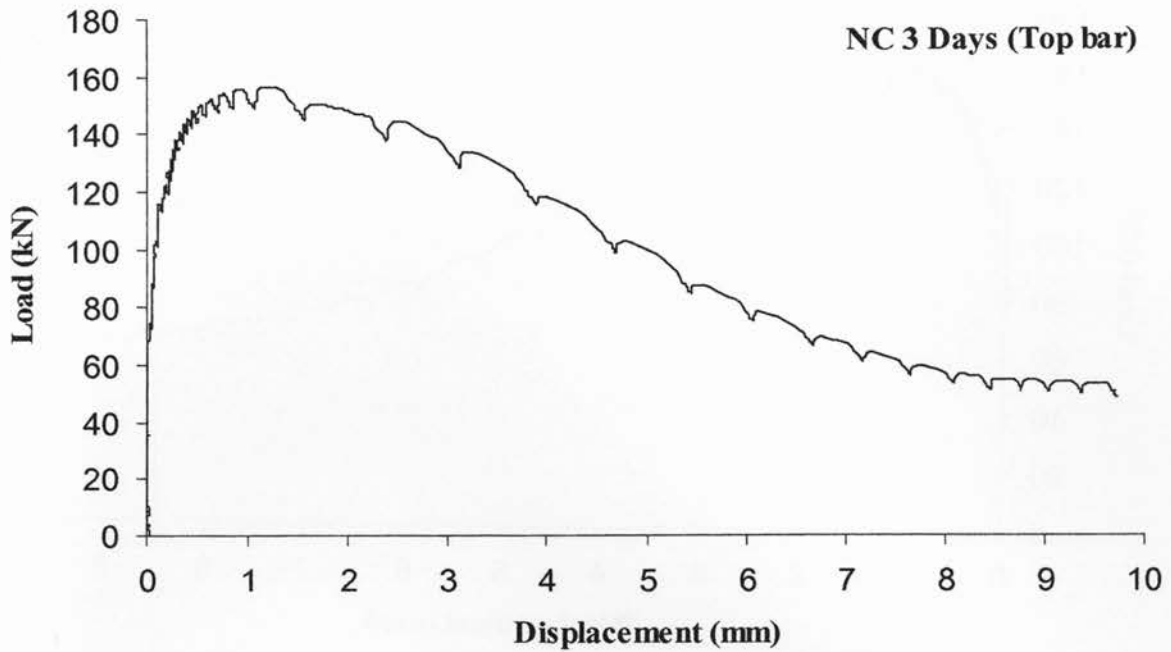
A 16: Experimental load-free end displacement (top bar embedded in the SCC beam at 7 days tested age) [Bond stress (MPa) = 0.106 Load (kN)]



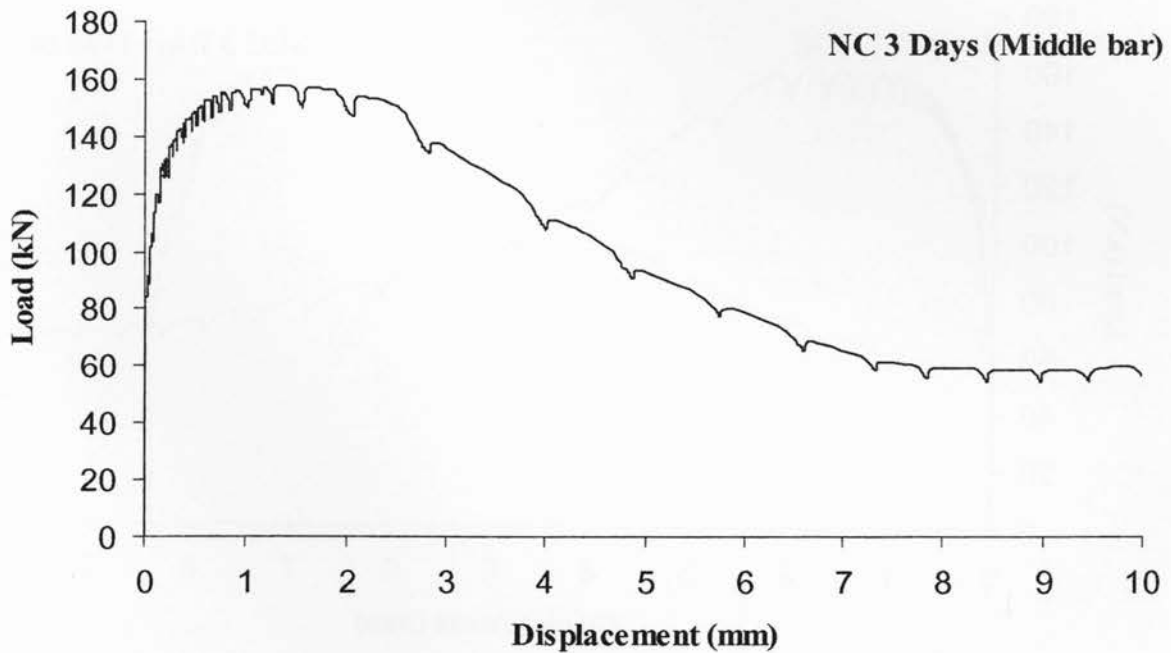
A 17: Experimental load-free end displacement (middle bar embedded in the SCC beam at 7 days tested age) [Bond stress (MPa) = 0.106 Load (kN)]



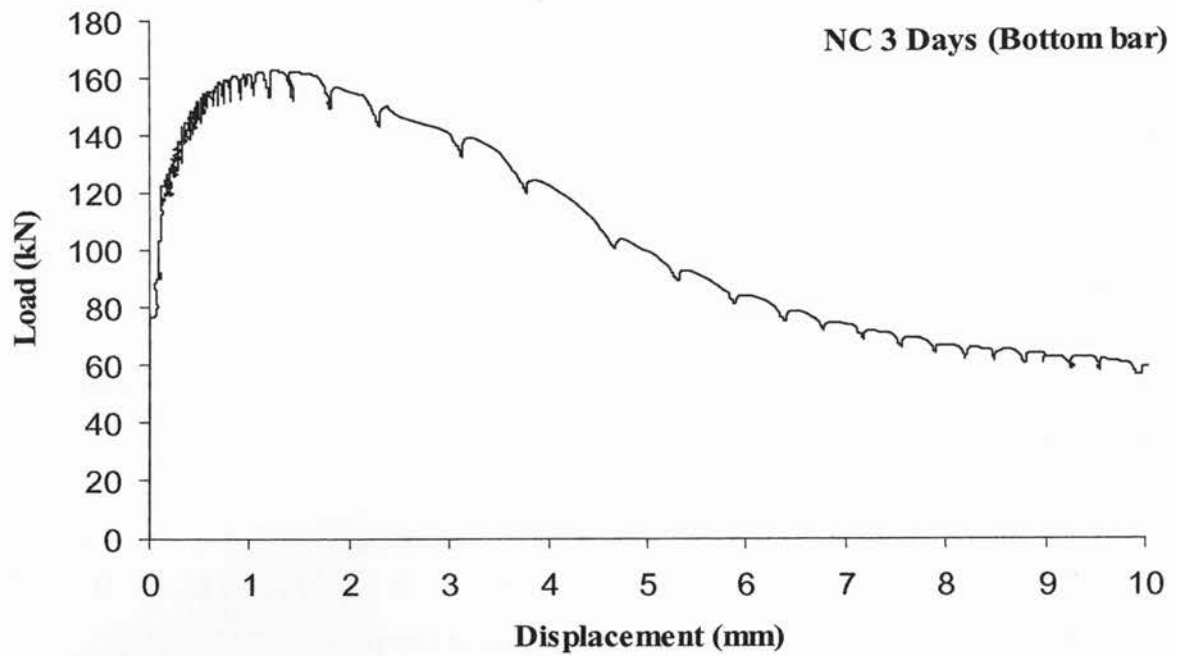
A 18: Experimental load-free end displacement (bottom bar embedded in the SCC beam at 7 days tested age) [Bond stress (MPa) = 0.106 Load (kN)]



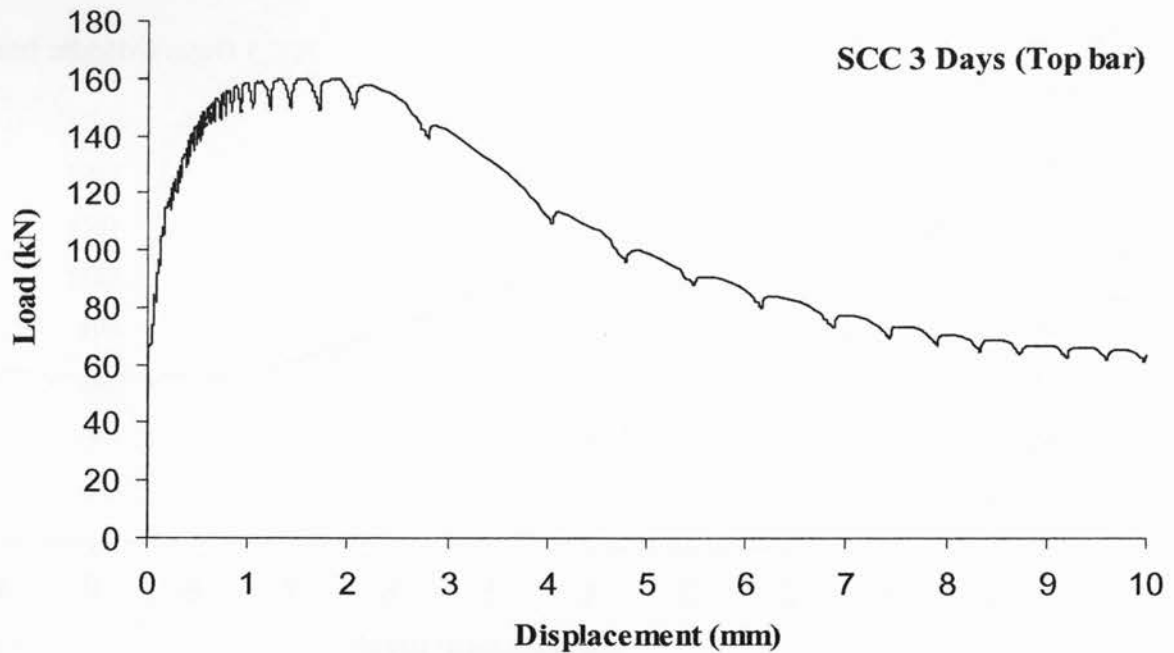
A 19: Experimental load-free end displacement (top bar embedded in the NC beam at 3 days tested age) [Bond stress (MPa) = 0.106 Load (kN)]



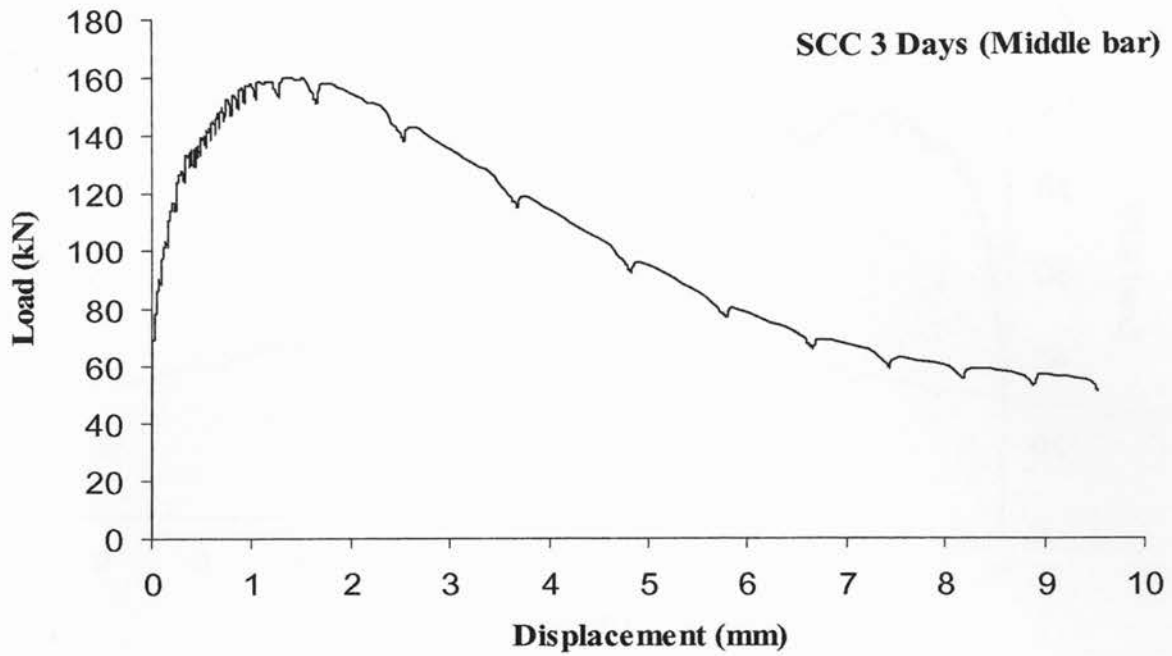
A 20: Experimental load-free end displacement (middle bar embedded in the NC beam at 3 days tested age) [Bond stress (MPa) = 0.106 Load (kN)]



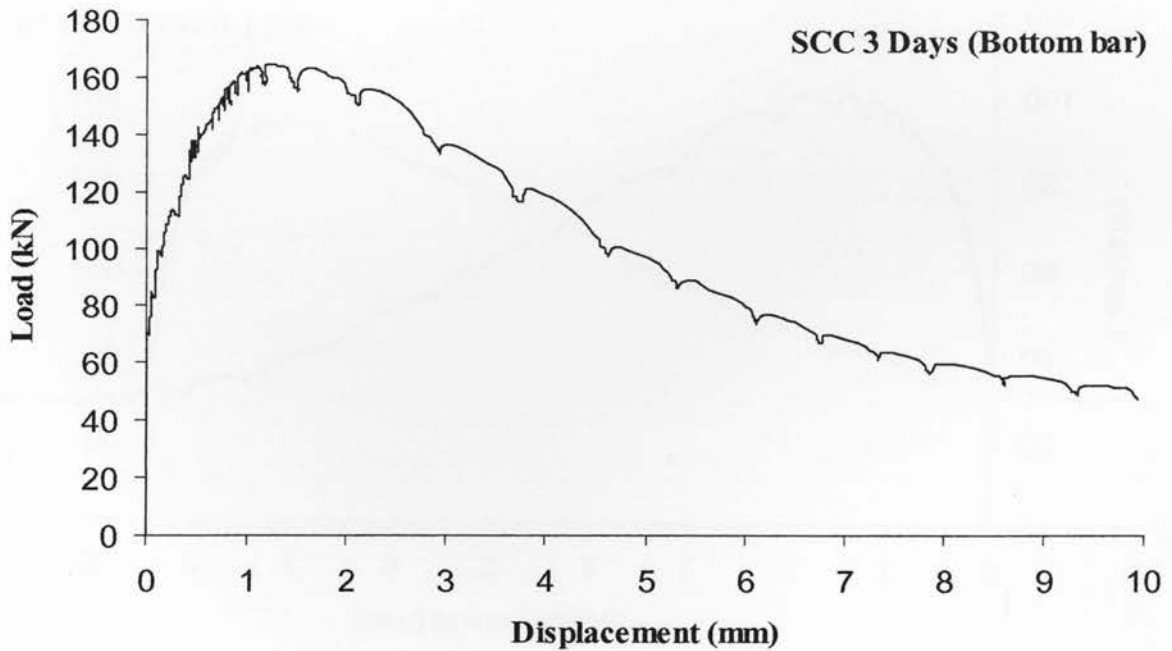
A 21: Experimental load-free end displacement (bottom bar embedded in the NC beam at 3 days tested age) [Bond stress (MPa) = 0.106 Load (kN)]



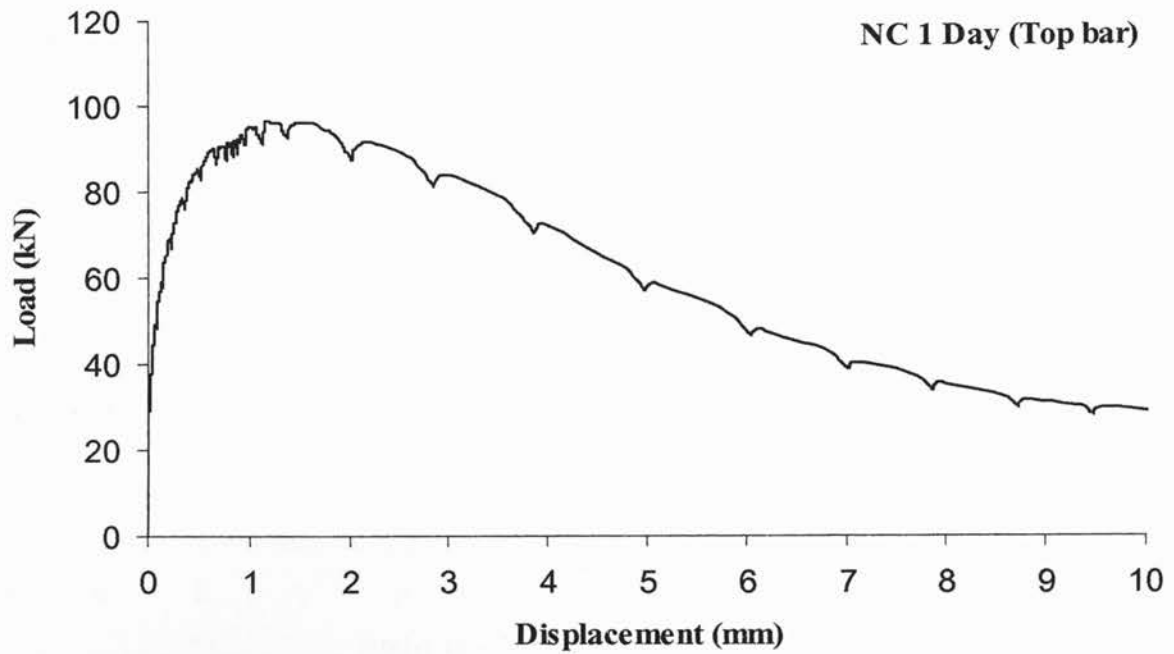
A 22: Experimental load-free end displacement (top bar embedded in the SCC beam at 3 days tested age) [Bond stress (MPa) = 0.106 Load (kN)]



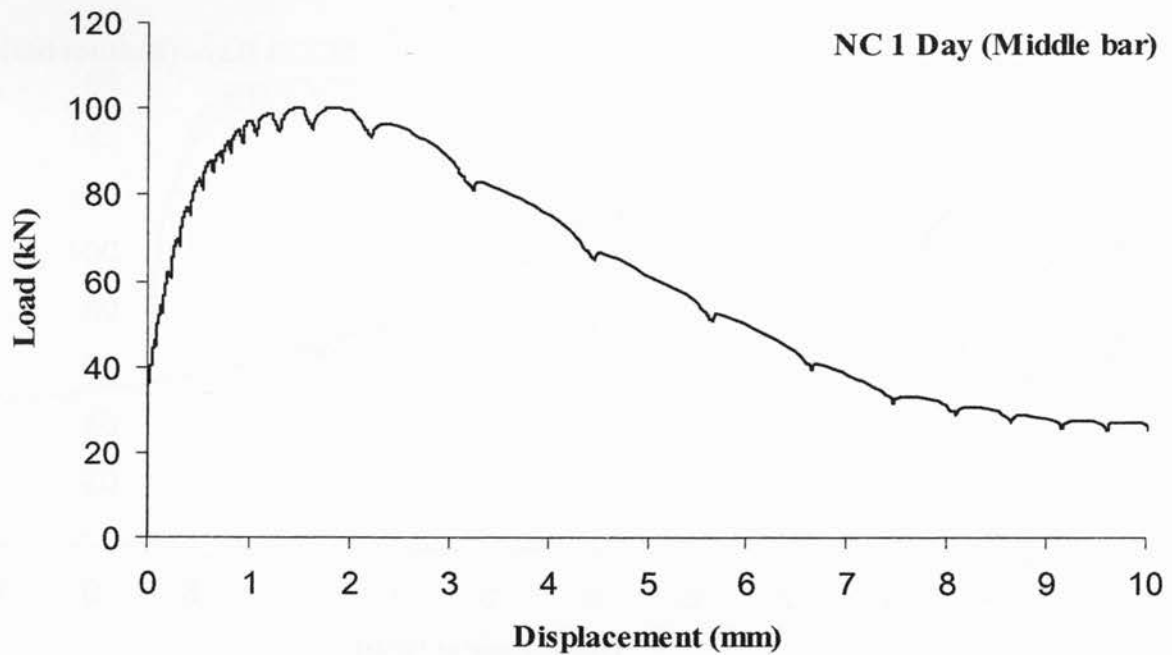
A 23: Experimental load-free end displacement (middle bar embedded in the SCC beam at 3 days tested age) [Bond stress (MPa) = 0.106 Load (kN)]



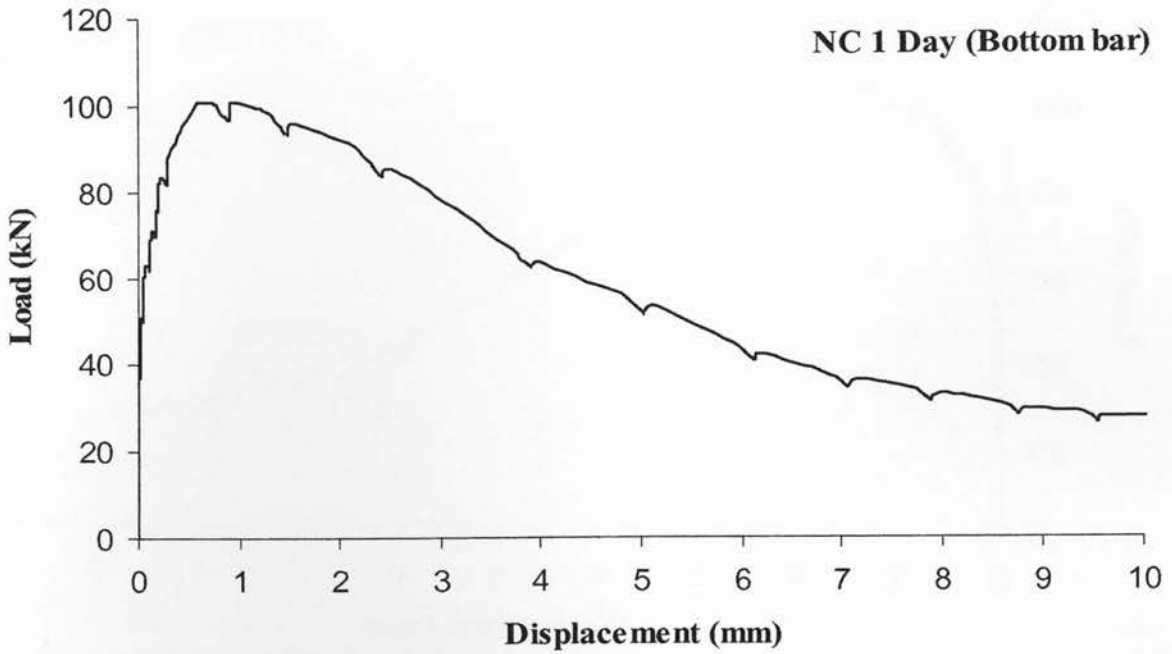
A 24: Experimental load-free end displacement (bottom bar embedded in the SCC beam at 3 days tested age) [Bond stress (MPa) = 0.106 Load (kN)]



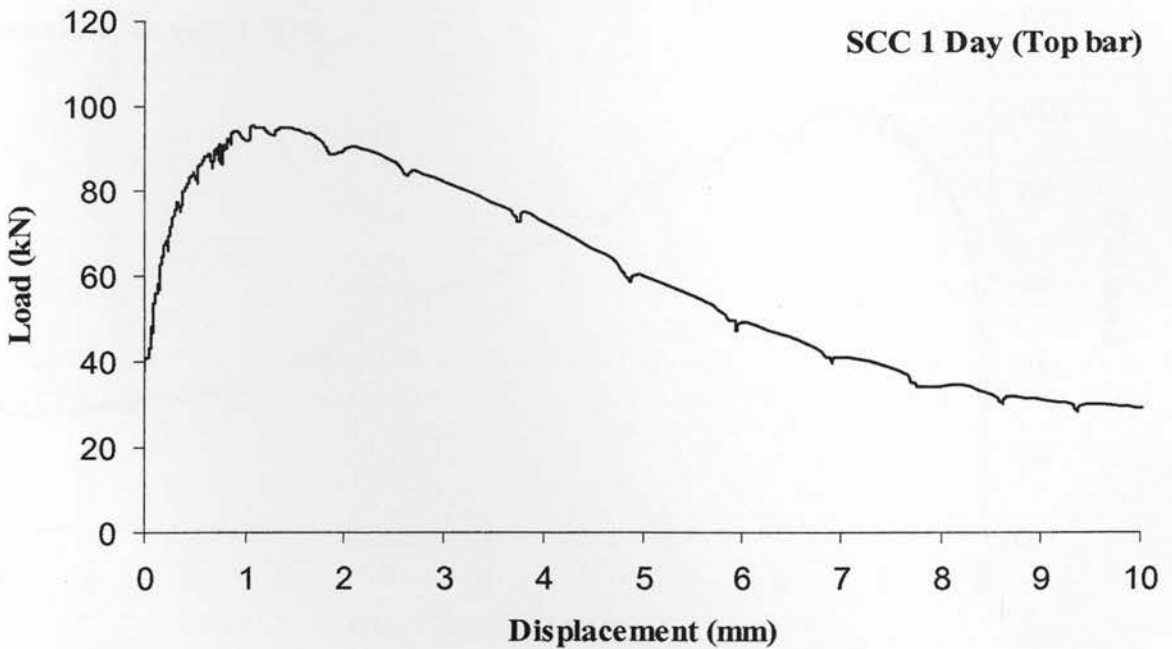
A 25: Experimental load-free end displacement (top bar embedded in the NC beam at 1 day tested age) [Bond stress (MPa) = 0.106 Load (kN)]



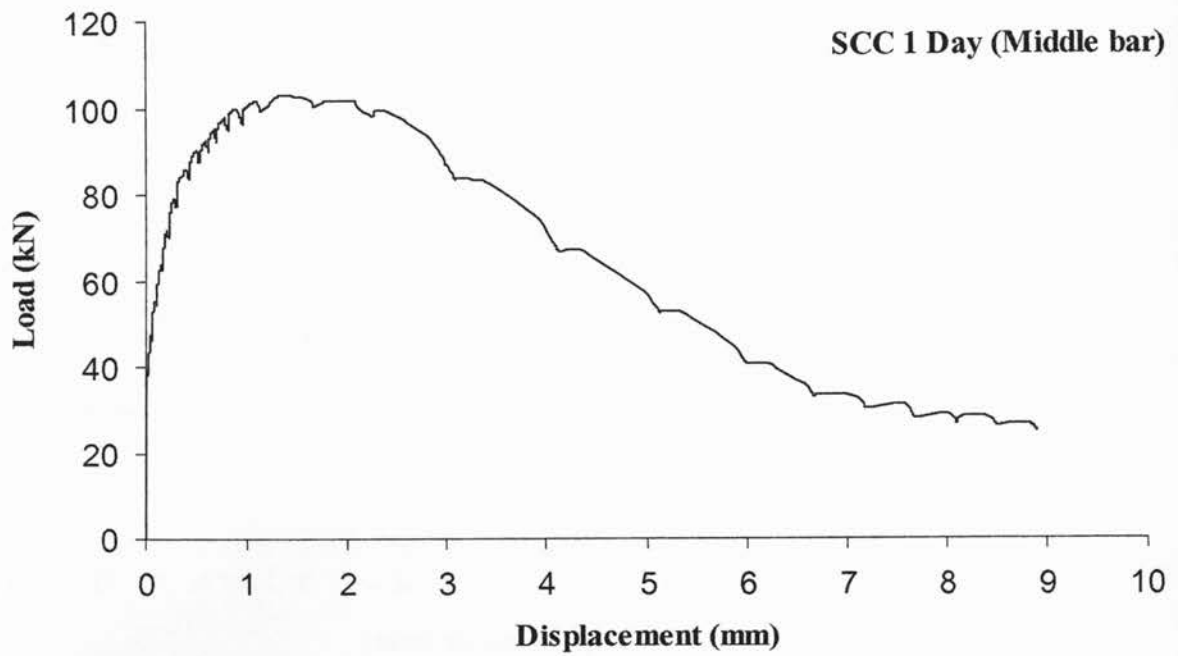
A 26: Experimental load-free end displacement (middle bar embedded in the NC beam at 1 day tested age) [Bond stress (MPa) = 0.106 Load (kN)]



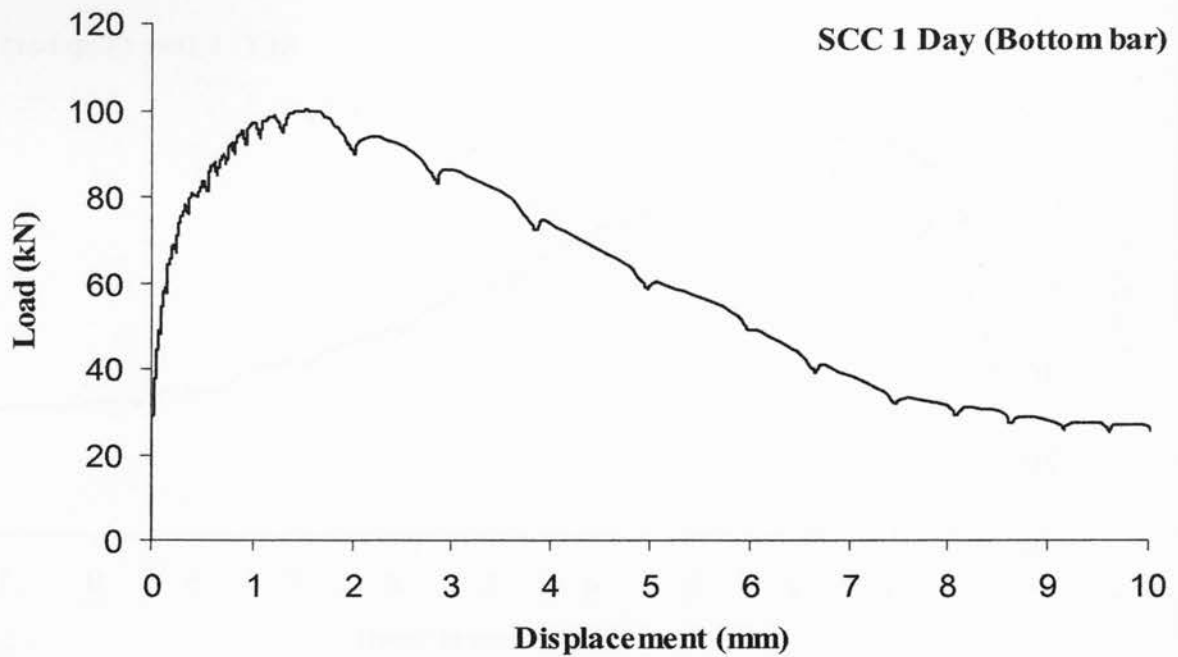
A 27: Experimental load-free end displacement (bottom bar embedded in the NC beam at 1 day tested age) [Bond stress (MPa) = 0.106 Load (kN)]



A 28: Experimental load-free end displacement (top bar embedded in the SCC beam at 1 day tested age) [Bond stress (MPa) = 0.106 Load (kN)]



A 29: Experimental load-free end displacement (middle bar embedded in the SCC beam at 1 day tested age) [Bond stress (MPa) = 0.106 Load (kN)]



A 30: Experimental load-free end displacement (bottom bar embedded in the SCC beam at 1 day tested age) [Bond stress (MPa) = 0.106 Load (kN)]

③ 15074-30